

AD-A281 985



ATION PAGE

Form Approved
OMB No. 0704-0188

6

average 1 hour per response including the time for reviewing instructions, searching existing data sources, gathering the necessary information, sending comments regarding this burden estimate or any other aspect of this collection of information, including suggestions for reducing this burden estimate, to the Office of Management and Budget, Paperwork Reduction Project (0704-0188) Washington, DC 20503

DATE

3. REPORT TYPE AND DATES COVERED

-THESIS/DISSERTATION

4. TITLE AND SUBTITLE

Development of An Automated Airfield
Dynamic Cone Penetrometer (AAOCP) Prototype And
The Evaluation of Unsaturated Airfield Seismic
Surveying Spectral Analysis of Surface Waves (SASW)
Technology

5. FUNDING NUMBERS

6. AUTHOR(S)

CAPTAIN David Weintraub, USAF

7. PERFORMING ORGANIZATION NAME(S) AND ADDRESS(ES)

AFIT Student Attending:

University of Florida

8. PERFORMING ORGANIZATION
REPORT NUMBER

AFIT/CI/CIA-

94-013D

9. SPONSORING/MONITORING AGENCY NAME(S) AND ADDRESS(ES)

DEPARTMENT OF THE AIR FORCE
AFIT/CI
2950 P STREET
WRIGHT-PATTERSON AFB OH 45433-7765

10. SPONSORING/MONITORING
AGENCY REPORT NUMBER

11. SUPPLEMENTARY NOTES

12a. DISTRIBUTION/AVAILABILITY STATEMENT

Approved for Public Release IAW 190-1
Distribution Unlimited
MICHAEL M. BRICKER, SMSgt, USAF
Chief Administration

327P

94-22513



13. ABSTRACT (Maximum 200 words)

DTIC
ELECTE
JUL 19 1994
S D

DTIC QUALITY INSPECTED 8

14. SUBJECT TERMS

15. NUMBER OF PAGES

282

16. PRICE CODE

94 7 18 053

17. SECURITY CLASSIFICATION
OF REPORT18. SECURITY CLASSIFICATION
OF THIS PAGE19. SECURITY CLASSIFICATION
OF ABSTRACT

20. LIMITATION OF ABSTRACT

DEVELOPMENT OF AN AUTOMATED AIRFIELD DYNAMIC CONE
PENETROMETER (AADCP) PROTOTYPE AND THE EVALUATION OF
UNSURFACED AIRFIELD SEISMIC SURVEYING USING SPECTRAL
ANALYSIS OF SURFACE WAVES (SASW) TECHNOLOGY

By

Captain David Weintraub, USAF

December 1993

Degree: PhD in Civil Engineering

Chairperson: John L. Davidson

Major Department: Civil Engineering, University of Florida

The mission of U.S. Air Force Combat Controllers is to infiltrate unused airfields. A specially trained evaluation team, carrying limited portable testing equipment, evaluates the unsurfaced airfield for use as a landing zone. The equipment used to evaluate the bearing capacity of the airfield is the Dynamic Cone Penetrometer (DCP).

Empirically based relationships are used to predict the type and number of aircraft passes on the unsurfaced airfield based on inputs from the DCP.

It was the goal of this research to improve on the field testing equipment used in the unsurfaced airfield evaluation process. The specific objectives were (a) to develop prototype airfield bearing test equipment that is less labor intensive than the currently used Dynamic Cone Penetrometer (DCP), while still providing accurate bearing capacity data, and (b) evaluate Spectral Analysis of Surface Wave (SASW) technology as a means of seismically surveying unsurfaced runways and aprons.

An Automated Airfield Dynamic Cone Penetrometer (AADCP)

prototype was developed to measure unsurfaced airfield bearing. Using correlations with the manual DCP and DCP-CBR relationships established in the literature, the AADCP can predict airfield bearing strengths. The AADCP was shown to be inherently less labor intensive than the manual DCP due to its pneumatic operation. In addition, SASW surveying techniques were successfully used to qualitatively detect soft layers at a soil site and a surveying technique was recommended to qualitatively compare profiles of an unsurfaced airfield.

Number of Pages: 290

Accession For	
NTIS GRA&I	<input checked="checked" type="checkbox"/>
DTIC TAB	<input type="checkbox"/>
Unannounced	<input type="checkbox"/>
Justification_____	
By_____	
Distribution/_____	
Availability Codes	
Dist	Special
A-1	

**DEVELOPMENT OF AN AUTOMATED AIRFIELD DYNAMIC CONE
PENETROMETER (AADCP) PROTOTYPE AND THE EVALUATION OF
UNSURFACED AIRFIELD SEISMIC SURVEYING USING SPECTRAL
ANALYSIS OF SURFACE WAVES (SASW) TECHNOLOGY**

By

Captain David Weintraub, USAF

December 1993

Degree: PhD in Civil Engineering

Chairperson: John L. Davidson

Major Department: Civil Engineering, University of Florida

The mission of U.S. Air Force Combat Controllers is to infiltrate unused airfields. A specially trained evaluation team, carrying limited portable testing equipment, evaluates the unsurfaced airfield for use as a landing zone. The equipment used to evaluate the bearing capacity of the airfield is the Dynamic Cone Penetrometer (DCP).

Empirically based relationships are used to predict the type and number of aircraft passes on the unsurfaced airfield based on inputs from the DCP.

It was the goal of this research to improve on the field testing equipment used in the unsurfaced airfield evaluation process. The specific objectives were (a) to develop prototype airfield bearing test equipment that is less labor intensive than the currently used Dynamic Cone Penetrometer (DCP), while still providing accurate bearing capacity data, and (b) evaluate Spectral Analysis of Surface Wave (SASW) technology as a means of seismically surveying unsurfaced runways and aprons.

An Automated Airfield Dynamic Cone Penetrometer (AADCP)

prototype was developed to measure unsurfaced airfield bearing. Using correlations with the manual DCP and DCP-CBR relationships established in the literature, the AADCP can predict airfield bearing strengths. The AADCP was shown to be inherently less labor intensive than the manual DCP due to its pneumatic operation. In addition, SASW surveying techniques were successfully used to qualitatively detect soft layers at a soil site and a surveying technique was recommended to qualitatively compare profiles of an unsurfaced airfield.

Number of Pages: 290

REFERENCES

- Bowles, J.E. 1988 Foundation Analysis and Design, 4th Edition, McGraw-Hill, Inc., New York, pp. 788.
- Brabston, W.N., and Hammitt, G.M., (1974) "Soil Stabilization for Roads and Airfields in the Theater of Operations," U.S. Army Engineer Waterways Experiment Station, AD-787-257.
- Brown, Randall W. Letter to 61 MAG/CC. 7 August 1986.
- Caudle, W.N., Pope, A.Y., McNeill, R.L., and Magason, B.E. (1977) "Feasibility of Rapid Soil Investigations Using High Speed Earth Penetrating Projectiles," International Symposium on Wave Propagation and Dynamic Properties of Earth Materials, Albuquerque, NM, (August).
- Chua, K. M., and Lytton, R. L., (1989) "Dynamic Analysis Using the Portable Pavement Dynamic Cone Penetrometer," Transportation Research Record 1192, TRB, National Research Council, Washington, D.C., pp. 27-38.
- Durgunoglu, H. T., and Mitchell, J. K., (1974) "Influence of Penetrometer Characteristics on Static Penetration Resistance," Proceedings of the European Symposium on Penetration Testing, Stockholm, pp. 133-139.
- Fenwick, W.B., (1965) "Description and Application of Airfield Cone Penetrometer," U.S. Army Engineer Waterways Experiment Station, Instruction Report No. 7.
- Hammitt, G.M., (1970) "Thickness Requirements For Unsurfaced Roads and Airfields," U.S. Army Engineer Waterways Experiment Station, Technical Report S-70-5, (July).
- Harrison, J. A., (1986) "Correlation of CBR and Dynamic Cone Penetrometer Strength Measurement of Soils," Technical Note No. 2, Australian Road Research, 16(2), (June), pp. 130-136.

- Harrison, J. A., (1989) "In Situ CBR Determination by DCP Testing Using a Laboratory-Based Correlation," Technical Note No. 2, Australian Road Research 19(4), December, pp. 313-317.
- Kleyn, E. G. (1975) "The Use of the Dynamic Cone Penetrometer," Transvaal Roads Department, Report 12/74, July, Pretoria, South Africa.
- Ladd, D.M. and Ulery, H.H. Jr., (1967) "Aircraft Ground Flotation Investigations; Part I, Basic Report," Technical Documentary Report AAFDL-TDR-66-43 Air Force Flight Dynamics Laboratory, WPAFB, Ohio.
- Ladd, D.C. (1965) "Ground Flotation Requirements for Aircraft Landing Gear," U.S. Army Engineer Waterways Experiment Station, Misc Paper No. 4-459.
- Livneh, Moshe, and Greenstein, Jacob, (1978) "A Modified California Bearing Ratio Test for Granular Materials," Geotechnical Testing Journal, ASTM, Vol 1, No. 3, Sep, pp. 141-147.
- Livneh, M., (1987) "The Correlation Between Dyanmic Cone Penetrometer Values (DCP) and CBR Values," Transportation Research Institute, Technion-Israel Institute of Technology, Pub. No. 87-065.
- Livneh, M., and Ishai, I., (1989) "Carrying Capacity of Unsurfaced Runways for Low Volume Aircraft Traffic - Phase I: Review of Current Technology," August, Technion-Israel Institute of Technology, Transportation Research Institute, Haifa, Israel, Prepared for AFESC, Tyndall AFB, FL 32403.
- Livneh, M., Ishai, I., and Livneh, N., (1990) "Carrying Capacity of Unsurfaced Runways for Low Volume Aircraft Traffic - Phase III: Application of the Dyanmic Cone Penetrometer," April, (Draft Copy), Technion-Israel Institute of Technology, Transportation Research Institute, Haifa, Israel, Prepared for AFESC, Tyndall AFB, FL 32403.
- MACP 50-8, (1989) "Combat Control - The Quick Action Force," Department of the Air Force - Military Airlift Command, Scott Air Force Base, Illinois, June.
- Melzer, K. J., and Smoltczyk, U., (1982) "Dynamic Penetration Testing - State of the Art Report," Proceedings of the Second European Symposium on Penetration Testing, Amsterdam, 24-27 May, pp. 191-202.

- Metcalf, J.B. (1976) "Pavement Materials - The Use of California Bearing Ratio Test in Controlling Quality," Report 48, Australia Road Research Board, Vertmont Victoria, Australia.**
- Meyerhof, G. G., (1961) "The Ultimate Bearing Capacity of Wedge-Shaped Foundations," Proceedings, Fifth International Conference on Soil Mechanics and Foundation Engineering, Vol. 2, pp. 105-109.**
- Molineux, C.E., (1955) "Remote Determination of Soil Trafficability By the Aerial Penetrometer," Report No. 77, Air Force Cambridge Research Center, Bedford, Mass.**
- Roesset, J.M., Chang, D., Stokoe, K., and Aouad, M. (1990) "Modulus and Thickness of the Pavement Surface Layer from SASW Tests," Transportation Research Record 1260, TRB, National Research Council, Washington, D.C., pp. 53-63.**
- Rohani, B. and Baladi, G.Y. (1981) "Correlation of Mobility Cone Index with Fundamental Engineering Properties of Soil," Miscellaneous Paper SL-81-4, U.S. Army Engineer Waterways Experiment Station, Vicksburg, MS.**
- Scala, A. J., (1956) "Simple Methods of Flexible Pavement Design Using Cone Penetrometers," New Zealand Engineering, Vol 11, No. 2, pp. 34-44.**
- Seed, B., Wong, R.T., Idriss, I.M., and Tokimatsu, K., (1986) "Moduli and Damping Factors for Dynamic Analysis of Cohesionless Soils," Journal of Geotechnical Engineering, November, Vol 112, No. 11.**
- Schmertmann, J.H. (1979) "Statics of SPT," Journal of the Geotechnical Division, ASCE, Vol. 105, No. GT5, Proc. Paper 14573.**
- Smith, R.B., and Pratt, D.N., (1983) "A Field Study of In-Situ California Bearing Ratio and Dynamic Cone Penetrometer Testing for Road Subgrade Investigations," Australian Road Research 13(4), December, pp. 283-294.**
- Stokoe, Kenneth H., Nazarian, S., Rix, Glenn J., Sanchez-Salinero, Ignacio, Sheu, J., and Mok, Y., (1988) "In Situ Seismic Testing of Hard-to-Sample Soils by Surface Wave Method," Proceedings, Earthquake Engineering and Soil Dynamics II, ASCE Specialty Conference - Recent Advances in Ground Motion Evaluation, June, Park City, Utah, pp. 264-278.**

- Townsend, F.C., Theos, J.F., Shields, M.D., Hussein, M., Coastal Caisson Drill Co., and Florida DOT, (1991) "Dynamic Load Testing of Drilled Shaft," March, Final Report to the Association of Drilled Shaft Contractors
- Turnbull, W. J., Maxwell, A.A. and Burns, C. D., (1961) "Strength Requirements in Unsurfaced Soils for Aircraft Operations," Proceedings of the 5th International Conference of Soil Mechanics and Foundation Engineering, Paris, pp. 347-357.
- Van Vuuren, D. J. (1969) "Rapid Determination of CBR with the Portable Dynamic Cone Penetrometer," The Rhodesian Engineer, September, Paper No. 105, pp. 852-854.
- Vesic, A. S., (1972) "Expansion of Cavities in Infinite Soil Mass," Journal of the Soil Mechanics and Foundations Division, March, pp. 265-290.
- Webster, Steve, L., Grau, Richard H., and Williams, Thomas P., (1992) "Description and Application of Dual Mass Dynamic Cone Penetrometer," Instruction Report GL-92-3, Waterways Experiment Station, Mississippi.
- Womack, L.M., (1965) "Tests with a C-130E Aircraft on Unsurfaced Soils," U.S. Army Engineer Waterways Experiment Station, Vicksburg, MS.

BIBLIOGRAPHY

- Air Force Engineering and Services Center, "Aircraft Characteristics for Airfield Pavement Design and Evaluation," Tyndall Air Force Base, 1990.
- Aun, O. T., and Hui, T. W., "The Use of a Light Dynamic Cone Penetrometer in Malaysia," 4th Southeast Asian Conference on Soil Engineering, Kuala Lumpur, Malaysia, 7-10 April 1975, pp. 3-62 - 3-79.
- Ayers, M. E., Thompson, M. R., and Uzarski, D. R., "Rapid Shear Strength Evaluation of In Situ Granular Materials," Transportation Research Record 1227, pp. 134-146.
- Cearns, P. J., and McKenzie, A., "Application of Dynamic Cone Penetrometer Testing in East Anglia," Penetration Testing in the UK, Thomas Telford, London, 1988, pp. 123-127.
- Chua, K. M., "Determination of CBR and Elastic Modulus of Soils using a Portable Pavement Dynamic Cone Penetrometer," ISOPT-1 Orlando, Fl, 20-24 March 1988.
- Harrison, J. A. 1987 (December). "Correlation Between California Bearing Ratio and Dynamic Cone Penetrometer Strength Measurements of Soils," Proceedings of Instn. Civil Engineers, Part 2, pp. 833-844.
- Headquarters, Department of the Army. 1990 (September). "Design of Aggregate Surfaced Roads and Airfields," Technical Manual TM 5-822-12, Washington, DC.
- Khedr, S. A., Kraft, D.C., and Jenkins, J. L., "Automated Cone Penetrometer: A Nondestructive Field Test for Subgrade Evaluation," Transportation Research Record 1022, pp. 108-115.
- Kleyn, E.G., Maree, J. H., Savage, P. F., "The Application of a Portable Pavement Dynamic Cone Penetrometer to Determine In-Situ Bearing Properties of Road Pavement Layers and Subgrades in South Africa," Proceedings of the Second European Symposium on Penetration Testing, Amsterdam, 24-27 May 1982, pp. 277-282.

- Livneh, M., "Validation of Correlations Between a Number of Penetration Tests and In Situ California Bearing Ratio Tests," *Transportation Research Record* 1219, pp. 56-67.
- Livneh, M., Ishai, I., "The Relationship Between In-situ CBR Test and Various Penetration Tests," *ISOPT-1 Orlando, Fl, 20-24 March 1988*, pp. 445-452.
- Livneh, M, and Ishai, I. 1987 (July). "Pavement and Material Evaluation by a Dynamic Cone Penetrometer," Proceedings of the Sixth International Conference on Structural Design of Asphalt Pavements, Vol. I, pp. 665-676, University of Michigan, Ann Arbor, MI.
- McElvaney, J., and Bunadidjatnika, I., "Strength Evaluation of Lime-Stabilised Pavement Foundations Using the Dynamic Cone Penetrometer," *Australian Road Research* 21(1), March 1991, pp. 40-52.
- Nazarian, Soheil, Stokoe, Kenneth H., Briggs, Robert C., and Rogers, Richard, "Determination of Pavement Layer Thicknesses and Moduli by SASW Method," *Transportation Research Record* 1190, pages 133-150, 1988.
- Overby, Charles, "A Comparison between Benkelman Beam, DCP, and Clegg-Hammer measurements for Pavement Strength Evaluation," *International Symposium on Bearing Capacity of Roads and Airfields, Norway, June 23-25, 1982*, pages 138-147.
- Schmertmann, J. H., and Palacios, A., "Energy Dynamics of SPT," *Journal of the Geotechnical Engineering Division*, GT8, August 1978, pp. 909-926.
- Smith, R. B., "Cone Penetrometer and In Situ CBR Testing of an active Clay," *ISOPT-1 Orlando, Fl, 20-24 March 1988*, pp. 459-465.
- Sowers, G. F., and Hedges, C. S., "Dynamic Cone for Shallow In-Situ Penetration Testing," *Vane Shear and Cone Penetration Resistance Testing of In-Situ Soils*, ASTM STP 399, Am. Soc. Testing Mats., 1966, pp. 29-37.
- U.S. Army Engineer Waterways Experiment Station, "Dynamic Cone Penetrometer - Instruction Manual, August 1989.
- Van Heerden, M. J., and Rossouw, A. J., "An Investigation to Determine the Structural Capacity of an Airfield Pavement Using the Pavement Dynamic Cone Penetrometer," *International Symposium on Bearing Capacity of Roads and Airfields, June 23-25, 1982 Trondheim, Norway*, pp. 1092-1094.

BIOGRAPHICAL SKETCH

David Weintraub earned a Bachelor of Science in Civil Engineering degree from the United States Air Force Academy in 1986. His first assignment was at Shaw AFB, SC. The basic skills as a civil engineer were acquired while he worked as a construction manager, runway project officer and a pavements engineer. As Deputy Chief of Contract Management at Shaw AFB, he coordinated inspection of \$20 million of Air Force construction and was part of a 1988 Unit Effectiveness Inspection "Excellent Rating" for the construction management section. As runway project officer, he was responsible for the construction and inspection of a \$10 million runway reconstruction project. My responsibilities included negotiating with contractors, writing and approving modifications, and review and approval of project material submittals for technical sufficiency. In addition, he authored the first TAC Runway Construction Management and Inspection Plan which later became the standard for all construction of runways in the Tactical Air Command. Based on this and other projects, he was presented the 1989 Tactical Air Command Design Excellence Award in Construction Management by the TAC commander. As a pavements engineer he contributed to the design of a \$3 million fighter parking ramp. His design duties included calculations of ramp grades, ramp and base thickness,

and the design of joint patterns. In addition, quarterly runway construction briefings to the wing, base, and squadron commanders honed his communication skills as did two years in the Shaw AFB Toastmasters Club.

His experience also includes leading a tiger team to Saudi Arabia to maintain and repair the USCENAF ELF-ONE E-3A Command Center. With an assignment to Squadron Officer School in-residence, and then the selection to AFIT at the University of Florida, his professional and engineering qualifications were greatly enhanced. The University of Florida accepted him in their civil engineering graduate construction management program in August of 1989 where he graduated in December of 1990. He later accepted a position in their PhD geotechnical engineering program in January of 1991. His next assignment is a base level job in Guam in January of 1994 and a follow on assignment as a Civil Engineering instructor at the United States Air Force Academy in January of 1996.

His off-base leadership experience has been enhanced tremendously with extra curricular activities such as a Gainesville youth soccer coach (11-14 year olds) for six seasons, leading a bi-monthly bible study for the last three years, and assisting with University of Florida Engineering fairs.

He is married to Ellen J. Weintraub. They have one daughter, Layna Jenee, and are awaiting their next child's birth in April of 1994.

**DEVELOPMENT OF AN AUTOMATED AIRFIELD DYNAMIC CONE PENETROMETER
(AADCP) PROTOTYPE AND THE EVALUATION OF UNSURFACED AIRFIELD
SEISMIC SURVEYING USING SPECTRAL ANALYSIS OF SURFACE WAVES (SASW)
TECHNOLOGY**

By

DAVID WEINTRAUB

**A DISSEPTATION PRESENTED TO THE GRADUATE SCHOOL OF THE UNIVERSITY
OF FLORIDA IN PARTIAL FULFILLMENT OF THE REQUIREMENTS FOR THE
DEGREE OF DOCTOR OF PHILOSOPHY**

UNIVERSITY OF FLORIDA

1993

Copyright 1993

by

David Weintraub

This dissertation is dedicated to my Lord and Savior Jesus Christ, my loving wife, Ellen, and my daughter, Layna Jenee. It is also dedicated to my father, Edward Weintraub, who passed away during this work but was extremely excited to have his son in the U.S. Air Force and studying for his doctorate degree.

ACKNOWLEDGEMENTS

There are several individuals to whom I owe a tremendous amount of appreciation in developing and preparing this dissertation. It is not often that a person can be surrounded by so many skillful professionals and technicians in one place.

Wisdom, knowledge, and understanding only come from one source, God the Father. The bible says that Jesus, His son, is the way, the truth and the life and that no one comes to the Father except through Him. The bible says that if anyone lacks wisdom, he should simply ask and it will be given unto him. I thank God that when I did ask that He was faithful to supply my every need. He inspired me and gave me direction in times when all my "ideas" ran out. I simply acknowledge that all creativity, wisdom, and understanding received in this dissertation was from God who worked through many of the people mentioned below.

Dr John Davidson served as my committee chairman, my coach, and friend. He was invaluable to this research effort with words of encouragement, direction, and focus. His editorial skills greatly enhanced my ability to communicate the ideas and concepts contained in this dissertation.

Dr David Bloomquist served as my "ultimate technical advisor." His ability to analyze a problem and reach a practical conclusion was phenomenal. My gratitude is extended to him for his countless hours of brainstorming with me and for teaching me to be quick on my feet.

Dr Mike McVay served as my theoretical advisor and has been a tremendous asset to the research. His ability to teach and apply theoretical concepts has made a lasting impression on my career. I want to thank him for forcing me to think logically, stand on my own to defend a subject matter, and listen carefully to what others have to say.

Dr Brisbane Brown served as the outside member on my committee. I personally thank Dr Brown for sharing his innovative ideas and taking the time to discuss them with me. His COE experience provided a practical insight into the project that otherwise would have been missed.

Captain Mike Coats and Captain Chris Foreman served as my Air Force project coordinators and did an outstanding job. I appreciate their professional support and interest in the project that allowed me to call them at any time to deal with a problem. Not many people have that kind of support. I was fortunate to have served with them on this dissertation project.

Dr Ralph "Rugby" Ellis served as my construction management advisor and was very supportive of my efforts. He has affectionately nicknamed this work, "Project

Thumper," and has been instrumental in shaping my professional development here at the University of Florida.

Dr Paul Thompson served as the Civil Engineering Department chairman while I attended the University of Florida. I want to thank him for the time he spent with me on career development as a civil engineer and an officer in the U.S. Air Force.

Ed Dobson served as my technical advisor extraordinaire. I want to thank Ed for his patience while spending time with me teaching the basics of shop mechanics, field testing, and tool maintenance. He has instilled in me the fact that everything has its place in the shop.

Bill Studstill and the "Boyz" (Hubert, Josh, Tom, and Karl) played a major supportive role in the completion of this project. I appreciate their time and energy helping me buy, install, and tear apart literally hundreds of odd parts and pieces. It is a blessing to see what happens when people are in unity.

The Machine Shop (Dale, Karl, Hermann, Tommy, Charlie, and Bill) were great friends throughout the manufacturing process of the project. With Dale and his ability to weld and machine intricate parts, the project seemed to run smoothly. I appreciate all his efforts.

Mr Pedro Ruesta, fellow PhD student, became a great friend of mine. His positive attitude and work ethic left an indelible mark on me. I am very appreciative of his

hours of feedback and encouragement throughout the project. His geotechnical computer skills were a tremendous benefit to the project.

TABLE OF CONTENTS

	Page
ACKNOWLEDGEMENTS.....	iv
LIST OF TABLES.....	xiii
LIST OF FIGURES.....	xiv
ABSTRACT.....	xviii
 CHAPTERS	
1 INTRODUCTION.....	1
1.1 Problem Statement.....	1
1.2 Objectives.....	5
1.3 Overview.....	6
2 REVIEW OF THE LITERATURE.....	9
2.1 Introduction.....	9
2.2 Unsurfaced Airfield Trafficability.....	9
2.2.1 Introduction.....	9
2.2.2 Measurement of Soil Trafficability...	12
2.3 Carrying Capacity of Unsurfaced Airfields...	12
2.3.1 Introduction.....	12
2.3.2 Airfield Cone Penetrometer (ACP).....	16
2.3.3 Dynamic Cone Penetrometer (DCP).....	21
2.3.3.1 Introduction.....	21
2.3.3.2 DCP Description.....	22
2.3.3.3 Correlation of CBR and DCP....	22
2.3.3.4 Dynamic Cone Penetrometer Mathematical Models	36
2.3.3.5 Force Analysis of the Dynamic Cone Penetrometer.....	46
2.3.3.6 Stress Wave Propagation.....	50
2.3.3.7 Other Dynamic Cone Penetrometers.....	54
2.3.4 Aerial Penetrometers.....	56
2.4 Seismic Surveying.....	59
2.4.1 Introduction.....	59
2.4.2 Surface Wave Propagation.....	60
2.4.3 SASW Field Testing and Equipment.....	63
2.4.4 Dispersion Calculations.....	65
2.4.5 Inversion Process.....	67
2.4.6 Qualitative Estimation of Density Using the SASW Method.....	70

2.4.7	Determining Surface Layer Thickness and Modulus Values.....	72
3	DEVELOPMENT AND DESCRIPTION OF THE AUTOMATED AIRFIELD DYNAMIC CONE PENETROMETER (AADCP) EQUIPMENT.....	82
3.1	Introduction.....	82
3.2	Selection of Testing System.....	82
3.2.1	Introduction.....	82
3.2.2	System Specifications.....	83
3.2.3	Review of Current Technology.....	85
3.3	Prototype Development.....	86
3.3.1	Rod and Guide Mounted to an Air Piston.....	86
3.3.2	Rotary Hammer.....	89
3.3.3	Cam Operated Lift and Drop Mechanism.....	91
3.3.4	Chain Driven Lifting-Drop Mechanism.....	94
3.3.5	Air Piston-Spring Lift and Drop Mechanism.....	96
3.3.6	Modifications of the Basic AADCP Design.....	101
3.3.6.1	Introduction.....	101
3.3.6.2	Air Exhaustion.....	101
3.3.6.3	Spring Reaction Force.....	103
3.3.6.4	Penetrometer Rod Modifications	105
3.4	Description of the Automated Airfield Dynamic Cone Penetrometer.....	108
3.4.1	Introduction.....	108
3.4.2	Penetration System.....	112
3.4.3	Control System.....	115
3.4.4	Power System.....	116
4	DESCRIPTION OF THE SPECTRAL ANALYSIS OF SURFACE WAVE EQUIPMENT.....	118
4.1	Introduction.....	118
4.2	Digital Analyzer.....	120
4.3	Signal Receivers and Impact Source.....	125
5	FIELD TESTING AND CORRELATION OF THE AUTOMATED AIRFIELD DYNAMIC CONE PENETROMETER (DCP) WITH THE DYNAMIC CONE PENETROMETER (AADCP).....	129
5.1	Introduction.....	129
5.2	Site Locations.....	129
5.3	Manual DCP Reliability Testing.....	134
5.3.1	Test Objectives.....	134
5.3.2	Test Procedures.....	135
5.3.3	Test Results.....	137

5.3.4	Discussion of Results.....	144
5.4	Manual DCP vs AADCP Testing.....	149
5.4.1	Test Objectives.....	149
5.4.2	Correlation Test Procedures.....	150
5.4.3	Correlation Test Results.....	152
5.4.4	Discussion of Correlation Test Results.....	162
6	EVALUATION OF SEISMIC SURVEYING FIELD TESTING USING SASW TECHNIQUES.....	168
6.1	Introduction.....	168
6.2	SASW Test Objectives.....	168
6.3	SASW Test Sites.....	169
6.4	SASW Test Procedures.....	169
6.5	SASW Test Results.....	174
6.6	Discussion of SASW Results.....	183
6.6.1	Kanapaha Site.....	183
6.6.2	FDOT Test Pit #1.....	183
7	CONCLUSIONS AND RECOMMENDATIONS.....	184
7.1	Conclusions.....	184
7.2	Recommendations for Future Testing.....	188
7.2.1	Airfield Evaluation Using SASW.....	188
7.2.2	Airfield Evaluation Using Robotics...	191
7.2.3	Modifications to the AADCP.....	191
APPENDICES		
A	DCP RELIABILITY TESTING DATA.....	193
A.1	Archer Landfill Manual DCP Raw Data and CBR Estimations.....	194
A.2	Archer Landfill Average Estimated CBR Calculations.....	196
A.3	Archer Landfill Estimated CBR Profile.....	197
A.4	Archer Landfill Manual DCP Blows vs Penetration.....	198
A.5	Maguire Housing Area Manual DCP Raw Data and CBR Estimations.....	199
A.6	Maguire Housing Area Average Estimated CBR Calculations.....	200
A.7	Maguire Housing Area Estimated CBR Profile..	201
A.8	Maguire Housing Area Manual DCP Blows vs Penetration.....	202
A.9	Lake Alice Pkg Lot Manual DCP Raw Data and CBR Estimations.....	203
A.10	Lake Alice Pkg Lot Average Estimated CBR Calculations.....	205
A.11	Lake Alice Pkg Lot Estimated CBR Profile....	206

A.12	Lake Alice Pkg Lot Manual DCP Blows vs Penetration.....	207
A.13	Lake Alice Shoreline Manual DCP Raw Data and CBR Estimations.....	208
A.14	Lake Alice Shoreline Average Estimated CBR Calculations.....	209
A.15	Lake Alice Shoreline Estimated CBR Profile..	210
A.16	Lake Alice Shoreline Manual DCP Blows vs Penetration.....	211
A.17	SW 24 Ave Quarry Manual DCP Raw Data and CBR Estimations.....	212
A.18	SW 24 Ave Quarry Average Estimated CBR Calculations.....	213
A.19	SW 24 Ave Quarry Estimated CBR Profile.....	214
A.20	SW 24 Ave Quarry Manual DCP Blows vs Penetration.....	215
A.21	Newberry Farm Manual DCP Raw Data and CBR Estimations.....	216
A.22	Newberry Farm Average Estimated CBR Calculations.....	217
A.23	Newberry Farm Estimated CBR Profile.....	218
A.24	Newberry Farm Manual DCP Blows vs Penetration.....	219
B	KANAPAHA SASW TESTING SITE DATA.....	220
B.1	Kanapaha Site Locations.....	221
B.2	Kanapaha Sites 1-6 Manual DCP Raw Data and CBR Estimations.....	222
B.3	Kanapaha Sites 1-6 Average Estimated CBR Calculations.....	224
B.4	Kanapaha Sites 1-6 Estimated CBR Profile....	225
B.5	Kanapaha Sites 1-6 Manual DCP Blows vs Penetration.....	226
B.6	Kanapaha Sites 7-12 Manual DCP Raw Data and CBR Estimations.....	227
B.7	Kanapaha Sites 7-12 Average Estimated CBR Calculations.....	228
B.8	Kanapaha Sites 7-12 Estimated CBR Profile...	229
B.9	Kanapaha Sites 7-12 Manual DCP Blows vs Penetration.....	230
B.10	Kanapaha Sites 13-16 Manual DCP Raw Data and CBR Estimations.....	231
B.11	Kanapaha Sites 13-16 Average Estimated CBR Calculations.....	232
B.12	Kanapaha Sites 13-16 Estimated CBR Profile..	233
B.13	Kanapaha Sites 13-16 Manual DCP Blows vs Penetration.....	234
C	AADCP AND DCP CORRELATION TESTING.....	235
C.1	Archer Landfill Spreadsheet 1.....	236

C.2	Archer Landfill Spreadsheet 2.....	237
C.3	Archer Landfill AADCP and DCP Blow Profile..	238
C.4	Archer Landfill DCP vs Depth.....	239
C.5	Archer Landfill CBR vs Depth.....	240
C.6	Maguire Field Spreadsheet 1.....	241
C.7	Maguire Field Spreadsheet 2.....	242
C.8	Maguire Field AADCP and DCP Blow Profile....	243
C.9	Maguire Field DCP vs Depth.....	244
C.10	Maguire Field CBR vs Depth.....	245
C.11	Lake Alice Parking Lot Spreadsheet 1.....	246
C.12	Lake Alice Parking Lot Spreadsheet 2.....	247
C.13	Lake Alice Parking Lot AADCP and DCP Blow Profile.....	248
C.14	Lake Alice Parking Lot DCP vs Depth.....	249
C.15	Lake Alice Parking Lot CBR vs Depth.....	250
C.16	Lake Alice Shore Line Spreadsheet 1.....	251
C.17	Lake Alice Shore Line Spreadsheet 2.....	252
C.18	Lake Alice Shore Line AADCP and DCP Blow Profile.....	253
C.19	Lake Alice Shore Line DCP vs Depth.....	254
C.20	Lake Alice Shore Line CBR vs Depth.....	255
C.21	FDOT Test Pit #1 Spreadsheet 1.....	256
C.22	FDOT Test Pit #1 Spreadsheet 2.....	257
C.23	FDOT Test Pit #1 AADCP and DCP Blow Profile.....	258
C.24	FDOT Test Pit #1 DCP vs Depth.....	259
C.25	FDOT Test Pit #1 CBR vs Depth.....	260
D	FORCE AND ENERGY MEASUREMENT OF THE AADCP AND DCP INSTRUMENTS.....	261
D.1	Force and Energy Measurement Test Equipment and Procedures.....	262
D.2	Force and Energy Measurement Results.....	264
D.3	Discussion of Force and Energy Measurement Results.....	268
E	INSTRUCTIONAL MANUAL FOR AADCP TESTING.....	270
E.1	AADCP General Description.....	272
E.2	Penetration System.....	274
E.3	Control System.....	277
E.4	Power System.....	278
E.5	AADCP Test Procedures.....	278
	REFERENCE LIST.....	282
	SUPPLEMENTARY REFERENCES.....	286
	BIOGRAPHICAL SKETCH.....	288

LIST OF TABLES

TABLE	Page
2.1 Classification of Continuous Dynamic Penetrometers.....	23
2.2 International Comparison of the Equation $\text{Log CBR} = A - B(\text{Log DCP})^C$	27
2.3 Common CBR-DCP Relationships.....	29
2.4 Variance Coefficient Values in CBR and DCP Tests.....	37
3.1 Potential Energy Calculations of Various Strokes.....	100
5.1 Manual DCP Raw Data and CBR Estimations (Archer Landfill).....	138
5.2 Average Estimated CBR Calculations.....	143
5.3 Summary of the Standard Deviations in DCP Reliability Testing at Six Sites.....	145
5.4 Summary of the Coefficient of Variability in DCP Reliability Testing at Six Sites.....	146
5.5 CV Values of All Testing Sites.....	163
6.1 Summary of Inversion Output of Site #6.....	176
E.1 AADCP Field Testing Form.....	280
E.2 AADCP Sample Data Correlation Worksheet.....	281

LIST OF FIGURES

Figure	Page
1.1 Unsurfaced Airfield Evaluation Process.....	2
2.1 Cone Index vs Moisture Content.....	11
2.2 Design Curve for the Single Wheel Carrying Capacity of Unsurfaced Runways.....	14
2.3 Design Curve for the Dual Wheel Carrying Capacity of Unsurfaced Runways.....	14
2.4 Comparison of Design Curves for the Carrying Capacity of Unsurced Runways for the C-130E.....	15
2.5 Airfield Cone Penetrometer.....	17
2.6 CBR vs Airfield Index.....	19
2.7 Dynamic Cone Penetrometer.....	24
2.8 Blows vs Penetration.....	25
2.9 Log Plot of CBR-DCP Relationship.....	30
2.10 Assumed Failure Plane Below CBR Plunger.....	32
2.11 Effect of Mold Size on CBR.....	33
2.12 Field CBR Equipment Assembled.....	35
2.13 Comparison of Predicted and Measured Cone Index for Clay Using Cavity Expansion Theory.....	43
2.14 Comparison of Predicted and Measured Cone Index for Mixed Using Cavity Expansion Theory.....	44
2.15 Comparison of Predicted and Measured Cone Index for Yuma Sand Using Cavity Expansion Theory	45
2.16 Failure Surface Observed with Wedge Penetration..	47
2.17 Comparison of Measured vs Predicted Friction Angle Using Plastic Failure Model.....	48
2.18 Dynamic Cone Penetrometer with Accelerometer Mounted to the Handle.....	49

2.19 Acceleration, Velocity, and Displacement Time Histories of DCP in Medium Stiff Granular Base Course Material.....	51
2.20 Calculated Force-Time History of the DCP in Granular Base Course Material.....	52
2.21 Aerial Penetrometer.....	57
2.22 Approximated Distribution of Vertical Particle Motion with Depth of Two Wavelengths.....	62
2.23 Configuration of SASW Equipment.....	64
2.24 Phase and Coherence Spectra.....	66
2.25 Composite Dispersion Curve.....	70
2.26 Final Shear Wave Velocity Profile.....	71
2.27 Qualitative Estimation of Densities Using Insitu and Empirical Shear Wave Velocities.....	73
2.28 Dispersion Curve for Rayleigh Waves Propagating in a Uniform Half-space.....	74
2.29 Dispersion Curve for Rayleigh Waves Propagating in a Softer Layer Over a Stiffer Half-space.....	76
2.30 Dispersion Curve for Rayleigh Waves Propagating in a Stiffer Layer Over a Softer Half-space.....	77
2.31 Determination of the Surface Layer Thickness from the Dispersion Curve for Rayleigh Waves.....	78
2.32 Dispersion Curve used to Determine Top Layer Thickness and Young's Modulus.....	79
2.33 Dispersion Curve used to Determine Top Layer Thickness and Young's Modulus.....	80
3.1 Rod and Guide Mounted to an Air Piston.....	87
3.2 Rotary Hammer.....	90
3.3 Cam Operated Lift and Drop Mechanism.....	93
3.4 Chain Driven Lifting-Drop Mechanism.....	95
3.5 Air Piston-Spring Lift and Drop Mechanism.....	97

3.6	Automated Air Piston-Spring Lift and Drop Mechanism.....	98
3.7	One-Way Gripper.....	104
3.8	Modified Solid Penetration Rod with Decoupling of Instrument and Penetration Rod.....	107
3.9	General View of the Automated Airfield Dynamic Cone Penetrometer.....	109
3.10	General Flow of AADCP Operation.....	110
3.11	Air Cylinder, Piston and Compression Spring.....	113
3.12	Quick Exhaust Valve.....	114
4.1	Source-Receiver Configuration of SASW Equipment..	119
4.2	HP 35665 Dual Channel Dynamic Signal Analyzer....	121
4.3	Complex Signal in Time and Frequency Domain.....	122
4.4	Phase of the Cross Power Spectrum and the Coherence Function.....	124
4.5	Receiver Spacing Arrangements for SASW Testing...	126
4.6	Manual DCP used as Impact Source for SASW Testing	127
5.1	Geographic Locations of Field Testing Sites.....	130
5.2	UF Campus Testing Sites.....	131
5.3	Off Campus Testing Sites.....	132
5.4	Soil Classification Site Summary.....	133
5.5	DCP Reliability Test Configuration.....	136
5.6	Manual DCP Blows vs Penetration Archer Landfill.....	141
5.7	Estimated CBR Profile Archer Landfill.....	142
5.8	DCP-AADCP Correlation Test Configuration.....	151
5.9	Sand and Silty-Sand Arithmetic Correlation of DCP and AADCP Instruments.....	153

5.10 Sand Arithmetic Correlation of DCP and AADCP Instruments.....	154
5.11 Silty-Sand Arithmetic Correlation of DCP and AADCP Instruments.....	155
5.12 Penetration Index from AADCP and DCP Instruments (Maguire Field).....	157
5.13 Number of Blows Versus Depth of AADCP and DCP Test Instruments at Maguire Field.....	158
5.14 AADCP and DCP Estimations of CBR Versus Depth (Maguire Field).....	159
5.15 Number of Blows Versus Depth Using Two Different Blow Rates at Maguire Field.....	160
6.1 Kanapaha Boring Log for SPT-3 near site #16.....	170
6.2 FDOT Test Pit #1 RAP Profile.....	171
6.3 Manual DCP Blow Profile of Site #6.....	175
6.4 Site #6 Field and Theoretical Dispersion Curves..	178
6.5 Shear Wave Velocity Profile of Site #6.....	179
6.6 Maximum Shear Modulus Profile of Site #6.....	180
6.7 Maximum Young's Modulus Profile of Site #6.....	181
6.8 FDOT Test Pit #1 Dispersion Curve RAP Material...	182
7.1 Proposed Seismic Surveying Configuration.....	189
7.2 Cumulative Dispersion Curves Over Several Survey Stations.....	190
D.1 Force Measurement Equipment.....	263
D.2 Velocity-Time Plot.....	265
D.3 Force-Time Plot.....	266
D.4 Energy-Time Plot.....	267
E.1 General Flow of AADCP Operation.....	273
E.2 Quick Exhaust Valve.....	276

**Abstract of Dissertation Presented to the Graduate School of
the University of Florida in Partial Fulfillment of the
Requirements for the Degree of Doctor of Philosophy**

**DEVELOPMENT OF AN AUTOMATED AIRFIELD DYNAMIC CONE
PENETROMETER (AADCP) PROTOTYPE AND THE EVALUATION OF
UNSURFACED AIRFIELD SEISMIC SURVEYING USING SPECTRAL
ANALYSIS OF SURFACE WAVES (SASW) TECHNOLOGY**

By

David Weintraub

December 1993

**Chairperson: John L. Davidson
Major Department: Civil Engineering**

The mission of U.S. Air Force Combat Controllers is to infiltrate unused airfields in enemy-controlled territory, access and report conditions, and control the airdrop for the entrance of the main army force. Once the airfield is secure, a specially trained evaluation team, carrying limited portable testing equipment, evaluates the unsurfaced airfield for possible use as a landing zone. The equipment used to evaluate the bearing capacity of the airfield is the Dynamic Cone Penetrometer (DCP). Empirically based relationships are used to predict the type and number of aircraft passes on the unsurfaced airfield based on inputs from the DCP.

It was the goal of this research to improve on the field testing equipment used in the unsurfaced airfield evaluation process. The specific objectives were (a) to

develop prototype airfield bearing test equipment that is less labor intensive than the currently used Dynamic Cone Penetrometer (DCP), while still providing accurate bearing capacity data, and (b) evaluate Spectral Analysis of Surface Wave (SASW) technology as a means of seismically surveying unsurfaced runways and aprons.

An Automated Airfield Dynamic Cone Penetrometer (AADCP) prototype was developed to measure unsurfaced airfield bearing. Using correlations with the manual DCP and DCP-CBR relationships established in the literature, the AADCP can predict airfield bearing strengths. The AADCP was shown to be inherently less labor intensive than the manual DCP due to its pneumatic operation. Though the AADCP is not field-ready due to weight and power restrictions, it is a viable prototype which can be modified to meet field conditions. In addition, SASW surveying techniques were successfully used to qualitatively detect soft layers at a soil site and a surveying technique was recommended to qualitatively compare profiles of an unsurfaced airfield.

CHAPTER 1

INTRODUCTION

1.1 Problem Statement

One of the greatest attributes of a modern air force is its ability to go anywhere, at any time, with the utmost speed. In the last decade, the United States Air Force has carried out this doctrine with tremendous skill. From Grenada in 1981 to Panama in 1985 to the recent Operation Desert Shield in 1991, our air force has shown that with proper training, equipment and leadership "quick reaction strike forces" can do the job.

In support of these strike forces is a team known as the Combat Control Team (CCT). The mission of U.S. Air Force Combat Control Team is to infiltrate unused airfields in enemy-controlled territory without being detected, access and report airfield conditions, and control the airdrop for the entrance of a main army force (MACP 50-5 1989). The airfield conditions are assessed by specially trained CCT runway evaluation teams, carrying limited portable testing equipment. Field test results are used as input data in empirically based models which predict the bearing strength of the unsurfaced runway and the type and number of allowable aircraft takeoffs and landings. Figure 1.1 is a

<u>DESCRIPTION</u>	<u>PAST AND PRESENT METHODS</u>
<u>PHASE I</u>	
RAW AIRFIELD DATA OBTAINED USING FIELD EQUIPMENT	FIELD CBR KIT ACP DCP
<u>PHASE II</u>	
FIELD DATA ENTERED INTO CBR-DCP EMPIRICAL MODEL TO OBTAIN CBR	KLEYN 1975 LIVNEH 1987 HARISON 1989 WEBSTER et al. 1992
<u>PHASE III</u>	
ESTIMATED CBR ENTERED INTO EMPIRICAL MODEL USED TO PREDICT NUMBER OF AIRCRAFT TAKEOFF AND LANDINGS	TURNBULL et al. 1961 LADD & ULERY 1967 HAMMITT 1970

Figure 1.1 Unsurfaced Airfield Evaluation Process

basic outline which describes the unsurfaced airfield evaluation process. The U.S. Air Force has primarily used two different portable penetrometer devices to evaluate the bearing strength of the landing sites in the last decade. They are the Airfield Cone Penetrometer (ACP) and the Dynamic Cone Penetrometer (DCP).

The Airfield Cone Penetrometer (ACP) was first used in this capacity in the early 1960s. This device uses a rod-cone assembly that is pushed into the ground by hand. The ACP measures the cone resistance using a spring loaded mechanism to a depth of about 24 inches but can penetrate deeper if necessary. However, the ACP penetration is limited by the vertical force which a CCT member can provide. At times, the CCT member is forced to hand auger through a stiff layer near the surface and then continue the ACP testing to the final test depth, usually 24 inches. In August of 1986, a C-130 aircraft punched through an unsurfaced landing zone which had been previously approved by a Combat Control Team (CCT) using the ACP as its evaluation device. Although there were several reasons for the punch-through, the two of most importance were the inability of the CCT member to penetrate the full 24 inches using the ACP device and the limited number of tests due to time constraints placed on the CCT members. It was later discovered that "the failed area was marked by a color change from the intact portion of the airfield. The color

change occurred when the airfield constructors placed a strong, lightweight, porous gravel over weak silt material to provide strength for their aircraft. Penetrometer measurements to a depth of 24 inches in 6 inch intervals would have revealed the problem (soft layer)" (Brown, personal communication). Since this incident, the Air Force has searched for alternative field equipment to measure bearing capacity of a landing zone. Today the state-of-the-art equipment used by the U.S.A.F. to evaluate the bearing capacity of the airfield is the Dynamic Cone Penetrometer (DCP).

The Dynamic Cone Penetrometer is a relatively lightweight, mobile testing device. It consists of a 17.6 pound sliding weight hand raised 22.6 inches and released to strike an anvil-rod-cone assembly. This energy drives the attached 39.4 inch rod into the ground. The cone is 0.79 inches in diameter and has a 60 degree cone apex. The number of inches per blow is defined as the DCP index value and is a measure of bearing strength. It is used in the correlations to estimate the number of safe takeoffs and landings of the unsurfaced airfield.

The DCP has been used by the Air Force successfully for the past six years. However, it does have some drawbacks. In an interview with the Combat Control School Instructors and with a former AFESC Pavement Evaluation Team Chief, the test is described as extremely labor intensive. Current

procedures provide for testing at 200 foot stations along 15 foot offsets of the centerline on the airfield. With such few data locations tested, under strict time constraints, it is feasible that the CCT members will leave the airfield without a full picture of its bearing strength. The U.S. Air Force therefore has requested that research be conducted to address the problems of field testing of unsurfaced airfields.

1.2 Objectives

To improve the technology in evaluations of unsurfaced airfields, a large research effort has been undertaken by HQ AFCESA/RACO. The major thrust of the U.S.A.F research was awarded in the late 1980's to Technion Israel Institute of Technology - Transportation Research Institute (TRI). TRI's goal is to improve the technology of evaluating and predicting the carrying capacity of unsurfaced airfields. They have emphasized the accuracy of the correlations used to predict the number of takeoff and landings and are presently including aircraft braking and turning stresses into the unsurfaced airfield evaluation process. Essentially, the Israeli effort is to update the second and third phases shown in Figure 1.1 using modern testing techniques and practices.

It is the general goal of this research to improve on the first phase of the unsurfaced airfield evaluation

process. In January of 1991, HQ AFCEA/RACO at Tyndall AFB, requested that a research effort be undertaken to propose new methodologies to evaluate bearing capacity of unsurfaced airfields. The following are specific objectives of this research effort:

(a) investigate the development of an unsurfaced airfield prototype device that is less labor intensive than the currently used Dynamic Cone Penetrometer (DCP) data.

(b) evaluate the Spectral Analysis of Surface Wave (SASW) technology as a means of assessing subsurface spatial variations throughout the unsurfaced runway and apron.

1.3 Overview

This dissertation has been divided into seven chapters. The first chapter defines the purpose and objectives of the research. The second chapter presents the reader with a literature review of past and present U.S.A.F. methods to evaluate carrying capacity of unsurfaced airfields. This chapter also presents an introduction to Spectral Analysis of Surface Wave (SASW) technology and its use in the seismic evaluation of soil sites.

The third chapter discusses the major phases of the AADCP prototype development and describes the final version of the AADCP in detail. The chapter begins with the rationale used to select the evaluation system, citing the various advantages and disadvantages of the available

systems. The chapter then introduces the several prototypes developed, in chronological order, leading up to the final AADCP design. Each prototype is discussed in detail and it is shown how the final version evolved from it. The chapter concludes with a detailed description of the final AADCP equipment, including the penetration device with its auxiliary equipment.

The fourth chapter concentrates on describing the equipment used in this research to accomplish the SASW test evaluation. It includes a discussion on the digital signal analyzer, signal receivers, and noise sources. The SASW evaluation was accomplished with equipment purchased by the Florida DOT (Gainesville Office). The fifth chapter describes the testing procedure and presents and discusses the results of field testing for the Automated Airfield Dynamic Cone (AADCP) prototype. This chapter presents and discusses the DCP field repeatability and DCP and AADCP prototype correlation testing.

The sixth chapter details the testing procedure for the evaluation of seismically surveying an unsurfaced airfield using the spectral analysis of surface wave (SASW) technology. It discusses the site locations where the evaluations took place, the testing procedures and test results.

Chapter seven presents the research conclusions and recommends a new methodology to evaluate unsurfaced

airfields. Several areas of future study are also discussed. There are five appendixes that contain the field data of the DCP reliability testing, SASW Kanapaha testing results, AADCP-DCP correlation results, force measurement results and AADCP instruction manual.

CHAPTER 2

REVIEW OF THE LITERATURE

2.1 Introduction

The purpose of this chapter is to provide the reader a background on past and present methods used by the U.S. Air Force to evaluate carrying capacity of unsurfaced airfields. In addition, this chapter presents an introduction to Spectral Analysis of Surface Wave (SASW) technology and its use in seismic evaluation of soil sites. The literature review begins with a discussion on unsurfaced airfield trafficability.

2.2 Unsurfaced Airfield Trafficability

2.2.1 Introduction

Trafficability of an airfield is determined by the shearing strength of the soil surface and subsurface and somewhat by the stickiness and slipperiness of the surface (Molineux 1955). In the event that shear strength is exceeded by an aircraft load, the surface fails and puts the aircraft at risk of immobility. In addition, once the surface has failed (formed a rut), the aircraft must overcome tremendous rolling resistance forces which put the aircraft in jeopardy of flight.

Unfortunately, it is impossible to label a particular area with a single trafficability rating over an extended period of time. Since trafficability, bearing and traction are based primarily on shearing strength, they are, like the strength, dependent on time, weather, and location. A few cycles of traffic can usually be sustained on dry soils. However, if moisture is added the shearing strength can be significantly decreased. The magnitude of this effect depends on the soil type. Generally fine-grained soils (silts and clays) will be more effected than coarse-grained soils (sands). Figure 2.1 shows the effects of moisture on the shearing strength of three fine-grained soils. The cone index is defined as the stress (force over area) required to penetrate a certain depth. Notice in Figure 2.1 that as the moisture content increases, the cone index decreases.

It is not an easy task to measure the trafficability of an airfield because there are so many changing variables involved in the process. This leads to the conclusion that a precise theoretical solution is virtually impossible. All the correlative studies performed on unsurfaced airfield evaluation techniques have been empirical in nature. The next section describes some of this work.

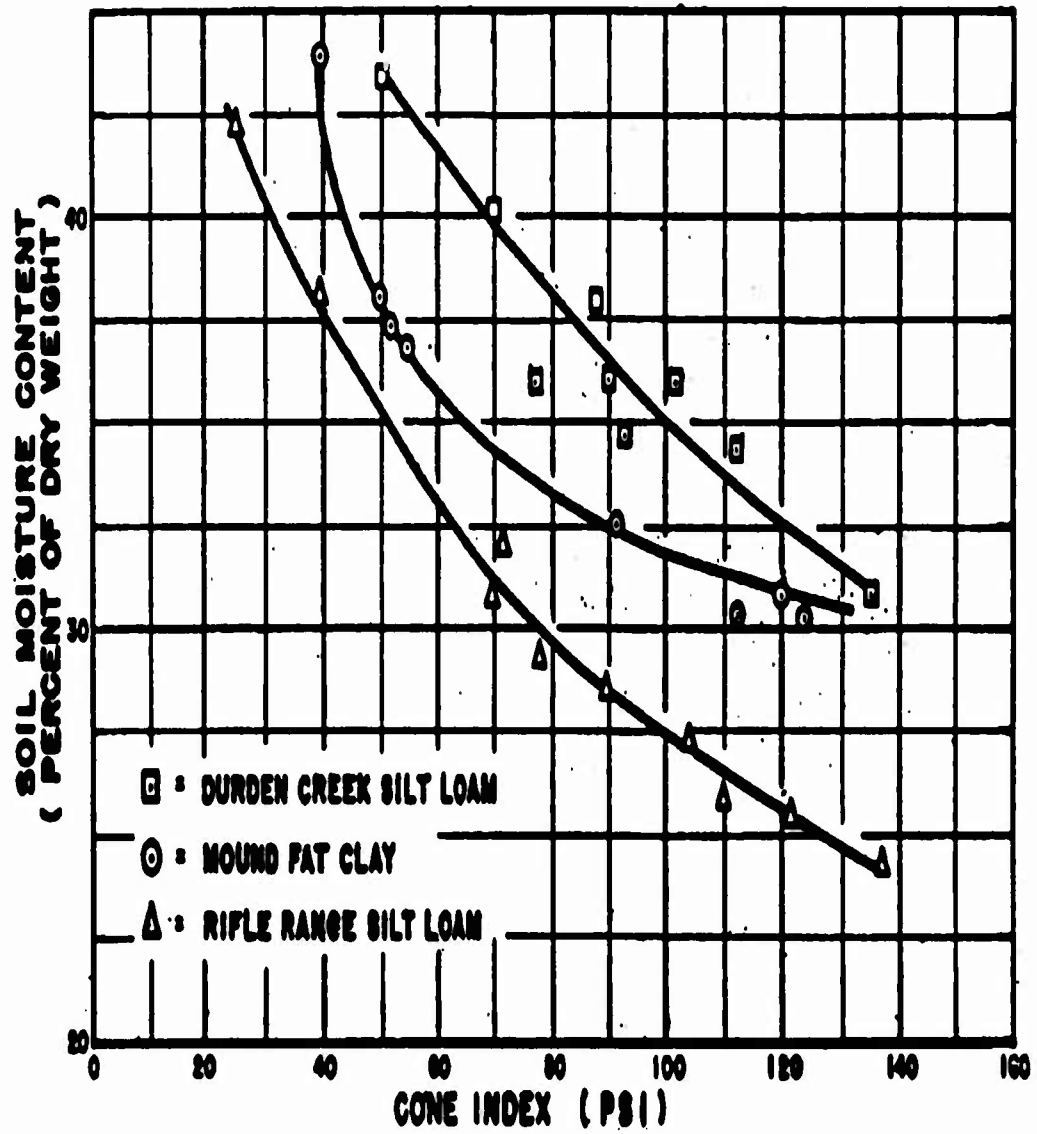


Figure 2.1 Cone Index vs Moisture Content
(Molineux 1955)

2.2.2 Measurement of Soil Trafficability

Since the late 1940's, the U.S. Air Force has sought after unique methods to rapidly determine the trafficability of aircraft on all types of soils. A direct means of soil trafficability measurement is required for the safe landing of military aircraft. Many methods have been used by the Air Force to determine insitu soil bearing strengths. The two most popular have been the Sub-grade Modulus method and the California Bearing Ratio method. However, these field testing methods require an extensive amount of time and equipment and are thus not applicable to a fast pace war-time environment. A number of simpler and less time consuming methods have been developed and tested over the last 40 to 50 years as discussed in the next section.

2.3 Carrying Capacity of Unsurfaced Airfields

2.3.1 Introduction

In the early 1960's, the U.S. Army conducted tests in an effort to determine the factors which effect the carrying capacity of an unsurfaced airfield (Turnbull et al. 1961). The study concluded that capacities should be based on the number of coverages of an aircraft to failure. Failure was defined as 1.5 inches of elastic deformation and 4 inches of plastic deformation. The study also concluded that the subgrade CBR averaged over various depths, the aircraft's equivalent single wheel load and the aircraft's tire

pressure were the factors which effect the number of coverages to failure. Correlations were then developed by using weighted carts, with specific tire pressures and aircraft loads, building low, medium and high CBR test sections, and measuring the number of passes to failure. Figures 2.2 and 2.3 display some of the results of this landmark study. Figure 2.2 shows that an aircraft with a tire pressure of 60 psi and a 30-kip single wheel load can operate 10 passes on an unsurfaced airfield with a CBR of 6.6.

Since the original 1961 study, several correlation studies have been completed. Moshe Livneh (Israeli Institute of Technology), in his 1989 draft report on "Carrying Capacity of Unsurfaced Runways for Low Volume Aircraft Traffic," compares several different design curves used to estimate the number of aircraft passes allowable for a C-130E Hercules aircraft. Figure 2.4 is a collection of design curves gathered in Livneh's research. Linveh points out that the selection of a design curve is very critical to the outcome of the design. For example, in Figure 2.4, the selection of a CBR of 6 with a 125 kip load reveals the number of passes to be 1.5, 6, or 90. It is one of the goals of Livneh's research to verify and update these designs curves so as to possibly close the gap in allowable aircraft passes.

The following sections, 2.3.2 and 2.3.3, describe in

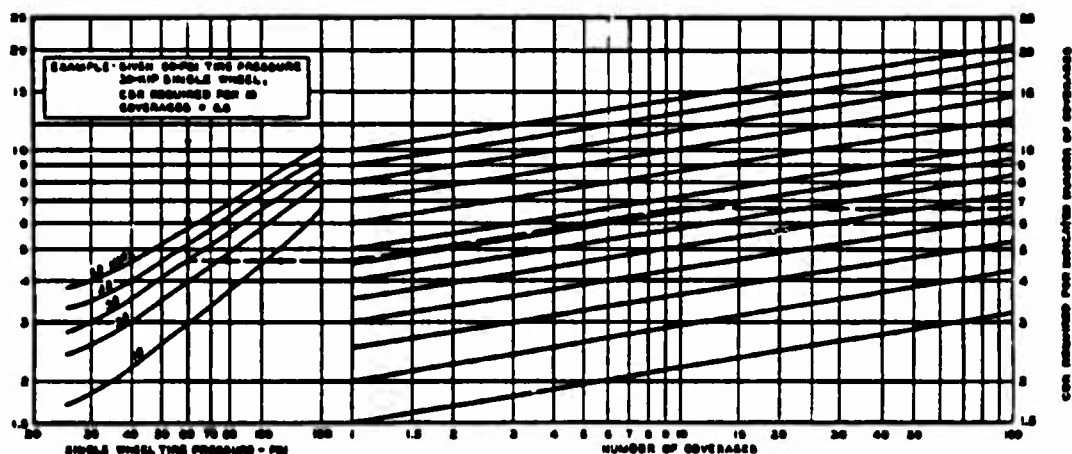


Figure 2.2 Design Curve For The Single Wheel Carrying Capacity of Unsurfaced Runways (Turnbull et al. 1961)

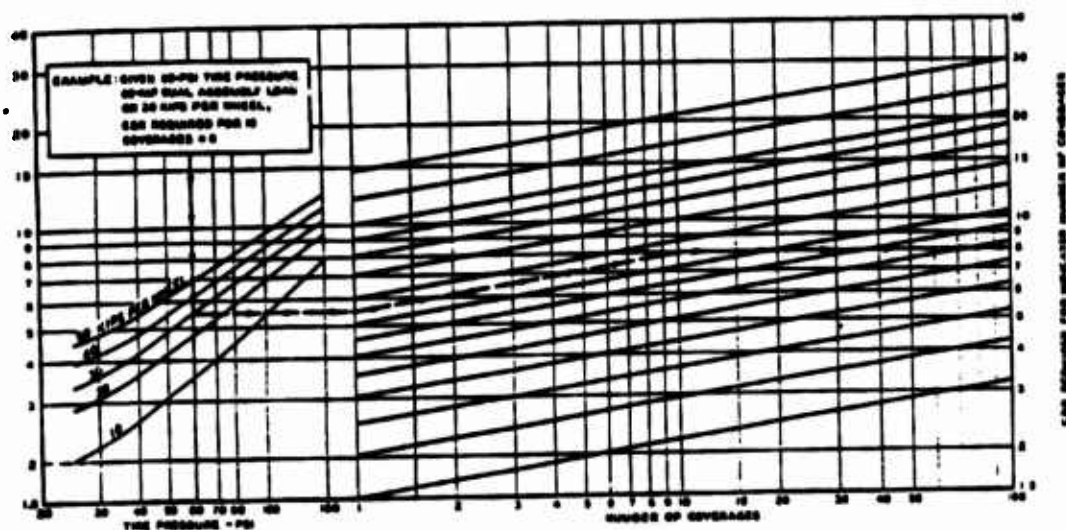
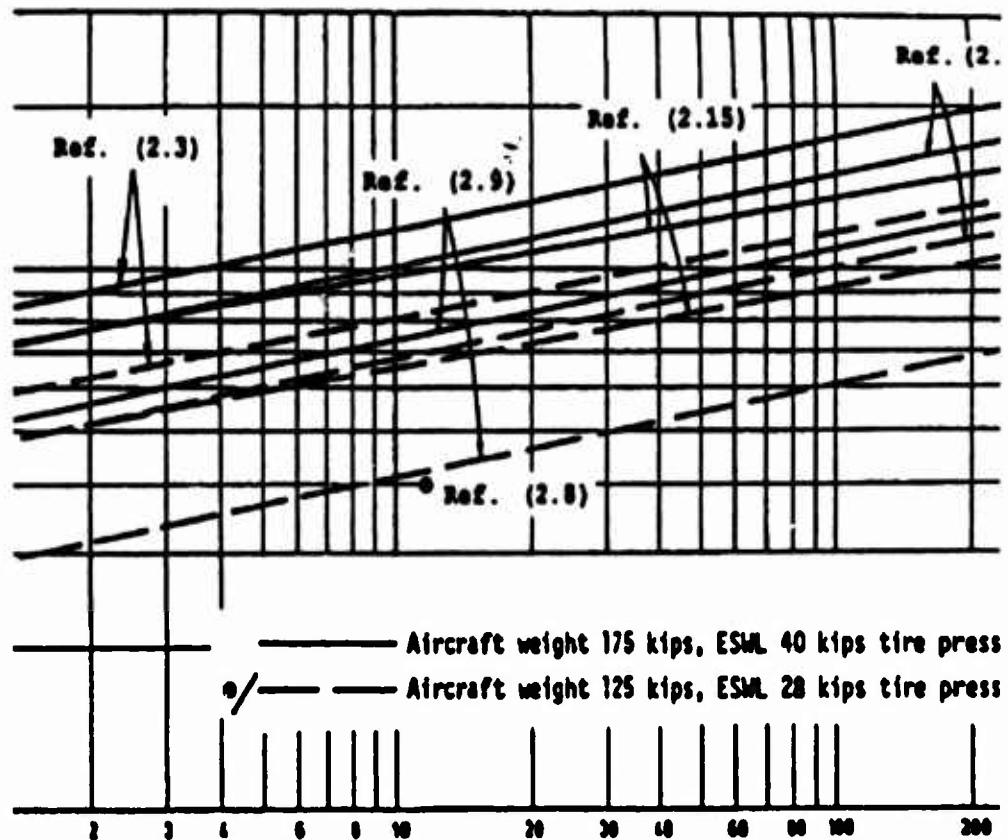


Figure 2.3 Design Curve For The Dual Wheel Carrying Capacity of Unsurfaced Runways (Turnbull et al. 1961)



Reference

2.3
2.5
2.8
2.9
2.15

Author

Turnbull et al. 1961
Womack 1965
Ladd 1965
Ladd 1967
Brabston et al. 1974

Figure 2.4 Comparison of Design Curves For The Carrying Capacity of Unsurfaced Runways For a C-130E (Livneh and Ishai 1989)

detail the two most popular portable insitu test methods used by the U.S. Air Force to measure the bearing strength of unsurfaced airfields. They are the Airfield Cone Penetrometer (ACP) and the Dynamic Cone Penetrometer (DCP). The measured field bearing strength is then correlated with the California Bearing Ratio (CBR) test to allow the CCT member to enter the design nomograph and determine a number of passes. These descriptions will include background information on each instrument and include the major advantages and disadvantages.

2.3.2 Airfield Cone Penetrometer (ACP)

The Airfield Cone Penetrometer, Figure 2.5, was designed to measure the bearing capacity of soils which support the operations of aircraft as well as vehicles. The ACP provides an investigator a soil index called the Airfield Index (AI). This is a measure of the bearing capacity of the soil tested and then is correlated with the California Bearing Ratio (CBR). The ACP is a hand-probe type instrument and consists of a 30 degree right circular cone with a base diameter of 1/2 inch and 48 inch long, 3/8 inch diameter rods. A housing near the top of the ACP contains an intertwined tension spring and a load indicator that directly reads the Airfield Index when the load is applied. The penetration rate is approximately one inch per second and readings are taken at two inch increments.

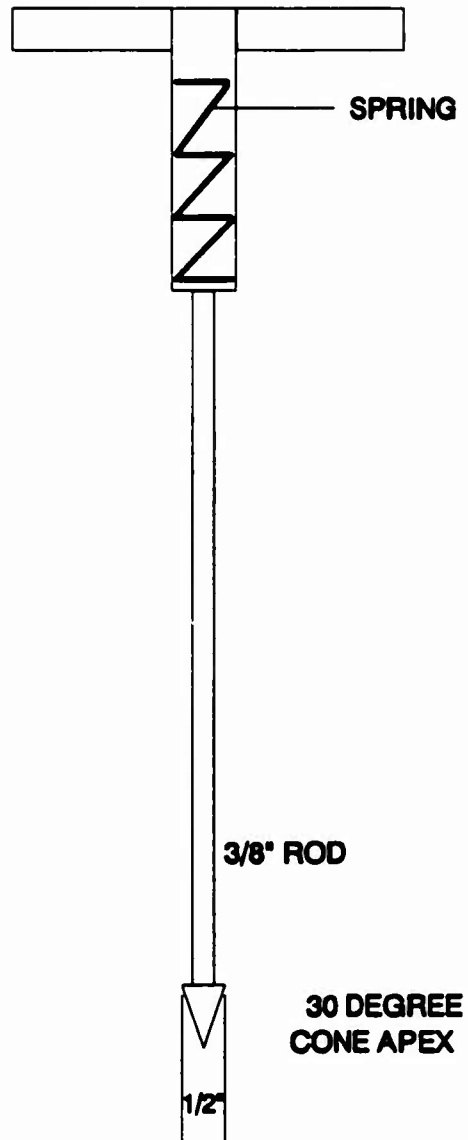


Figure 2.5 Airfield Cone Penetrometer

Five penetrations at each location in an "X" configuration are made with a depth of penetration of at least 24 inches. Figure 2.6 shows correlations of AI vs CBR for various soil types (Fenwick 1965). The long-dash dark line in this figure represents the currently used relationship. It applies to both cohesive and granular soils and has the equation:

$$\log \text{CBR} = -0.22 + 1.10 (\log \text{AI} + 0.13) \quad (2.1)$$

The ACP was used by the Air Force to measure bearing capacity from the mid-1950s to the mid-1980s. However, the device had a number of limitations. The first limitation relates to the correlation of the AI and CBR values. Livneh and Ishai (1989) made a study of the confidence intervals in these correlations. The confidence interval is used to determine the probability that the stated correlation is within a certain range of results. If a normally distributed population is assumed, a 95% confidence interval is equal to $\pm \text{Log } 2.7$. This in essence means for a predicted value of Y, the range is between $2.7(Y)$ and $(Y)/2.7$. Therefore, if a 10 CBR is predicted by the ACP, there is a 95% probability that the actual CBR value is within the range 3 to 40. Such a range corresponds to a number of aircraft passes somewhere between zero and one thousand. Obviously, this wide margin is not acceptable. Livneh and Ishai (1989) conclude that the ACP method of estimating field CBR values was liable to

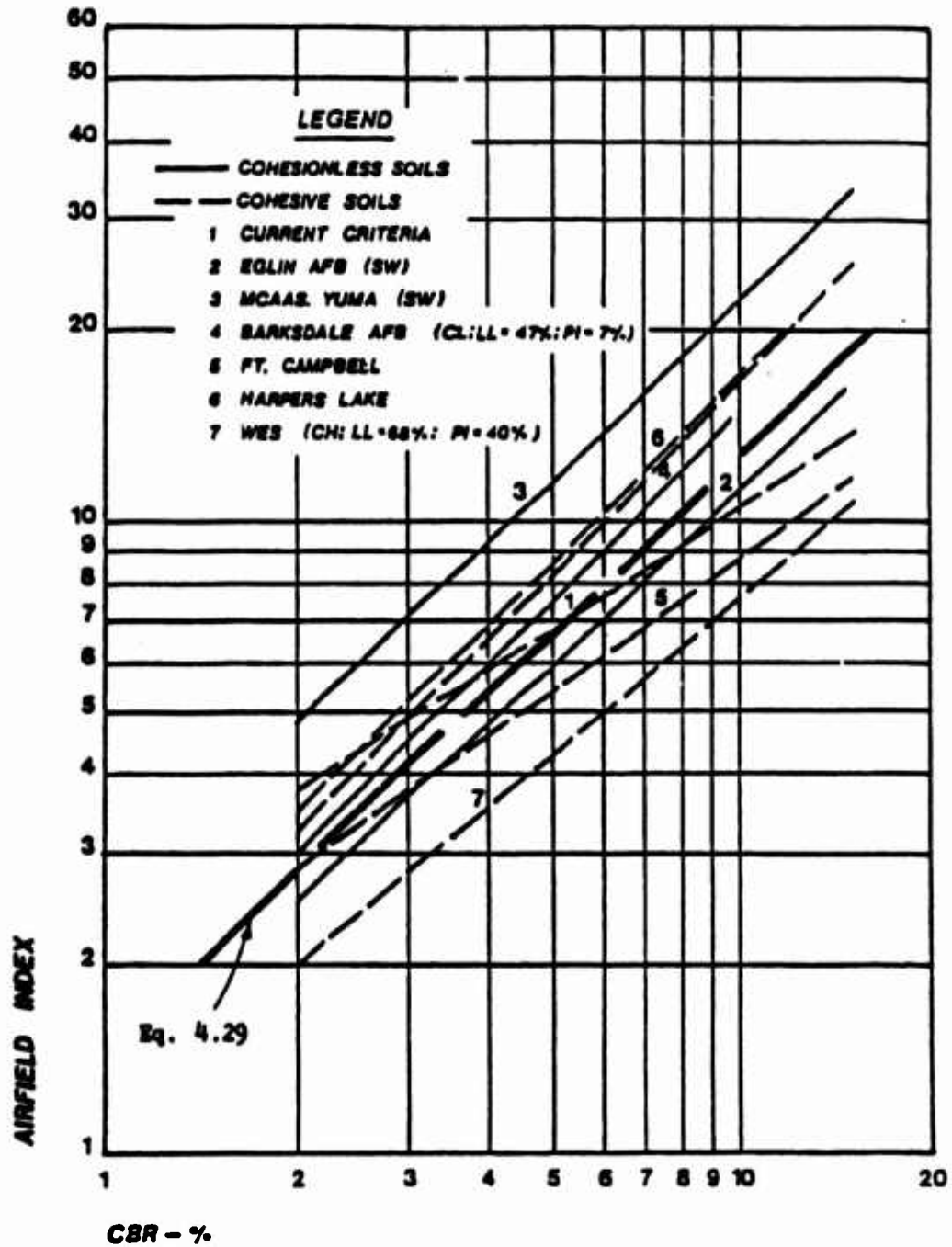


Figure 2.6 CBR vs Airfield Index
(Fenwick 1965)

significantly mislead when used to determine a predicted coverage value.

A second limitation of the ACP was in the accuracy of the values on the nomographs which were compiled more than 40 years ago using outdated aircraft tire configurations. In addition, the nomographs do not take into account the braking, turning and thrust stresses that are applied by modern aircraft.

A third limitation concerns the CBR range of the ACP which is from zero to 15. This means that the ACP cannot cover the entire range of normal unsurfaced airfield values which is between CBR values of 3 to 30. This last limitation is somewhat the culprit in the 1986 Operation Blast Furnace accident where it was found that the ACP could not penetrate through a stiff layer of material overlaying a soft clay. Although, there were other reasons for the punch through of the landing gear, the inability of the ACP to penetrate a stiff layer was high on the list (Brown 1986).

In an effort to overcome these limitations, the U.S. Air Force switched in the mid 1980's to the Dynamic Cone Penetrometer (DCP) to measure carrying capacity of unsurfaced airfields. In addition, the Technion-Israel Institute of Technology Transportation Research Institute was contracted by the U.S. Air Force to improve the technology of predicting the carrying capacity of contingency and forward unsurfaced runways by means which

ensure a high degree of reliability. The objectives included (Livneh and Ishai 1989)

(a) development of an improved design nomograph correlated with operational landings of C-130E aircraft and simulation of other aircraft using large scale wheel-track testing and mobility number;

(b) development of a carrying capacity model which includes effects of remolding characteristics of soil, braking, reverse thrust and turning operations; and

(c) application of Dynamic Cone Penetrometer (DCP) technology to accurately determine soil strength in the field.

2.3.3 Dynamic Cone Penetrometer (DCP)

2.3.3.1 Introduction

In the last seven years, the U.S. Air Force has adopted the Dynamic Cone Penetrometer as the preferred light-weight bearing capacity testing device. In general, the advantages of the DCP are its cheapness, simplicity and capability of providing rapid measurement of insitu strength of subgrades in a non-destructible manner (Harison 1989). The original DCP developed by Scala in 1956 was used to evaluate the insitu CBR of cohesive soils (Scala 1956). Today, the DCP has become a part of a much larger family of dynamic cones which are used to estimate properties of soils and in the design of both shallow and pile foundations (Melzer and

Smoltczyk 1982). Penetrometers used for continuous dynamic testing were divided into four basic categories depending on the size of the hammer dropped. Table 2.1 shows the arbitrary classifications of the four categories. The DCP used by the Air Force falls into the "DPL" or light category since it has an 8 kg hammer.

2.3.3.2 DCP Description

The DCP, adopted by the U.S. Air Force, consists of a 16 mm diameter steel rod with a cone at one end driven by an attached falling weight at the other end, Figure 2.7. The angle of the cone is 60 degrees and the base diameter is 20 mm. The additional 4 mm on the cone was designed to prevent resistance to penetration along the 16 mm steel rod. The DCP uses a sliding 8 kg hammer falling 575 mm to drive the cone to a depth of up to 1 meter. Two people are required to operate the DCP. One person lifts and drops the weight while the other measures the depth of penetration. During the test, a plot of the number of blows versus depth is recorded, Figure 2.8. The number of inches per blow is defined as the DCP value. This value is then also used to correlate the DCP test to the CBR test.

2.3.3.3 Correlation of CBR and DCP

In Section 2.3.1, a discussion was presented concerning the variables which effect the carrying capacity of an

Table 2.1 Classification of Continuous Dynamic Cone Penetrometers (Melzer and Smoltczyk 1982)

TYPE	ABBREVIATION	MASS (KG)
LIGHT	DPL	≤ 10
MEDIUM	DPM	10 - 40
HEAVY	DPH	40 - 60
SUPER HEAVY	DPSH	> 60

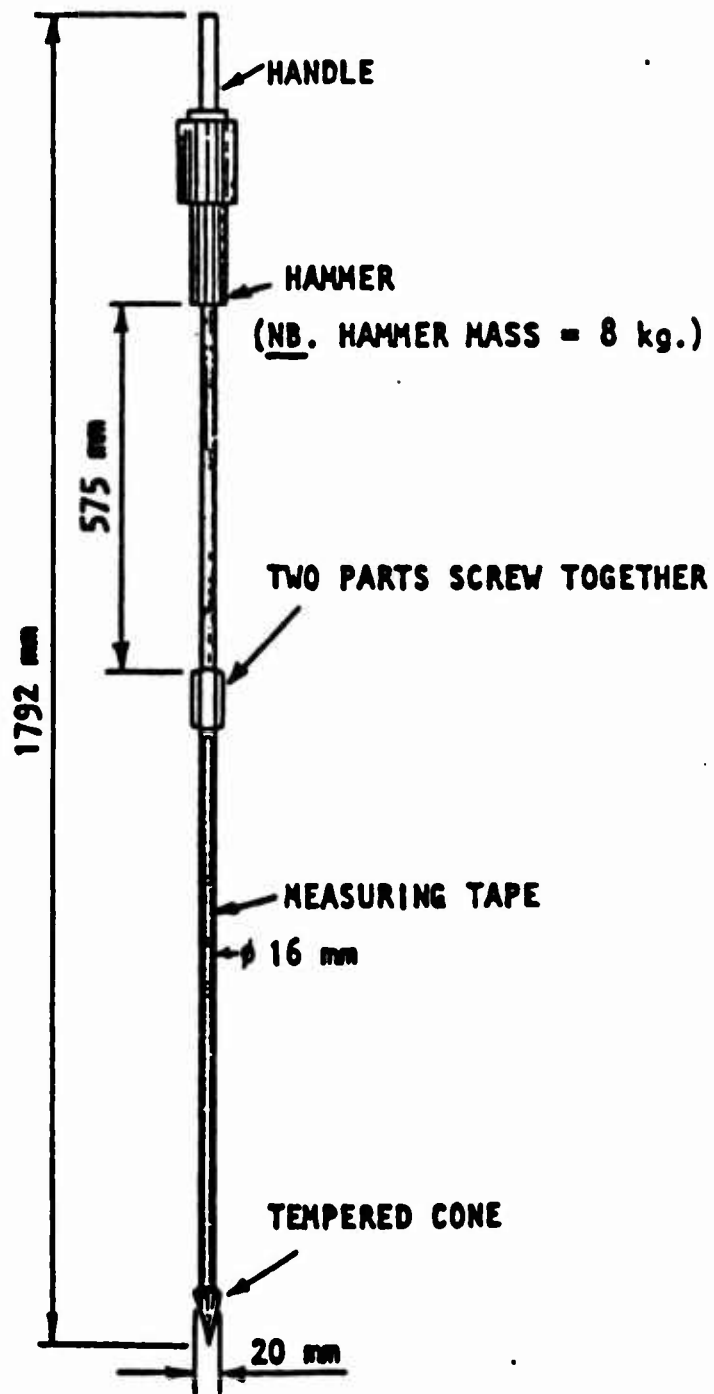


Figure 2.7 Dynamic Cone Penetrometer

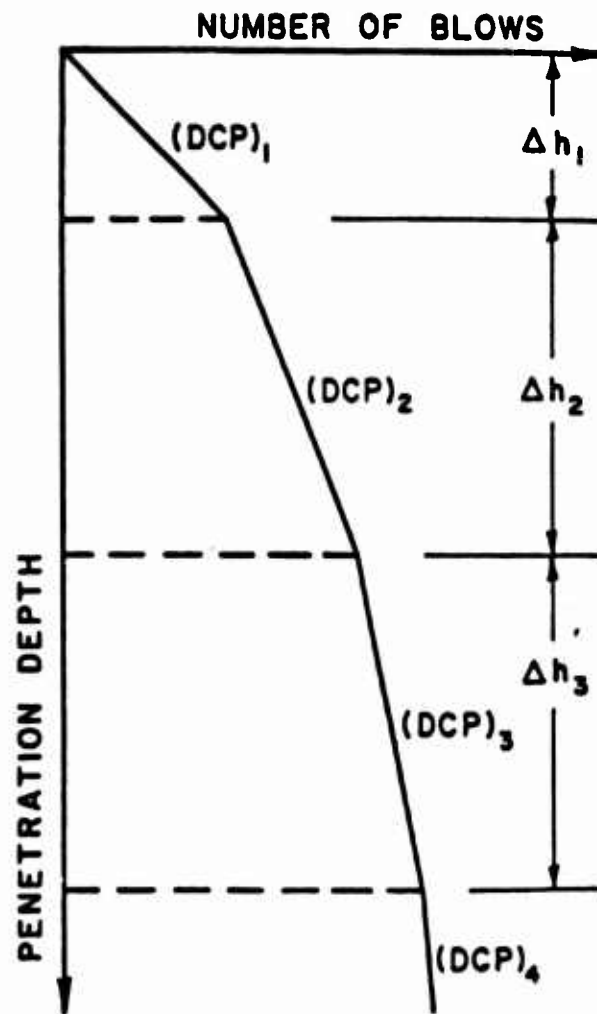


Figure 2.8 Blows vs Penetration

unsurfaced runway. One of those factors was the bearing capacity of the airfield as measured by the California Bearing Ratio (CBR) test. This test, developed by the California Division of Highways and later adopted by the U.S. Corps of Engineers, was the most widely known strength test used in the 1950's. The test involves using a standard piston to penetrate a specimen inside a mold in the laboratory after soaking 1 days. The load at 0.1 or 0.2 inches of penetration is compared to the load required to penetrate a standard specimen at the same depth. This ratio is known as the California Bearing ratio. Later this test was adapted into a corresponding field test. The same piston dimensions were used and insitu bearing measured at different depths. However, in the field, reaction frames were required for the piston to push against. Often the mass of a large truck was used for this reaction. Because of the unique combat control mission where timing, secretiveness and mobility were paramount, large reaction frames could not be used. Therefore, Airfield Cone Penetrometers and Dynamic Cone Penetrometers were used to measure a type of bearing capacity as discussed in the previous sections. A correlation is required to bridge the gap between the known bearing capacity in terms of the DCP and the unknown bearing capacity in terms of the CBR. CBR-DCP relationships have been studied for the past four decades. Table 2.2 shows several of the relationships in

Table 2.2 International Comparison of the Equation
 $\text{Log CBR} = A - B(\text{Log DCP})^C$ (Livneh and Ishai 1989)

A	B	C	Types of Material	Country of Origin
2.555	1.145	1	All types	Australia
2.810	1.320	1	All types	Indonesia
2.600	0.310	1	Sands	Australia
2.340	0.868	1	Low clays	Australia
1.995	0.725	1	Intermediate clays	Australia
2.370	0.944	1	Clays	Australia
2.407	1.020	1	Silts and clays	Australia
2.840	1.210	1	Silts	Australia
2.300	0.973	1	High clays	Australia
2.555	1.135	1	Samples confined in CBR moulds	England
2.765	1.135	1	Unconfined samples	England
2.940	1.100	1	Subbases	England - Sudan
3.170	1.415	1	Subbases	England - Sudan
2.222	0.785	1	Expansive clays	England - Sudan
3.070	1.280	1	Expansive clays	England - Sudan
2.200	0.710	1.5	All types	Israel
2.317	0.8577	1	All types	Sudan - England
2.500	1.310	1	All types	Belgium
2.300	1.200	1	All types, samples confined in CBR moulds	South Africa
2.095	1.200	1	All types, unconfined samples	South Africa
2.002	1.301	1	All types	South Africa

use today. In general, they have the form

$$\text{Log CBR} = A - B(\text{Log DCP})^C \quad (2.2)$$

where

CBR = California Bearing Ratio (in percent)

DCP = DCP index value

A = constant

B = constant

C = exponent

Some of the more generally accepted relationships are listed in Table 2.3 along with the type of testing procedure. Figure 2.9 shows several of those CBR-DCP correlations in a graphical format.

The laboratory-based research involves the preparation of two identical samples with the same water content, compactive effort, and mold size. The samples are subjected to a circular steel surcharge weight with a hole in the center. This allows for penetration of the piston in the CBR test and the cone tip in the DCP test. Normal procedures are used to run the CBR and DCP tests. Harison (1986) found that soaking the samples had an insignificant effect on the CBR-DCP relationship, changing the moisture content and dry density also did not affect the relationship and that a Log-Log representation was more suitable than an inverse model.

Laboratory testing has been an accepted means of determining CBR-DCP relationships. However, there are problems with the testing procedure. It has been observed

Table 2.3 Common CBR-DCP Relationships

REFERENCE TEST CBR-DCP EQUATION
Kleyne (1975) Laboratory Testing $\text{Log CBR} = 2.62 - 1.27(\text{Log DCP})$
Smith and Pratt (1983) Field Testing $\text{Log CBR} = 2.56 - 1.15(\text{Log DCP})$
Livneh (1987) Laboratory Testing $\text{Log CBR} = 2.20 - 0.71(\text{Log DCP})^{1.5}$
Harison (1989) Laboratory Testing $\text{Log CBR} = 2.55 - 1.14(\text{Log DCP})$
Webster et al. (1992) Field Testing $\text{Log CBR} = 2.46 - 1.12(\text{Log DCP})$

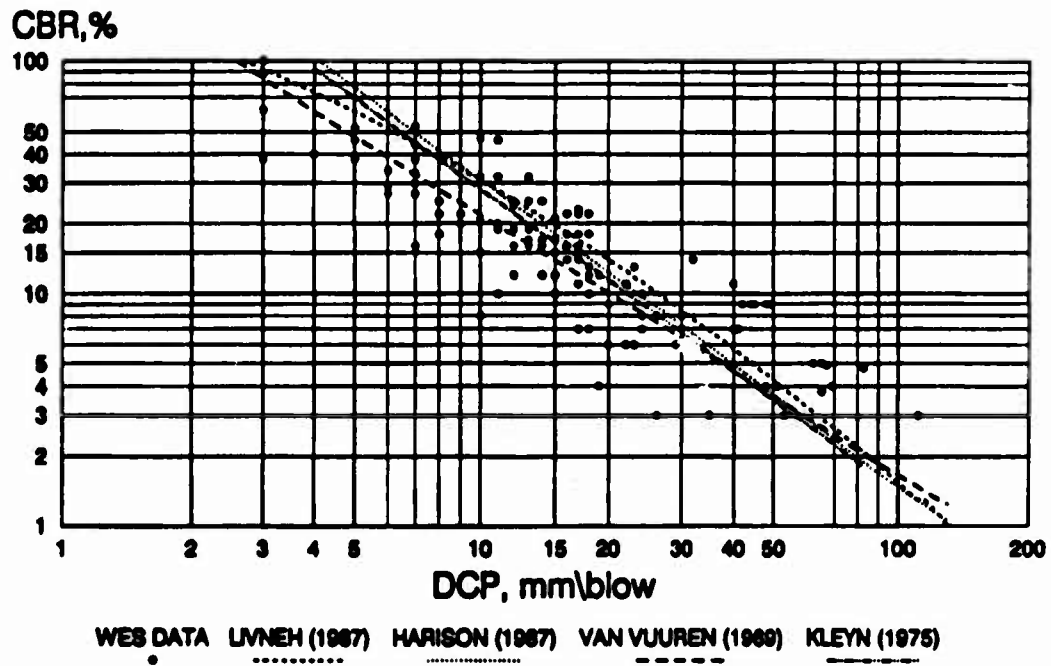


Figure 2.9 Log Plot of CBR-DCP Relationship
(Webster et al. 1992)

that laboratory-based CBR tests of granular materials give higher CBR results than tests carried out in the field (Livneh and Greenstein 1978). This variation is due to the geometry of the testing mold and the specimen preparation procedures. Figure 2.10 shows the assumed failure mechanism of the plunger in the laboratory and the field. In the laboratory, the failure plane is obstructed by the sides of the mold which increases the net resistance to the plunger. In addition, lateral precompression of the specimen during the compaction procedures contributes to the increase in CBR results. Figure 2.11 demonstrates the effect of an increase in mold diameter and the reductions in CBR value (Metcalf 1976).

Based on these results, some design agencies, including the Corps of Engineers, have introduced other procedures for estimating CBR design values. The Corps of Engineers relates plasticity and gradation to the granular base CBR values. Livneh and Greenstein (1978) suggest using a theoretical derivation based on a modified CBR test which controls lateral pressure. A third method is to simply measure the field CBR values using either the DCP and its correlation to the CBR or using the field CBR test procedure which is considered to be destructive and very time consuming.

The field CBR test equipment consists of some kind of a reaction platform, generally a 2 1/2 ton truck, a jack,

(a)

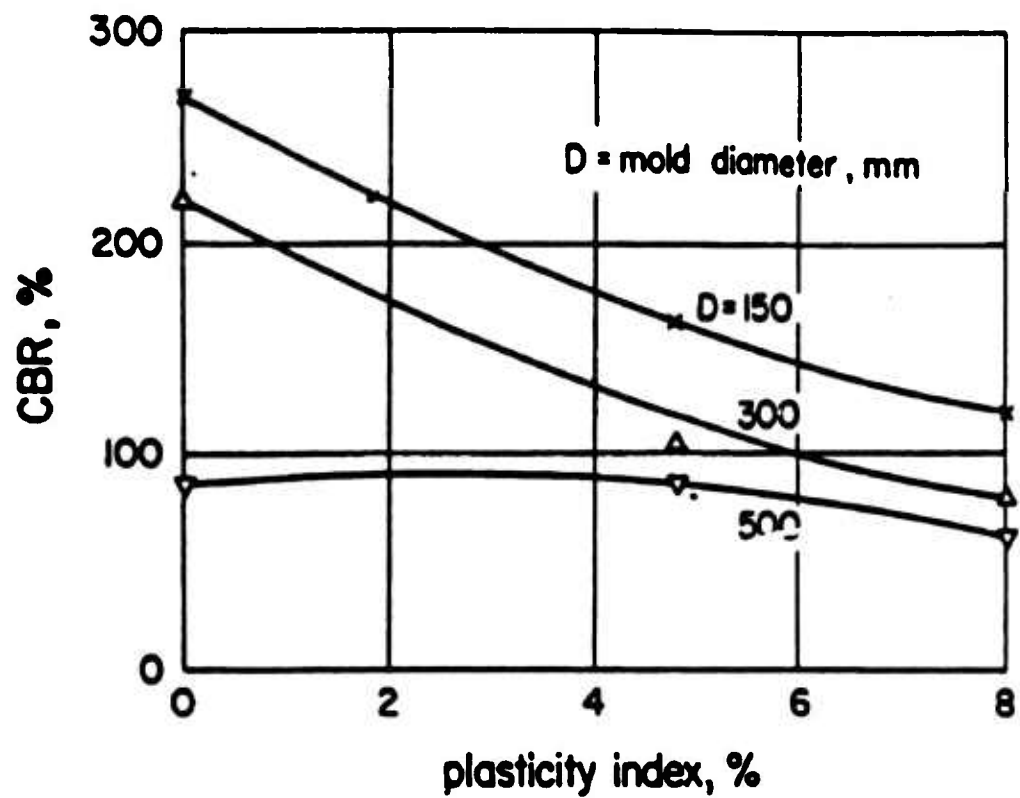


Figure 2.11 Effect of Mold Size on CBR (Metcalf 1976)
Copyright ASTM - Reprinted with permission

proving ring, penetration piston, dial gages, surcharge weights and deflection beam. Figure 2.12 shows the apparatus assembled. Using a stop watch and dial gages, the piston is jacked into the soil at 0.05 inches per minute. Proving ring readings are taken at 0.025 inch increments to a final penetration of 0.5 inches.

Tests correlating insitu CBR and DCP have been conducted by Smith and Pratt in 1983. Their relationship is expressed as:

$$\text{Log CBR} = 2.56 - 1.15 (\text{Log DCP}) \quad (2.3)$$

and is extremely close to Harison's (1989) laboratory CBR-DCP relationship which was modified to include the confining effect:

$$\text{Log CBR} = 2.55 - 1.14 (\text{Log DCP}) \quad (2.4)$$

This suggests a greater level of confidence between the field and laboratory correlations of the CBR-DCP relationships than previously thought.

A major advantage of using the DCP over the field CBR is the decrease in amount of time it takes to run a DCP test versus a CBR test. However, if the reliability of the DCP is not as good or better than the CBR field test, then the adoption of this test to evaluate unsurfaced airfields is questionable. Two papers, Smith and Pratt (1983) and

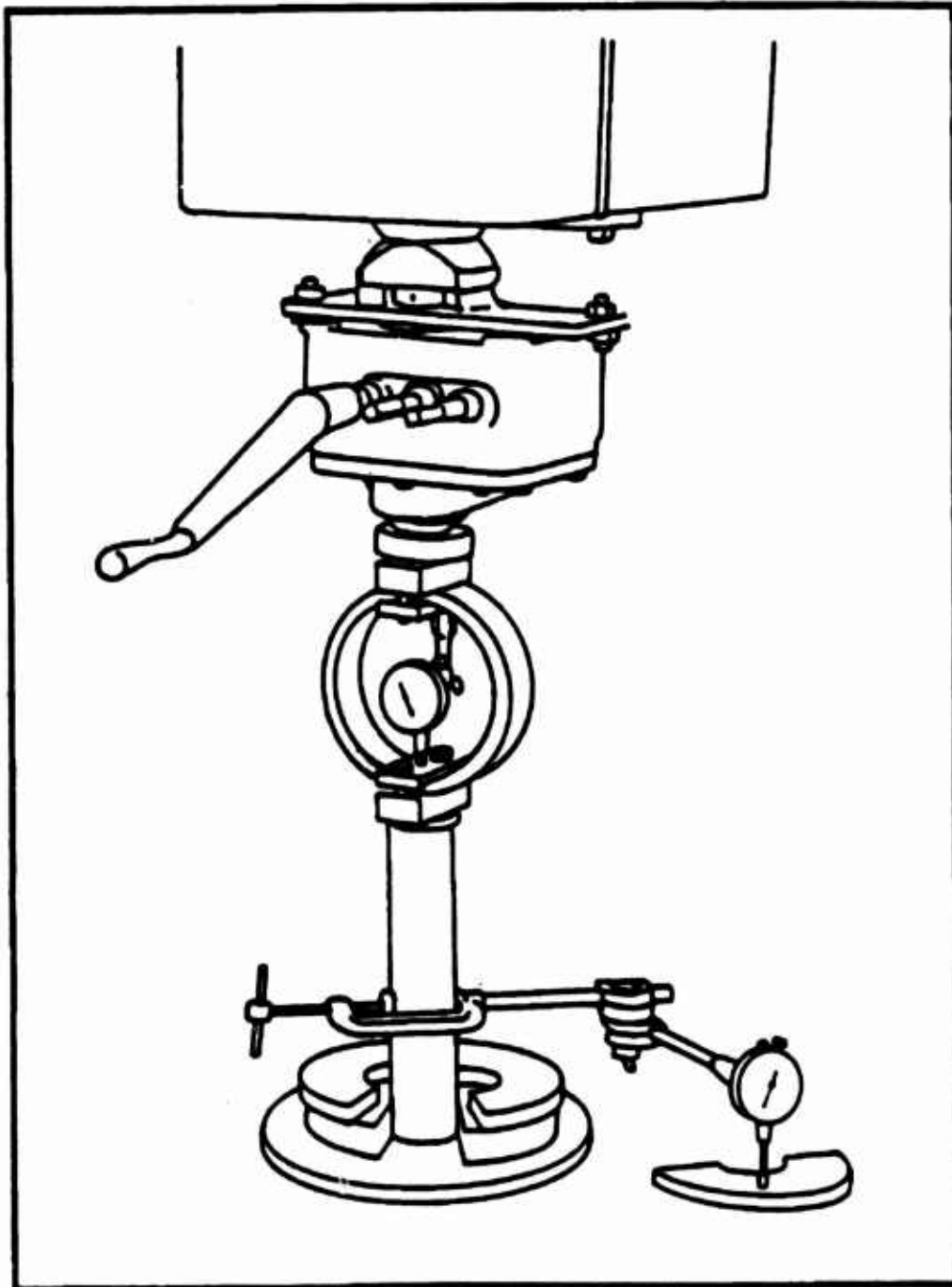


Figure 2.12 Field CBR Equipment Assembled

Livneh and Ishai (1989), have tested the degree of repeatability of the DCP and both have concluded that the DCP is more repeatable than the field CBR test. The measurement used to compare the test's repeatability is the coefficient of variation (CV), the ratio of standard deviation to mean.

Smith and Pratt (1983) concluded that the coefficient of variation of field CBR for a material was around 60 percent while that of the laboratory DCP was around 40 percent. Livneh and Ishai (1989) reported lower values as shown in Table 2.4. The maximum coefficient of variation obtained for the field DCP was 23 percent while the maximum for the CBR test was 32 percent.

This section has presented a number of empirical CBR-DCP correlations. In the following section (2.3.3.4) a discussion is presented on mathematical models used to describe the penetration of a DCP.

2.3.3.4 Dynamic Cone Penetrometer Mathematical Models

The accepted model used to represent the CBR-DCP relationship is the log-log model. It can be derived from the rational pile formula discussed by J.E. Bowles (Bowles 1988). This formula is the basis for nearly all the pile-driving formulas used today and is centered around the principles of impulse-momentum. Impulse is a measure of a force during the time the force acts and is expressed as:

**Table 2.4 Variance Coefficient Values in CBR and DCP Tests
(Livneh and Ishai 1989)**

Test	SITE 4	SITE 1	SITE 8	SITE 6
TYPE OF TEST: SAMPLE SURFACE OR FIRST DEPTH				
CBR	0.10	0.32	0.30	---
DCP LAB	0.16	0.12	0.21	0.14
DCP FIELD	0.12	0.07	0.23	0.13
TYPE OF TEST: SAMPLE BOTTOM OR SECOND DEPTH				
CBR	0.15	0.37	0.32	0.14
DCP LAB	0.14	0.15	0.21	0.14
DCP FIELD	0.09	0.07	0.17	0.05

$$I = \int F dt \quad (2.5)$$

where

I = impulse

F = force

t = time

Momentum is the product of mass and velocity and is expressed as:

$$L = mv \quad (2.6)$$

where

L = momentum

v = velocity

m = mass

The principle of linear impulse and momentum is defined as the initial momentum plus the impulse equals the final momentum and is expressed as:

$$\begin{aligned} L_{initial} + Impulse &= L_{final} \\ m(v_i) + \int F dt &= m(v_f) \end{aligned} \quad (2.7)$$

Based on these relationships, the point resistance of the DCP is related to the depth of penetration by the following expression (Harison 1986):

$$R = \frac{[(W_1) \times (H)]}{D} \times \frac{[(W_1) + (e^2 \times W_2)]}{(W_1 + W_2)} \quad (2.8)$$

where

- R = point resistance
- W_1 = weight of hammer
- W_2 = weight of instruments
- H = height of hammer fall
- D = penetration depth
- e = coefficient of restitution

Note: Only impact losses are included in Equation 2.8 for simplicity; other losses might include: rod loss and soil loss.

A closer inspection of the pile driving equation and some separation of terms reveals the work-energy theorem:

$$(\text{Energy In}) = (\text{Work Out}) + (\text{Impact Losses})$$

$$(W_1 \times H) = (R \times D) + [W_1 \times \frac{W_2 \times (1 - e^2)}{(W_1 + W_2)}] \quad (2.9)$$

The point resistance value, R, is a measure of the strength of the material tested. Therefore, it is assumed that R is a function of other strength parameters such as CBR and therefore the following equation can be written:

$$\text{CBR} = A \times (D)^{-1} \quad (2.10)$$

where

A = a constant

However, because the impulse-momentum equation includes

losses such as impact, the equation might be re-arranged as

$$\text{CBR} = A \times (D)^{-B} \quad \text{or} \quad (2.11)$$

$$\text{Log CBR} = \text{Log } A - B \times \text{Log}(D) \quad (2.12)$$

Equation 2.12 is now in the commonly used form to express the CBR-DCP relationship. Equation 2.10 is called the inverse model and has been used by Smith and Pratt (1983) to express CBR-DCP relationships. However, Equation 2.10 is not commonly used.

One of the aims of Livneh and Ishai's (1989) research was to search the literature for a theoretical derivation which would relate the DCP values with the basic soil strength properties of cohesion and angle of internal friction. The theoretical derivation is used to verify the empirical correlation between the CBR and DCP.

The DCP test consists of dropping a 17.6 lb weight 22.6 inches onto an anvil. The anvil is connected to a 39 inch vertical rod and cone assembly that penetrates the unsurfaced airfield. The fundamentals of dynamics show that the maximum amount of dynamic energy from one blow of the DCP is:

$$dE = W \times h \quad (2.13)$$

where

dE = dynamic energy

W = weight of hammer

h = hammer drop height

Due to friction, heat and other energy losses, the entire potential energy does not reach the DCP cone tip.

Therefore, Livneh et al. (1990) describe the DCP's apparent energy transfer efficiency factor (n) as:

$$n = dE_i / dE \quad (2.14)$$

where

dE_i = quasi-static energy for one blow

n = apparent energy transfer efficiency factor

In other words, n is a measure of how well the DCP transfers energy to the cone tip. Livneh et al. (1990) conclude that the n value for the DCP test is between 0.40 and 0.50 based upon several correlation investigations. The total quasi-static energy (E_i) is given by:

$$E_i = W \times h \times N \times n \quad (2.15)$$

where,

N = total number of blows

Using Schmertmann's paper on "Statics of the SPT"

(Schmertmann 1979), Livneh wrote the basic equilibrium equation for the DCP as

$$W \times H \times N \times n = L \times F \quad (2.16)$$

where

L = depth of DCP penetration

F = quasi-static force required to cause dynamic penetration

Since the DCP value is defined by

$$DCP = L / N \quad (2.17)$$

Livneh presents the following correlation:

$$\begin{aligned} \text{DCP} &= (W \times h \times n) / F & (2.18) \\ &= (17.6 \times 22.6 \times 0.45) / F \\ &= 179 / F \end{aligned}$$

where

DCP is given in in/blow

F is given in lbs

It can be seen that the force F is the key to determining the relationship between the DCP and the cohesion and angle of internal friction of the soil. Theoretical derivations based on either cavity expansion theory or on plastic failure theory are used.

Rohani and Baladi (1981) present a failure model for the relationship between Cone Index (CI) and the material's strength characteristics. It is based on cavity expansion (Vesic 1972) in an infinite soil mass and on the empirical assumption that the cone penetrometer shears the surrounding soil during its penetration process. The theory combines the shear strength expression, the internal pressure of an expanding spherical cavity in an unbounded elastic-plastic medium, and the geometry of a penetrating cone to derive an expression for CI for granular and cohesive materials. A comparison of calculated and the measured CI values shows a remarkably good correlation, Figures 2.13, 2.14 and 2.15.

A second failure model, using the plastic failure mechanism to determine the quasi-static force required to

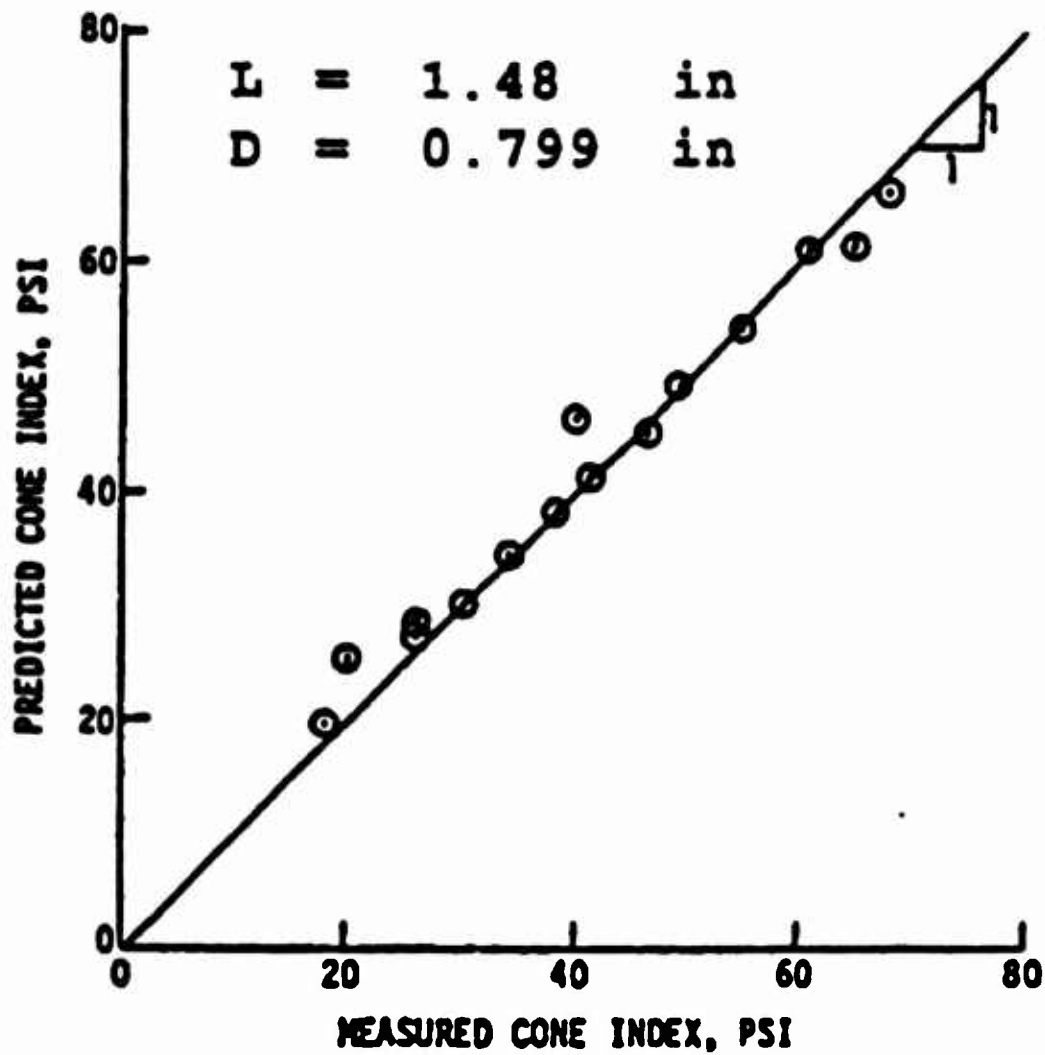


Figure 2.13 Comparison of Predicted and Measured Cone Index for Clay Using Cavity Expansion Theory (Rohani and Baladi 1981)

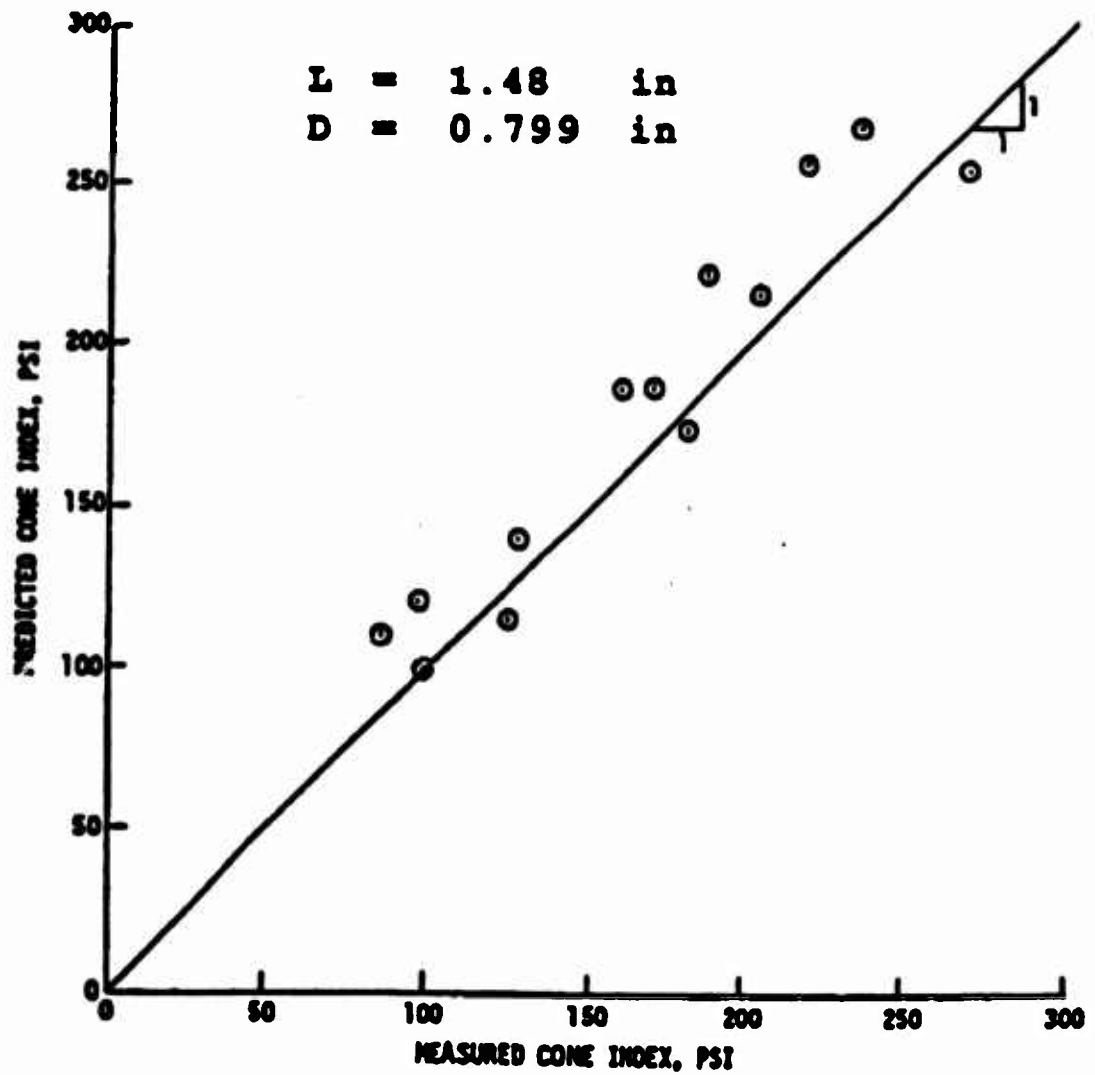


Figure 2.14 Comparison of Predicted and Measured Cone Index for Mixed Soil Using Cavity Expansion Theory (Rohani and Baladi 1981)

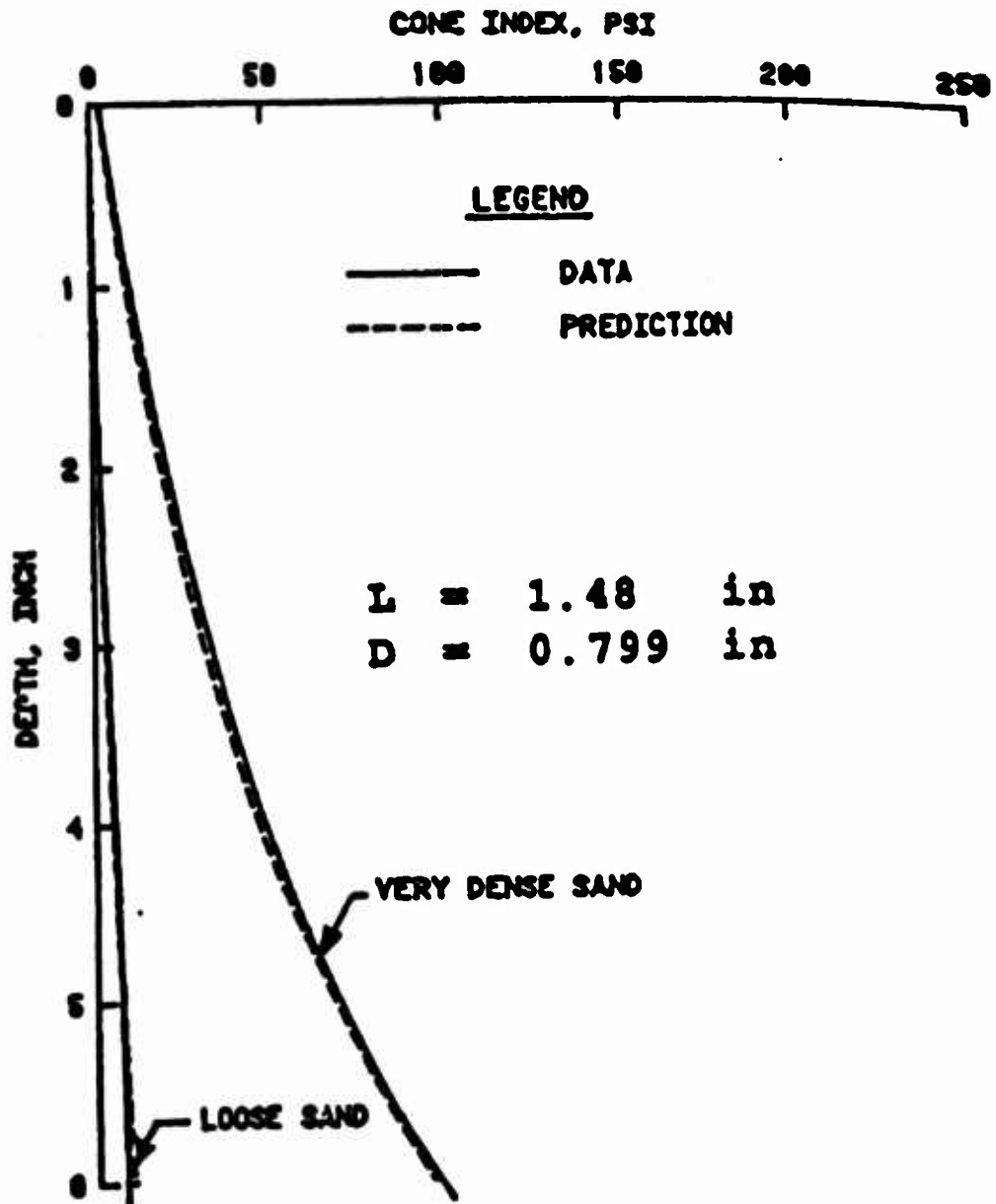


Figure 2.15 Comparison of Predicted and Measured Cone Index for Yuma Sand Using Cavity Expansion Theory (Rohani and Baladi 1981)

penetrate a DCP cone, was introduced by Durgunoglu and Mitchell (1974). They used Meyerhoff's "Ultimate Bearing Capacity of Wedge-Shaped Foundations" (Meyerhof 1961) research. The failure surface, shown in Figure 2.16, closely represented the failure planes observed using wedge shaped penetrometers at shallow depths. Using the observed failure mechanism and equilibrium analysis of the failure zones, a penetration resistance equation can be written:

$$q_r = [c(N_c)(\epsilon_c)] + [B_\gamma(N_\gamma)(\epsilon_\gamma)] \quad (2.19)$$

where

q_r = ultimate unit tip resistance

c = unit cohesion

γ = mass density

B = penetrometer diameter

N_c and N_γ = penetration resistance factors

ϵ_c and ϵ_γ = shape factor

Figure 2.17 shows fairly good agreement of friction angles predicted using penetration resistance factors versus measured values.

2.3.3.5 Force Analysis of the Dynamic Cone Penetrometer

A method to generate the force history of the DCP instrument was demonstrated by Chua and Lytton (1989). A 100,000 G accelerometer was screw-mounted to the top of the DCP handle, Figure 2.18, and the acceleration-time history was recorded for each blow. The recording was triggered

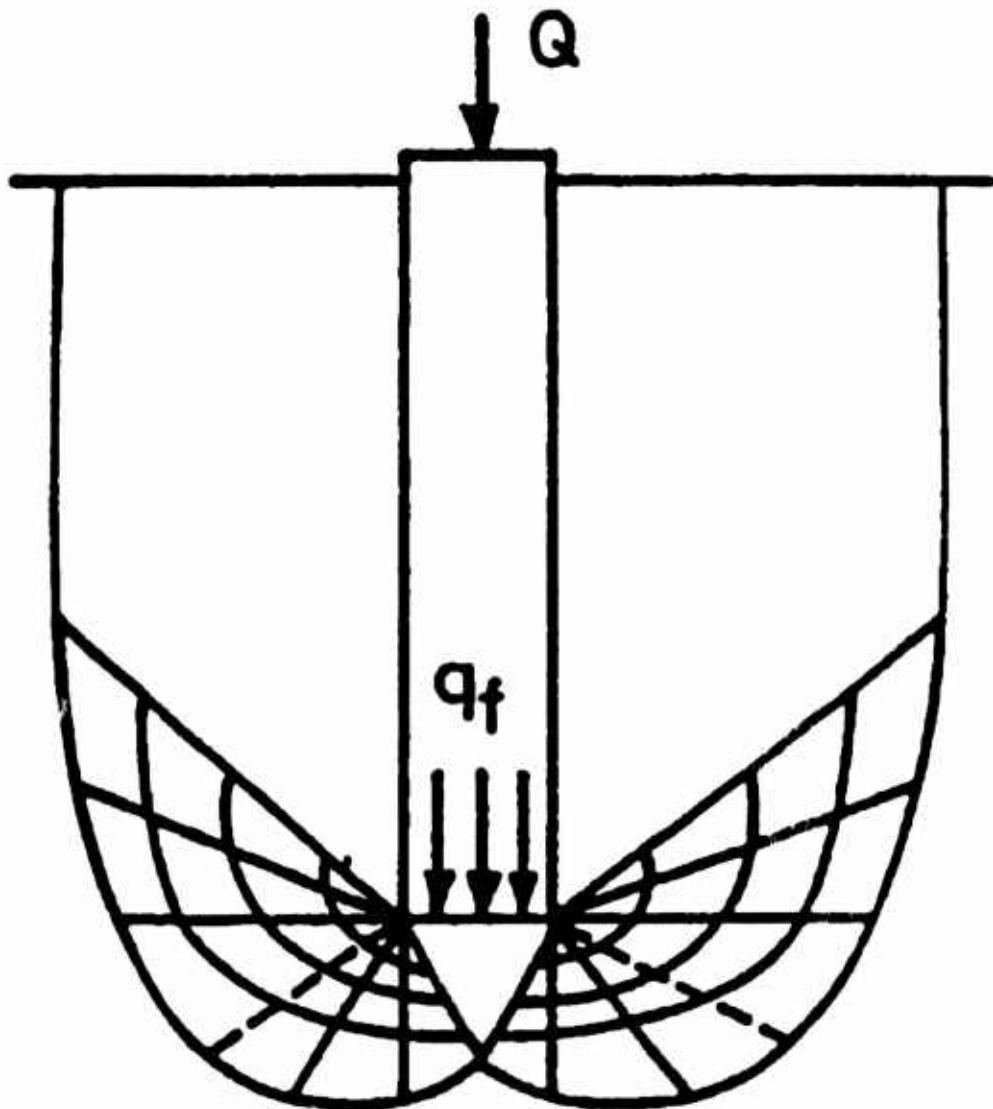


Figure 2.16 Failure Surface Observed with Wedge Penetration (Durgunoglu and Mitch, *)

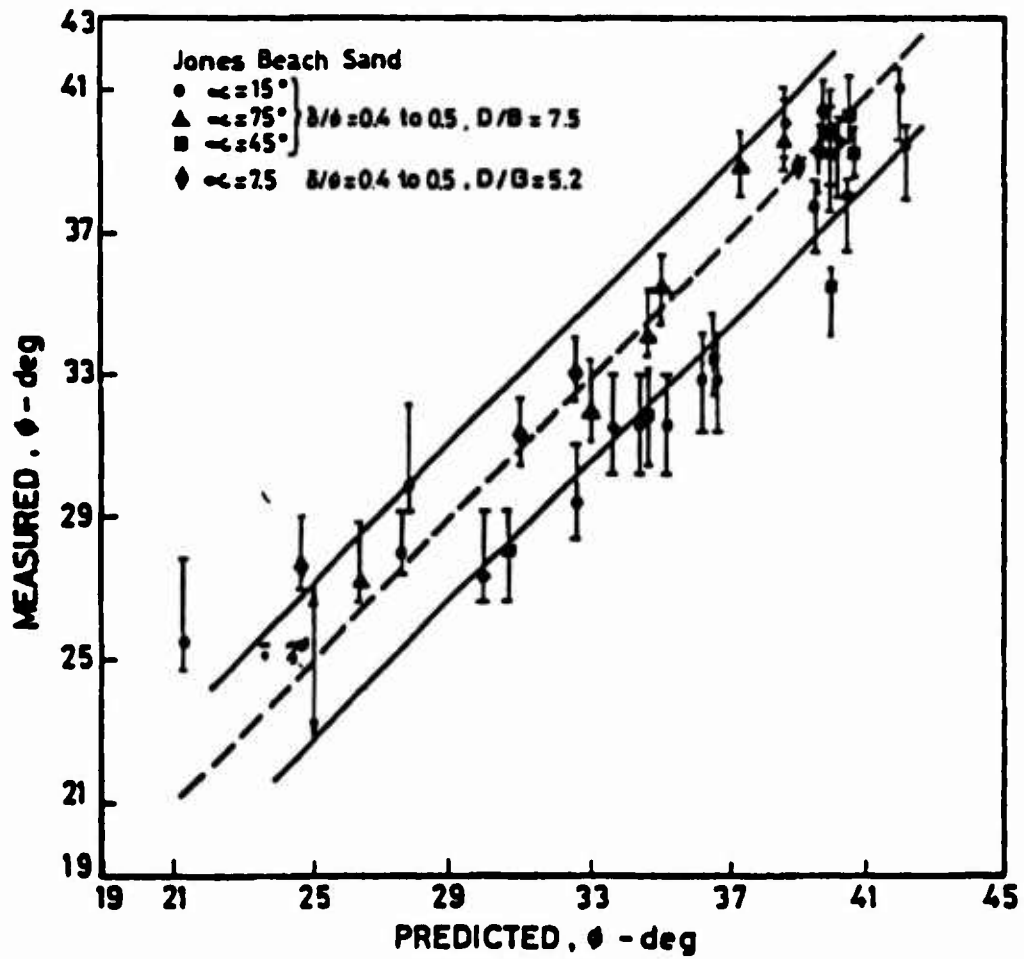


Figure 2.17 Comparison of Measured vs Predicted Friction Angle Using Plastic Failure Model (Durgunoglu and Mitchell 1974)

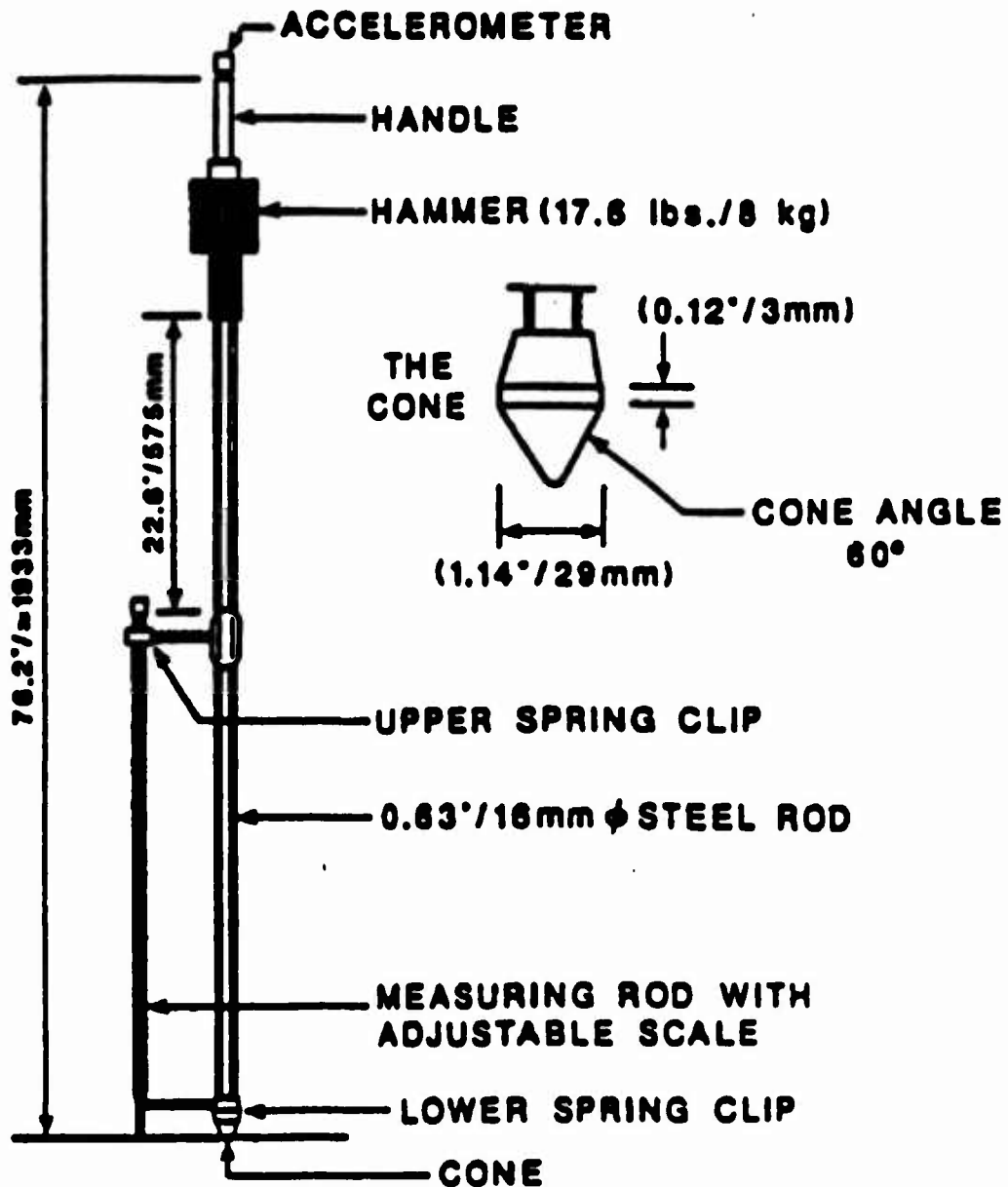


Figure 2.18 Dynamic Cone Penetrometer With Accelerometer Mounted To The Handle (Chua and Lytton 1989)

by the impact of the hammer. By integrating the acceleration-time signal, the velocity-time and displacement-time histories were generated. Figure 2.19 shows these signals of a test performed in a granular base course material. Using a computer program that models dynamic response under load, the force history of the sliding hammer onto the anvil were generated. Figure 2.20 shows triangular shaped force impulses estimated by matching measured and calculated acceleration signals.

2.3.3.6 Stress Wave Propagation

When a rod is suddenly struck by a force, F , at one end at time, t , then at the first instant of time, all of its particles are still at rest. A very short time later, dt , a section of the rod, dL , is compressed an amount, dd . A wave speed or wave propagation velocity, can be defined as

$$c = dL/dt \quad (2.20)$$

The wave speed is the speed with which a compression or tension zone moves along a rod. The deformation of a point, dd , can also be written as

$$dd = (F) (dL) / (A) (E) \quad (2.21)$$

where

A = area of rod

E = elastic modulus

The change in particle velocity of this point is

$$dv = dd/dt \quad (2.22)$$

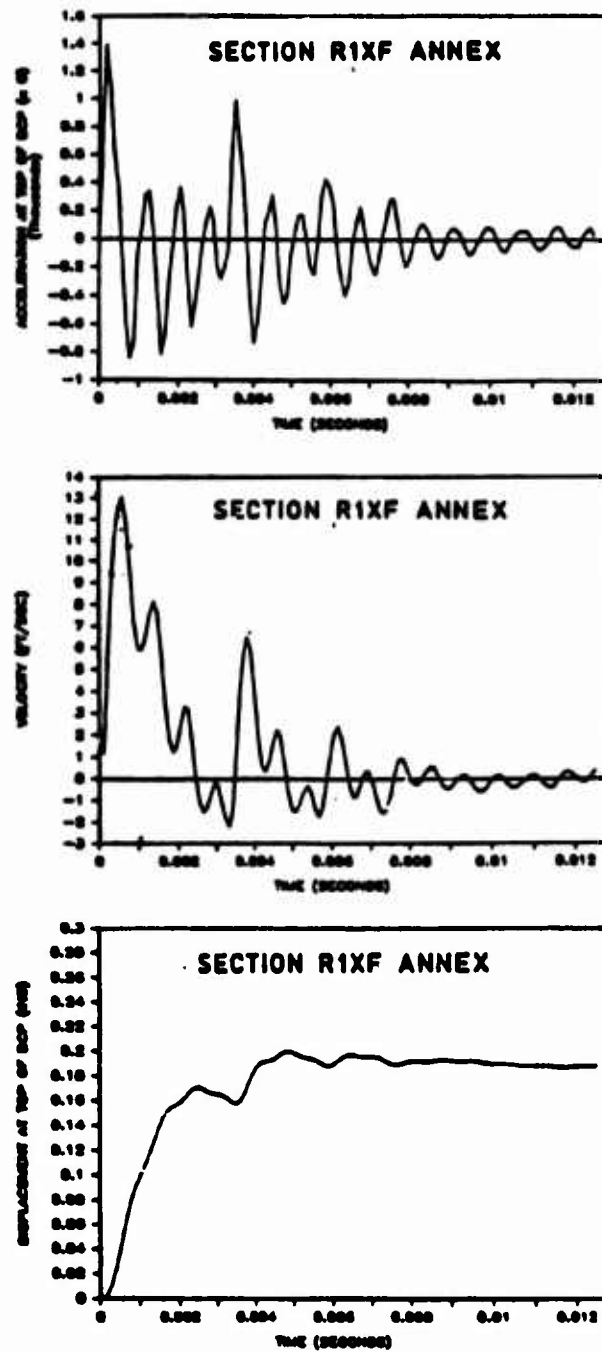


Figure 2.19 Acceleration, Velocity, and Displacement Time Histories of DCP in Medium Stiff Granular Base Course Material (Chua and Lytton 1989)

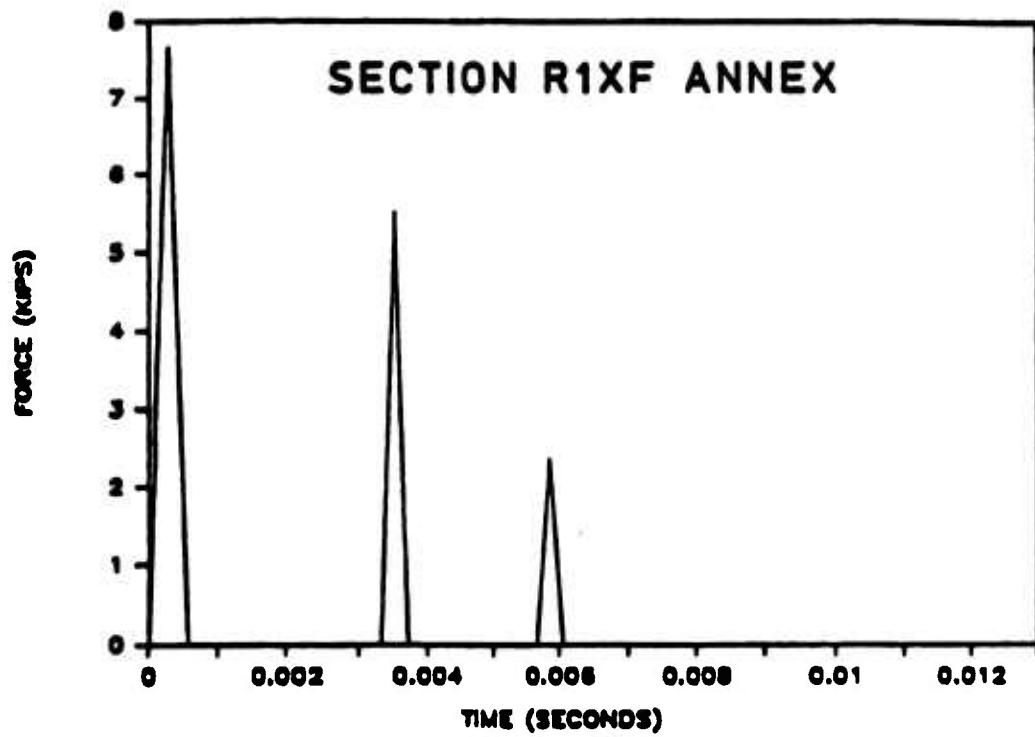


Figure 2.20 Calculated Force-Time History of the DCP in Granular Base Course Material (Chua and Lytton 1989)

$$dv = (F) (dL) / (A) (E) (dt)$$

$$dv = (F) (c) / (E) (A)$$

The particle speed is the speed with which a particle in a rod moves as a wave passes. The acceleration of this point is

$$a = dv/dt \quad (2.23)$$

$$a = (F) (c) / (E) (A) (dt)$$

From Newton's Second Law and the definition of mass, m ,

$$F = (m) (a) \quad (2.24)$$

$$m = (dL) (A) (\rho) \quad (2.25)$$

where

$$\rho = \text{mass density}$$

then

$$F = (dL) (A) (\rho) [(F) (c) / (E) (A) (dt)]$$

or by canceling out F and A

$$c = \sqrt{\frac{E}{\rho}} \quad (2.26)$$

The wave speed is a function of the material properties of the rod in which it travels.

The stress in the penetration rod is

$$\sigma = F/A \quad (2.27)$$

$$\sigma = E\epsilon \quad (2.28)$$

where

$$\epsilon = dd/dL \text{ (strain)}$$

Consequently, the stress in the penetration rod is

$$\sigma = (E) (dd/dl) \quad (2.29)$$

Using Equation 2.20 and re-arranging for velocity, v , the stress is

$$\begin{aligned}\sigma &= [E][dd/(c)(dt)] \\ &= [(E)(v)]/[c]\end{aligned}\tag{2.30}$$

Multiplying the stress by area of the rod, A ,

$$F = \left[\frac{(E)(A)}{(c)} (v) \right]\tag{2.31}$$

The term EA/c is called impedance, I , and is calculated using Young's modulus, the cross sectional area of the rod, and the wave speed from Equation 2.26. This term implies that the rod offers a resistance or impedes the change in velocity. Equation 2.31 suggests that if the particle velocity of the penetration rod can be measured, then the force in the rod can be determined. An accelerometer is used for this purpose.

An accelerometer, mounted to the penetration rod, and an oscilloscope are used to measure, record, and integrate an acceleration-time signal. The integration of the signal reveals a velocity-time plot which can be then used to plot a force-time graph of the penetration rod. This plot would be similar to Figure 2.20.

2.3.3.7 Other Dynamic Cone Penetrometers

During the literature search, two unique DCP penetrometers were discovered. They are the Dual Mass DCP and the Automated Dynamic Cone Penetrometer.

The Dual Mass DCP, invented by Webster et al. (1992), consists of the same basic dimensions as the standard DCP except that the mass can be either 17.6 lbs or 10.1 lbs. The mass is converted from 17.6 to 10.1 by removing an outer steel sleeve attached by a set screw. Webster reports that the cone penetration of one 17.6 lb blow of the hammer is about twice that of the 10.1 lb blow. The purpose of the dual hammer weight is that the 17.6 lb hammer is best suited for stiff materials whereas the 10.1 lb hammer was found more suitable and yields better results in soils of CBR less than ten. The testing procedure is also the same as the standard DCP except that the DCP index derived from the 10.1 lb hammer is multiplied by two to equal the standard DCP index. In addition, a specially designed disposable cone was designed to reduce the effort in removing the DCP from the ground. The cone remains in the ground after testing and is replaced before each successive test. Webster concludes that this disposable cone can double the number of DCP tests per day.

The Automated DCP, invented by Livneh et al. (1992), consists of a mobile air compressor, a falling weight mechanism, a lifting and release mechanism and a penetration rod. Basically, the system uses compressed air to raise the 8 kg mass to the desired height and adjustable brackets to release the mass onto the penetration rod. Livneh reports that the automatic DCP device provides very similar results

to those produced by the manual DCP. He concludes that the automated DCP device is fully recommended as an efficient substitute for the manual device, from the point of view of both precision and technical testing. Livneh also reported that statistical analysis demonstrated that automated Dynamic Cone Penetrometer results were independent of the blow-rate in the range of 24 to 40 blows per minute. Forty blows per minute was the fastest practical rate tested.

2.3.4 Aerial Penetrometers

Because of the inaccessibility of some landing sites, due to hostile enemy, rough terrain, or insitu time testing restraints, aerial penetrometers have been developed to measure bearing capacity. Since the early 1940s, the Department of Defense has investigated projectile devices launched from the air to improve the penetration of bombs. One of the earliest investigations studied the penetration of a cannon ball into earth revetments. Using projectile bombing technology, the Air Force Cambridge Research Center developed an aerial penetrometer to measure bearing capacity in remote sites. The penetrometer shown in Figure 2.21 was an aluminum cylinder two feet long, one and one half inches in diameter and weighed two pounds. It was dropped by hand over the site. Each penetrometer was rated at a certain capacity calibrated with known cone index standards. Either

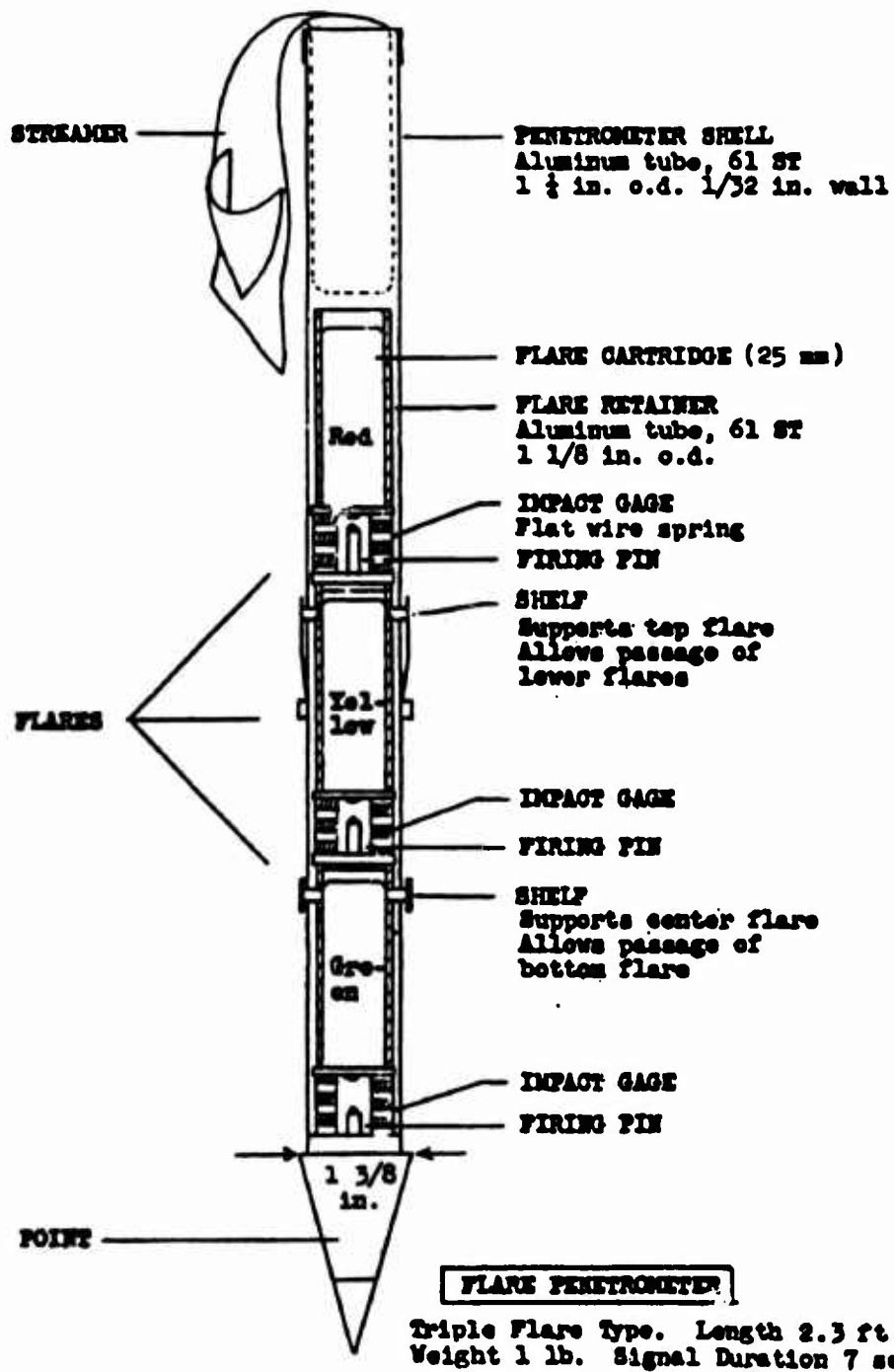


Figure 2.21 Aerial Penetrometer (Molineux 1955)

springs, for low ratings, or shear pins, for high ratings, were activated by the impact of the ground. A shot-gun type cartridge was triggered if the rating of the site was as strong or stronger than the rating of the penetrometer, and a flare would be fired about 200 feet into the air from the penetrometer. When used in a water environment, such as a beach head, a dye would replace the flare. If a pilot were to fly over a site dropping these projectiles, he would look for the flares to fire in a consistent manner and would know if the site was acceptable for his aircraft. In later versions of this type of aerial penetrometer, three different color flares were used, indicating different cone indices. In some versions, a radio telemetered indicator was placed inside the penetrometer and radio signals would be transmitted back to the pilot with test results. The transmitter was capable of transmitting up to four miles away for 30 minutes at a time.

In the 1960s, when technology allowed the projectile to be instrumented, a projectile was designed to actually penetrate the ground, with little deviation in the line of flight and with instrumentations on board such as an accelerometer to measure decelerations. The Sandia Corporation was a major research group that contributed heavily to the large scale earth penetrometer research.

The Sandia program used projectiles from 1 to 18 inches in diameter that were dropped in free fall from helicopters.

The projectile would penetrate up to 300 feet in soil. It was found in their research that "for a given projectile impacting vertically at a given velocity, the deceleration and depth depend on the properties of the soil and rock media being penetrated" (Caudle et al. 1977). It was then surmised that if decelerations, depth and impact velocities were known for a given projectile, then the properties of the earth penetrated could be determined.

Though the aerial penetrometer technology seemed promising, several limitations prevented the program from making a large impact in the field. The first limitation was the erroneous data provided to the pilot if the projectile were to strike a stone, clump of moss, animal hole or any number of other obstacles. Secondly, the number of penetrometer required to accurately measure the bearing capacity of an airfield was estimated to reach up in the hundreds if the site was a non-homogeneous soil with an area of 150 ft x 1800 ft (Molineux 1955). Finally, if the area investigated prevented full penetration of the projectile, the area would have to first cleared of projectiles before any landing operations could be made.

2.4 Seismic Surveying

2.4.1 Introduction

In the United States Air Force, Combat Controllers are used to evaluate unsurfaced airfields for possible use as a

landing zone. Today, the evaluation is accomplished by the Dynamic Cone Penetrometer test method. Since this method, described earlier, can effectively test only one location at a time, it is proposed in this research to use insitu seismic methods to complement the evaluation. Today's seismic methods include the crosshole, downhole, surface refraction, and reflection methods and spectral analysis of surface waves. Of these methods, spectral analysis of surface waves had the potential of being the most promising method of evaluation. It precluded the use of destructive and time consuming boreholes and provided a means of evaluation where a stiff material overlaid a soft material. The Spectral Analysis of Surface Waves (SASW) method of insitu soil investigation is a seismic test which places both the source and receivers on the ground surface. Two receivers placed at varying spacings use waves generated by a vertical impact load to measure surface wave properties between the receivers. An inversion program is used to estimate the shear wave velocity and shear modulus profiles. These profiles can be used by the combat controller to compare results at different stations down the unsurfaced airfield.

2.4.2 Surface Wave Propagation

A surface wave created by a vertical impact propagates through a layered soil in a dispersive manner. The velocity

of the wave is dependent on the wavelength (or frequency) of the wave. The variation of velocity with frequency is called dispersion and occurs because waves of different wavelengths sample different layer depths. Low frequency waves propagate with longer wavelengths and therefore sample deeper layers. High frequency waves propagate with shorter wavelengths in the near surface layers. As the wavelength increases, particle motion is found in the deeper layers, as shown in Figure 2.22. The velocity of the wave is influenced by the properties of the layer in which the particle motion occurred. In Figure 2.22(c), the properties of the surface layer, the base and some of the subgrade effect the velocity of that wave. In Figure 2.22(b), particle motion is limited to the surface layer and therefore the velocity of the wave is only effected by that layer. This technique allows surface waves to sample the different layers by creating a wide range of frequencies (or wavelengths). The surface wave velocity is then compared with the corresponding wavelength and plotted on a dispersion curve (discussed later). Using an inversion process, the shear wave velocity of the different layers can be calculated.

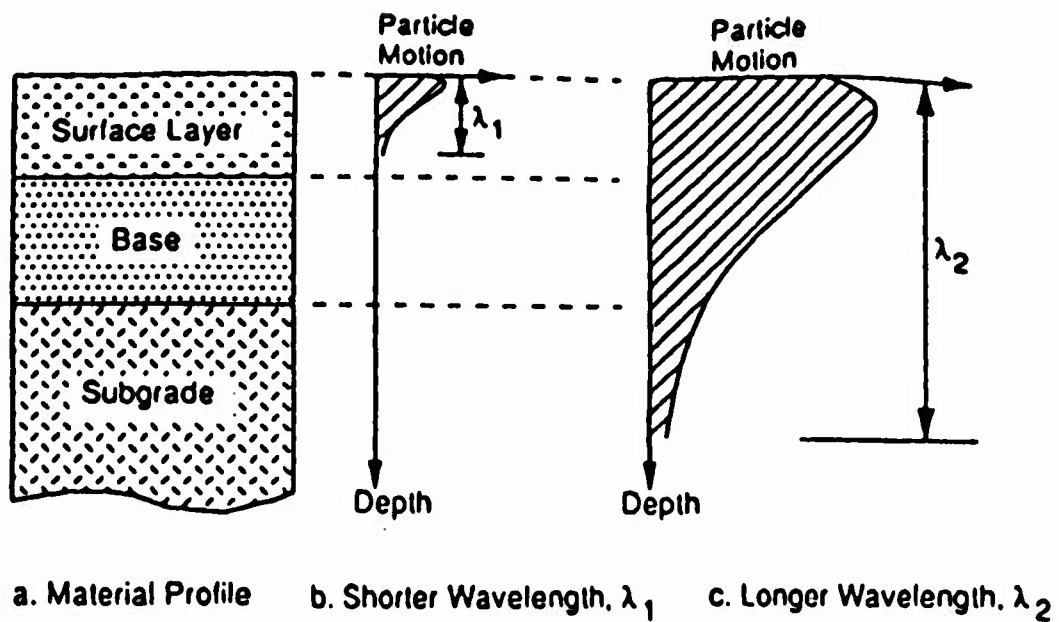


Figure 2.22 Approximate Distribution of Vertical Particle Motion with Depth of Two Wavelengths

2.4.3 SASW Field Testing and Equipment

The field SASW equipment consists of an impact source, seismic receivers, and a recording device as shown in Figure 2.23. The impact source is generally some type of drop hammer. At close receiver spacings (2 to 8 feet) hand-held hammers are used while at greater spacings (8 to 16 feet) sledge-hammers are generally used. Stokoe et al. (1988) have investigated using 150 to 2000 lb dropped weights with good success and have suggested using bulldozers and dynamic compaction weights to create the very low frequencies required for depths of 500 feet. However, the larger weights are quite destructive and could be prohibitive on some sites. A piezoelectric shaker can be used to generate high frequencies in the 1 to 50 kHz range for evaluation of near surface layers.

Once the source has impacted, two vertical receivers monitor the surface wave. The frequencies of the wave influence the type of receiver used. Vertical velocity receivers with natural frequencies of 1 to 4.5 Hz perform well at soil sites (5 to 500 Hz) and piezoelectric accelerometers do well at pavement sites where frequencies range from 1 to 50kHz (Stokoe et al. 1988). SASW testing is usually done with receivers at different spacings using one common centerline midway between receivers. Spacings between receivers at a soil site can be 4, 8, 16, 32, 64,

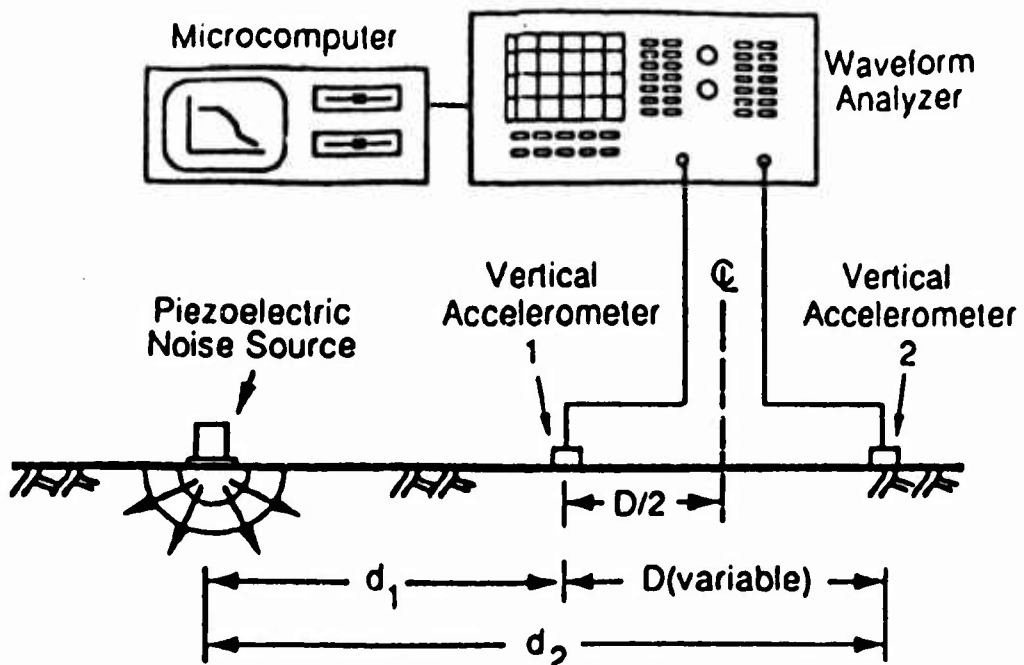


Figure 2.23 Configuration of SASW Equipment
 Copyright ASCE - Reprinted with permission

and 128 feet. These spacings can be used to evaluate to depths of 60 feet.

The recording devise is usually some kind of dynamic signal analyzer with a micro-computer. The digital signal analyzer is a digital oscilloscope that has the ability to perform calculations in either the time or frequency domains. Figure 2.24 shows some typical field data at one receiver spacing. The phase of the cross power spectrum plots the phase difference between receivers as a function of frequency. The phase difference is used to generate the dispersion curve discussed later. The coherence is a measure of the quality (signal to noise ratio) of the signals recorded. A ratio of one signifies a high quality signal while a ratio of zero indicates poor quality.

2.4.4 Dispersion Calculations

The dynamic digital analyzer collects the time records of each receiver spacing and transforms them into records of the frequency domain using a fast fourier transform algorithm. Inside the frequency domain, the phase difference (θ) between two receivers is plotted against frequency. The time delay from one receiver to the other is a function of frequency and is

$$t(f) = \theta_{yx}(f) / 2\pi f \quad (2.32)$$

where

$$\theta_{yx}(f) = \text{phase of cross power spectrum (radians)}$$

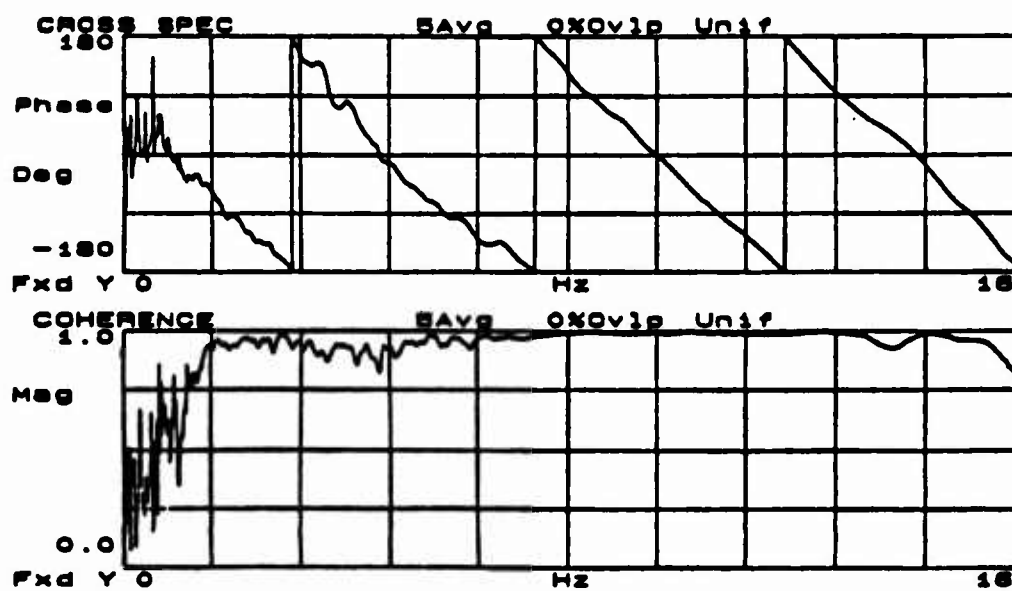


Figure 2.24 Phase and Coherence Spectra

f = frequency (Hertz)

The surface wave velocity is

$$V_R(f) = D/t(f) \quad (2.33)$$

where

D = distance between receivers

The wavelength of the surface wave, λ_R , is

$$\lambda_R = V_R/f \quad (2.34)$$

These calculations in Equations 2.32, 2.33, and 2.34 are preformed by a micro-computer for each frequency and the result is plotted as a dispersion curve. Each dispersion curve generated from specific receiver spacings is merged to form one integrated dispersion curve as shown in Figure 2.25.

2.4.5 Inversion Process

The purpose of the inversion process is to back calculate shear velocity and moduli of the differing soil layers. The process used today is an iterative procedure that matches a theoretical dispersion curve with the experimental dispersion curve obtained in the field. Each iteration assumes a shear wave velocity and thickness of layer and modifies accordingly to obtain similarity between experimental and theoretical curves. Figure 2.26 is an example of a Final Shear Wave Velocity Profile.

The Young's modulus of the surface layer can also be determined once the phase velocity of the surface layer has

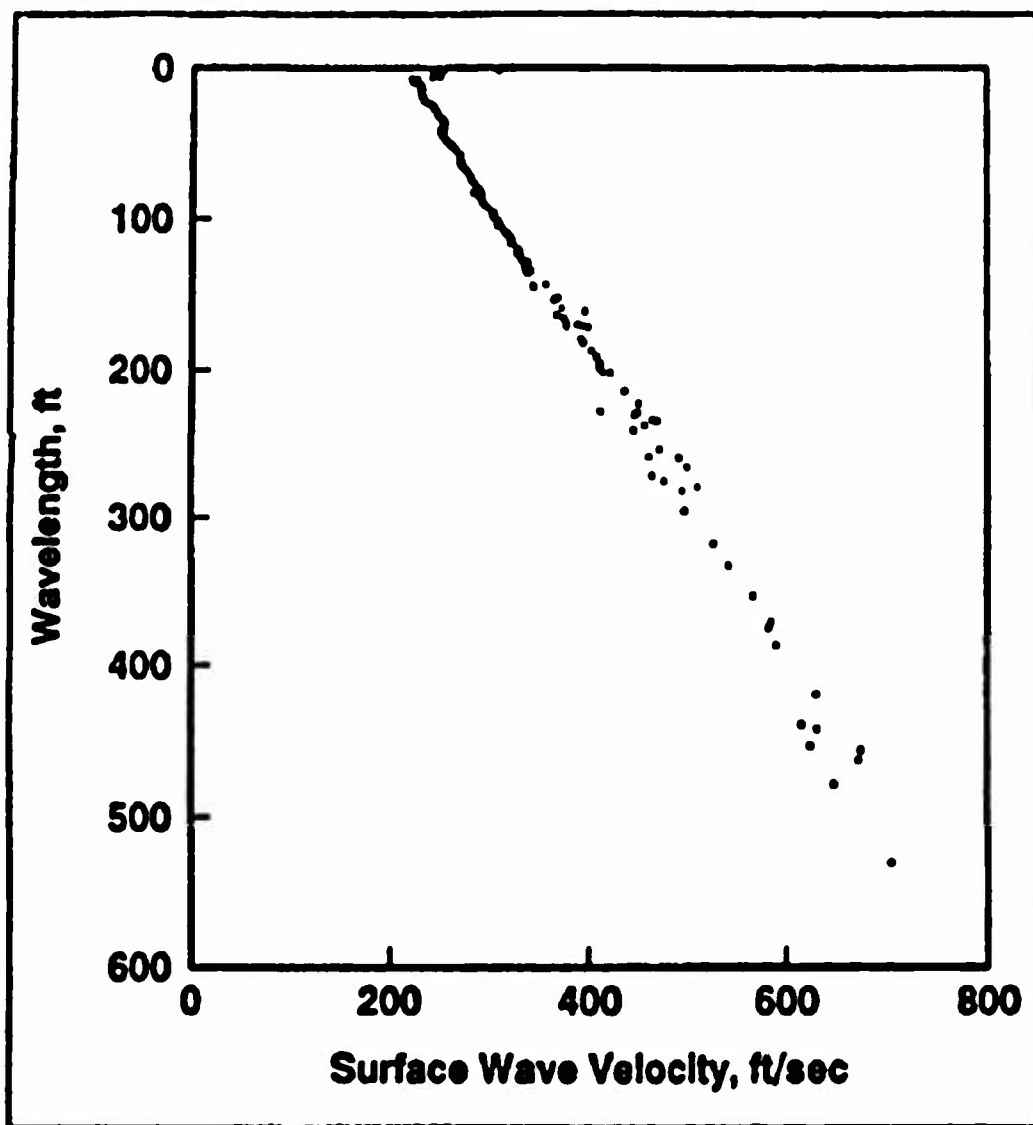


Figure 2.25 Composite Dispersion Curve

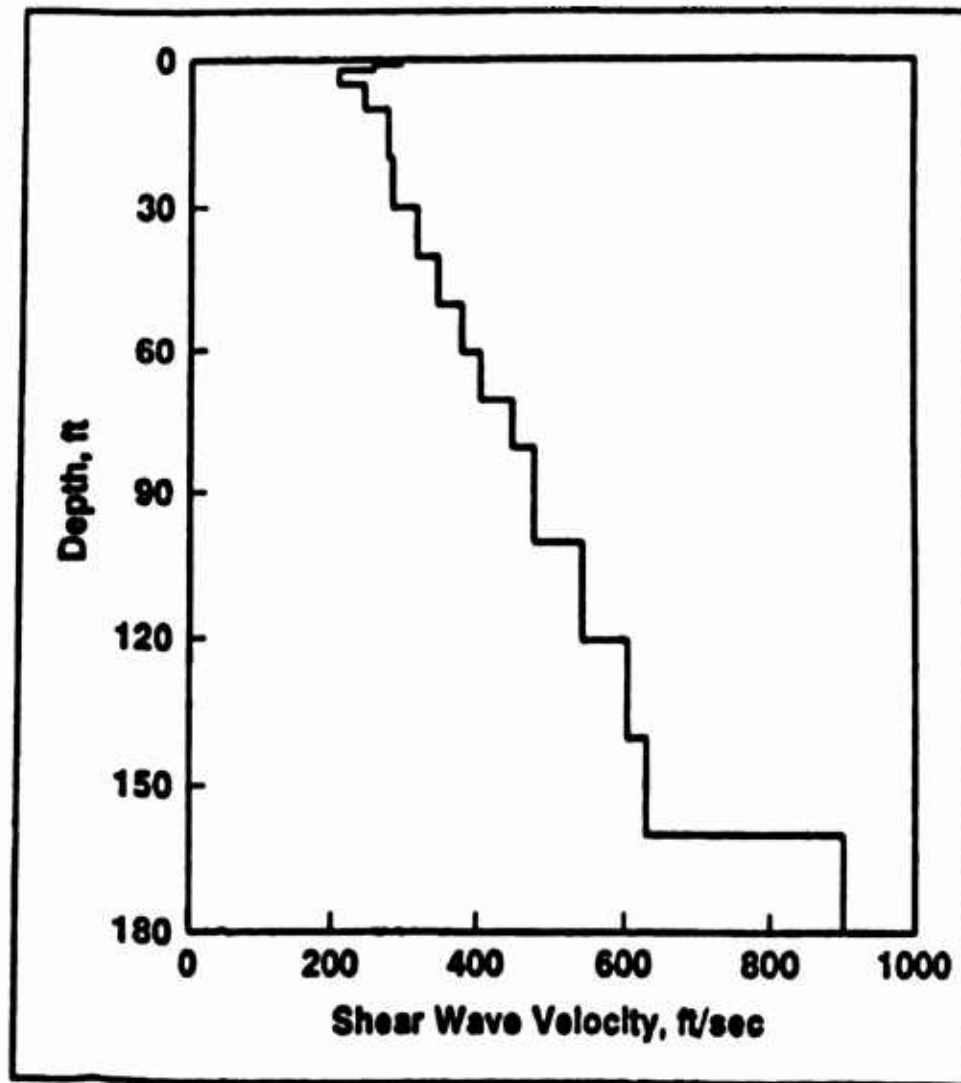


Figure 2.26 Final Shear Wave Velocity Profile

been measured (Roesset et al. 1991):

$$V_s = CV_R \quad (2.35)$$

$$G_{(max)} = (\gamma/g) (V_s)^2 \quad (2.36)$$

$$E_{(max)} = 2G(1+\nu) \quad (2.37)$$

where

$$C = 1.135 - 0.182\nu \quad (\text{for } \nu \geq 0.1)$$

G = shear modulus

γ = total unit weight

g = acceleration due to gravity

E = Young's modulus

ν = poisson's ratio

Since measurements are seismically made with strains below 0.001 percent, equations 2.36 and 2.37, represent maximum moduli values.

2.4.6 Qualitative Estimation of Density Using the SASW Method

One of the by-products of obtaining the shear wave velocity of a site is that in-situ densities can be inferred. Stokoe et al. (1988) demonstrate that this can be done for sands and gravels by comparing measured shear wave velocities with values calculated using an empirical relationship developed by Seed et al. (1986). A small strain value of shear modulus, G_{max} , is given by

$$G_{max} = (1000)K_2(\sigma'_m)^{0.50} \quad (2.38)$$

where

K_2 = empirical constant which takes into account density (void ratio)

σ_m' = mean effective principle stress.

Shear modulus and shear velocity are related by Equation 2.39:

$$G = (\gamma/g)V_s^2 \quad (2.39)$$

where

γ = total unit weight

g = gravitational acceleration

Stokoe et al. (1988) demonstrate that if equations 2.38 and 2.39 are combined, the shear wave velocity can be expressed as

$$V_s = [(1000)(g/\gamma)(K_2)]^{0.50} (\sigma_m')^{0.25} \quad (2.40)$$

Using Equation 2.40, the variation of shear velocity with depth and density can be evaluated at a site.

Using a qualitative approach, Stokoe et al. (1988) suggest assuming different values of K_2 which reflect various densities. For example, values such as 30, 50, and 70 represent loose, medium dense and very dense sands while values of 40, 80, and 120 might be used for gravel. In addition, σ_m' must be calculated for each depth using the expression

$$\sigma_m' = (\sigma_v')(1 + 2K_0)/3 \quad (2.41)$$

where

σ_v' = vertical effective stress

K_0 = coefficient of earth pressure at rest

However, Stokoe et al. (1988) caution that by using Equation 2.41 there are at least five assumptions implicitly made:

- (1) level ground
- (2) principal stresses are oriented in the vertical and horizontal directions
- (3) the intermediate and minor principal stresses are equal
- (4) age of deposit can be neglected
- (5) little or no cementation exists

Stokoe et al. (1988) demonstrated this technique using three sites that were hard to sample with traditional methods.

Figure 2.27 present results from the sites in terms of shear velocity, depth, and density. Figure 2.27(a) shows a very loose layer between 10 and 40 feet in the Spirit Lake area, Figure 2.27(b) shows a loose layer between 4 and 16 feet and Figure 2.27(c) demonstrates the effects of compactions efforts at Jackson Lake Dam, Wyoming.

2.4.7 Determining Surface Layer Thickness and Modulus Values

The goal of SASW testing is to determine the stiffness of layers by using the dispersive properties of surface waves. Measurements of surface wave phase velocity and wavelength of a uniform surface layer can then be used in Equations 2.35, 2.36, and 2.37 of Section 2.4.5 to determine

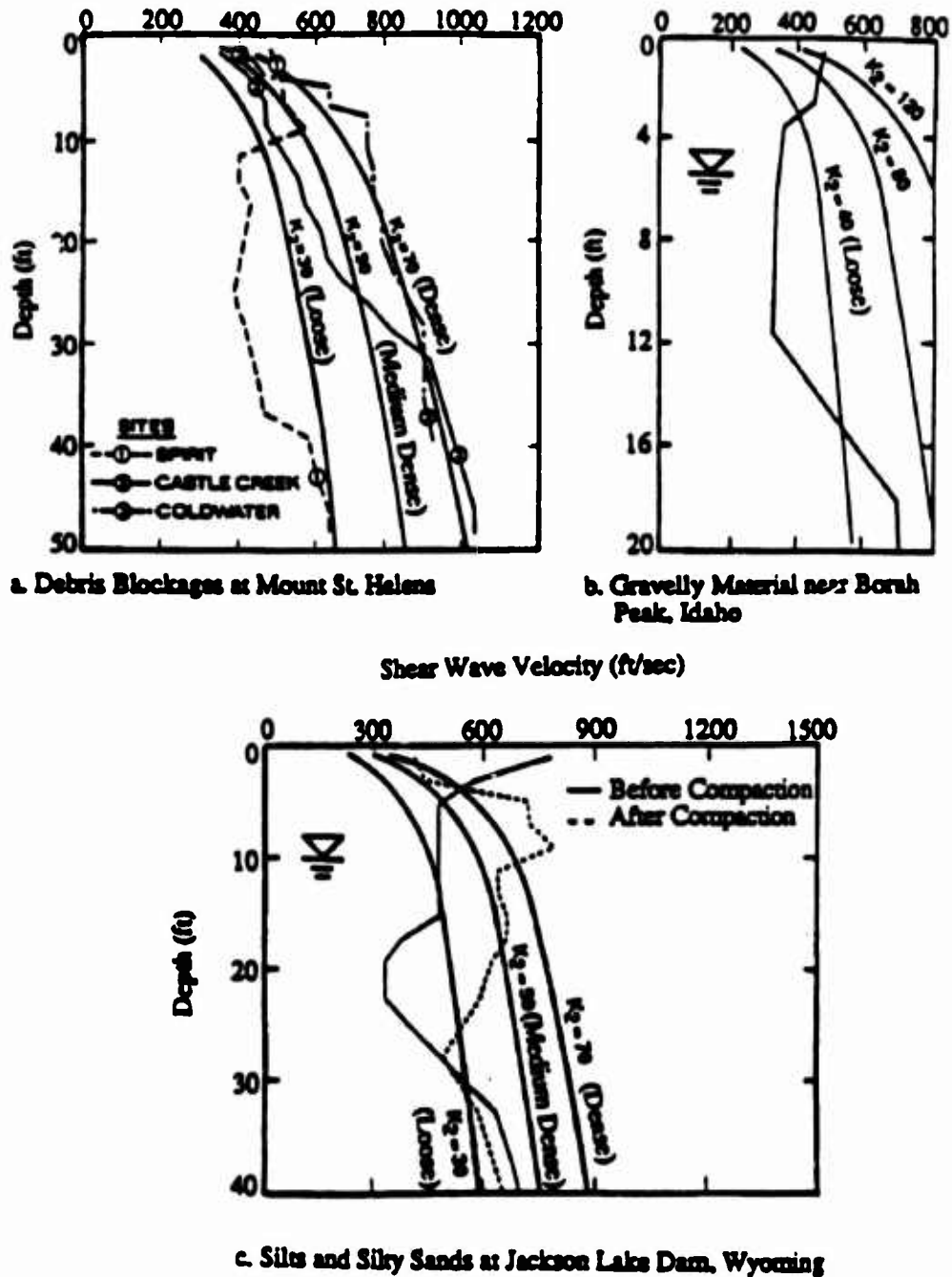


Figure 2.27 Qualitative Estimation of Densities Using Insitu and Empirical Shear Wave Velocities (Stokoe et al. 1988)
 Copyright ASCE - Reprinted with permission

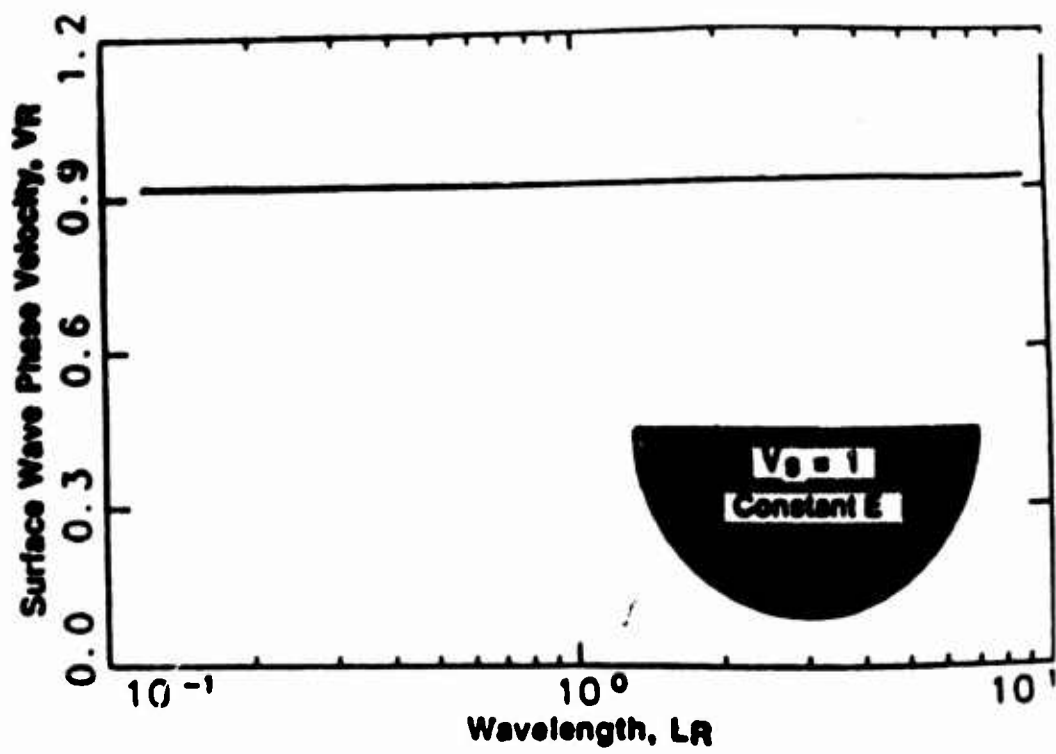


Figure 2.28 Dispersion Curve for Rayleigh Waves Propagating in a Uniform Half-space (Roesset et al. 1990)

wave propagation in a uniform half-space. In this figure, the surface wave phase velocity is independent of the wavelength because the section has uniform stiffness.

Figure 2.29 shows a dispersion curve for Rayleigh waves propagating in a soft over stiffer half-space. Notice that at short wavelengths, the surface wave phase velocity is equal to the value of the surface layer. As the wavelength increases, however, the surface velocity is effected by the stiffer material below and the averaging of the two layers results in a higher surface wave phase velocity. Figure 2.30 shows a stiff over soft half-space since the short wavelengths (high frequencies) have a higher surface wave phase velocity than the long wavelengths (low frequencies). This would simulate a base course over a subgrade. Roesset et al. (1990) suggests that since the short-wavelengths sample only the stiffness of the top layer, then the shear wave velocity, shear modulus, and Young's modulus of the top layer may be calculated using Equations 2.35, 2.36, and 2.37. In addition, Roesset et al. (1990) point out that using the critical wavelength shown in Figure 2.31, the thickness of the top layer may be estimated. Roessett et al. (1990) reported on the two pavement sections shown in Figures 2.32 and 2.33. Figure 2.32 shows a section with an average surface wave phase velocity of 4,500 ft/sec which translates into a Young's modulus of 2.8×10^8 psf. Roessett et al. (1990) conclude that this value

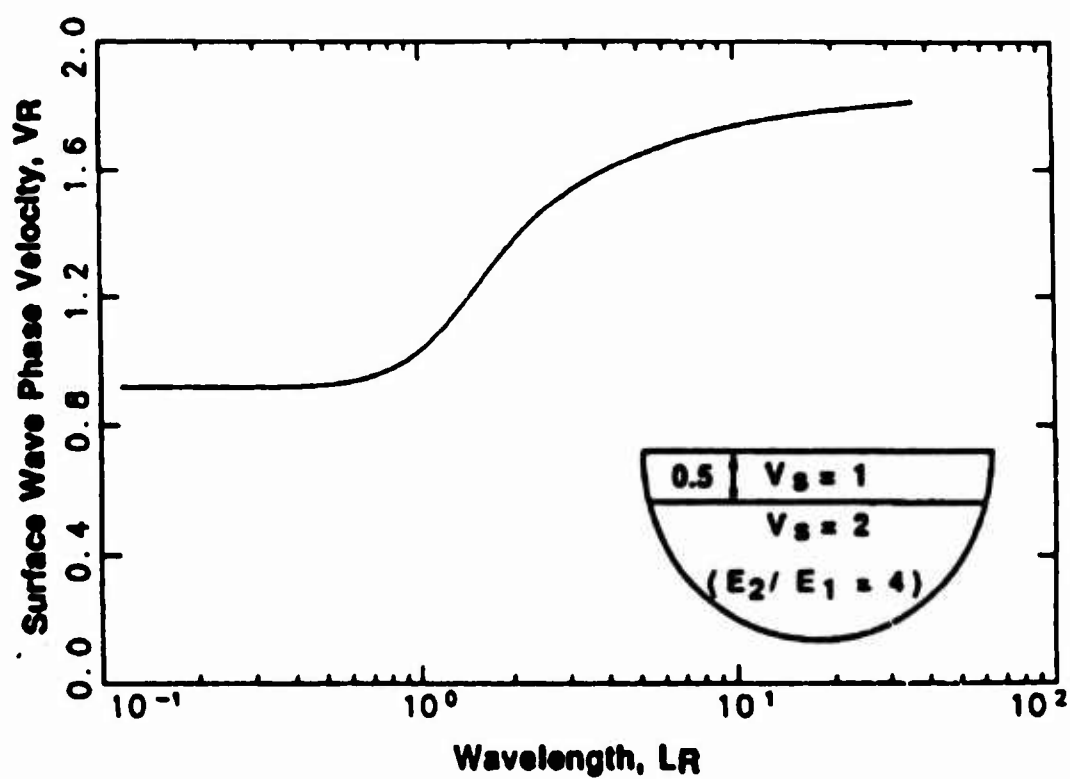


Figure 2.29 Dispersion Curve for Rayleigh Waves Propagating in a Softer Layer Over a Stiffer Half-space (Roesset et al. 1990)

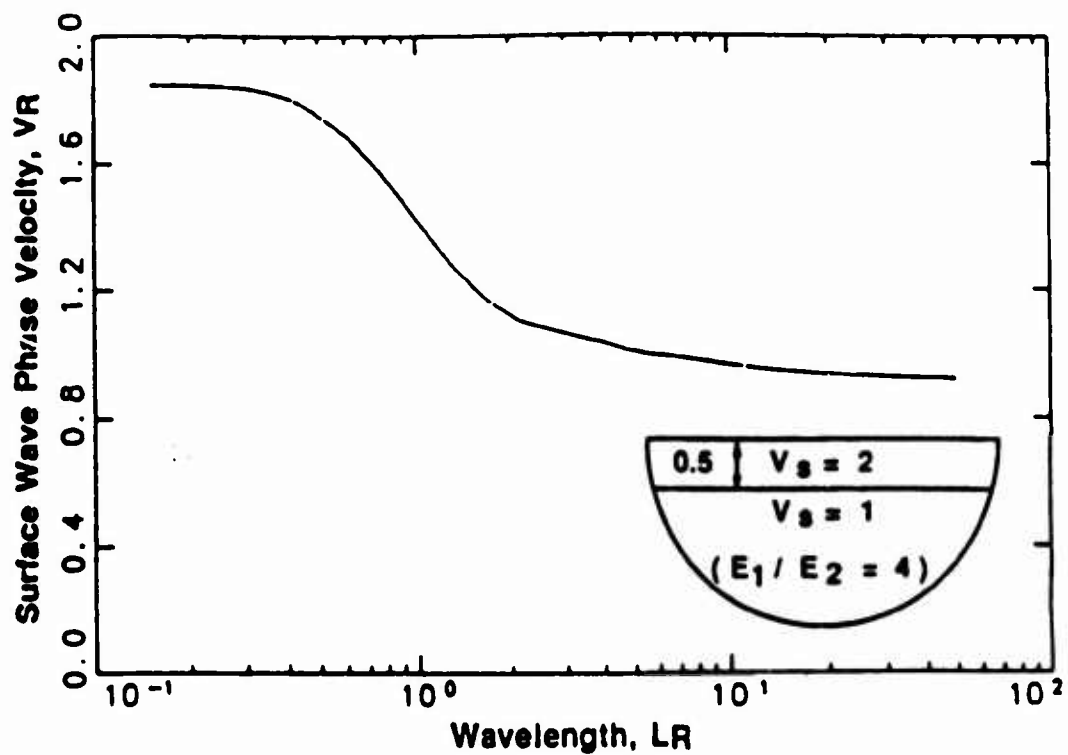


Figure 2.30 Dispersion Curve for Rayleigh Waves Propagating in a Stiffer Layer Over a Softer Half-space (Roesset et al. 1990)

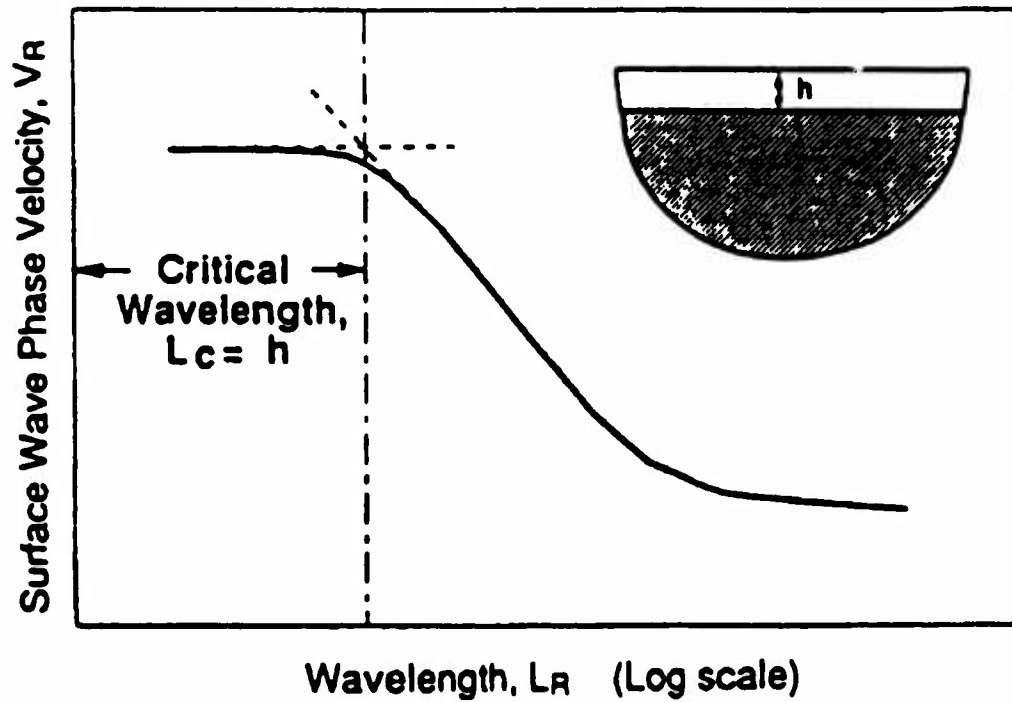


Figure 2.31 Determination of the Surface Layer Thickness from the Dispersion Curve for Rayleigh Waves (Roesset et al. 1990)

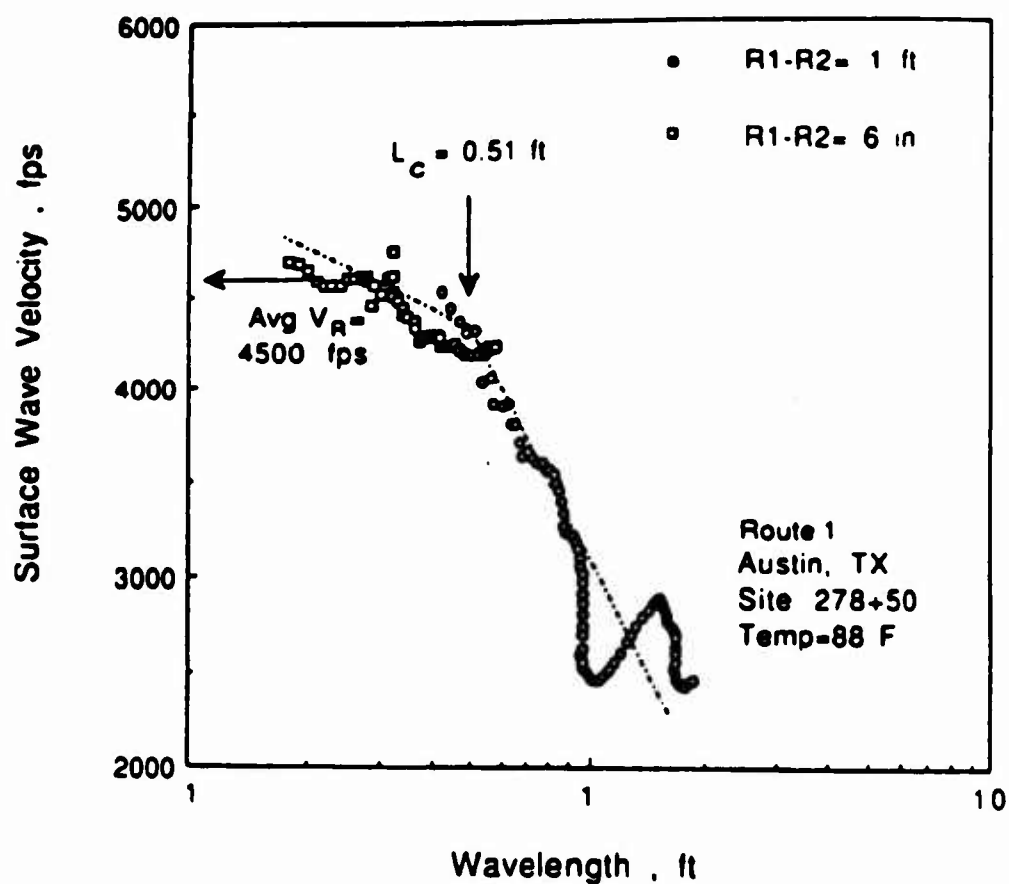


Figure 2.32 Dispersion Curve used to Determine Top Layer Thickness and Young's Modulus (Roesset et al. 1990)

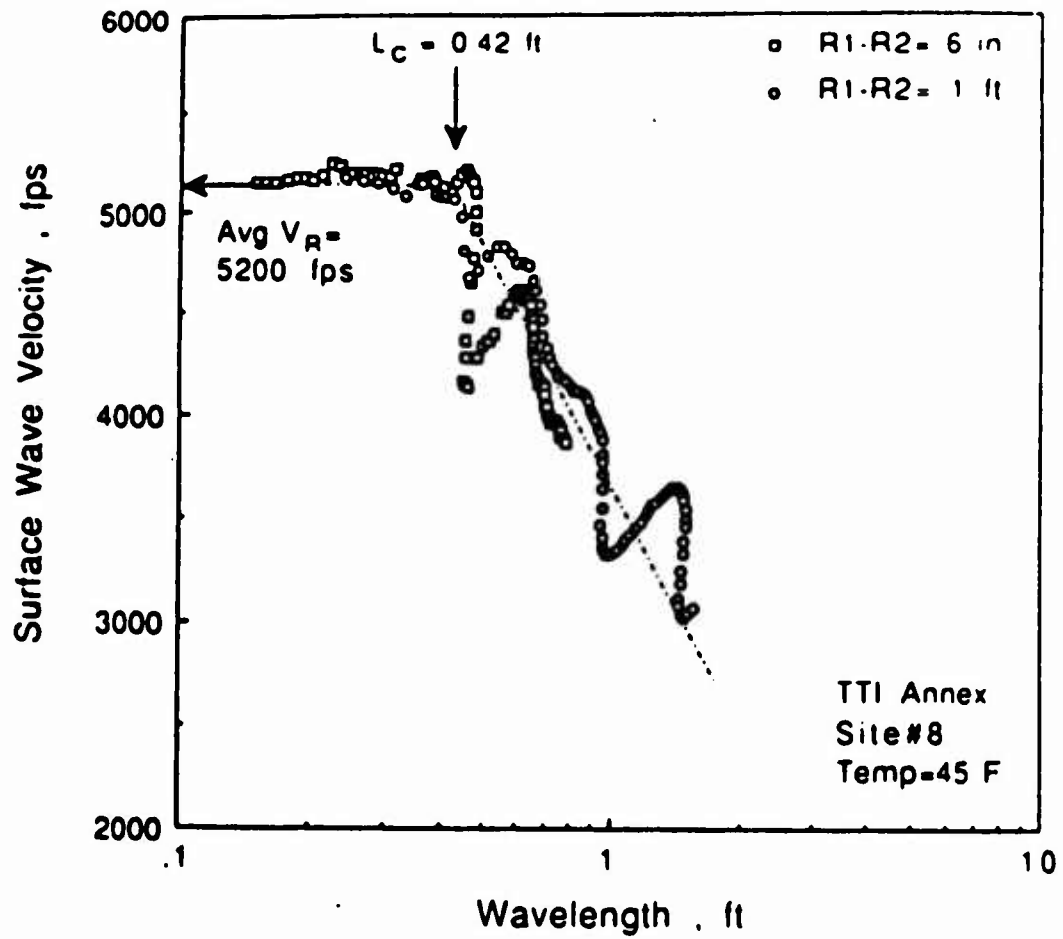


Figure 2.33 Dispersion Curve used to Determine Top Layer Thickness and Young's Modulus (Roesset et al. 1990)

is high because moduli measured at strain levels associated with seismic testing are maximum values. Also shown in Figure 2.32 is a prediction of top layer thickness of 6.12 inches as compared to cores of 6.96 inches, which compares reasonably well. Figure 2.33 shows similar data with a Young's modulus value of 2.7×10^6 psf and estimated surface layer thickness of 5.04 inches. The cored thickness was 5.04 inches also and compares very favorably.

It has been the intent of this chapter to provide the reader with the necessary background to logically follow and understand the research presented in the following chapters. This chapter has discussed basic airfield trafficability concepts, U.S.A.F. unsurfaced airfield evaluation techniques and seismic surveying using spectral analysis of surface waves. Chapter 3 will present the design and development of the Automated Airfield Dynamic Cone Penetrometer (AADCP).

CHAPTER 3
DEVELOPMENT AND DESCRIPTION OF THE AUTOMATED AIRFIELD
DYNAMIC CONE PENETROMETER (AADCP)

3.1 Introduction

The purpose of this chapter is to present the major phases of the AADCP prototype development. The chapter begins with the rationale used to select the penetration system, citing the various advantages and disadvantages of each system. The various prototypes developed are then presented. Each is discussed in detail and it is shown how it contributed to the final version. The chapter concludes with a detailed description of the final version of the AADCP equipment, including the penetration device and its auxiliary equipment.

3.2 Development and Selection of Testing System

3.2.1 Introduction

The first phase of this research project was to develop and design an alternative DCP testing system. Though the manual DCP has been used by the Air Force quite successfully for the last five years, it does have a single major drawback. It is extremely labor intensive and hence time

consuming. This was brought out in interviews with both the Combat Control School instructors and with the former AFESC Pavement Evaluation Team Chief. The Air Force therefore seeks an alternative testing procedure.

3.2.2 System Specifications

In discussions with the Air Force, the following list was created to identify system specifications. These specifications would enhance the DCP testing technology and would help provide a blueprint for any new DCP system. The most important system attributes are speed, mobility and repeatability of testing. Depending on the site conditions, the manual DCP can require up to 150 blows in one location. A second test is usually performed to ensure statistical accuracy and a third test is required if the number of blows of the first and second tests are not relatively close. In the worst case, a manual DCP test can last 12 minutes per penetration or 36 minutes per test location. With 20 test locations required over a 3500 foot unsurfaced airfield, the total time of testing for a two man crew could be 12 hours. Any significant decrease in testing time would lower the combat exposure of the airfield controllers.

The mobility of the instrument is important to the Air Force in that it must be able to be transported into various scenarios. The Air Force Combat Controllers, one of the main users of the DCP, have mission statements that require

the ability to airdrop in land or water, traverse mountainous terrain, and cross dessert terrain. The new instrument must be adaptable to these types of environments. In addition, the instrument should be as repeatable as the manual DCP to ensure consistent reliable results. It has previously been shown in Section 2.3.3.3 that the DCP is more reliable than the field CBR test which it was developed to duplicate. The new system should have the same characteristics.

Another important system attribute discussed with Air Force Combat Controllers was a total weight limitation. A practical limit was that each member of a two man team would carry 20 - 30 lbs. Ease of maintenance and a total research budget of \$10,000 were other Air Force constraints.

In addition to the above DCP testing enhancements, it was proposed to include some type of technology that would evaluate spatial variation of the unsurfaced runway. It was discussed that some kind of seismic non-destructive testing would be used. Chapter Four details the spectral analysis of surface waves technique which can provide useful soil information to evaluate the unsurfaced airfield.

Therefore an appropriate problem statement is to develop an unsurfaced airfield prototype device that would be less labor intensive than the currently used Dynamic Cone Penetrometer (DCP) test, as fast or faster to perform than the DCP test, and would have an associated non-destructive

testing component to evaluate non-test zones for spatial variation, while still providing accurate bearing capacity data.

3.2.3 Review of Current Technology

The purpose of a review of current test methods is to determine if an existing system or part thereof could be used to solve the problem statement. It was quite evident that any type of laboratory testing would be too time consuming and therefore not a viable option. A list of geotechnical insitu field testing devices was compiled to analyze their applicability. The list includes

- (a) Hand Cone Penetrometer
- (b) Electric Cone Penetrometer
- (c) Dilatometer
- (d) Plate Load Test
- (e) Screw Plate Test
- (f) Dynamic Cone Penetrometer
- (g) Standard Penetration Test
- (h) Seismic Testing
- (i) Electrical Resistivity

In review of this list, it became obvious that some are eliminated because of equipment size and logistics. In general, the tests requiring quasi-static penetration or static loading are eliminated, such as the electric cone, dilatometer, plate load, and screw plate tests, because of

the large reaction forces required. Hand-held penetrometers, such as the airfield cone penetrometer (ACP), discussed in section 2.3, can not be penetrated into some of the stiffer soils and have questionable reliability.

It was therefore decided that the device should be dynamic in form. The standard penetration test was rejected because the equipment is too heavy and bulky for mobility purposes. The manual DCP test described in Section 2.3.3, with its characteristics of manageable size and good penetration potential, has performed satisfactorily in the evaluation of unsurfaced airfields. It was therefore decided to direct the research effort towards producing an automated form of this test.

3.3 Prototype Development

This section describes the various prototypes developed over the course of the research. In general, each prototype developed tested different principles associated with the penetration system. The final version described in detail in Section 3.4, was simply a combination of the various designs.

3.3.1 Rod and Guide Mounted to an Air Piston

The first prototype consisted of a 40-inch penetration rod mounted to an air piston, Figure 3.1. One end of the penetration rod screwed directly into the piston rod while



Figure 3.1 Rod and Guide Mounted to an Air Piston

the other end fitted into a 5-inch guided rod-cone tip assembly. The cone tip is the same as used in the manual DCP with a sixty degree apex and a 20 mm cross section diameter. A vertical stanchion was used to guide the system into the ground. The 40-inch rod was lifted and driven down by air pressure. The rod struck the guide to advance the cone tip.

Preliminary testing showed that the penetration rod which carried the weight of the piston apparatus did not move. The movement came from the air piston rising and falling with each blow. Consequently, the cone tip could not penetrate.

It became obvious that the prototype required a locking device at the vertical stanchion to hold the weight of the air piston while the penetration rod was retracted away from the cone tip. Once the retraction occurred, the return blow could then strike the cone tip. The locking device could release its hold on the air piston at the time of the blow, allowing the entire system to penetrate. The locking device solution was difficult to develop. Ideas such as pneumatic locking pins and pneumatic air grippers were discussed. No solution was completely satisfactory and therefore the locking device was put on hold until an alternative solution could be designed. However, the idea of a rod striking inside a cone tip led to the inner-outer rod system used in Section 3.3.4.

3.3.2 Rotary Hammer

An alternative solution to the rod and guide assembly mounted to an air piston was the rotary hammer approach, Figure 3.2. A rotary hammer uses a small cam to propel a horizontal impactor which strikes a penetration rod. The penetration rod is forced through the medium at very high vibratory speeds. An electric-powered rotary hammer was mounted to a vertical stanchion to penetrate in the vertical direction Figure 3.2. The plan was to slow down the blow rate to 1 or 2 per second (60-120 bpm) and record how long it took to penetrate particular depths. Knowing the time taken and the frequency of the hammer, the number of blows required to penetrate each layer could be calculated. In addition, penetration versus time could be plotted to yield an inches per blow value, equivalent to the DCP value. The advantages of using a rotary hammer were its unique capability of driving a rod through the stiffest materials in a relatively short period of time. A 40-inch rod was machined to fit a Ryobi rotary hammer. An attempt was made to verify the manufacturers claim of 3750 blows per minute (bpm). Using an oscilloscope in the soils lab, sixty blows per minute was measured as opposed to the manufacturers claim of more than six times that number. Field tests proved very successful. The device easily penetrated the stiffest of materials, including asphalt. Efforts were made to buy a variable rate gas-powered rotary

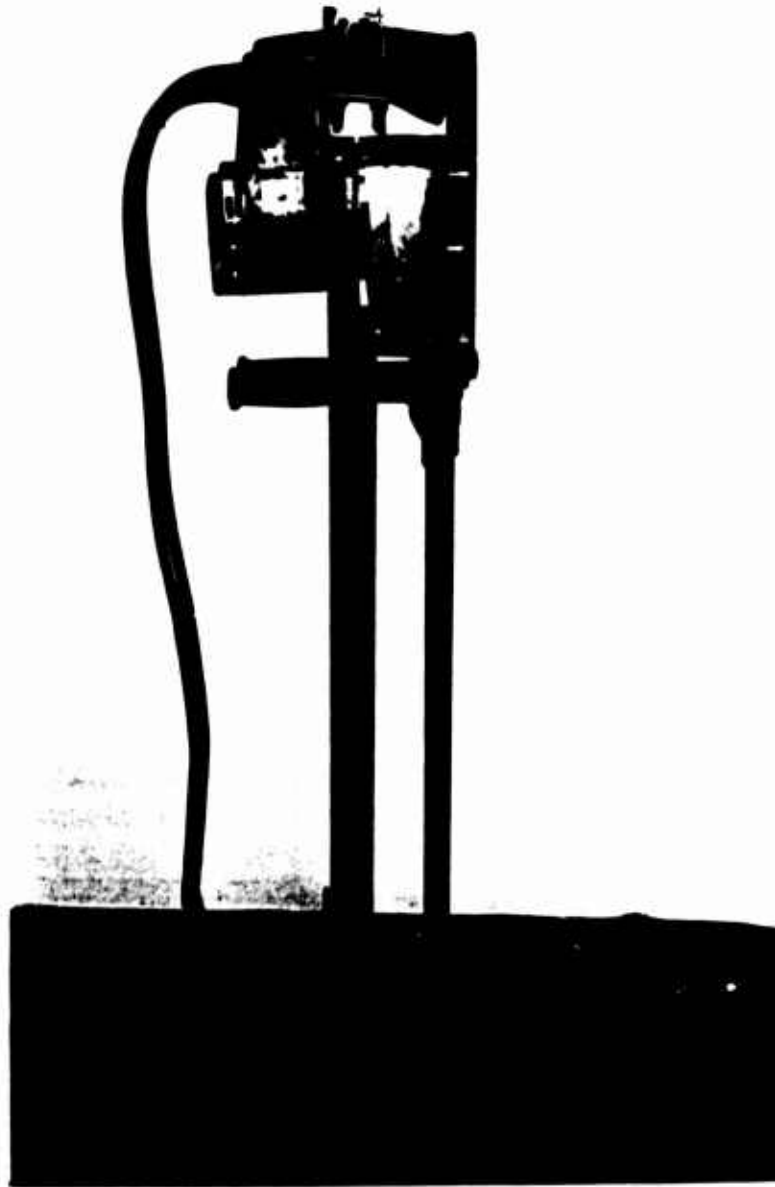


Figure 3.2 Rotary Hammer

hammer. This would have provided independence from an electrical source and the possibility of slowing the bpm rate down to around 40 bpm. However, no such piece of equipment could be found. With further inspection of this system, the contribution to penetration of the tremendous vibrations on the rod became an area of concern. It was concluded that the manual DCP had a different type penetration than the vibrating rotary hammer and that the hammer did not model the manual DCP energy impact well enough to warrant continued effort in this direction.

The Ryobi rotary hammer prototype was not successful. However, this prototype led to the purchase of a variable speed gas-powered reciprocating saw. It was anticipated that the back and forth motion of this saw would produce a penetration similar to that of the rotary hammer, and it had the advantage of being variable speed and gas powered. Unfortunately, when a penetration rod was retro-fitted to the saw and field tested, the saw was not built ruggedly enough to withstand the vibrations of penetration.

3.3.3 Cam Operated Lift and Drop Mechanism

An entirely new concept was conceived based on a cam and roller assembly. This prototype provides the potential energy of a manual DCP, 398 in-lbs (17.6 lb weight dropping 22.6 inches), by using a spring-mass system. The potential energy of a spring-mass system is:

$$PE = [(1/2)(K)(X^2)] + [(W)(X)] \quad (3.1)$$

where

PE = potential energy

K = spring constant

X = compression of spring

W = weight

Consequently, a 2 lb penetration rod raised 3 inches by a 90 lb/in spring produces 411 in-lbs of potential energy which is very close to the energy of a manual DCP.

$$\begin{aligned} PE &= 1/2 K X^2 + W x \\ &= (1/2)(90)(3^2) + (2)(3) \\ &= 411 \text{ in-lbs} \end{aligned}$$

This prototype used a hand crank and cam to compress a spring attached to a penetration rod, Figure 3.3. Once the cam reached its release point the spring was uncoiled and caused the rod to strike against the cone tip. Two methods were used to rotate the cam, a hand turned version and a 1/2-inch drill version. Both methods were successful in penetration, however, the drill version required some type of electrical power source. Preliminary penetration results demonstrated that the spring and rod assembly provided an effective means of driving a rod into the ground while monitoring the penetrations per blow. The spring-mass system used in this particular design represented a major breakthrough in the project. The idea of replacing the force of a falling weight with that of a spring was pursued



Figure 3.3 Cam Operated Lift and Drop Mechanism

in each of the subsequent prototypes. However, because a major thrust of the project was to automate the DCP and because of the lack of electricity in the field, a new lifting mechanism was required. The following two sections describe the attempts made in this direction.

3.3.4 Chain Driven Lifting-Drop Mechanism

The idea for a gas-powered chain driven lifting-drop mechanism came from the Marshall mix design equipment, in which a drop hammer is lifted by a chain rotating on gears. A chain lifting mechanism was utilized in this project as shown in Figure 3.4. A gas powered reciprocating saw engine was used to drive a bicycle chain which had lifting prongs attached to its links. The lifting prongs caught a roll pin placed in the vertical rod-spring assembly and compressed the spring. When the lifting prongs reached the top of the upper gear, the spring and mass were released to strike.

One of the new design features in this prototype was an inner hammer and outer penetration rod system. The lifting prongs actually lifted an inner hammer rod that slid down through an outer penetration rod. The impact load was taken at the cone tip and not at the top of the penetration rod. This allowed the striking motion of the inner rod to move independently from the outer rod which rigidly supported the weight of the entire penetrating system. This inner and outer rod system solved the problem mentioned in Section



Figure 3.4 Chain Driven Lifting-Drop Mechanism

3.3.1. where a locking device was necessary.

Testing showed that the gas-powered motor rotated the gear and chain at an unsafe rate. It was discovered that the variable speed motor required at least 750 rpm's to engage the clutch. To compensate, additional gears were designed to accommodate the speed of the motor and it was found that an 8-inch gear was required. Due to geometric space constrictions, the gas-powered chain motor lifting mechanism was no longer pursued. However, the inner-outer rod system and the spring-mass system were carried over to the next prototype.

3.3.5 Air Piston-Spring Lift and Drop Mechanism

At this time, it was decided to return to the original idea of using an air piston, however, not to drive the penetration rod but to compress the spring, see Figure 3.5. The air piston was mounted to the top of the spring-rod assembly and used as the lifting force. The system, when tested, showed that it was possible to drive a rod into the ground and therefore worthy of some fine tuning efforts.

A second air piston prototype, Figure 3.6, was manufactured out of aluminum and included an inner/outer rod-spring assembly, vertical stanchion, portable air compressor, air tank, double solenoid air valve, quick release exhaust valves, and a 12 VDC battery. The system works as follows. First, air is inserted into the cylinder



Figure 3.5 Air Piston-Spring Lift and Drop Mechanism

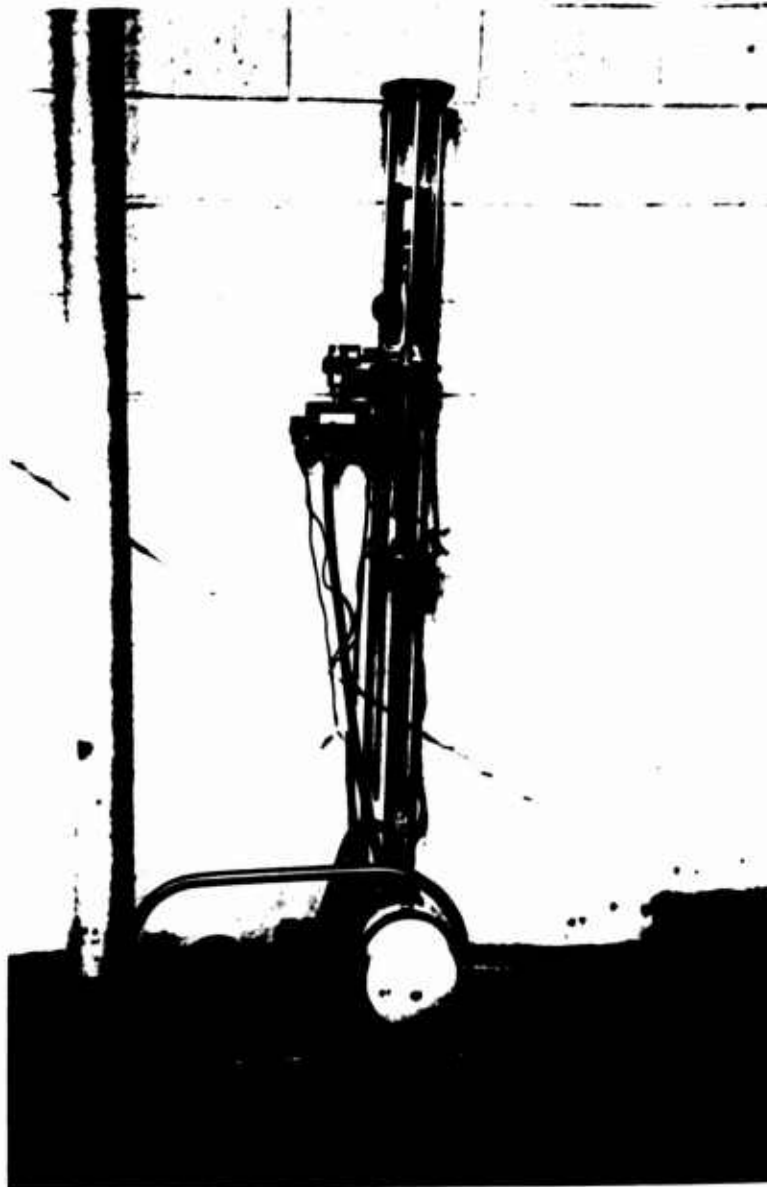


Figure 3.6 Automated Air Piston-Spring Lift and Drop Mechanism

to lift the piston. When the piston, which has a magnet attached, moves up to the top position switch, the switch is magnetically closed. This sends a signal to the 3-way solenoid valve to cease providing air and to exhaust the pressurized cylinder air out through the quick exhaust valves. "Instantly" the air is released and the attached spring drives the inner rod down onto the cone tip. Once the cone tip begins penetration, the entire driving mechanism is lowered because it is rigidly attached to the outer penetration rod. The lower position switch is then triggered as the magnetic piston moves by this sensor and the air begins to again lift the piston.

It was from this basic air piston lifting design that the automated airfield dynamic cone penetrometer was built. Numerous modifications and tests have been performed with the goal of matching the driving energy and the repeatability of the manual DCP. In order to match the penetration index (inches per blow) of the manual DCP, an energy analysis of the system was necessary. As noted in Section 2.3, the DCP has an 17.6 lb weight dropping 22.6 inches which provides about 400 in-lbs of potential energy. In order to store 400 in-lbs of potential energy in the AADCP, the spring and rod weight would have to be chosen carefully. Table 3.1 provides of list of possible combinations which could be used to satisfy the potential energy requirement. In addition, a reaction force necessary

Table 3.1 Potential Energy Calculations of Various Strokes

DCP = 17.6 * 22.4 = 394.24 IN*LBS			
PE = [1/2 * K * X^2] + [W * X]			
K (LBS/IN)	X (INCHES)	PE (IN*LBS)	UPLIFT (LBS)
79900.0	0.1	400	7990
19950.0	0.2	400	3990
8855.6	0.3	400	2657
4975.0	0.4	400	1990
3180.0	0.5	400	1590
2205.6	0.6	400	1323
1618.4	0.7	400	1133
1237.5	0.8	400	990
976.5	0.9	400	879
790.0	1	400	790
195.0	2	400	390
85.6	3	400	257
47.5	4	400	190
30.0	5	400	150
20.6	6	400	123
14.9	7	400	104
11.3	8	400	90
8.8	9	400	79
7.0	10	400	70
5.7	11	400	63
4.7	12	400	57
4.0	13	400	52
3.4	14	400	47
2.9	15	400	43
2.5	16	400	40
2.2	17	400	37
1.9	18	400	34
1.7	19	400	32
1.5	20	400	30

to stabilize the spring when released is also shown. Various size spring were tested for efficient penetration with the 280 lb/in spring being most suitable. The required compression for this spring is just 1.5 inches. Other factors which were evaluated when selecting the spring were the spring constant vs required air pressure to lift, volume of air pressure required, and rate of air exhausting.

3.3.6 Modifications of the Basic AADCP Design

3.3.6.1 Introduction

After preliminary field testing of the basic design of the AADCP it was discovered that the instrument was requiring considerably more blows per inch than the manual DCP. Several design modifications were made to solve this problem.

3.3.6.2 Air Exhaustion

The first problem was that the air was not exhausting fast enough. This meant that the piston and spring were slowed on the down stroke and prevented from impacting the cone tip with the desired force. The solution to this problem was to first shorten the stroke length. With a shorter stroke length less volume of air was required and therefore less time to get the air out of the piston on the down stroke. To complement the shorter stroke length, the three-way air valve and the quick release valve were moved

as close to the air cylinder as possible. Close nipples were used to thread the quick release valve into the cylinder and thread the three-way solenoid valve into the quick release valve. Since the stroke was shortened, the spring constant had to be increased from 10 lbs/inch with a 9 inch stroke to 385 lbs/inch and a 1.5 inch stroke. A further solution to the problem of air not escaping fast enough was to increase the number of quick release valves and increase the size of the valve opening. Originally, a single 3/8" diameter quick release valve was used to exhaust the air. However, a significant increase in the penetration index (inches/blow) resulted when three 3/8" quick release valves were used and an even greater improvement occurred when one 3/4" quick release valve was used. There was no significant change when three 3/4" quick release valves were used. To accommodate a single 3/4" valve, a new base to the air cylinder was designed for optimum air flow.

A final modification was to pressurize the top of the cylinder. This places pressure on the top side of the piston and assists on the down stroke. This had some positive effect on the penetration efficiency. A spinoff of this solution was to drill several holes in the top of the air cylinder. This allowed the piston to drop more easily on the down stroke and avoid any suction resistance on the top side. In general, this modification was easier and more practical to maintain than pressurizing the top cylinder and

therefore was chosen. The combination of a single 3/4" quick release valve connected directly to the air cylinder, a three way solenoid valve threaded into the quick release valve, using a one to two inch stroke, and a fully opened top cylinder provided the lowest air resistance possible.

3.3.6.3 Spring Reaction Force

It was observed that the force of impact increased tremendously when the previous sections modifications were implemented. However, the relatively large impact created another problem. During preliminary field testing, a relatively large rebound force lifted the testing instrument off the ground. It was deduced that the spring required a reaction to push against in order to release its energy in the downward direction. In an effort to provide a spring reaction, a specially designed one-way gripper was mounted to the penetration rod, Figure 3.7.

The idea behind the one-way gripper was to allow the penetration rod to drive in the downward direction but not rebound in the upward direction. The gripper consisted of a post-tensioning chuck. The chuck had special inclined gripper teeth set inside a narrow barrel that allowed penetration in one direction but locked tight against the rod if movement occurred in the opposite direction. Once the rod was successfully prevented from lifting up, the force was carried through the chuck's threads and was

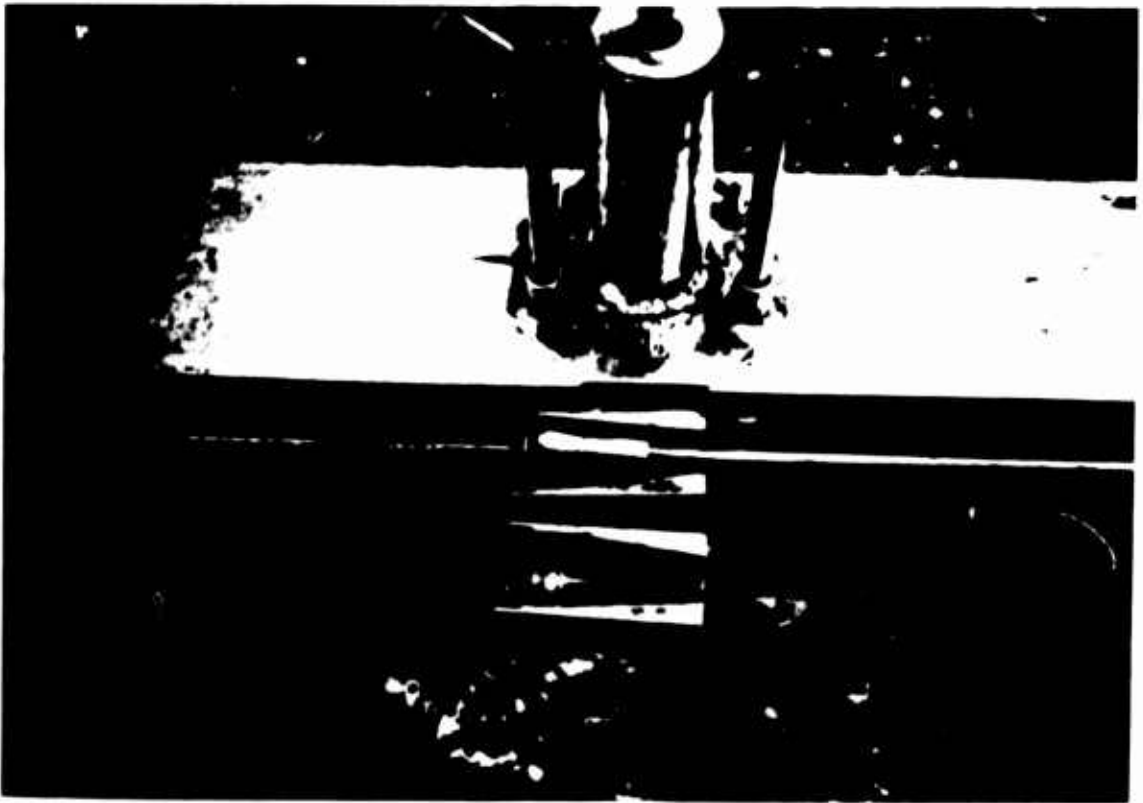


Figure 3.7 One-Way Gripper

resisted by the two operators standing on a platform threaded to the post-tensioning chuck. In field testing of the gripper, the penetration rod was successfully prevented from lifting in the upward direction. However, the post-tensioning gripper scarred the penetration rod to a point that after several tests the rod no longer fit snugly inside the gripper teeth. It was decided that this approach to preventing rebound was not a possible long-term solution.

3.3.6.4 Penetration Rod Modifications

The original AADCP rod and cone diameters were 16 and 20 mm respectively with a 60 degree tip. In an effort to increase the penetration efficiency of the AADCP, the rod and cone diameter were reduced to 12.7 mm and 16 mm respectively. The cone tip was also changed to 30 degrees. In addition, the hammer impact location was changed by replacing the inner-outer rod system with a single solid penetration rod system.

It was apparent, after informal testing, that the decrease in diameter of the cone and the rod and the change in impact location had a small but positive effect on the penetration efficiency. The number of blows per inch were reduced from 18 to 12.

It was suggested that the driving of the penetration rod depends on the ratio of the mass of the hammer to the mass of the penetration rod. Bowles suggests a ratio of 0.5

to 1.0 for a single-acting pile driver (Bowles 1990). It became obvious that the goal was to increase the mass of the hammer and decrease the mass of the penetration rod. However, in the current AADCP model, the piston, spring, and accessories were all welded to the penetration rod and therefore must be included in its mass. To correct this problem the penetration rod was modified to allow the rod to separate from the piston assembly after each blow. This was accomplished by allowing the instrument to rest on top of a collar which was attached to the outside cylinder, Figure 3.8. When the blow struck, the penetration rod separated from the instrument and penetrated into the ground alone. Field testing showed a dramatic increase in penetration efficiency. The previous relative penetration index was decreased from 18 blows per inch to 6 blows per inch. The manual DCP averaged approximately one to two blows per inch.

It was evident that the increase in hammer mass, the decrease in rod diameter and cone apex, and the decoupling of the instrument mass from the penetration rod mass made a dramatic increase in penetration efficiency. It was decided to return the rod and cone dimensions to those of the manual DCP to better compare the two instruments, even though a loss in penetration efficiency was possible.

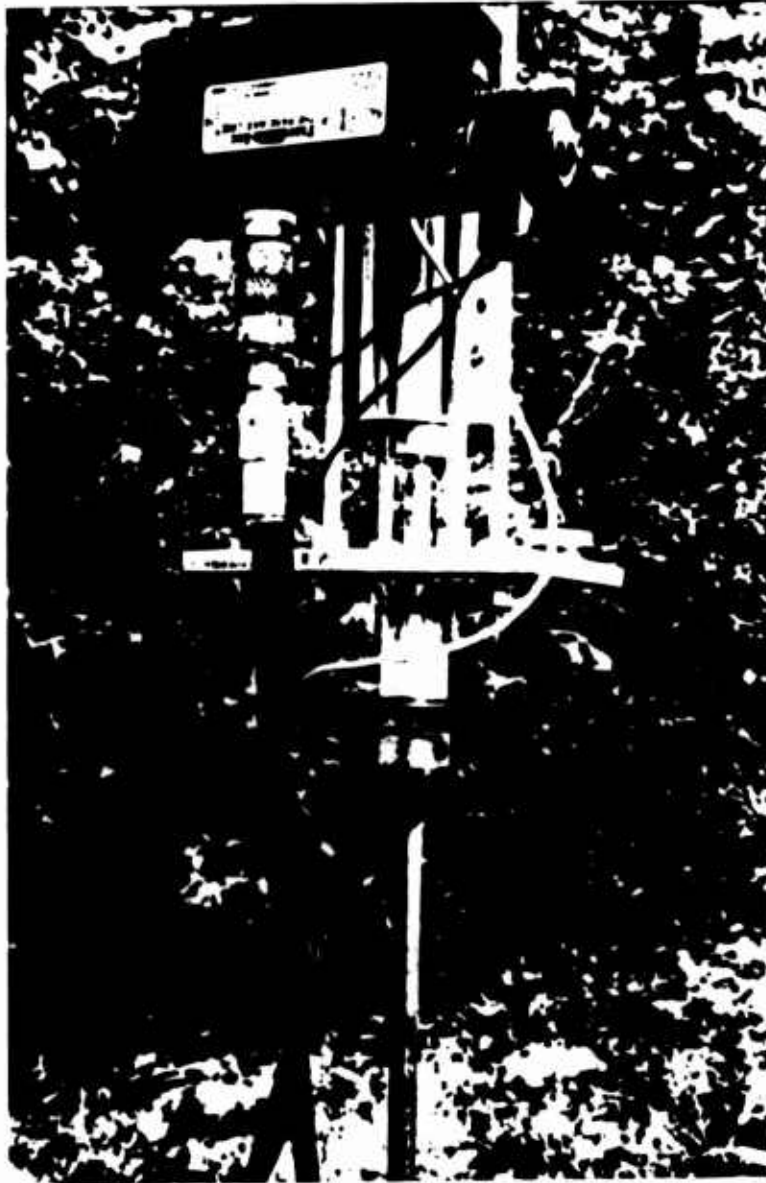


Figure 3.8 Modified Solid Penetration Rod with Decoupling of Instrument and Penetration Rod

3.4 Description of the Automated Airfield Dynamic Cone Penetrometer (AADCP)

3.4.1 Introduction

The purpose of this section is to provide a complete description of the final version of the Automated Airfield Dynamic Cone Penetrometer (AADCP). The AADCP is composed of three basic components, the penetration system, the control system and the power system. The AADCP is shown in Figure 3.9. The penetration system consists of the penetration rod, cone tip, anvil, pneumatic air cylinder and piston, hammer, compression spring, counter weight and quick exhaust valve. The control system includes the piston position switch, the double solenoid air valve, the trigger switch, the vertical tape measuring rod, and the digital counter. The power system consists of the gas powered motor, air compressor, air tank, and 12 volt DC battery.

In general, the AADCP works somewhat like a single acting pile driver. The AADCP requires two operators with one person reading the measuring rod and the other operating the trigger switch. Testing begins by an operator turning the toggle switch to the "on" position which allows air to flow into the cylinder, Figure 3.10. Notice in Figure 3.10 that the toggle switch has a lead to the positive side of the battery and one to the fill side of the solenoid. The air, supplied by an adjacent air compressor to port 1, travels through the fill side of the directional control valve from port 1 to port 2. Port 2 is directly connected



Figure 3.9 General View of the Automated
Airfield Dynamic Cone Penetrometer

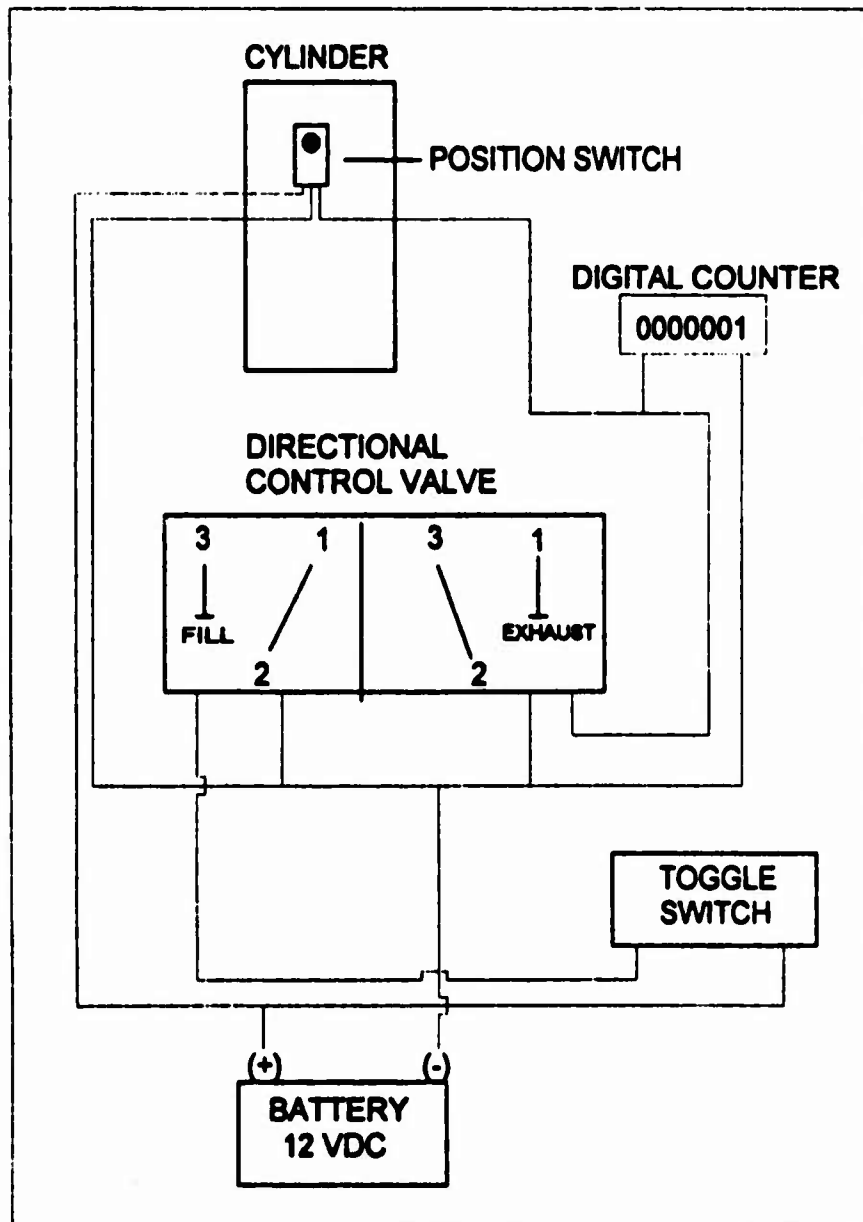


Figure 3.10 General Flow of AADCP Operation

to the air cylinder and acts as a pivot point for air to fill and exhaust the cylinder. Notice that when it is time to exhaust the air that port 2 pivots and is now connected with port 3 on the exhaust side of the directional control valve. As the 90 psi pressurized air fills the cylinder, the piston is raised approximately two inches. The air overcomes the resistance of both the hammer mass and the 285 lb/in spring. Generally, 90 psi of air pressure is required to raise the piston two inches. Once the piston reaches the top of the stroke, a magnet attached to the piston, triggers the position switch mounted on the outside of the cylinder. The position switch then sends a signal to the exhaust side of the directional control valve to stop the air flow into the cylinder and to exhaust this air. Notice in Figure 3.10, the position switch has three leads with two of them connected to the battery terminals. The third lead is connected to the exhaust side of the directional control valve. Immediately, the piston is driven down by the spring and mass of the hammer and strikes the anvil which is rigidly connected to the penetration rod. The trigger operator starts the process again by moving the toggle switch back to the "on" position. This is the basic operation of the AADCP. The following sections describe the various functions of the AADCP in more detail.

3.4.2 Penetration System

The penetration system consists of the penetration rod, the cone tip, the anvil, the hammer, the pneumatic air cylinder, the compression spring, the counter weight and the quick exhaust valve. The penetration steel rod has a diameter of 16 mm and can penetrate to a depth of 36 inches. The hardened steel cone tip, which is threaded to the penetration rod, has a diameter of 20 mm and a 60 degree cone apex. The air cylinder has a 2.5 inch diameter piston that has a 10 inch stroke capability with no attached mass, Figure 3.11. Notice in Figure 3.11 that an 11 lb mass is mounted to the piston rod. This leaves a maximum of two inches in stroke. The compression spring is mounted inside the piston with teflon guide rings used to stabilize the spring. The spring rests on top of the piston and pushes against the top of the cylinder when compressed. The operating air pressure is approximately 90 psi. A 20 lb weight, shown in Figure 3.9 is used to counter the large rebound force from the compression spring.

One of the key elements of the penetration system is the quick exhaust valve, Figure 3.12(a). This valve is used to expel the air inside the cylinder as quickly as possible. As previously mentioned, once the position switch triggers the exhaust side of the directional control valve, the air into the cylinder is cutoff, port 1 closed, and the air begins to exhaust from port 2 to port 3 through the

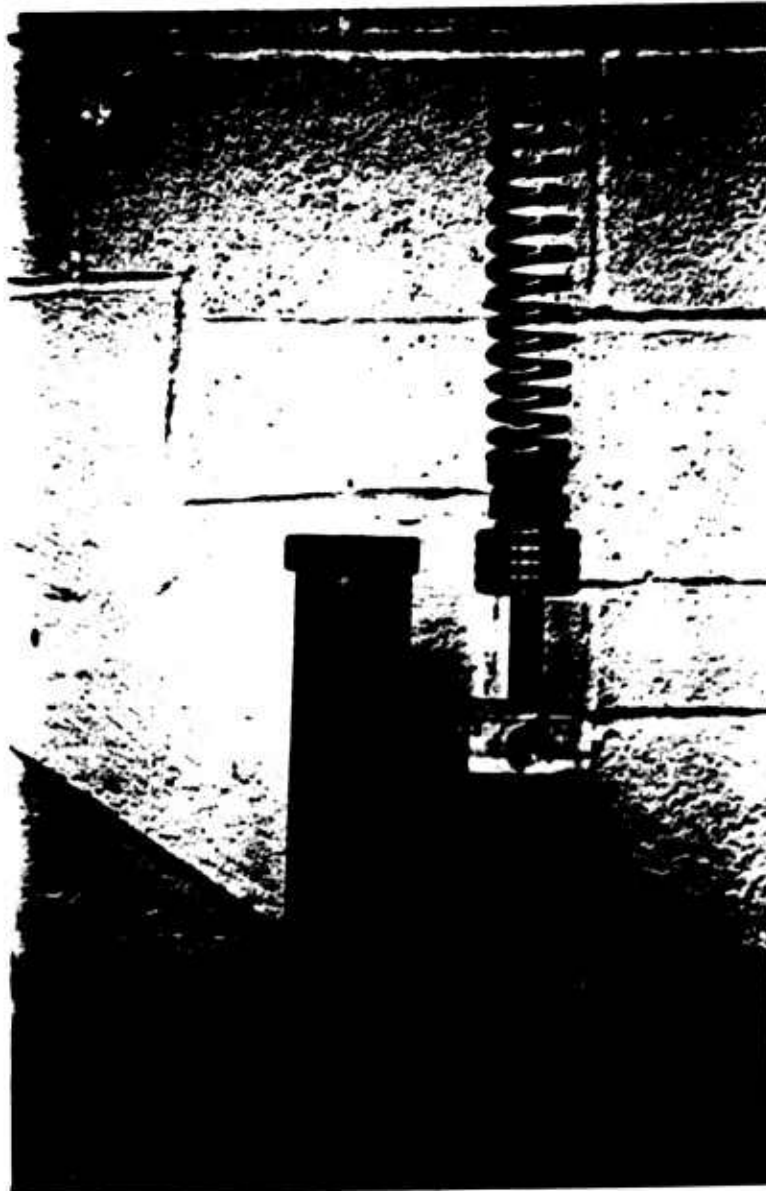
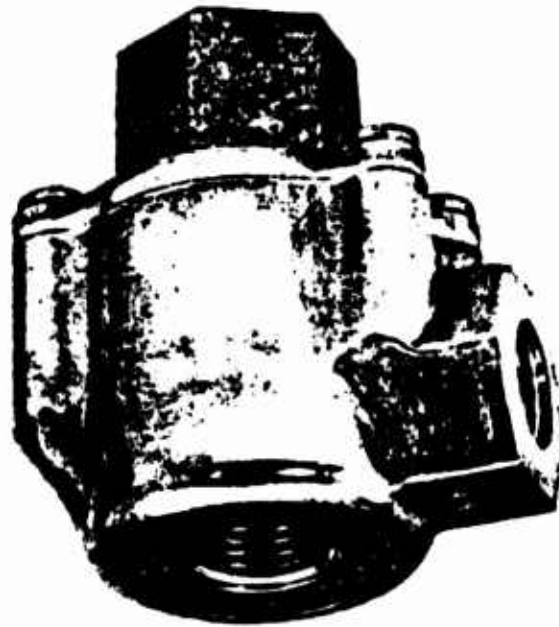
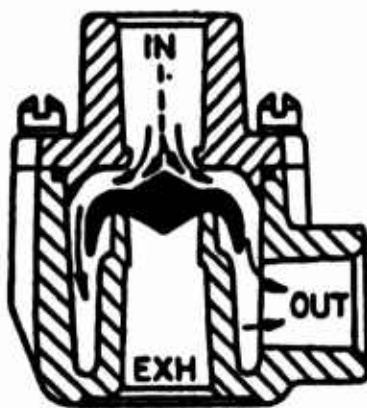


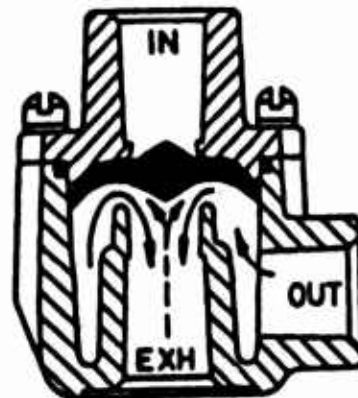
Figure 3.11 Air Cylinder, Piston and Compression Spring



A



B



C

Figure 3.12 Quick Exhaust Valve

directional control valve. Since the openings inside the directional control valve are relatively small, the air does not escape fast enough through the valve. However, the drop in pressure from the directional control valve creates a backpressure on the quick exhaust valve diaphragm which "instantly" dumps the air out of its large 3/4" exhaust port, Figure 3.12(c). Figure 3.12(b) shows the filling of the air cylinder through the exhaust valve while Figure 3.12(c) shows the air exhausting out the valve. Notice the pressure of the in-coming air forces the diaphragm to block the exhaust port during filling and the backpressure causes the diaphragm to seal the "in" port during the exhaustion phase.

3.4.3 Control System

The control system consists of the piston position switch, the directional control valve, the toggle switch, the digital blow counter, and the vertical tape measure. The purpose of the control system is to direct the air flow into and out of the cylinder. When the piston is at the bottom (striking) position, high pressure air flows through the normally open solenoid valve into the quick exhaust valve and then into the cylinder. The piston rises and eventually aligns with the top position switch. The top position switch is a magnetic operated switch that is activated when the piston travels near its position. The

magnet, mounted in the piston, closes the top position switch which sends a 12 VDC impulse to the solenoid valve. The solenoid valve then ceases the flow of air into the piston and forces the air to escape through its exhaust port.

The other control components are the trigger switch and the digital blow counter. The trigger switch is used to pulse the fill side of the directional control valve as discussed in the previous section. The digital blow counter is activated by the impulse from the position switch. Each time the piston rises to the top position, the counter is pulsed. A measuring rod, divided into tenths of an inch, is used to measure the penetration.

3.4.4 Power System

The power system includes the gas powered motor, air compressor, air tank, and 12 volt DC battery. A light-weight gas powered motor ideally should run the air compressor. However, the focus of this research was to design and develop a penetration system. It was decided that an electric air compressor run by a gas powered generator would suffice to supply the 90 psi air pressure. A 12 volt DC battery was used to power the solenoids, digital blow counter and the position switches.

An alternative power method was evaluated to lower the total weight of the power equipment. Light weight

high pressure aluminum air tanks were investigated for possible use to replace the gas powered motor and air compressor. The high pressure cylinders were rated in the range of 1800 to 3000 psi.

The typical unsurfaced landing strip for a C-130 is 3500 feet long and 60 feet wide. Based on manual DCP testing, one test location might require 150 blows. With an average of 20 tests per landing site, the required number of blows per landing strip is 3000. Since the air cylinder is 2.5 inches diameter and the piston stroke is a maximum of three inches, the volume of air required per blow is 0.0085 cubic feet. The total required air volume is then 25 cubic feet at 100 psi.

The available high pressure cylinder can provide 0.077 cubic feet at 3000 psi and which equates into 2.2 cubic feet of compressed air at 100 psi. This translates into requiring 12 high pressure air cylinders which weigh 6.5 lbs each. Therefore it was concluded that the high pressure air cylinder was not an acceptable option for providing air pressure to the penetration system.

CHAPTER 4

SPECTRAL ANALYSIS OF SURFACE WAVE EQUIPMENT

4.1 Introduction

An important parameter which can be used to predict the behavior of a soil skeleton is the shear modulus. Geotechnical engineers often use seismic methods to obtain a measure of the shear modulus. They measure the velocity of a shear wave passing through a material and then relate this to the shear modulus by a fundamental relationship. The most common methods of shear wave velocity measurement are the crosshole and downhole methods. However, these methods require either boreholes or that probes be placed in the ground. This is time consuming, expensive, and, depending on site conditions, may be difficult to accomplish.

A relatively new seismic method, known as the Spectral Analysis of Surface Waves (SASW), is an alternative method which uses no intrusive procedures, Figure 4.1. A vertical load is applied to the ground and surface waves are monitored by receivers placed on the ground surface at various distances apart from each other. A digital signal analyzer, microcomputer, and SASW software are used to collect, sort and analyze the signals and run an

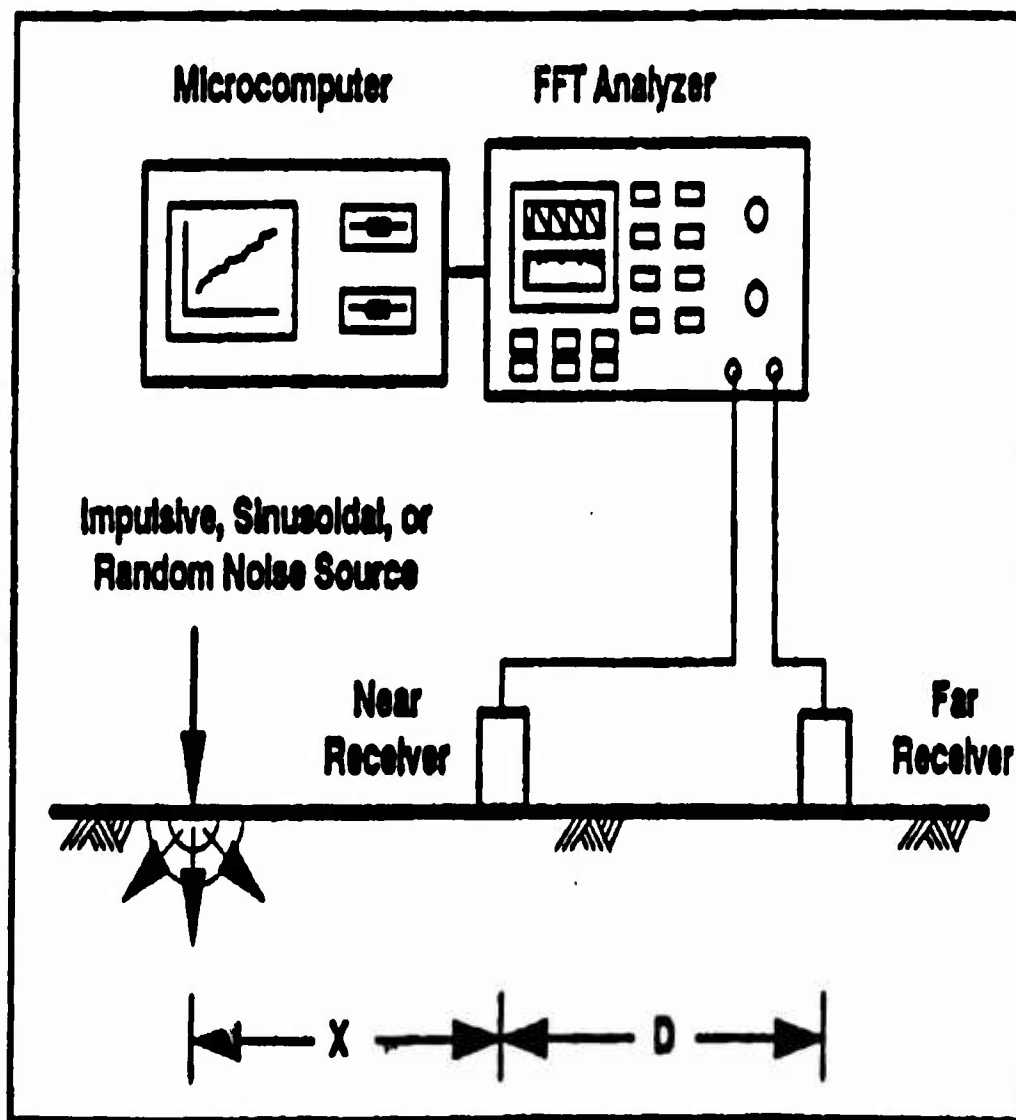


Figure 4.1 Source-Receiver Configuration of SASW Equipment

inversion program that produces a shear wave velocity and shear modulus profile.

The SASW method is described in detail in Chapter Two's literature review, Section 2.4. This chapter will concentrate on describing the equipment used in this research to run the SASW test method. It includes a discussion on the digital signal analyzer, signal receivers and impact source. The SASW research was carried out with equipment bought by the Florida DOT and loaned to the researcher.

4.2 Digital Signal Analyzer

The digital signal analyzer used in this research was a HP 35665 Dual Channel Dynamic Signal Analyzer, Figure 4.2. The signal analyzer is used to capture, store and process the receiver outputs. The signal analyzer is capable of calculating Fast Fourier Transforms (FFT) on recorded data in real time. This FFT capability at the testing site allows the operator to view the quality of data collected and make modifications to either the source or signal analyzer. According to Stokoe et al. (1988), the reason for using spectral analysis is that data can be evaluated that could not be easily gathered by using the time domain. For example, Figure 4.3(a) displays a signal in the time domain while Figure 4.3(b) displays a signal in the frequency domain. The waves in Figure 4.3(a) are relatively

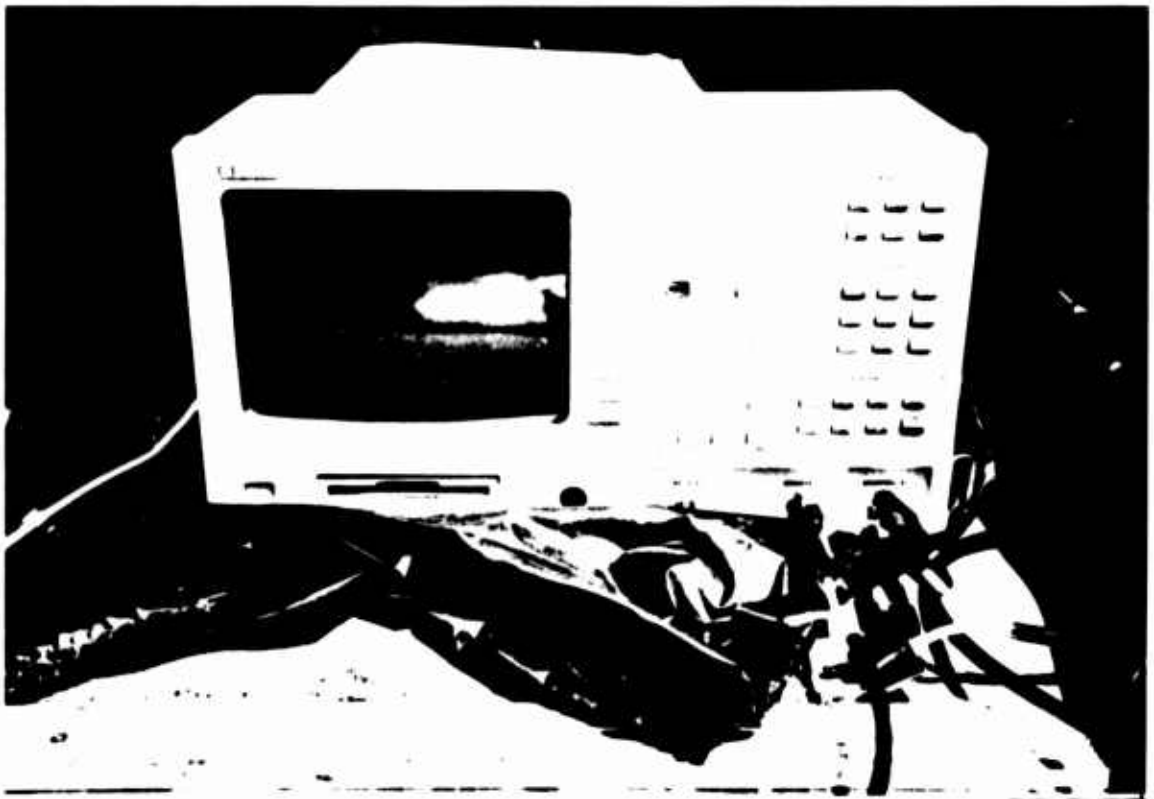
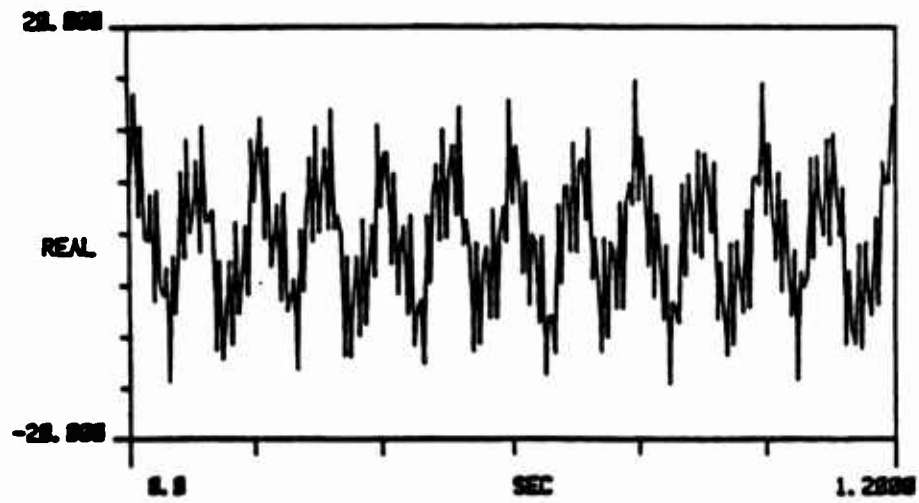
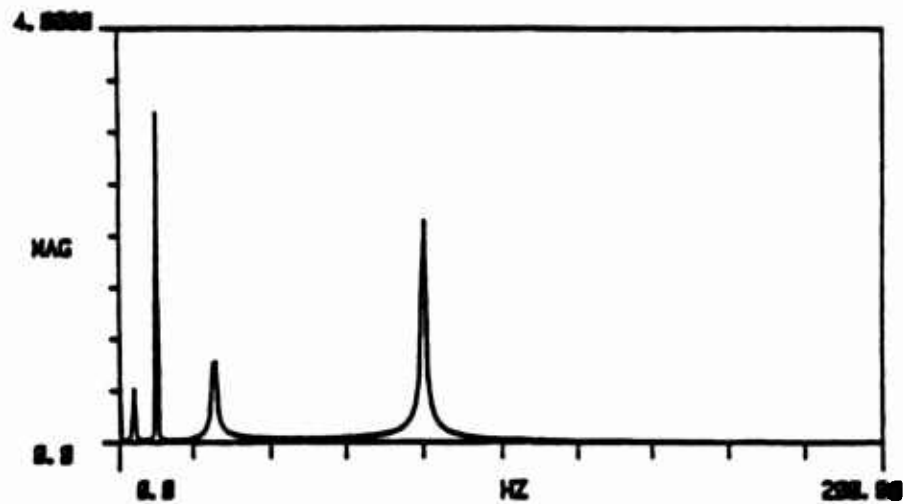


Figure 4.2 HP 35665 Dual Channel Dynamic Signal Analyzer



(a) Signal in the time domain.



(b) Signal in the frequency domain.

Figure 4.3 Complex Signal in Time and Frequency Domain

indistinguishable from each other while in Figure 4.3b are much more pronounced. Each wave and its relative contribution to the waveform are observed while the amplitude and phase of each frequency are easily identified in the frequency domain.

A second reason for using the spectral analysis technique is that most of the data obtained in the frequency domain do not require a synchronized signal. The averaging of input signals and the inherent trigger delays do not necessarily affect the data as they would in the time domain. Lastly, the frequency domain simplifies the mathematical operations and is similar to solving non-integer exponents using a logarithmic technique.

The signal analyzer records the time histories of the two receivers, $x(t)$ and $y(t)$. These time histories are transformed to the frequency domain resulting in the linear spectra of the two signals. A cross power spectrum, $G_{yx}(f)$, is then generated by multiplying $Y(f)$ by the complex conjugate of $X(f)$. The coherence function is created in a similar manner. The cross power spectrum and coherence are both generated by the signal analyzer and are shown in Figure 4.4. The coherence function is the signal to noise ratio and should be nearly one for acceptable data.

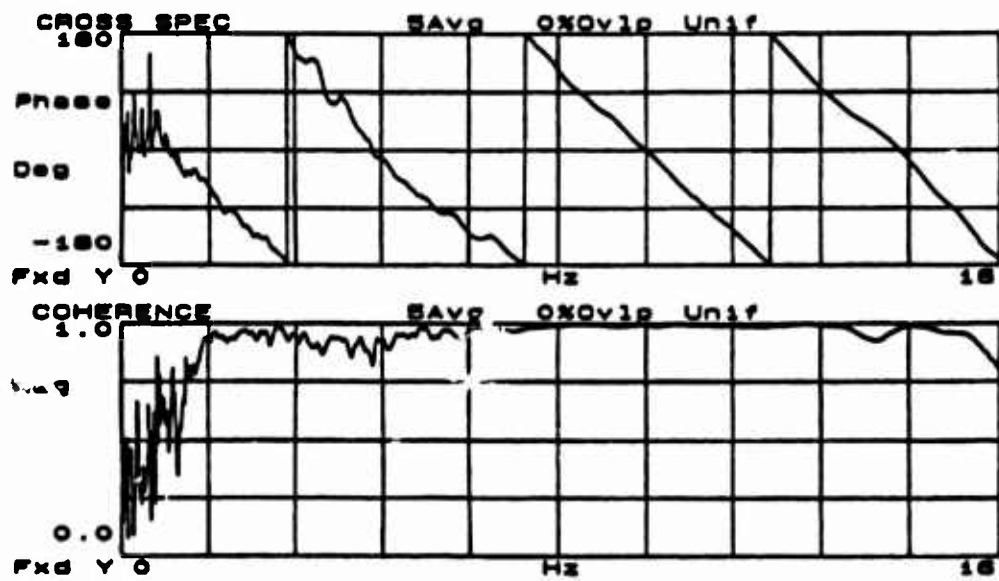


Figure 4.4 Phase of the Cross Power Spectrum and the Coherence Function

4.3 Signal Receivers and Impact Source

In general, the range of frequencies governs the choice of receivers. Velocity transducers or geophones (1-4.5 Hz) work well with soil sites that have frequencies between 1 and 500 Hz. Piezoelectric accelerometers, used for high frequency tests, are used on pavements with frequencies between 1 kHz to 50 kHz. A piezoelectric accelerometer utilizes a mass in direct contact with some type of piezoelectric component. When a varying motion is applied to the accelerometer, the mass causes a force against the piezoelectric component which causes a proportional electrical charge to occur. This charge is then amplified and used as an input for the digital analyzer. To optimize the amount of data collected, accelerometers are used at close spacings with high frequencies while geophones are used at larger spacings where low frequency R-waves are prevalent.

The distance between receivers is based on the required depth of the shear wave velocity profile. For example, receiver spacings of 0.5 to 2 feet would be used for a near surface investigation while 1 to 200 feet are used at sites where depth is important. Figure 4.5 shows some typical receiver spacing arrangements used for near surface investigations such as for an unsurfaced airfields.

It was generally found that a three foot spacing between receivers was the most efficient spacing. During

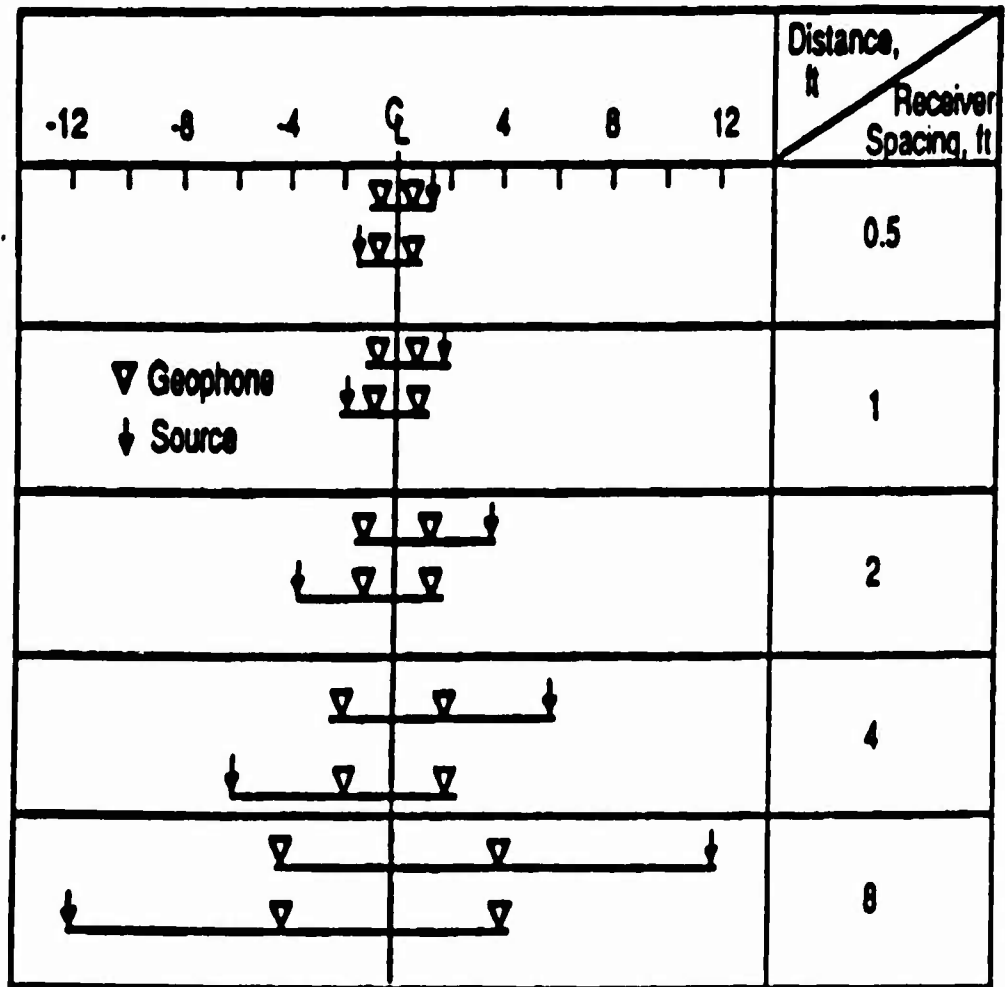


Figure 4.5 Receiver Spacing Arrangements for SASW Testing

the SASW unsurfaced airfield testing, the main impact source was the manual DCP as shown in Figure 4.6. It was found that the DCP was an excellent source with spacing between three and nine feet. It is generally accepted that the spacing between receivers is approximately equal to the depth surveyed. Since the CCT member is interested in the first 24 inches of the unsurfaced runway, it was decided that a three foot interval would be acceptable.



Figure 4.6 Manual DCP Used as Impact Source for SASW Testing

CHAPTER 5

FIELD TESTING AND CORRELATION OF THE AUTOMATED AIRFIELD DYNAMIC CONE PENETROMETER (AADCP) WITH THE MANUAL DYNAMIC CONE PENETROMETER (DCP)

5.1 Introduction

The purpose of this chapter is to present and discuss the results of the Dynamic Cone Penetrometer (DCP) and the Automated Airfield Dynamic Cone Penetrometer (AADCP) field testing. The chapter will describe the various sites used for testing, present DCP field repeatability and DCP-AADCP correlation testing.

5.2 Site Locations

The selection of sites for the DCP reliability testing was based primarily on soil classifications. The major classifications found in the Alachua County area were sand, silt-sand and clay. It was decided to locate two sites in each type of soil. In addition to these six sites an FDOT test pit was also used to ensure testing in uniform conditions, for a total of seven sites. The geographic locations of the sites are shown in Figures 5.1, 5.2 and 5.3. A soil classification summary is shown in Figure 5.4. The sites and their corresponding numbers are:

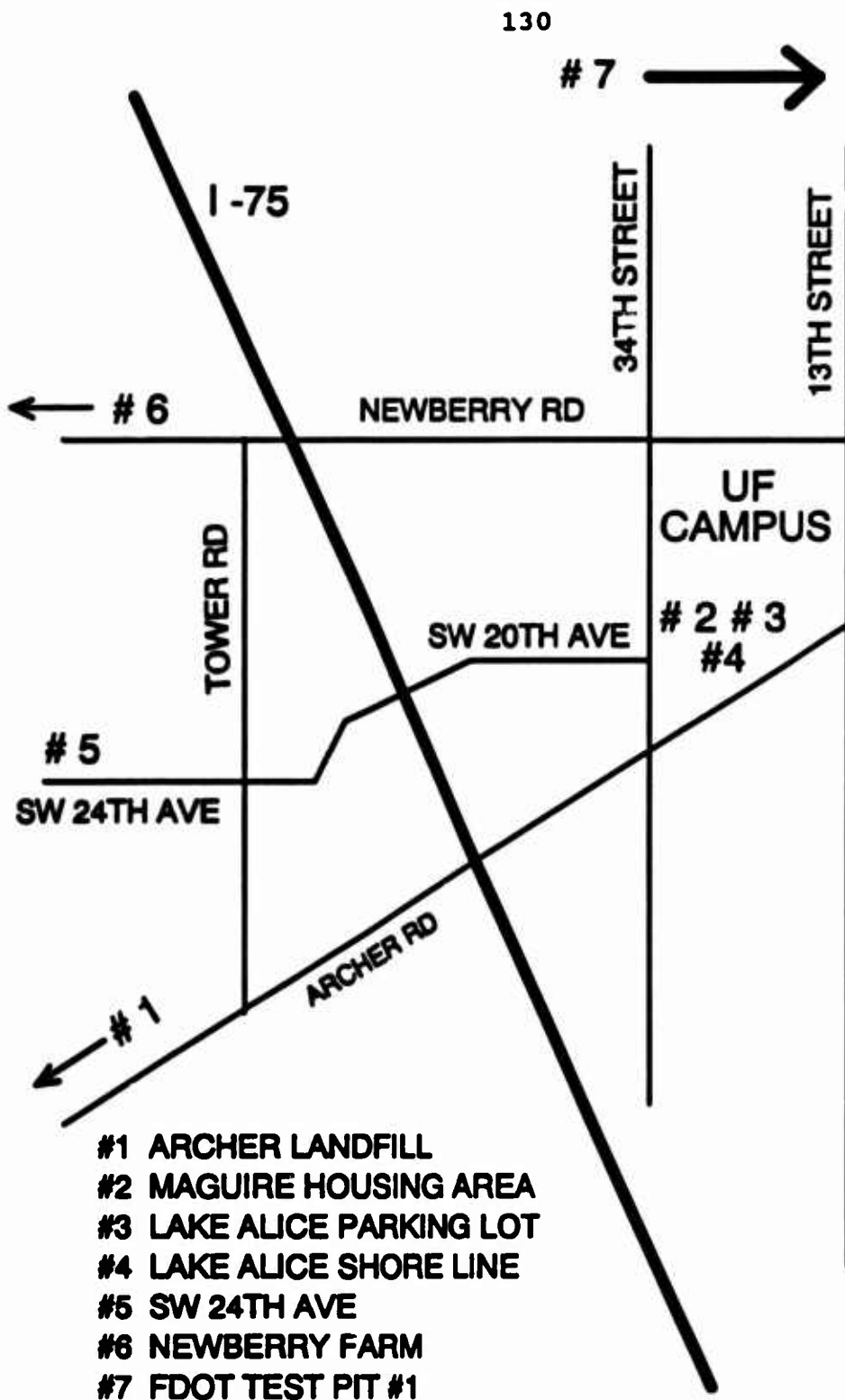


Figure 5.1 Geographic Locations of Field Testing Sites

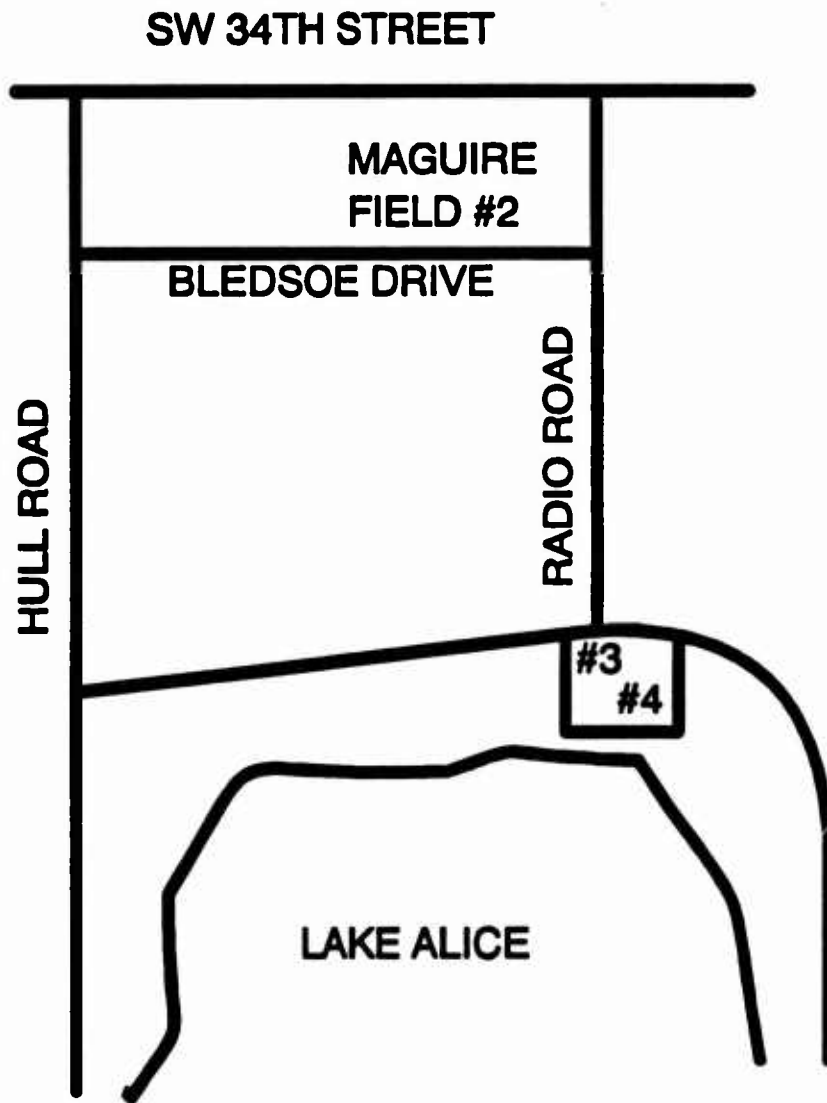
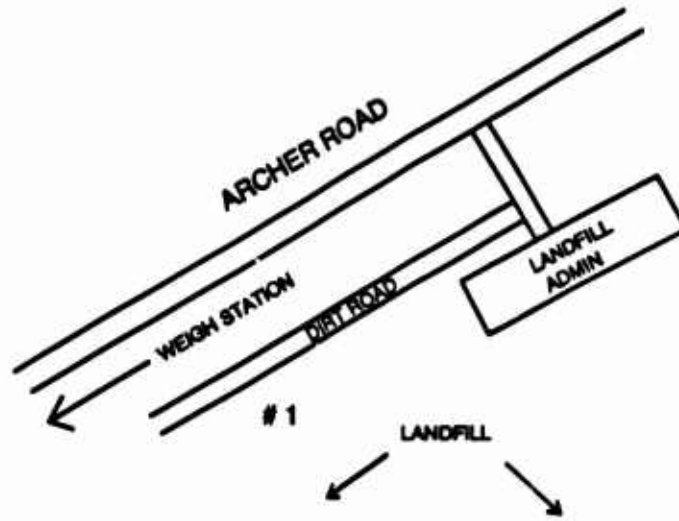
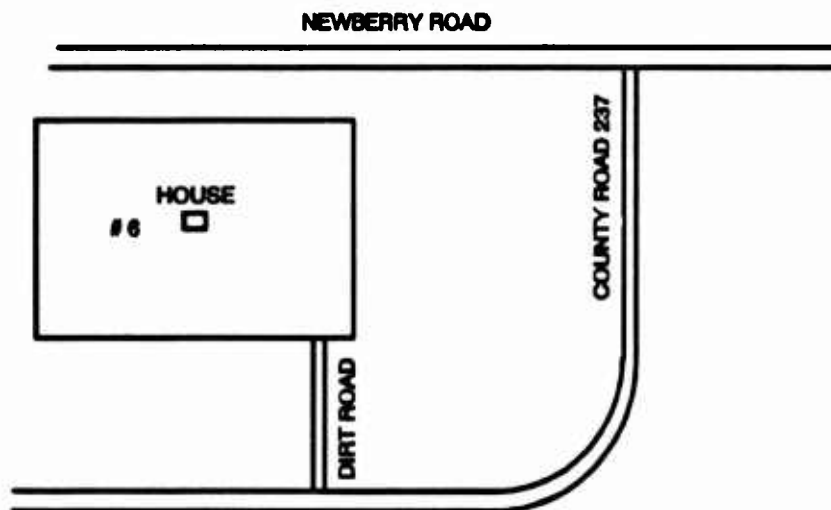


Figure 5.2 UF Campus Testing Sites



(A)



(B)

Figure 5.3 Off Campus Testing Sites
(A) Archer Landfill (B) Newberry Farm

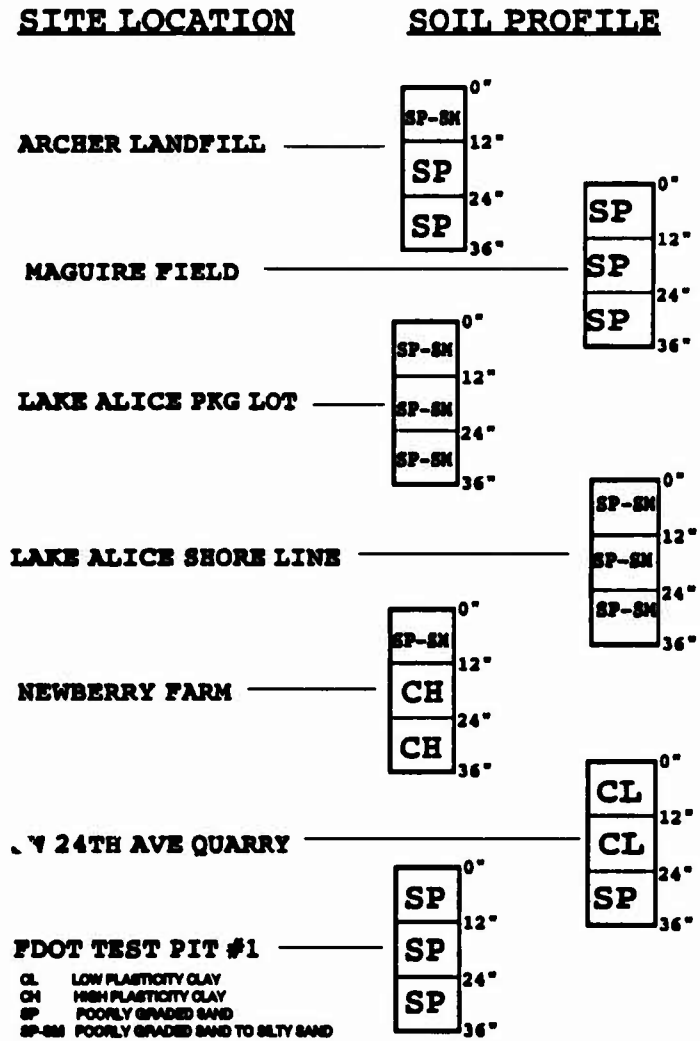


Figure 5.4 Soil Classification Site Summary

Archer Landfill (1), Maguire Field (2), Lake Alice Parking Lot (3), Lake Alice Shore Line (4), SW 24 AVE Quarry (5), Newberry Farm (6) and FDOT Test Pit #1 (7). The Archer landfill, Maguire Field, and FDOT Test Pit #1 are the sand sites, the Lake Alice Parking Lot and Shore Line are the silty-sand sites, and the Newberry Farm and SW 24 AVE Quarry are the clay sites.

5.3 Manual DCP Reliability Testing

5.3.1 Testing Objectives

The objectives of reliability testing of the manual DCP were threefold. First, the reliability testing will re-establish that the manual DCP is a repeatable and consistent instrument in the field. Previous research such as Smith and Pratt (1983) and Livneh and Ishai (1989) have established that the manual DCP is more repeatable than the CBR test. In this research it is intended to establish the consistency of the manual DCP by performing DCP testing at the six field sites. The second objective was to use the reliability testing to provide the author the opportunity to become completely familiar with the manual DCP and to evaluate its advantages and disadvantages prior to developing an automated version. The third objective of the reliability testing was to locate and analyze six sites to determine their suitability for later manual and automated DCP correlation testing. Borings were made the at six sites

and the soil analyzed to ensure the sites covered the sand, silty-sand, and clay classifications discussed in the previous section.

5.3.2 Testing Procedures

Prior to the manual DCP reliability testing borings were made to a depth of 48 inches to determine the layering of the soil. A hand auger was used and samples were placed in glass specimen jars for laboratory classification testing. The results of the laboratory testing are shown in Figure 5.4. Next, a small grid was etched on the ground with the bore hole in the center. Generally, the pattern used was as shown in Figure 5.5. Six manual DCP tests were performed around each borehole with spacing between tests of six to twelve inches.

The manual DCP, as described earlier in Chapter 2, is a falling weight penetrometer that measures the bearing strength of shallow soils. The 17.6 lb weight is raised manually by the operator and is released to impact an anvil 22.6 inches away. The impact is transferred to the cone tip through a 48 inch long rod. Two operators are required to run the test with one lifting the hammer and the other recording penetrations after each blow. It is important for the operator to keep the instrument as vertical as possible to prevent side friction from effecting the penetration results. Also, the operator lifting the weight should be

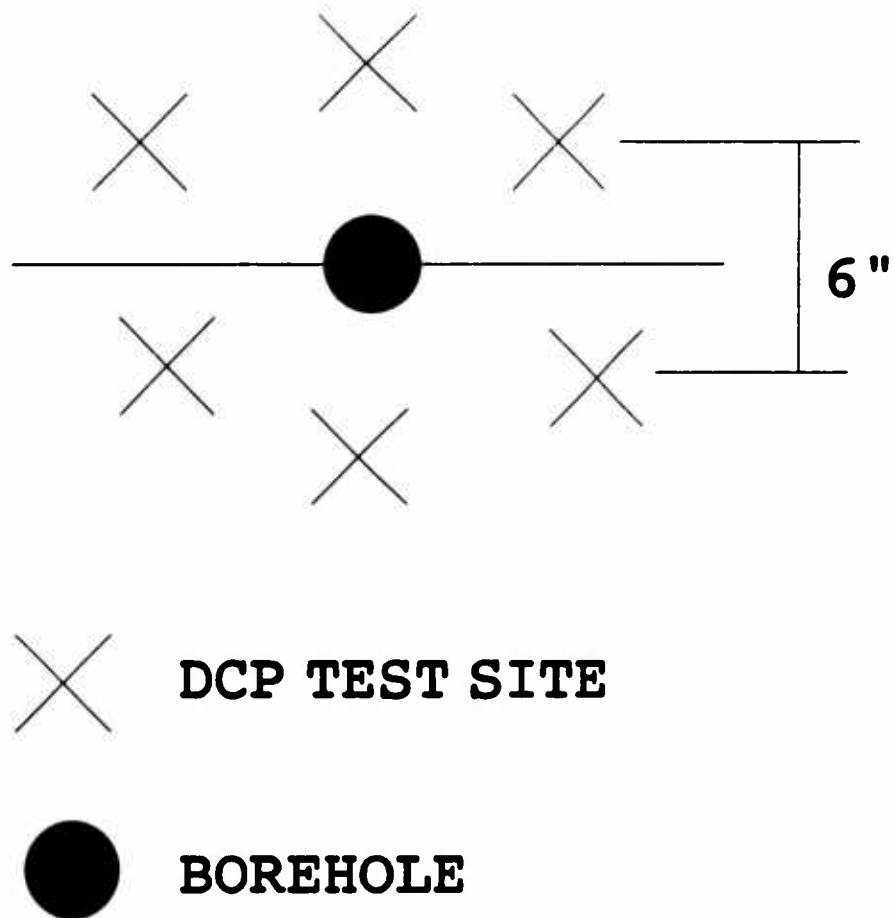


Figure 5.5 DCP Reliability Test Pattern

careful to consistently lift the weight to the top of the stroke and resist leaning on the instrument after each blow.

Once the DCP has completely penetrated the ground, the operator uses the hammer to impact the DCP out of the ground. Because the cone tip (20 mm) is larger than the rod diameter (16 mm) it is sometimes very difficult to extract the rod. At times the amount of energy to pull the rod out of the ground is greater than the energy required to put it in. Webster et al. (1991) solved this problem by designing a disposable cone tip. This research did not use the disposable tips but recommend their use in the final version of the AADCP.

5.3.3 Test Results

The DCP reliability testing results come in the form of several plots. The Archer Landfill site was selected as a site for discussion. This site consisted of very uniform, medium dense sand. Results from all the sites are presented in Appendix A in their entirety. Table 5.1 presents the raw data from the Archer Landfill site and also the CBR estimations obtained from known empirical relationships. The left-hand side of the table presents the cumulative penetrations per blow. For example, on the tenth blow the six manual DCP tests had penetrated 11.0, 11.4, 11.8, 11.8, 11.4, and 11.0 inches, respectively. The middle section of the table calculates the DCP penetration

**Table 5.1 Manual DCP Raw Data and CBR Estimations
(Archer Landfill)**

ARCHER LANDFILL

CUMMULATIVE DCP PENETRATION (INCHES)							DCP VALUES (IN/BLOW)						WES DCP-CBR CORRELATION					
BLOW	TEST 1	TEST 2	TEST 3	TEST 4	TEST 5	TEST 6	DCP 1	DCP 2	DCP 3	DCP 4	DCP 5	DCP 6	CBR 1	CBR 2	CBR 3	CBR 4	CBR 5	CBR 6
1	-1.6	-1.6	-1.4	-1.3	-0.8	-1.0	1.6	1.6	1.4	1.6	0.8	1.0	4.0	4.0	5.3	4.0	10.0	7.8
2	-3.4	-3.6	-4.0	-4.2	-3.2	-3.4	1.8	2.0	2.6	2.4	2.4	2.4	4.0	3.6	2.7	2.9	2.9	2.9
3	-5.2	-5.2	-6.0	-6.5	-5.0	-5.0	1.8	1.8	2.0	1.8	1.8	1.8	4.0	4.0	3.6	4.8	4.0	4.8
4	-6.4	-6.8	-7.2	-7.2	-6.4	-6.8	1.2	1.6	1.2	1.4	1.4	1.8	8.4	4.8	6.4	5.3	5.3	4.6
5	-7.4	-7.6	-8.2	-8.4	-7.6	-7.6	1.0	1.0	1.0	1.2	1.2	1.0	7.8	7.8	7.8	8.4	8.4	7.8
6	-8.4	-8.8	-9.2	-9.2	-8.6	-8.4	1.0	1.0	1.0	0.8	1.0	0.8	7.8	7.8	7.8	13.8	7.8	10.0
7	-9.0	-9.8	-10.0	-10.0	-8.4	-8.4	0.8	0.8	0.8	1.0	0.8	1.0	13.8	10.0	10.0	7.8	10.0	7.8
8	-9.8	-10.2	-10.4	-10.8	-10.0	-10.0	0.8	0.8	0.4	0.8	0.8	0.8	10.0	13.8	21.8	10.0	13.8	13.8
9	-10.4	-10.8	-11.2	-11.2	-10.8	-10.8	0.8	0.8	0.8	0.4	0.8	0.8	13.8	13.8	10.0	21.8	10.0	10.0
10	-11.0	-11.4	-11.8	-11.8	-11.4	-11.0	0.8	0.8	0.8	0.8	0.8	0.2	13.8	21.8	13.8	13.8	13.8	47.3
11	-11.4	-12.0	-12.2	-12.4	-12.0	-11.8	0.4	0.8	0.4	0.8	0.8	0.8	21.8	13.8	21.8	13.8	13.8	13.8
12	-11.8	-12.4	-12.8	-13.0	-12.8	-12.0	0.4	0.4	0.8	0.8	0.8	0.4	21.8	21.8	13.8	13.8	13.8	21.8
13	-12.2	-12.8	-13.2	-13.8	-13.0	-12.6	0.4	0.4	0.4	0.8	0.4	0.8	21.8	21.8	21.8	10.0	21.8	13.8
14	-12.8	-13.2	-13.8	-14.2	-13.4	-13.0	0.4	0.4	0.8	0.4	0.4	0.4	21.8	21.8	13.8	21.8	21.8	21.8
15	-13.0	-13.8	-14.2	-14.8	-14.0	-13.6	0.4	0.8	0.4	0.8	0.8	0.8	21.8	13.8	21.8	13.8	13.8	13.8
16	-13.4	-14.2	-14.8	-15.0	-14.8	-14.0	0.4	0.4	0.4	0.2	0.8	0.4	21.8	21.8	21.8	47.3	10.0	21.8
17	-13.8	-14.8	-15.0	-15.4	-15.2	-14.4	0.4	0.4	0.4	0.4	0.4	0.4	21.8	21.8	21.8	21.8	21.8	21.8
18	-14.2	-15.0	-15.4	-15.8	-15.6	-14.8	0.4	0.4	0.4	0.4	0.4	0.4	21.8	21.8	21.8	21.8	21.8	21.8
19	-14.8	-15.2	-15.8	-16.2	-16.0	-15.0	0.4	0.2	0.4	0.4	0.4	0.2	21.8	47.3	21.8	21.8	21.8	47.3
20	-14.8	-15.8	-16.2	-16.8	-16.4	-15.8	0.2	0.4	0.4	0.4	0.4	0.8	47.3	21.8	21.8	21.8	21.8	13.8
21	-15.8	-16.8	-16.8	-17.0	-16.8	-16.0	0.2	0.4	0.4	0.4	0.4	0.4	47.3	21.8	21.8	21.8	21.8	21.8
22	-15.2	-16.2	-16.8	-17.2	-17.0	-16.6	0.2	0.2	0.2	0.2	0.2	0.8	47.3	47.3	47.3	47.3	47.3	13.8
23	-15.8	-16.8	-17.2	-17.8	-17.4	-17.0	0.4	0.4	0.4	0.4	0.4	0.4	21.8	21.8	21.8	21.8	21.8	21.8
24	-16.8	-17.0	-17.8	-18.0	-17.8	-17.4	0.4	0.4	0.4	0.4	0.4	0.4	21.8	21.8	21.8	21.8	21.8	21.8
25	-16.4	-17.2	-17.8	-18.4	-18.2	-17.8	0.4	0.2	0.2	0.4	0.4	0.2	21.8	47.3	47.3	21.8	21.8	47.3
26	-16.8	-17.8	-18.2	-18.8	-18.4	-17.8	0.4	0.4	0.4	0.2	0.2	0.2	21.8	21.8	21.8	47.3	47.3	47.3
27	-17.2	-17.8	-18.4	-19.0	-18.8	-18.0	0.4	0.2	0.2	0.4	0.2	0.2	21.8	47.3	47.3	21.8	47.3	47.3
28	-17.4	-18.2	-18.8	-19.2	-19.0	-18.4	0.2	0.4	0.2	0.2	0.4	0.4	47.3	21.8	47.3	47.3	21.8	21.8
29	-17.8	-18.4	-19.0	-19.4	-19.2	-18.6	0.2	0.2	0.4	0.2	0.2	0.4	47.3	47.3	21.8	47.3	47.3	21.8
30	-17.8	-18.8	-19.2	-19.8	-19.6	-19.2	0.2	0.2	0.2	0.4	0.4	0.4	47.3	47.3	47.3	21.8	21.8	21.8
31	-18.8	-19.8	-19.8	-20.0	-20.0	-19.4	0.2	0.4	0.4	0.2	0.4	0.2	47.3	21.8	21.8	47.3	21.8	47.3
32	-18.4	-19.8	-19.8	-20.2	-20.2	-19.6	0.4	0.2	0.2	0.2	0.2	0.2	21.8	47.3	47.3	47.3	47.3	47.3
33	-18.8	-19.8	-20.0	-20.8	-20.4	-19.8	0.2	0.4	0.2	0.4	0.2	0.2	47.3	21.8	47.3	21.8	47.3	47.3
34	-18.8	-19.8	-20.2	-20.8	-20.8	-20.2	0.2	0.2	0.2	0.2	0.4	0.4	47.3	47.3	47.3	47.3	21.8	21.8
35	-19.2	-20.0	-20.8	-21.0	-21.2	-20.4	0.4	0.2	0.4	0.2	0.4	0.2	21.8	47.3	21.8	47.3	21.8	47.3
36	-19.4	-20.2	-21.0	-21.2	-21.4	-20.6	0.2	0.2	0.4	0.2	0.2	0.2	47.3	47.3	21.8	47.3	47.3	47.3
37	-19.8	-20.4	-21.2	-21.8	-21.6	-21.0	0.2	0.2	0.2	0.4	0.2	0.4	47.3	47.3	47.3	21.8	47.3	21.8
38	-19.8	-20.6	-21.4	-22.0	-22.0	-21.2	0.2	0.2	0.2	0.4	0.4	0.2	47.3	47.3	47.3	21.8	21.8	47.3
39	-20.2	-21.0	-21.8	-22.2	-22.2	-21.4	0.4	0.4	0.4	0.2	0.2	0.2	21.8	21.8	21.8	47.3	47.3	47.3
40	-20.4	-21.2	-22.0	-22.4	-22.4	-21.8	0.2	0.2	0.2	0.2	0.2	0.2	47.3	47.3	47.3	47.3	47.3	47.3
41	-20.8	-21.4	-22.2	-22.8	-22.8	-22.0	0.2	0.2	0.2	0.2	0.2	0.4	47.3	47.3	47.3	47.3	47.3	21.8
42	-21.8	-21.8	-22.4	-23.0	-22.8	-22.2	0.4	0.4	0.2	0.4	0.2	0.2	21.8	21.8	47.3	21.8	47.3	47.3
43	-21.4	-22.0	-22.8	-23.2	-23.0	-22.4	0.4	0.2	0.4	0.2	0.2	0.2	21.8	47.3	21.8	47.3	47.3	47.3
44	-21.8	-22.2	-23.0	-23.4	-23.4	-22.8	0.4	0.2	0.2	0.2	0.4	0.2	21.8	47.3	47.3	47.3	21.8	47.3
45	-22.0	-22.4	-23.2	-23.8	-23.8	-23.0	0.2	0.2	0.2	0.2	0.4	0.4	47.3	47.3	47.3	47.3	21.8	21.8

Table 5.1 (Continued) Manual DCP Raw Data and CBR Estimations
(Archer Landfill)

CUMMULATIVE DCP PENETRATION (INCHES)							DCP VALUES (IN/BLOW)						WES DCP-CBR CORRELATION					
TEST	TEST	TEST	TEST	TEST	TEST	TEST	DCP	DCP	DCP	DCP	DCP	DCP	CBR	CBR	CBR	CBR	CBR	CBR
BLOW	1	2	3	4	5	6	1	2	3	4	5	6	1	2	3	4	5	6
46	-32.2	-32.6	-33.4	-34.0	-34.6	-35.2	0.2	0.2	0.2	0.4	0.2	0.2	47.3	47.3	47.3	21.8	47.3	47.3
47	-32.4	-32.8	-33.6	-34.2	-34.8	-35.4	0.2	0.2	0.4	0.2	0.2	0.2	47.3	47.3	21.8	47.3	47.3	47.3
48	-32.6	-33.0	-34.0	-34.6	-34.4	-35.0	0.2	0.2	0.2	0.4	0.2	0.2	47.3	47.3	47.3	21.8	47.3	47.3
49	-33.0	-33.4	-34.2	-34.8	-34.6	-34.9	0.4	0.4	0.2	0.2	0.2	0.4	21.8	21.8	47.3	47.3	47.3	21.8
50	-33.2	-33.6	-34.6	-35.0	-35.0	-34.2	0.2	0.4	0.4	0.2	0.4	0.2	47.3	21.8	21.8	47.3	21.8	47.3
51	-33.4	-34.0	-34.8	-35.2	-35.2	-34.6	0.2	0.2	0.2	0.2	0.2	0.4	47.3	47.3	47.3	47.3	47.3	21.8
52	-33.6	-34.2	-35.0	-35.4	-35.4	-34.6	0.2	0.2	0.2	0.2	0.2	0.2	47.3	47.3	47.3	47.3	47.3	47.3
53	-34.0	-34.4	-35.4	-35.8	-35.8	-35.0	0.4	0.2	0.4	0.2	0.2	0.2	21.8	47.3	21.8	47.3	47.3	47.3
54	-34.2	-34.6	-35.6	-36.0	-36.0	-35.2	0.2	0.2	0.2	0.2	0.4	0.2	47.3	47.3	47.3	47.3	21.8	47.3
55	-34.6	-35.0	-35.8	-36.0	-36.2	-35.4	0.4	0.4	0.2	0.2	0.2	0.2	21.8	21.8	47.3	47.3	47.3	47.3
56	-34.8	-35.2	-36.0	-36.2	-36.4	-35.6	0.2	0.2	0.2	0.2	0.2	0.2	47.3	47.3	47.3	47.3	47.3	47.3
57	-35.0	-35.4	-36.2	-36.4	-36.6	-35.8	0.2	0.2	0.2	0.2	0.4	0.4	47.3	47.3	47.3	47.3	21.8	21.8
58	-35.2	-35.6	-36.4	-36.6	-37.0	-36.2	0.2	0.2	0.2	0.4	0.2	0.2	47.3	47.3	47.3	21.8	47.3	47.3
59	-35.6	-36.0	-36.8	-37.0	-37.2	-36.4	0.4	0.2	0.4	0.2	0.2	0.2	21.8	47.3	21.8	47.3	47.3	47.3
60	-35.8	-36.0	-37.0	-37.2	-37.6	-36.8	0.2	0.2	0.2	0.2	0.4	0.4	47.3	47.3	47.3	47.3	21.8	21.8
61	-36.0	-36.2	-37.2	-37.4	-37.6	-37.0	0.2	0.2	0.6	0.2	0.2	0.2	47.3	47.3	19.8	47.3	47.3	47.3
62	-36.2	-36.4	-36.8	-37.6	-38.0	-37.4	0.2	0.2	0.4	0.4	0.2	0.4	47.3	47.3	21.8	21.8	47.3	21.8
63	-36.4	-36.6	-36.2	-36.6	-36.2	-37.0	0.2	0.4	0.2	0.2	0.2	0.2	47.3	21.8	47.3	47.3	47.3	47.3
64	-36.6	-37.0	-36.8	-36.2	-36.4	-37.8	0.2	0.2	0.6	0.2	0.2	0.2	47.3	47.3	19.8	47.3	47.3	47.3
65	-36.8	-37.2	-36.8	-36.4	-36.6	-36.0	0.2	0.2	0.2	0.2	0.2	0.2	47.3	47.3	47.3	47.3	47.3	47.3
66	-37.0	-37.4	-36.2	-36.6	-36.6	-36.4	0.2	0.2	0.2	0.4	0.2	0.4	47.3	47.3	47.3	21.8	47.3	21.8
67	-37.2	-37.6	-36.4	-36.2	-36.0	-36.6	0.2	0.4	0.2	0.4	0.2	0.2	47.3	21.8	47.3	21.8	47.3	47.3
68	-37.4	-38.0	-36.6	-36.4	-36.2	-36.8	0.2	0.2	0.2	0.2	0.2	0.4	47.3	47.3	47.3	47.3	47.3	21.8
69	-37.6	-38.4	-36.8	-36.6	-36.4	-36.2	0.4	0.4	0.4	0.2	0.2	0.2	21.8	21.8	21.8	47.3	47.3	47.3
70	-38.2	-38.6	-36.2	-36.6	-36.6	-36.4	0.4	0.2	0.2	0.2	0.4	0.2	21.8	47.3	47.3	47.3	21.8	47.3
71	-38.6	-38.6	-36.4	-36.6	-36.2	-36.8	0.4	0.2	0.2	0.2	0.4	0.2	21.8	47.3	47.3	47.3	21.8	47.3
72	-38.8	-38.8	-36.8	-36.2	-36.4	-36.8	0.2	0.2	0.4	0.2	0.2	0.2	47.3	47.3	21.8	47.3	47.3	47.3
73	-39.2	-39.2	-31.6	-36.4	-36.6	-36.6	0.4	0.2	0.2	0.2	0.2	0.2	21.8	47.3	47.3	47.3	47.3	47.3
74	-39.4	-39.4	-31.2	-36.8	-31.6	-36.2	0.2	0.2	0.2	0.4	0.4	0.2	47.3	47.3	47.3	21.8	21.8	47.3
75	-39.6	-39.6	-31.6	-31.2	-31.2	-36.6	0.2	0.4	0.4	0.4	0.2	0.4	47.3	21.8	21.8	21.8	47.3	21.8
76	-39.8	-39.2	-31.6	-31.4	-31.4	-36.8	0.2	0.4	0.2	0.2	0.2	0.2	47.3	21.8	47.3	47.3	47.3	47.3
77	-39.8	-39.4	-32.2	-31.6	-31.6	-31.6	0.2	0.2	0.4	0.2	0.2	0.2	47.3	47.3	21.8	47.3	47.3	47.3
78	-39.2	-39.6	-32.4	-32.0	-32.0	-31.4	0.2	0.4	0.2	0.4	0.4	0.4	47.3	21.8	47.3	21.8	21.8	21.8
79	-39.4	-31.6	-32.6	-32.2	-32.4	-31.8	0.2	0.2	0.2	0.2	0.4	0.4	47.3	47.3	47.3	47.3	21.8	21.8
80	-39.6	-31.4	-32.8	-32.4	-32.6	-32.0	0.2	0.4	0.4	0.2	0.2	0.2	47.3	21.8	21.8	47.3	47.3	47.3
81	-31.0	-31.6	-30.4	-32.6	-32.6	-32.2	0.4	0.2	0.4	0.2	0.2	0.2	21.8	47.3	21.8	47.3	47.3	47.3
82	-31.4	-31.8	-30.6	-32.6	-32.6	-32.4	0.4	0.2	0.2	0.2	0.2	0.2	21.8	47.3	47.3	47.3	47.3	47.3
83	-31.6	-32.0	-34.0	-32.2	-32.2	-32.0	0.2	0.2	0.4	0.4	0.2	0.4	47.3	47.3	21.8	21.8	47.3	21.8
84	-31.8	-32.4	-34.2	-33.4	-33.4	-36.8	0.2	0.4	0.2	0.2	0.2	0.2	47.3	21.8	47.3	47.3	47.3	47.3
85	-32.2	-32.6	-34.4	-36.8	-33.6	-33.4	0.4	0.4	0.2	0.4	0.4	0.4	21.8	21.8	47.3	21.8	21.8	21.8
86	-32.4	-33.2	-34.6	-34.2	-34.2	-36.6	0.2	0.4	0.4	0.4	0.4	0.2	47.3	21.8	21.8	21.8	21.8	47.3
87	-32.6	-36.4	-35.2	-34.8	-34.8	-34.0	0.2	0.2	0.4	0.4	0.6	0.4	47.3	47.3	21.8	21.8	19.8	21.8
88	-33.0	-36.6	-35.4	-34.6	-35.2	-34.2	0.4	0.2	0.2	0.2	0.4	0.2	21.8	47.3	47.3	47.3	21.8	47.3
89	-33.4	-33.8	-35.8	-36.0	-35.4	-34.6	0.4	0.2	0.4	0.2	0.2	0.4	21.8	47.3	21.8	47.3	47.3	21.8
90	-33.6	-34.2	-36.0	-36.2	-35.8	-34.8	0.2	0.4	0.2	0.2	0.4	0.2	47.3	21.8	47.3	47.3	21.8	47.3
91	-34.0	-34.4		-36.8	-36.0	-35.2	0.4	0.2		0.4	0.2	0.4	21.8	47.3		21.8	47.3	21.8
92	-34.2	-34.8		-36.8		-36.4	0.2	0.4		0.2		0.2	47.3	21.8		47.3		47.3
93	-34.6	-36.0		-36.2		-36.0	0.4	0.2		0.4		0.6	21.8	47.3		21.8		19.8
94	-34.8	-35.4					0.2	0.4					47.3	21.8				
95	-35.2	-36.8					0.4	0.2					21.8	47.3				
96	-35.4	-36.0					0.2	0.4					47.3	21.8				
97	-35.6						0.2						47.3					
98	-36.0						0.4						21.8					

index. This index is the penetration per blow. An empirical formula relates the DCP index to the CBR value which is shown on the right-hand side of the table. The empirical formula used is from Webster et al. (1992) and was discussed in Chapter 2:

$$\text{Log CBR} = 2.46 - 1.12 (\text{Log DCP}) \quad (5.1)$$

Figures 5.6 and 5.7 graph the information presented in Table 5.1. Figure 5.6 plots the number of blows versus penetration into the ground. The slope of the curve in Figure 5.6 is the DCP index at that depth. A change in slope indicates a change in the strength of the ground penetrated. If the slope is steep then the material is relatively weak because it takes relatively few blows to penetrate a set distance. However, if the slope is shallow then the material is relatively strong because it requires many blows to penetrate the same depth.

Figure 5.7 plots depth versus the CBR calculated using Webster's empirical CBR-DCP relationship. Table 5.2 shows the data used to plot Figure 5.7. In this figure the average CBR is calculated over five inch intervals to a depth of 35 inches per test. Also shown are site averages, standard deviations and coefficient of variability for each depth of interest. The numbers in Table 5.2 were calculated using a spreadsheet macro. The purpose of the macro was to

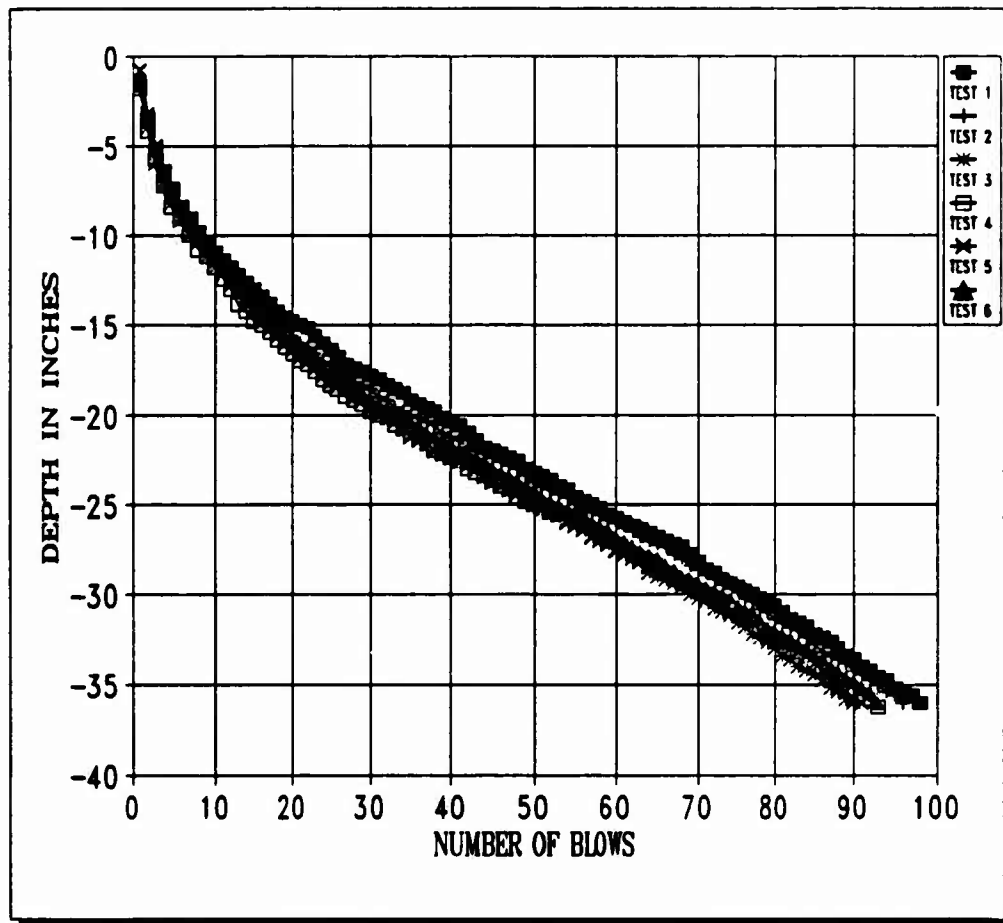


Figure 5.6 Manual DCP Blows vs Penetration
(Archer Landfill)

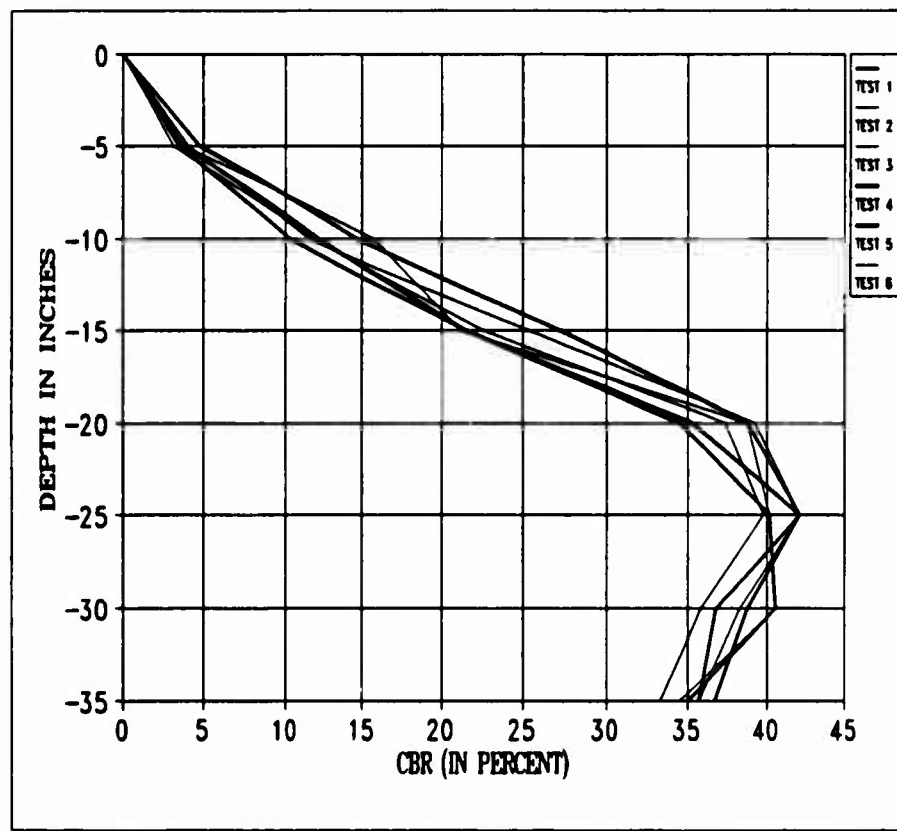


Figure 5.7 Estimated CBR Profile
(Archer Landfill)

**Table 5.2 Average Estimated CBR Calculations
(Archer Landfill)**

D E P T H*	AVG CBR 1	AVG CBR 2	AVG CBR 3	AVG CBR 4	AVG CBR 5	AVG CBR 6	CBR SITE AVG	ST DEV	CV
-5	4.8	4.1	3.1	3.8	3.5	3.8	3.8	0.5	13.6
-10	14.7	11.5	11.9	12.3	10.3	15.8	12.7	1.9	14.8
-15	27.2	25.3	22.6	21.5	21.6	21.2	23.3	2.3	9.7
-20	38.8	39.2	37.4	35.3	34.5	38.8	37.3	1.8	4.9
-25	42.2	42.2	39.8	42.2	40.2	40.2	41.1	1.1	2.6
-30	36.8	38.3	35.8	38.8	40.6	40.6	38.5	1.8	4.6
-35	35.7	35.7	33.4	36.7	35.0	34.5	35.1	1.0	2.9

*** Depth is in inches.**

calculate the CBR value at specific depths. The macro averages the CBR values in a range of 2.5 inches above and below the specified depth. The spreadsheet macro compares estimated CBR values at a specific depth and writes the average CBR value over a five inch interval for each test as shown in Table 5.2. Table 5.3 is a summary of the standard deviations and Table 5.4 is a summary of the coefficients of variability of the six sites. The standard deviation (s) is a measure of the variability of the CBR while the coefficient of variation (CV) is a measure of the CBR's relative dispersion from the mean. Their respective equations are:

$$s = \left[\frac{\sum (X_i - \bar{X})^2}{(n-1)} \right]^{1/2} \quad (5.2)$$

$$CV = \frac{s}{\bar{X}} \quad (5.3)$$

5.3.4 Discussion of Results

The objectives of the reliability testing were to re-establish the reliability of the DCP, to evaluate the advantages and disadvantages of the DCP prior to prototype development, and to locate sites suitable for DCP-AADCP correlation testing. The following discussion is based on these objectives.

**Table 5.3 Summary of Standard Deviations in DCP
Reliability Testing at Six Sites**

MEAN DEPTH (INCHES)	ARCHER LANDFILL CBR	MAGUIRE FIELD CBR	LAKE ALICE SHORE LINE CBR
-5	0.5	0.8	1.3
-10	1.9	1.9	3.6
-15	2.3	1.8	3.9
-20	1.8	0.9	3.1
-25	1.1	2.9	3.5
-30	1.8	4.6	2.9
-35	1.0	1.3	3.8
MEAN DEPTH (INCHES)	LAKE ALICE PARKING LOT CBR	SW 24TH AVE QUARRY CBR	NEWBERRY FARM CBR
-5	4.0	1.0	0.4
-10	2.8	0.9	0.9
-15	2.6	3.0	1.8
-20	3.4	3.5	1.6
-25	5.2	3.7	1.4
-30	4.8	7.2	1.6
-35	9.6	6.9	2.8

**Table 5.4 Summary of the Coefficient of Variability in
DCP Reliability Testing at Six Sites**

MEAN DEPTH (INCHES)	ARCHER LANDFILL CBR	MAGUIRE FIELD CBR	LAKE ALICE SHORE LINE CBR
-5	13.6	10.4	9.1
-10	14.8	15.1	17.4
-15	9.7	8.5	15.8
-20	4.9	3.6	20.5
-25	2.6	12.1	28.6
-30	4.6	23.3	18.9
-35	2.9	8.9	30.4
MEAN DEPTH (INCHES)	LAKE ALICE PARKING LOT CBR	SW 24TH AVE QUARRY CBR	NEWBERRY FARM CBR
-5	10.9	29.1	22.6
-10	7.1	36.4	22.6
-15	7.4	50.0	43.9
-20	8.3	52.9	27.4
-25	13.7	28.2	17.5
-30	12.9	57.6	18.7
-35	26.9	52.0	32.0

It can be seen from the Archer Landfill data and the corresponding data in Appendix A that the DCP provides both reliable and consistent results when tested in a uniform insitu site. Note in Figures 5.6 and 5.7 at the Archer Landfill site that the six tests plot in a narrow band. Maguire Field, Lake Alice Shore Line and Parking Lot demonstrate similar results for the six field tests. However, the Newberry Farm and SW 24th Ave Quarry sites have some dispersion in their respective blow vs penetration plots. This dispersion signifies that the two sites have a non-uniform profile.

During DCP field repeatability testing, the advantages and disadvantages of the DCP testing device were noted. The advantages of the DCP device were:

- (a) its ease of operation
- (b) low maintenance
- (c) high mobility
- (d) the data reduction procedures were simple and basic enough for someone at any engineering level to accomplish. The disadvantages were:

- (a) labor intensive over long periods of time (especially in a stiff soil)
- (b) penetration rod difficult to remove from ground
- (c) requires two full time operators
- (d) human error possible, e.g., miscounting blows

In order to evaluate the sites for possible use in the DCP-AADCP correlation testing an evaluation of the field

data is required. A discussion of the results of the DCP reliability testing begins with Figure 5.6. This plot is the penetration of the DCP with number of blows. The first item of interest in this plot is the change in slope at a depth of approximately twelve inches. This change in slope from relatively steep to shallow indicates a stiffer underlying soil which requires more blows to penetrate. Additionally, Figure 5.6 reveals that a fairly consistent bearing layer exists from about 12 to 35 inches. Figure 5.7 is a profile of the estimated CBR using the WES CBR-DCP relationship developed by Webster et al. (1992). This figure basically emulates Figure 5.6 since it is based on the DCP penetration index values. This plot shows an increasing CBR profile up to a depth of 25 inches followed by a slight reduction between 25 and 35 inches.

Another point that should be made about Figures 5.6 and 5.7 is the repeatability of the DCP. Since the Archer Landfill site was a soil site with a uniform sand, it is not surprising to see how close the six tests were to each other. Tables 5.2, 5.3, and 5.4 demonstrate just how close the six tests at each of the sites compared to each other. Since the standard deviation and the coefficient of variation measure test variances and repeatability they provide a good means of comparing successive tests. Livneh and Ishai (1989) suggested that a CV value of 30 was a representative value obtained for the field CBR test. This

value can then be used to evaluate DCP reliability testing and determine whether the DCP instrument is suitable for correlation testing.

It can be seen from the coefficient of variation summary, Table 5.4, that some sites have higher variability than others. The Archer landfill site reads the best with CV values well under 30 while the SW 24th Ave Quarry site reads the worst with values of 50. The two clay sites, SW 24 AVE Quarry and Newberry Farm, were surrounded by non-uniform soil layering. The Quarry clay site is located on top of some soft limestone with sporadic layering of a tan sand. The Newberry farm site is also located in a non-uniform site with several sinkholes known to be present. The low coefficient of variation values found at the sand and silty-sand sites indicate that the DCP test can be used, at these sites, as a standard with which other devices can be compared. Therefore, correlation testing should be performed only at Archer Landfill, Maguire Field, Lake Alice Shore Line, Lake Alice Parking Lot, and in the FDOT site.

5.4 Manual DCP vs AADCP Testing

5.4.1 Test Objectives

The major objective of the DCP vs AADCP testing was to produce field testing data that could be used to correlate the two instruments. The correlation could then be used to estimate a DCP penetration index. This index can then in

turn be used to estimate a CBR profile of the testing site. The thrust of the DCP-AADCP testing involved penetration field testing at the sites discussed in Section 5.2. Additional comparative testing was accomplished by statistically measuring the repeatability of the AADCP and manual DCP instruments. Finally, AADCP blow rate was tested to determine if it has any bearing on test results.

5.4.2 Correlation Test Sites and Procedures

Correlation testing was performed at five sites; FDOT, Archer Landfill, Maguire Field, Lake Alice Parking Lot, and Lake Alice Shore Line. The first DCP-AADCP correlation testing was carried out in Test Pit #1 at the FDOT facilities on Waldo Road. This site was chosen for its uniform, stiff sand properties. It consisted of 48 inches of uniform Fairbanks sand with an average surface CBR of 30. Three manual DCP and three AADCP tests were performed in a test pattern spacing six to twelve inches apart, Figure 5.8.

The manual DCP was performed at all sites in a standard manner as described in Chapter 2. The AADCP testing consisted of attaching the air supply to the pneumatic cylinder, connecting the 12 VDC battery to the three-way solenoid valve and attaching a measuring rod to the instrument. Air pressure was released into the air lines at about 100 psi pressure which was required to compress the spring. The hand switch was used to trip the solenoid

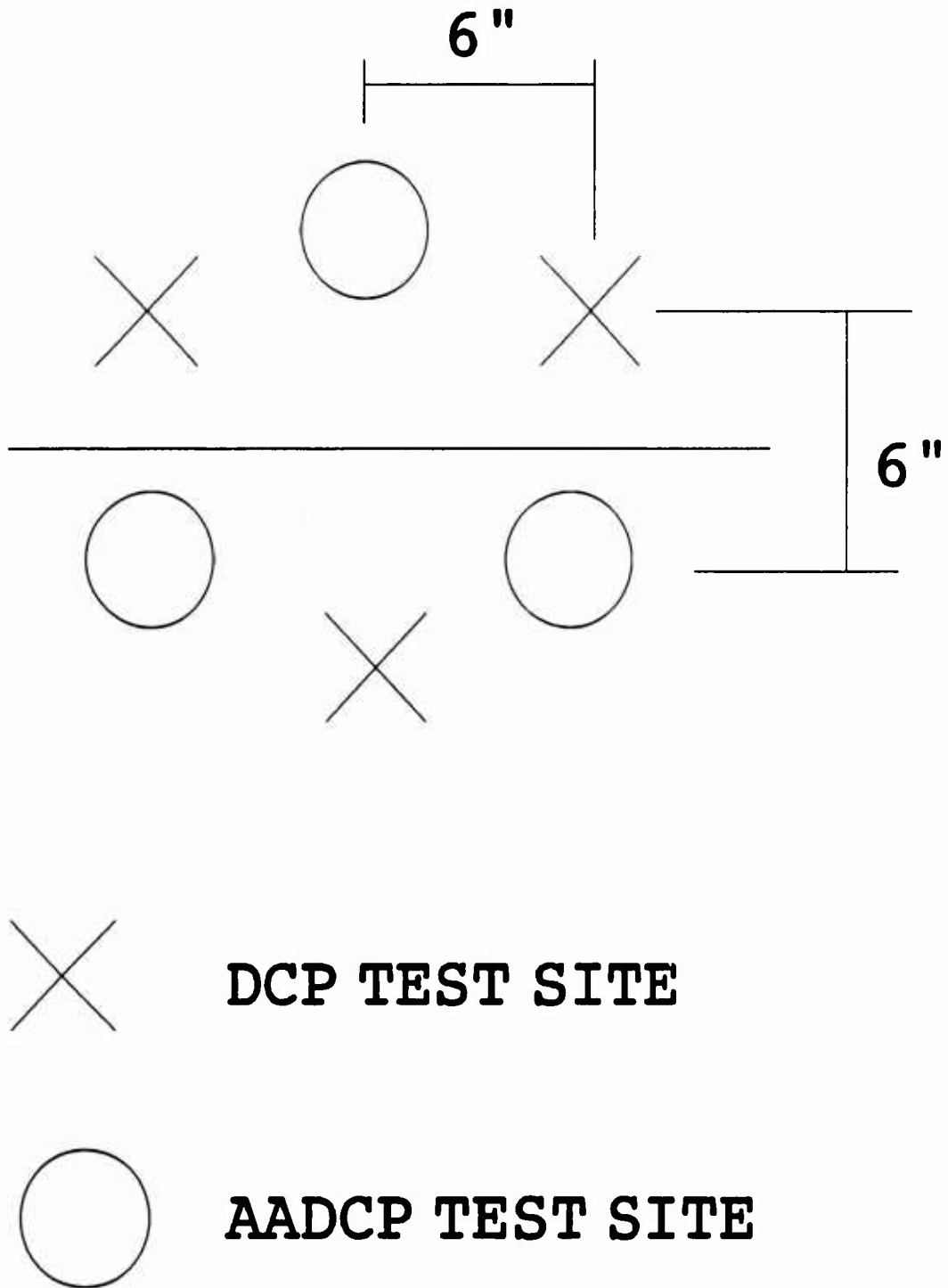


Figure 5.8 DCP-AADCP Correlation Test Configuration

valve to allow air into the air cylinder while the counter was triggered to measure the number of blows. The hand-switch allowed air into the cylinder while the position switch was used to redirect the air out of the cylinder and release the hammer. Generally, a measurement was made every five blows. The stiffer the soil, the greater the number of blows before a measurement was made, generally five to ten blows.

5.4.3 Correlation Test Results

The results of correlation testing at the five sites are shown in Figures 5.9, 5.10 and 5.11. These figures present the regression used to correlate the DCP and AADCP test instruments. In Figure 5.9, the equation which fits all the data is:

$$\text{DCP} = 2.27 \text{ AADCP} - 0.12 \quad (5.4)$$

The arithmetic regression technique was chosen over log-log or semi-log formats because of its higher R-squared value. The R-squared value is a measure of how well the data fit the line. A value greater than 0.90 is usually considered to indicate a good fit. The arithmetic R-squared value for all five sites was 0.85 while the log and semi-log values were somewhat less than 0.85. Each point on Figure 5.9 represents the penetration index of each instrument at the

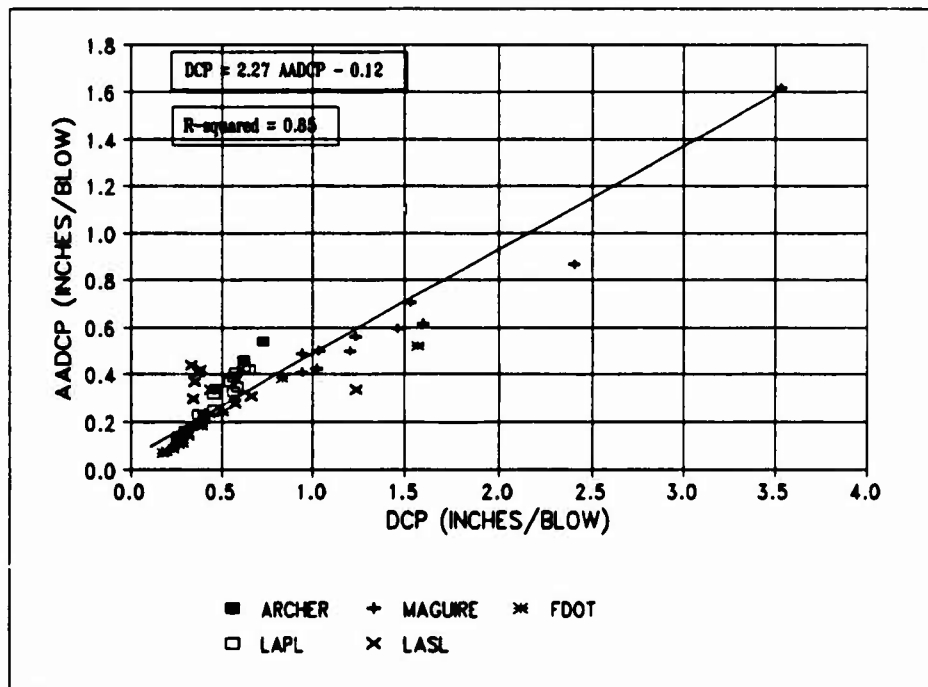


Figure 5.9 Sand and Silty-Sand Arithmetic Correlation of DCP and AADCP Instruments

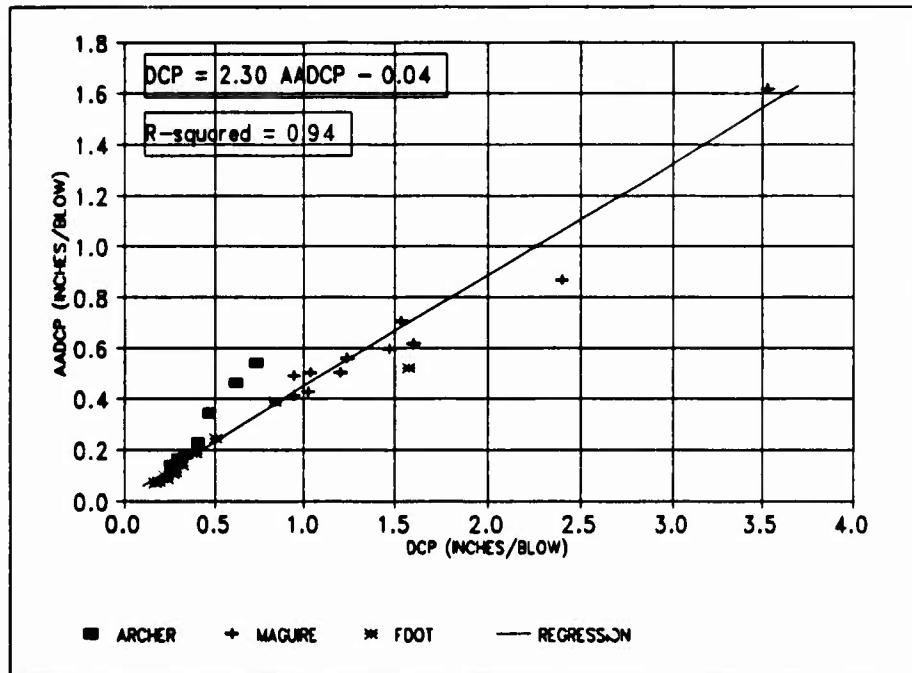


Figure 5.10 Sand Arithmetic Correlation of DCP and AADCP Instruments

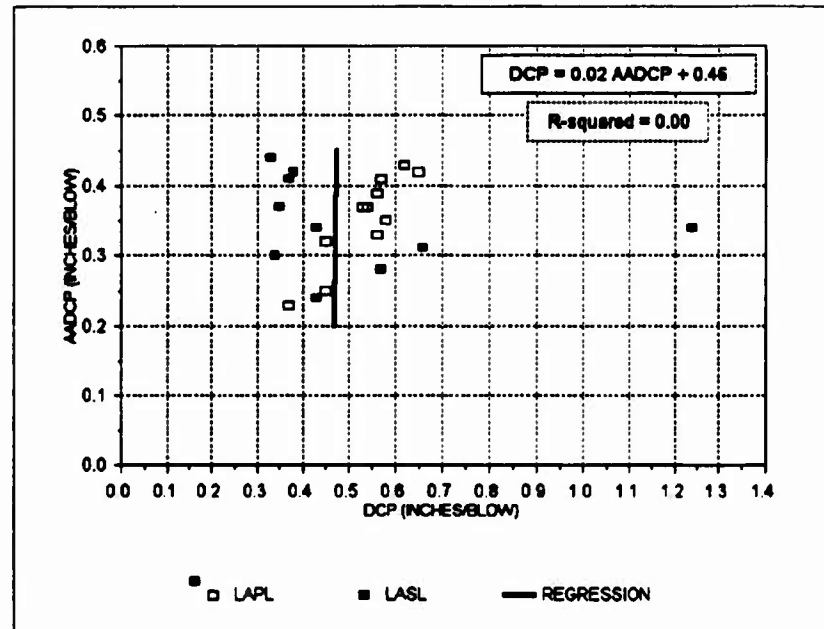


Figure 5.11 Silty-Sand Arithmetic Correlation of DCP and AADCP Instruments

same depth. The penetration index is the increment of penetration for one blow and is measured as inches per blow. Figure 5.9 includes all five sites. Figures 5.10 and 5.11 present correlations for the sand and silty-sand sites, respectively. Their respective correlation equations and R-squared values are:

$$\text{Sand:} \quad \text{DCP} = 2.30 \text{ AADCP} - 0.04 \quad R^2 = 0.94 \quad (5.5)$$

$$\text{Silty-Sand:} \quad \text{DCP} = 0.02 \text{ AADCP} - 0.46 \quad R^2 = 0.00 \quad (5.6)$$

Using Equation 5.5 for sands, a plot of estimated DCP penetration index (from AADCP results) and actual DCP indexes versus depth was created. Equation 5.5 was used for all the sand sites while Equation 5.4 was used for the silty-sand sites. Equation 5.6 was not used since the R^2 value was so low which essentially means that no practical correlation exists which will fit the line. Figure 5.12 is an example of the penetration index vs depth plot from the Maguire Field testing site. This plot was created by first obtaining DCP and AADCP penetration indexes at equivalent depths using the number of blows versus depth data in the field. These points correspond with the AADCP and DCP symbols on Figure 5.12. Figure 5.13 is an example of number of blow vs depth plot used in the penetration index calculations. Spreadsheets shown in Appendix C were used to help organize and calculate these values. AADCP values were

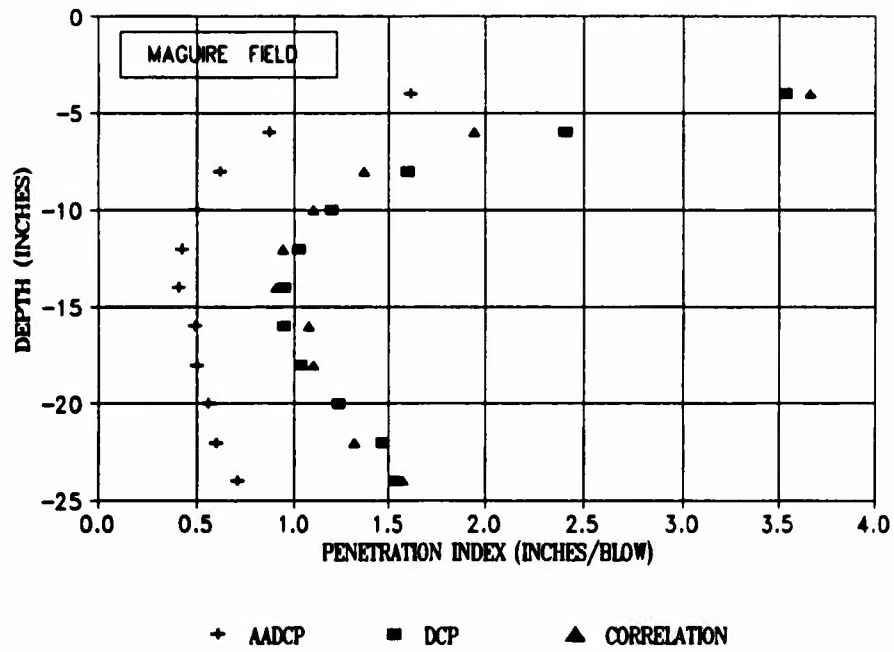


Figure 5.12 Penetration Index Profile From AADCP and DCP Instruments (Maguire Field)

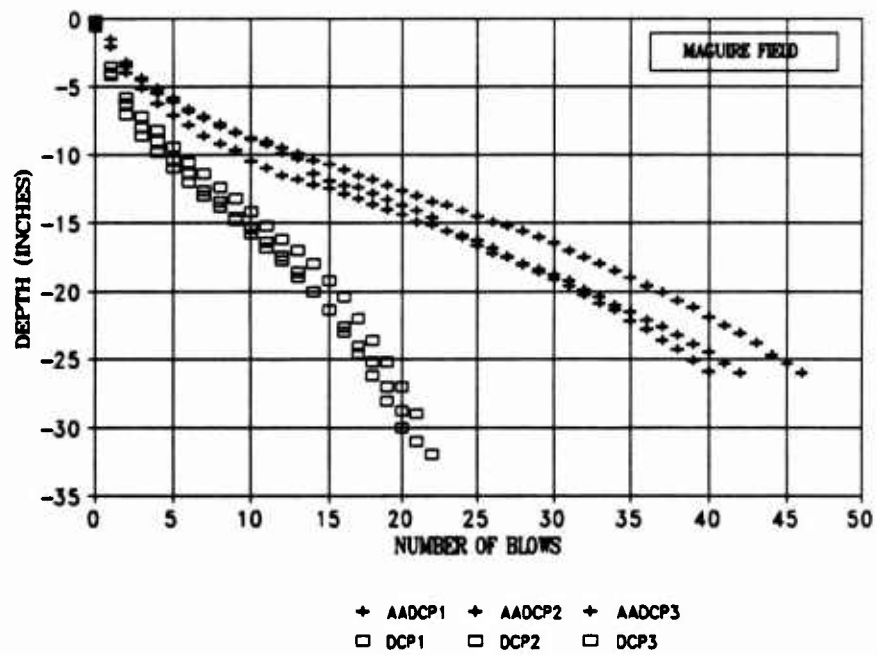


Figure 5.13 Number of Blows Versus Depth of AADCP and DCP Test Instruments at Maguire Field

plugged into Equation 5.5 at their respective depths to obtain (estimated) values of the penetration index for comparison with the actual DCP penetration index values. These correlation points are labeled with filled triangles in Figure 5.12. Based on field data measurements, Equation 5.5, and Webster's (1992) DCP-CBR correlation, the AADCP can be used to estimate CBR bearing values at a site. Figure 5.14 shows a CBR profile of Maguire Field using this method.

An experiment was conducted using different AADCP blow rates. Results are presented in Figure 5.15. A total of four tests were performed with two different blow rates. A blow rate of 10 blows per minute (bpm) was selected to simulate manual testing of the DCP while the 30 bpm rate was the fastest practical for the AADCP. The blow rate testing was only accomplished at Maguire Field.

Correlation testing results are presented in Appendix C in their entirety. For each of the five testing sites, tables used to calculate DCP and CBR values, plots of depth vs blows, depth vs penetration index and depth vs CBR are included.

The reliability of the AADCP instrument can be statistically measured by comparing the three tests at each site. The penetration indexes of the three tests are compared by calculating the mean, standard deviation, and coefficient of variation at a particular depth. The penetration indexes are determined by averaging them over a

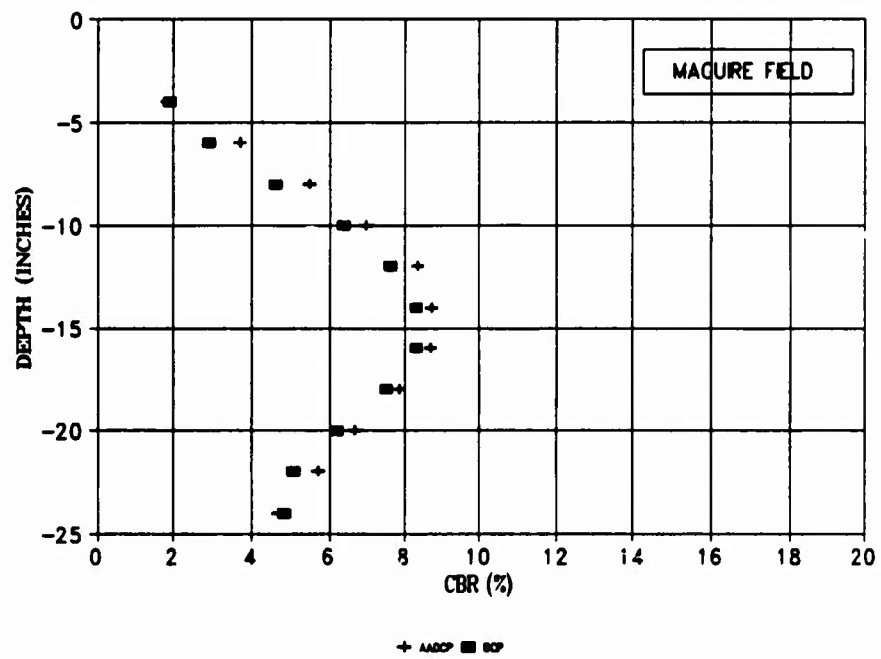


Figure 5.14 AADCP and DCP Estimations of CBR Versus Depth (Maguire Field)

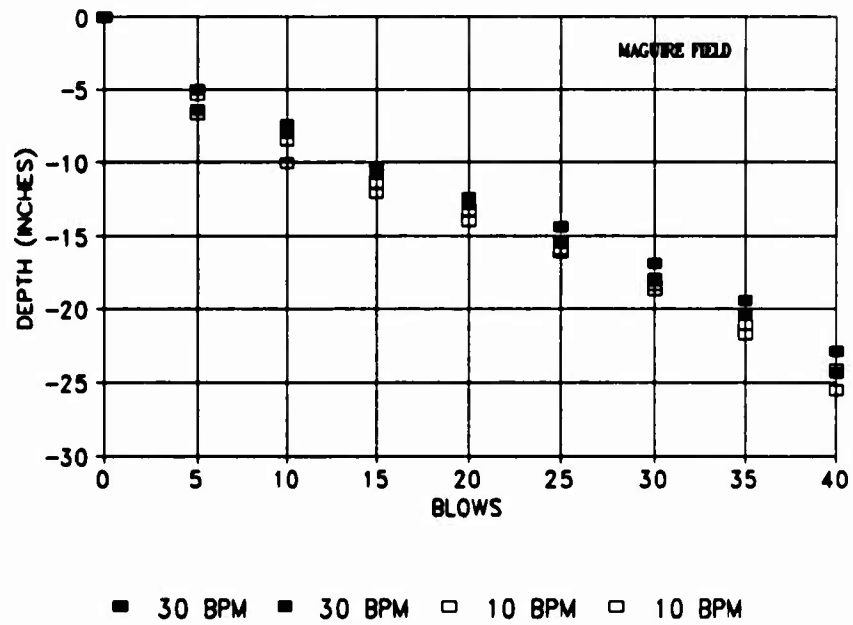


Figure 5.15 Number of Blows Versus Depth Using Two Different Blow Rates at Maguire Field

two inch interval, one inch above and below the depth. Appendix C displays the repeatability data from all the testing sites. Table 5.5 is a summary of the coefficient of variabilities (CV) of the AADCP and DCP instruments for all the testing sites. The CV is the percentage of deviation from the mean value of the three tests and is a measure of the relative dispersion. As discussed in Section 5.3.3, the coefficient of variation is a measure of repeatability.

5.4.4 Discussion of Correlation Test Results

The AADCP-DCP correlation results are shown in Figures 5.9, 5.10 and 5.11. The best correlation was Figure 5.10 for sand sites with an R-squared value of 0.94. The worst correlation was Figure 5.11 for silty-sand sites with an R-squared value of 0.00. An R-squared value of 0.00 means that there is not one line for which all the data have a good fit. The reason for the differences in R-squared values of the sand and silty-sand sites is probably related to the uniformity of the sites. Since it is difficult in the field to find completely uniform sites, spacial soil variations can cause scatter in the correlations. The R-squared value for all the sites of 0.85 is reasonably acceptable. It was decided to use the sand correlation for the sand sites and the sand and silty-sand correlation for the silty-sand sites. Using Equation 5.4 which is based on Figure 5.9,

Table 5.5 CV Values of All Testing Sites

SITE	MIN	MIN	MAX	MAX	AVG	AVG
	CV	CV	CV	CV	CV	CV
	AADCP	DCP	AADCP	DCP	AADCP	DCP
ARCHER	0.00	0.00	18.95	19.68	11.62	6.16
MAGUIRE	0.00	0.00	47.34	33.07	18.23	10.62
FDOT	2.37	0.44	23.06	11.30	10.65	6.59
LAPL	6.73	3.21	58.23	31.53	28.10	15.77
LASL	3.77	0.64	21.65	19.49	12.49	7.58
AVERAGE	2.57	0.86	33.84	23.01	<u>16.22</u>	<u>9.34</u>

it can be stated that the AADCP requires about 2.3 times more blows than the manual DCP to penetrate the same depth in sands and silty-sands. In an attempt to measure the force in both automated and manual rods, dynamic field measurements of both instruments were taken. Results are presented in Appendix D. No conclusions could be reached from the dynamic testing in comparison with the correlation results.

The accuracy of the correlation equations can be seen graphically in the estimation of DCP penetration index from AADCP data versus manual DCP values. Figure 5.12 shows results from Maguire Field site. The corresponding plots for the other sites are included in Appendix C. In general, the correlation equations did a good job of estimating the DCP penetration index values at the three sand sites and a poor job of estimating the index values at the two silty-sand sites. The Maguire Field and FDOT sites seemed to have the best results while the two silty-sand sites have poorer correspondence. Of course, the accuracy depends on the correlation equation. Notice in Figure 5.9 that the data closest to the regression line include Maguire Field and FDOT while the data the furthest from the regression line include the silty-sand sites. Consequently, where the data are relatively close to the regression line, then the estimated CBR data from the AADCP and that from the DCP devices are in good agreement. In Figure 5.14 the two

estimated CBR's are basically the same. The corresponding graph in Appendix C, Figure C.25, for the FDOT site shows that the estimated CBR's are the same to a depth of about 12 inches and then separate to a depth of 24 inches. Notice in the FDOT DCP profile plot, C.24, that at 12 inches the estimated DCP and DCP values separate at values of DCP less than 0.5. This is the precise range in which the FDOT data shown in Figure 5.9 are the least accurate.

It is also concluded that the most accurate range of CBR values is between 5% and 40%. Note in Figure C.25 that the AADCP approximately matches the results of the DCP up to a CBR of 35-40% and in Figure C.10 the CBR is matched as low as 3-5%. Considering that the Webster (1992) DCP-CBR equation is exponential and plotted on a log-log scale, this range of CBR is acceptable because values less than 0.2 inches/blow (DCP index) can lead to significant variation of the CBR above 40%. It was observed during field testing that values less than 0.2 cannot be consistently and accurately recorded. This was due to the graduation of the measuring rods. Notice that Webster's DCP-CBR correlation for penetration indexes of 0.2 and 0.1 gives CBR's of approximately 50% and 100% respectively.

An experiment was conducted using different AADCP blow rates which simulate the manual DCP and the fastest AADCP rate practical. Figure 5.15 shows an investigation into the effect of AADCP blow rates on the penetration. There were

two blow rates of 30 blows per minute and 10 blows per minute. Based on Figure 5.15, it is concluded that the blow rate has no effect on the penetration of the AADCP rod. This is in agreement with the Livneh et al. (1992) report which stated that penetration is unaffected by the rate of blows of up to 60 blows per minute.

Another conclusion which can be drawn from Figure 5.12 concerns the shape of the AADCP and DCP penetration index curves. Plots of DCP and AADCP penetration indexes versus depth show that they have the same shape and therefore suggest that both instruments detect changes in layer stiffness at approximately the same depths. In Appendix C, the Lake Alice Parking Lot and FDOT penetration index plots, C.14 and C.24, respectively, reveal the same agreements. The Archer Landfill and Lake Alice Shore Line are less conclusive.

The results of the reliability tests are presented in Table 5.5. and Appendix C. The average CV values for all the sites using the AADCP and DCP instruments are 16.22 and 9.34, respectively. These values are quite good and demonstrate that the AADCP and DCP test instruments essentially have the same reliability.

During the field testing, an effort was made to evaluate the advantages of the AADCP and DCP instruments. The following were considered advantages of each device:

Advantages of the DCP

- (a) ease of transportation
- (b) cheaper to manufacturer
- (c) established correlation of over 35 years
- (d) ease of maintenance

Advantages of the AADCP

- (a) ease of operation over large number of tests
- (b) field testing can be performed by one operator
- (c) digital blow counter reduces operator error i.e.,
miscounting blows
- (d) tests at a normal blow rate of 30 bpm and
therefore is faster to perform than the manual DCP
blow rate of 10 bpm
- (e) data acquisition easier to document with separate
measuring rod

CHAPTER 6

EVALUATION OF SEISMIC SURVEYING FIELD TESTING USING SPECTRAL ANALYSIS OF SURFACE WAVES (SASW) TECHNIQUE

6.1 Introduction

The purpose of this chapter is to evaluate the Spectral Analysis of Surface Waves (SASW) technique as a means of assessing subsurface spacial variations throughout a simulated unsurfaced runway and apron. The chapter discusses the test objectives, test sites, and test procedures used to evaluate the testing. Finally, the results of the SASW field testing are presented and discussed.

6.2 SASW Test Objectives

The objective of the field SASW testing was to evaluate whether or not the technique could be used to complement DCP testing of an unsurfaced runway. It was necessary to evaluate the sensitivity of the SASW testing technique in determining spacial variations to a depth of 36 inches. Comparison of shear wave velocities was used as a means of locating lower strength material and of estimating the surface layer thickness (Roesset et al. 1991).

6.3 SASW Test Sites

The test sites for the SASW testing were chosen based upon diversity and accessibility. The first test site was the FDOT Kanapaha material storage area off of Archer Road in Gainesville, Florida. This site consisted of a variable layer of tan sand with sporadic soft limestone pinnacles rising at times to near surface depth. Figure 6.1 shows a typical boring log from the area. This site was chosen for its many variations within five feet of the surface. Sixteen separate seismic surveys were performed at the Kanapaha site. The purpose of the large number of tests was to survey a fairly well known site that contained small limestone cavities near the surface.

The second test site was located at the Waldo Road FDOT soil testing laboratory. Test Pit #1 consisted of a very stiff 10.5 inch recycled asphalt (RAP) material overlaying a 48 inch sand subbase, Figure 6.2. This site was chosen for its stiff over soft layer geometry which simulates an unsurfaced airfield.

6.4 SASW Test Procedures

The SASW testing equipment, as described in Chapter 4, is sensitive to the environment and great care should be taken in setting up the equipment. The digital analyzer was set up first in a central location near the testing site. A gas powered generator, which provided power for the digital

DEPTH FEET	SOIL DESCRIPTION	STANDARD PENETRATION TEST	NO. OF BLows	TEST DATE	LOGS
0	TOE SAND				
1					
5	TOE SOFT LIMESTONE	8	12	1	
10		4	7	2	
15		14	23	3	
20		11	21	4	
25	TOE SOFT LIMESTONE				
30		28	26	5	
35		27	46	6	
40		26	54	7	
45		27	44	8	
50		26	51	9	
55		29	68	10	
60		28	63	11	
65		31	72	12	

Figure 6.1 Kanapaha Boring Log for SPT-3 near site #16
(Townsend et al. 1991)

FDOT TEST PIT #1

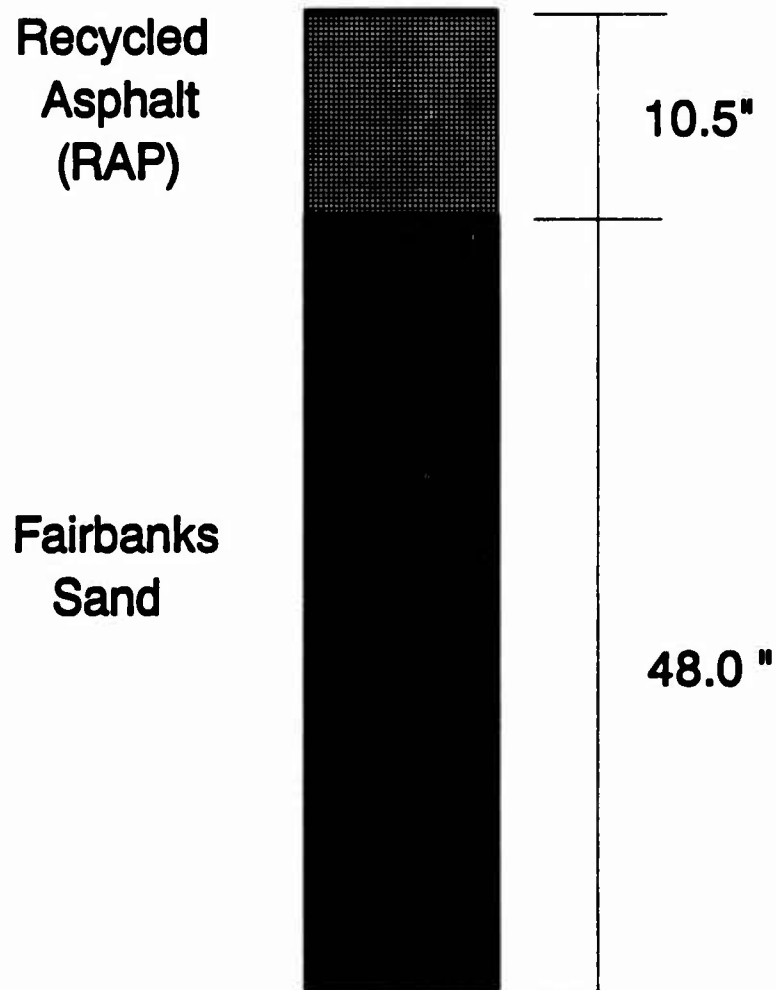


Figure 6.2 FDOT Test Pit #1 RAP Profile

analyzer, was located behind a vehicle to prevent errant vibrations. Once the test site was chosen, a line of testing was determined with geophone spacings of three feet or 1.5 feet from an imaginary centerline. The geophones were leveled with nearby soil so that full contact was made with the base of the geophone. The geophone cables were connected to the digital analyzer in the 1 and 2 channel positions.

The digital analyzer setup depends on the type of material being tested. In general, the frequency, record length, pre-trigger, and channel input ranges are determined by a trial and error procedure. During the testing at Kanapaha, the frequency span was set at 200 Hz, the record length was set at one second, the pre-trigger was set at 10 percent of the record length or 100 milliseconds, and channel one and two input ranges were set at 2.0 and 0.5 volts. The channel input ranges are actually the sensitivities of the geophones. The input ranges were different because the geophone nearest the impact source requires less sensitivity than the further geophone.

With the digital analyzer and geophones in place, the impact source (DCP) was positioned three feet (geophone spacing) away from the number one channel geophone. One blow from the DCP triggers the digital analyzer which first displayed the signal in a real time voltage-time plot and then immediately displayed the signal in the frequency

domain in the form of a phase of the cross power and coherence spectra. A second blow of the DCP triggered a second real time voltage-time plot, a cross power and coherence spectra and then immediately an average of the current and previous cross power spectrum signals. In general, if the second signal did not visibly differ from the average signal in shape and form, then two signals were adequate. However, the digital analyzer could average several signals if required.

The cross power and coherence spectra were reviewed carefully to determine if the coherence was approximately equal to one and that no obvious extraneous vibrations or reflections were recorded. However, if part of the coherence was approximately one in a particular frequency range, the operator had the option of saving the signal and later during the inversion phase eliminating the less desirable parts of the signal. The ability of the operator to read and evaluate this screen cannot be overstated. Only with training and experience can one adequately evaluate the cross power and coherence screen. Once the operator decided the signal was acceptable, the screen was saved and recorded on a floppy disc. This procedure was then repeated for other geophone spacings.

6.5 SASW Test Results

Of the sixteen sites surveyed, there was one site with a cavity near the surface. Site number six contained a small 16 inch deep cavity starting at a depth of 18 inches. The cavity was found using the manual DCP. Figure 6.3 shows the DCP blow profile from site #6. Notice that from about 18 inches to 34 inches the slope of the penetration index is vertical which means a large penetration with one blow or a cavity. Once the cavity was discovered, the manual DCP was used to determine its boundaries. The cavity was determined to be at a depth of 18 inches, 24 inches long and 16 inches in height.

The results of the SASW analysis were generated first from the waveform analyzer which captured, stored, and processed the output of each geophone. For each spacing, three and nine feet, the time and frequency spectra were recorded from the two signals. Matrix calculations were made on these results and a dispersion curve was developed. The dispersion curve is a plot of surface wave velocity vs wavelength. Several dispersion curves were combined into a single composite curve for this site #6. The dispersion curve took about fifteen minutes to develop. Finally, an inversion process was used to compare the composite dispersion curve of site #6 with a theoretical curve based on different stiffness profiles. The inversion data took two hours to develop. Table 6.1 is a summary of the

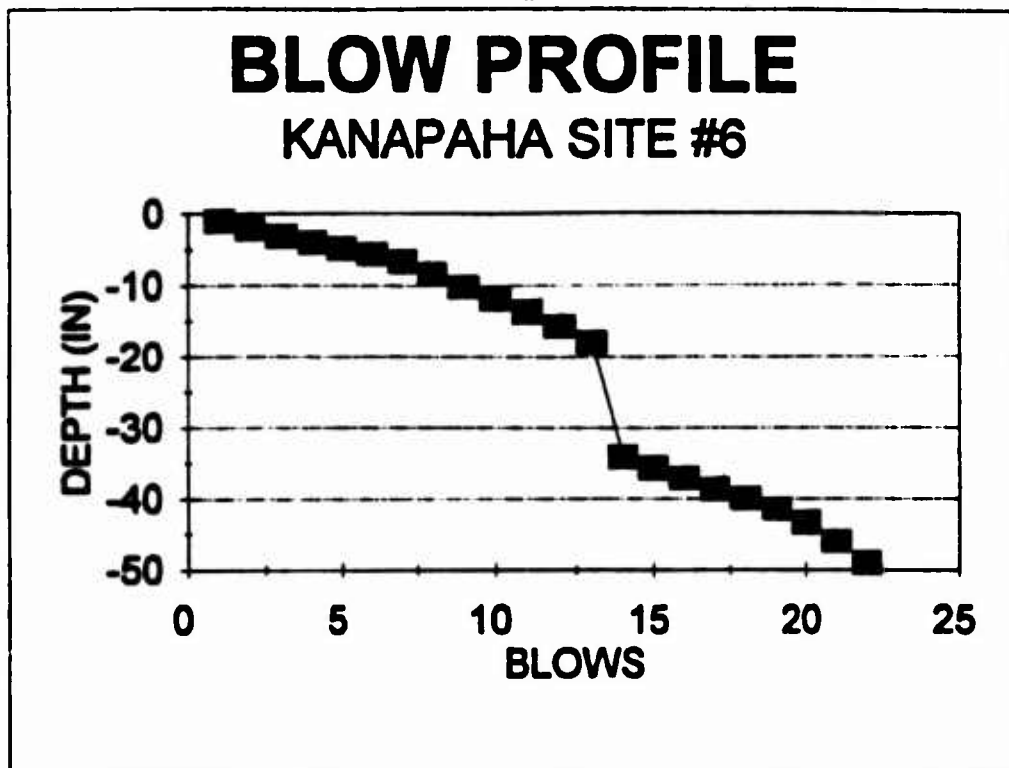


Figure 6.3 Manual DCP Blow Profile of Site #6

Table 6.1 Summary of Inversion Output of Site #6

SOLUTION INFORMATION

LAYER NO.	LAYER THICKNESS	TOTAL DEPTH	SHEAR WAVE VELOCITY		MASS DENSITY	POISSON RATIO	DAMPING	SAT
			(REAL)	(IMAG)				
1	1.00	1.00	299.77	.00	3.40	.30	.00	U
2	1.00	2.00	849.93	.00	3.40	.30	.00	U
3	1.00	3.00	550.13	.00	3.40	.30	.00	U
4	1.00	4.00	550.36	.00	3.40	.30	.00	U
5	1.00	5.00	1000.04	.00	3.40	.30	.00	U
6	1.00	6.00	1000.05	.00	3.40	.30	.00	U
7	4.00	10.00	1100.11	.00	3.40	.30	.00	S
	HALF SPACE		1199.97	.00	3.40	.30	.00	S

LAYER NUMBER	VELOCITIES		MODULI	
	SHEAR	COMPRESSION*	SHEAR	YOUNGS
1	299.77	560.81	.306E+06	.794E+06
2	849.93	1590.07	.246E+07	.639E+07
3	550.13	1029.19	.103E+07	.268E+07
4	550.36	1029.63	.103E+07	.268E+07
5	1000.04	1870.90	.340E+07	.884E+07
6	1000.05	1870.92	.340E+07	.884E+07
7	1100.11	4800.00	.411E+07	.107E+08
HALF SPACE	1199.97	4800.00	.490E+07	.127E+08

inversion output. Figure 6.4 is a plot of the Kanapaha site #6 field and theoretical dispersion curves. This figure shows how well the program matched the field data. From the theoretical dispersion curve, the shear wave velocity, maximum shear modulus and maximum Young's modulus profiles are determined and are plotted in Figures 6.5, 6.6, and 6.7.

The second set of results presented are from Test Pit #1 FDOT Waldo road test site. This site, as shown in Figure 6.2, had 10.5 inches of recycled asphalt and a 48 inch Fairbanks sand subbase. Results were generated using the same SASW process as described above with one exception. This site used accelerometers on the stiff upper-layer instead of the geophones used in the soil site of Kanapaha. As discussed in Section 2.4.3, pavement sites have frequencies much higher than those at soil sites.

Test Pit #1 results are presented in Figure 6.8 as a two-layer dispersion curve. An attempt was made to run the inversion program in order to generate a theoretical dispersion curve and the shear wave and modulus profiles. It was however found that the software could not properly calculate the theoretical dispersion curve when a stiff layer overlies a soft layer. Alternative inversion software was not available as of the writing of this report.

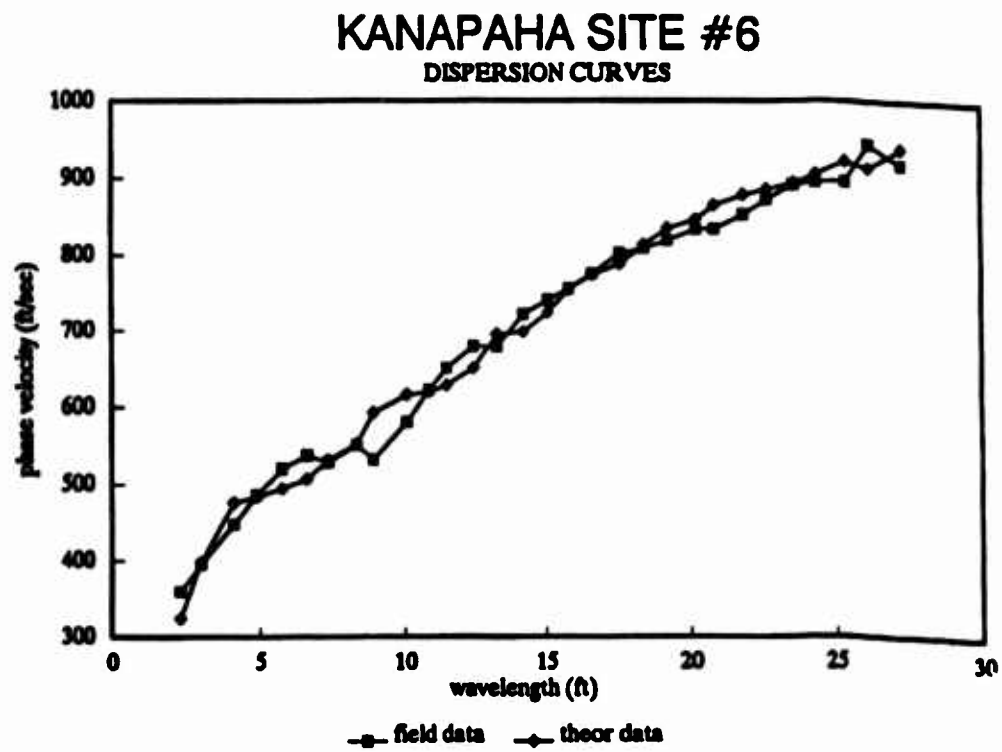


Figure 6.4 Site #6 Field and Theoretical Dispersion Curves

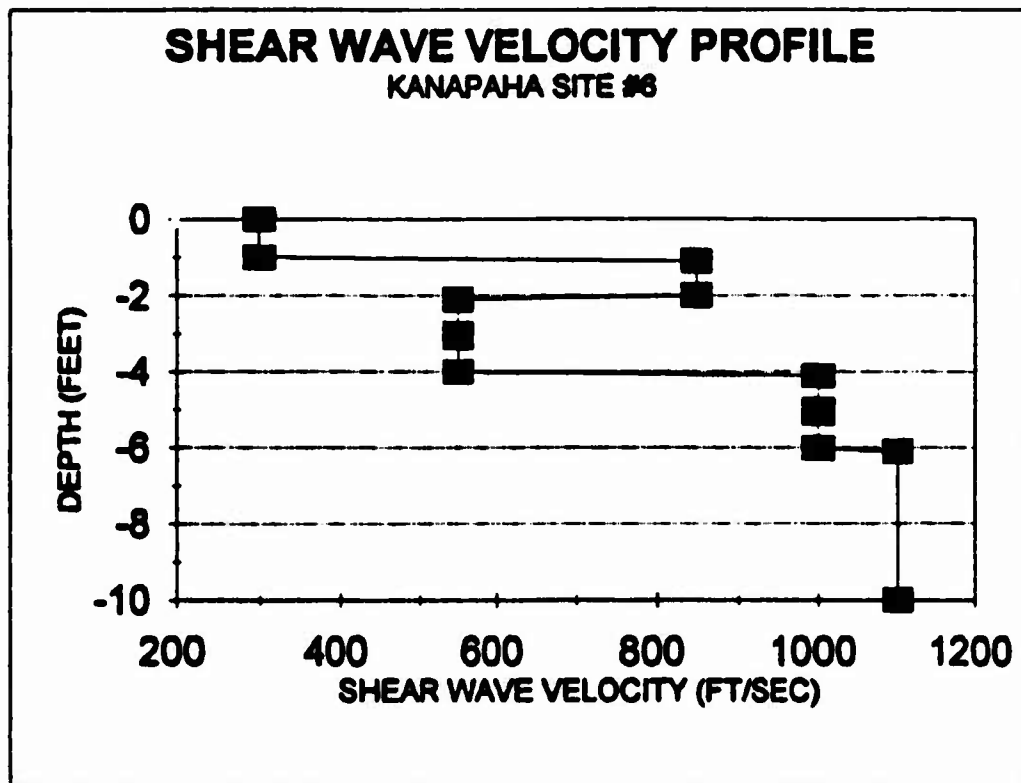


Figure 6.5 Shear Wave Velocity Profile of Site #6

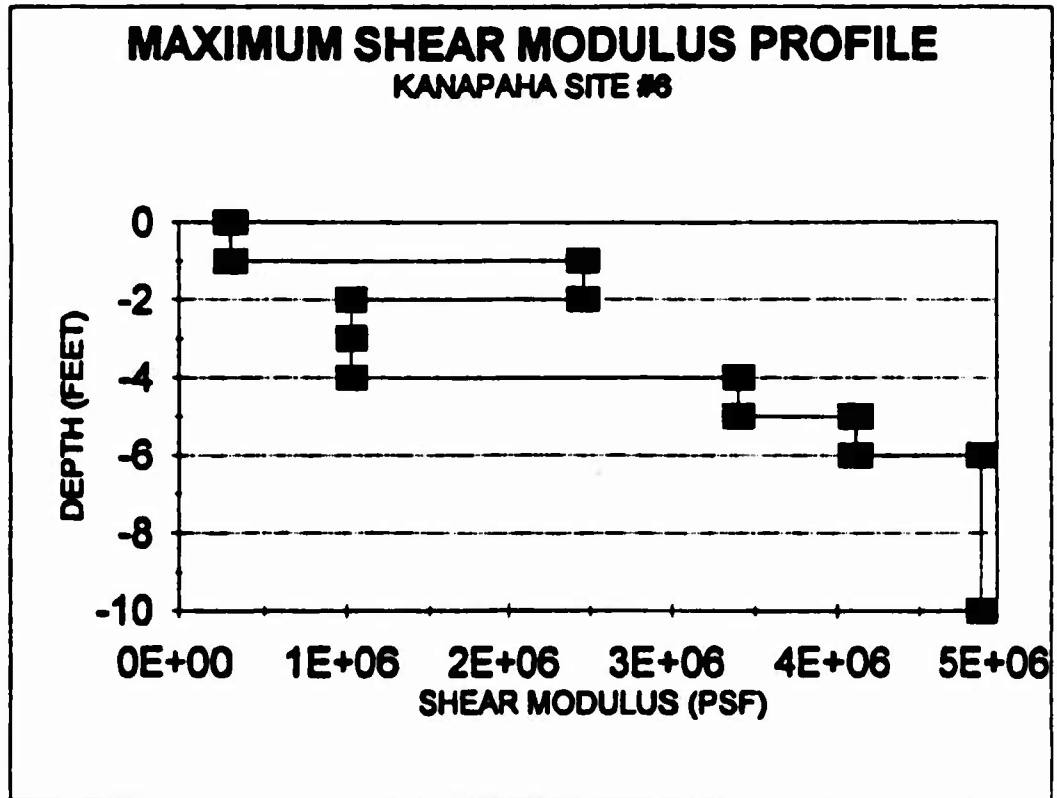


Figure 6.6 Maximum Shear Modulus Profile of Site #6

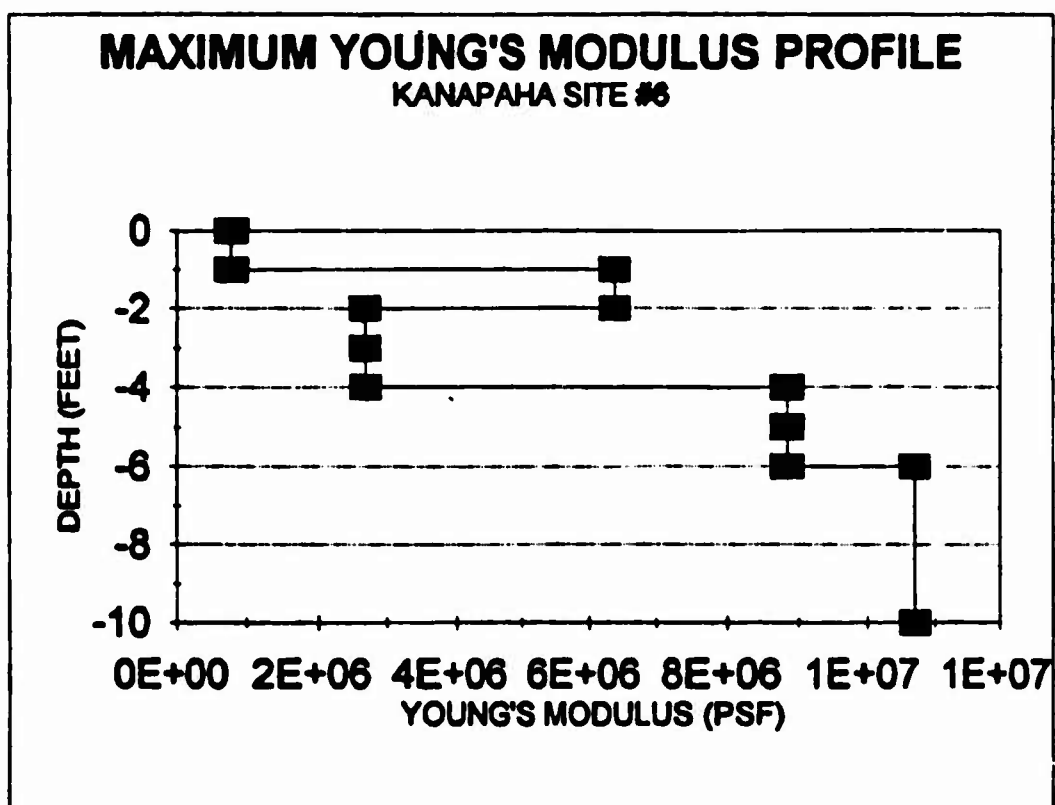


Figure 6.7 Maximum Young's Modulus Profile of Site #6

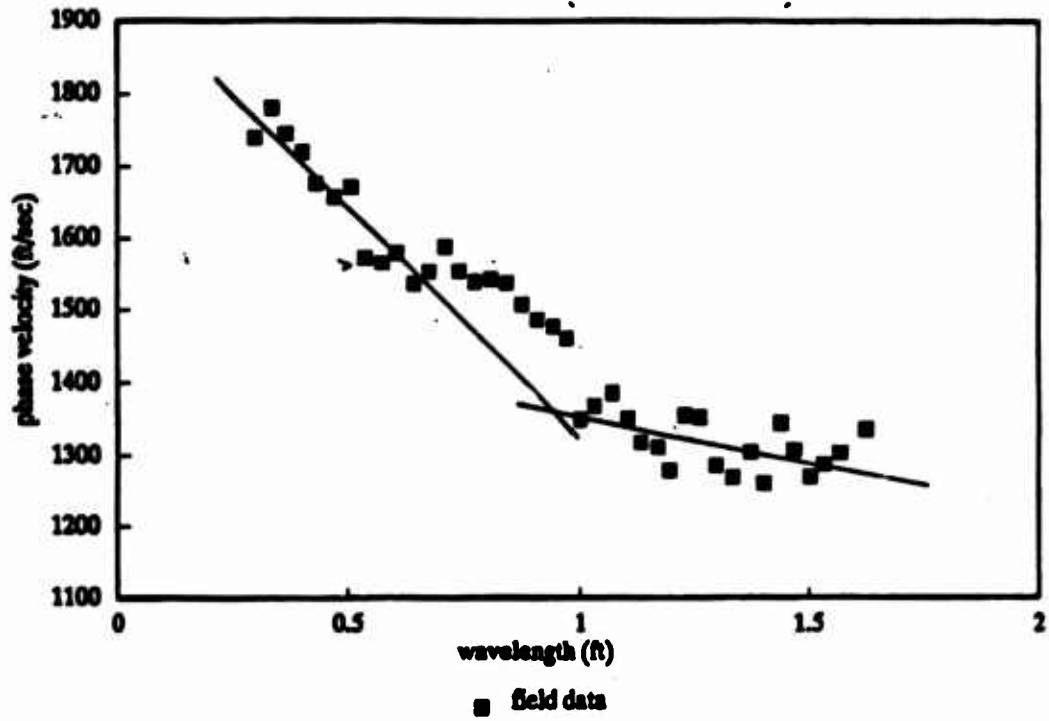


Figure 6.8 FDOT Test Pit #1 Dispersion Curve
RAP Material

6.6 Discussion of SASW Results

6.6.1 Kanapaha Site

The results for the Kanapaha site are shown in Figures 6.3 through 6.7. Since Figure 6.3 reveals a cavity at the 18 to 34 inch depth, it should be detected by the SASW technique in Figures 6.5 through 6.7. All three of these figures show a decrease in shear wave velocity or modulus in the range of 24 to 48 inches. Otherwise the velocity and modulus values show a continuous increase with depth. In Table 6.1, the inversion output shows six one foot layers, one four foot layer, and the half space. The lower than expected values in layers 3 and 4 indicate qualitatively that a softer layer exists in site #6.

6.6.2 FDOT Test Pit #1

Figure 6.8 displays the field dispersion plot for Test Pit #1. Using a technique developed by Roesset et al. (1991) the thickness of the pavement surface layer can be estimated as described in Section 2.4.7. The first step is to note the location of the change in slope of the data in the dispersion curve. This location, as drawn on Figure 6.8, is equal to a wavelength of 0.9 feet which is approximately equal to the thickness (10.5 inches or 0.875 feet) of the RAP material. This suggests that the dispersion curve, which takes 10 minutes per site to generate, can be used to verify the surface layer thickness.

CHAPTER 7

CONCLUSION AND RECOMMENDATIONS

7.1 Conclusions

It was the goal of this research to improve on the first phase of the unsurfaced airfield evaluation process, i.e., the gathering of raw airfield bearing data. The primary research effort has focused on developing airfield bearing test equipment which is equally acceptable but less labor intensive than the currently used Dynamic Cone Penetrometer (DCP). A secondary goal was to evaluate Spectral Analysis of Surface Wave (SASW) technology for use as a seismic surveying technique of non-test zones for spatial variations throughout the unsurfaced runway and aprons. From the study performed the following conclusions may be drawn.

1. The manual DCP test instrument provides consistent and repeatable results when performed in uniform insitu soil sites.
2. The manual DCP test can be used as a standard with which to compare alternative DCP prototypes, based on its relatively low coefficient of variation values.

3. A prototype Automated Airfield Dynamic Cone Penetrometer (AADCP) was designed and manufactured which penetrates the ground in much the same manner as the manual DCP. The AADCP was shown to be inherently less labor intensive than the manual DCP due to its pneumatic operation. Though the AADCP is not field-ready due to weight and power restrictions, it is a viable prototype which could be modified as explained in the recommendations section.

4. Automated Airfield Dynamic Cone Penetration Testing was performed at one site at two different blow rates. There was no significant influence of blow rate on the depth versus number of blows plot, i.e., data fell within the band of natural scatter of AADCP testing.

5. Plots of DCP and AADCP penetration indexes versus depth have the same shape and therefore suggest that both instruments detect changes in layer stiffness.

6. Correlation testing between the manual Dynamic Cone Penetrometer and the Automated Airfield Dynamic Cone Penetrometer was performed. The correlation equations and R-squared values were:

(a) For all five sites combined

$$\text{DCP} = 2.27 \text{ AADCP} - 0.12$$

$$R^2 = 0.85$$

(b) For the three sand sites

$$\text{DCP} = 2.30 \text{ AADCP} - 0.04$$

$$R^2 = 0.94$$

(c) For the two silty-sand sites

$$\text{DCP} = 0.02 \text{ AADCP} + 0.46$$

$$R^2 = 0.00$$

7. The Automated Airfield Dynamic Cone Penetrometer requires approximately 2.3 blows for every one blow of the manual DCP to achieve the same penetration.

8. Profiles of field CBR's can be determined from the Automated Airfield Dynamic Cone Penetration Test using the correlations of 6a and 6b. above and the Webster et al. equation, (5.1).

9. For practical purposes the AADCP CBR range of accuracy is 5% to 40% as shown in Appendix C CBR profiles. Since standard cargo aircraft, i.e., C-130, require at least a CBR of 10%, this range is still useful to determine the number of aircraft takeoffs and landings.

10. Statistical analysis was applied to the correlation test results of the AADCP and the DCP instruments. According to the statistical analysis using the coefficient of variation, the AADCP and DCP instruments have similar relative dispersions of their penetration indexes.

11. During the field testing, an effort was made to evaluate the advantages of the AADCP and DCP instruments.

The following were considered advantages of each device:

Advantages of the DCP

- (a) ease of transportation
- (b) cheaper to manufacturer
- (c) established correlation over 35 years
- (d) ease of maintenance

Advantages of the AADCP

- (a) ease of operation over large number of tests
- (b) field testing can be performed by one operator
- (c) operator error reduced with electronic blow counter, i.e., miscounting blows
- (d) higher blow rate decreases testing time
- (e) data acquisition easier to document with separate measuring rod

12. The SASW seismic survey technique can be used to detect soft layers and cavities qualitatively by analyzing a theoretical shear wave velocity profile. A decrease in shear wave velocity from 849 ft/sec to 550 ft/sec indicated a soft layer at site #6 in Kanapaha.

13. Using a dispersion curve, which takes 10 to 15 minutes per site to generate, the thickness of the base coarse layer of an unsurfaced airfield can be estimated by the method introduced by Roesset et al. (1991) and described in Chapter 6.

7.2 Recommendations for Future Testing

7.2.1 Airfield Evaluation Using SASW

Based on the results in Chapters 5 and 6, the unsurfaced airfield evaluation procedure should be re-evaluated. It is suggested to use the Spectral Analysis of Surface Waves seismic surveying technique to complement the Automated Airfield Dynamic Cone Penetrometer prototype in a full scale field evaluation of an unsurfaced runway. This field testing would first consist of using the SASW seismic technique to survey the unsurfaced airfield and parking ramp. The seismic survey would consist of comparing field dispersion curves at the present station spacing of 150-200 feet. Figure 7.1 shows the proposed test configuration while Figure 7.2 displays a cumulative dispersion curve over several survey stations. Note in Figure 7.1 that the seismic survey using two geophones staggers across the centerline within a 30 foot primary landing zone centered on a 60 foot wide unsurfaced airfield. It is recommended that additional testing be attempted using a multiple channel analyzers with 4 to 6 channels. This could tremendously increase the efficiency of the seismic survey. Figure 7.2 shows several dispersion curves plotted together for easy comparison. The traces for stations 1+50, 3+50 and 5+50 are quite similar while that for station 7+50 does not quite match up in phase velocity. A decision might therefore be made to perform a DCP test at station 7+50. Using the

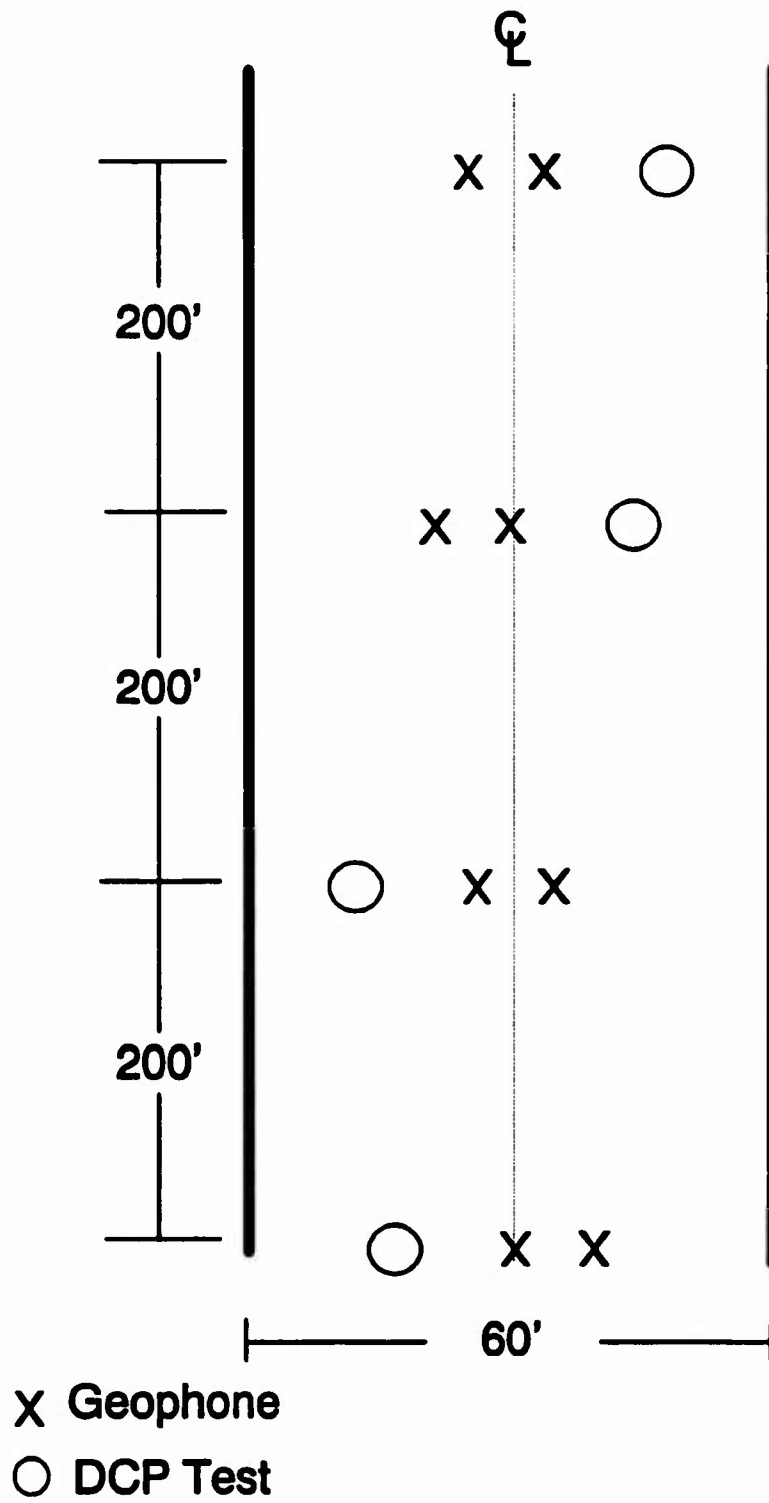


Figure 7.1 Proposed Seismic Surveying Configuration

DISPERSION CURVE

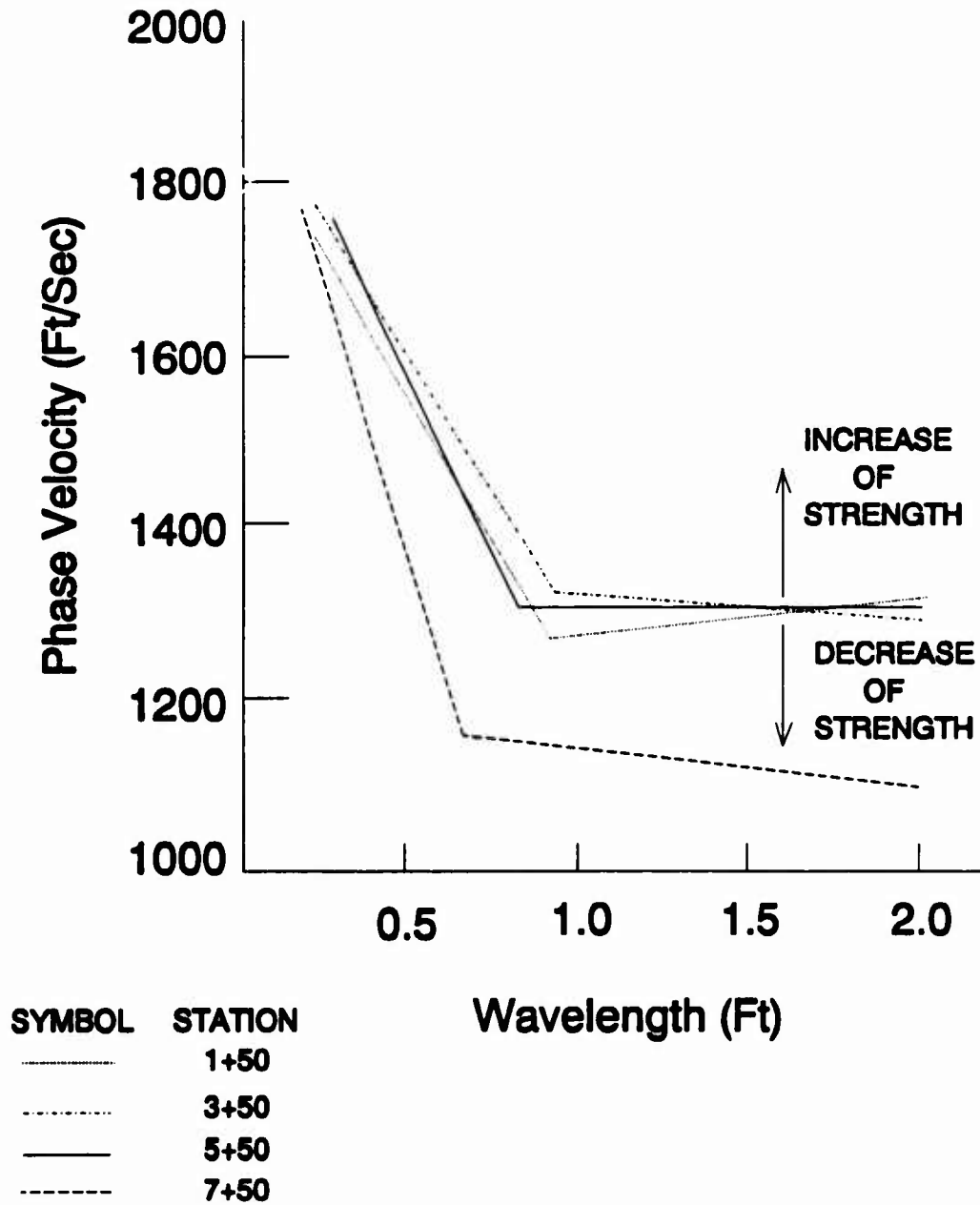


Figure 7.2 Cumulative Dispersion Curves Over Several Survey Stations

technique of overlying successive dispersion curves could decrease the number of DCP tests required to evaluate the unsurfaced airfield.

7.2.2 Airfield Evaluation Using Robotics

During the literature review phase of this research, the idea of using a robotic device to meet the research goals was considered. Based on the aerial penetrometers dropping from low flying aircraft, a robot device could be parachuted into the unsurfaced airfield. The robot could then be remotely controlled by either a party on the ground or airborne in a nearby aircraft. A research effort should be made in this area.

7.2.3 Modifications to the AADCP Prototype

Further study should be carried out on the Automated Airfield Dynamic Cone Penetrometer (AADCP) prototype. The following topics are suggested:

- (1) Study a reduction in weight using carbon kevlar components instead of aluminum

- (2) Study an alternative method of providing compressed air into the air cylinder including compressed air bottles and light weight gas-powered engines

- (3) Study an alternative method to provide the spring reaction force used to counteract the spring rebound force

- (4) Study an alternative method to allow air to escape

quickly out of the air cylinder.

(5) Study a direct correlation between the AADCP and the CBR.

Appendix A

DCP RELIABILITY TESTING DATA

This appendix presents all the data from the DCP reliability testing at the six test sites. The sites were Archer landfill, Maguire Field, Lake Alice Parking Lot, Lake Alice Shoreline, SW 24 Ave Quarry, and Newberry farm. The data presented for each site consist of the cumulative DCP penetrations, the calculated DCP values, and the WES CBR-DCP correlations. In addition, the averaged estimated CBR calculations over five inch intervals are presented. These averages were used to plot CBR profiles as discussed in Chapter 5. Also included for each site is a plot of the number of blows versus depth, developed by using the raw data.

ARCHER LANDFILL

CUMULATIVE DCP PENETRATION (INCHES)							DCP VALUES (IN/BLOW)						WEB DCP-CBR CORRELATION					
TEST	TEST	TEST	TEST	TEST	TEST	TEST	DCP	DCP	DCP	DCP	DCP	DCP	CBR	CBR	CBR	CBR	CBR	CBR
BLOW	1	2	3	4	5	6	1	2	3	4	5	6	1	2	3	4	5	6
1	-1.0	-1.0	-1.4	-1.0	-0.0	-1.0	1.0	1.0	1.4	1.0	0.0	1.0	4.0	4.0	6.0	4.0	10.0	7.0
2	-0.4	-0.0	-4.0	-4.0	-0.0	-0.4	1.0	2.0	2.0	0.4	0.4	0.4	4.0	0.0	0.7	0.0	0.0	0.0
3	-0.0	-0.0	-0.0	-0.0	-0.0	-0.0	1.0	1.0	2.0	1.0	1.0	1.0	4.0	4.0	0.0	4.0	4.0	4.0
4	-0.4	-0.0	-7.0	-7.0	-0.4	-0.0	1.0	1.0	1.0	1.4	1.4	1.0	0.4	4.0	0.4	0.0	0.0	4.0
5	-7.4	-7.0	-0.0	-0.4	-7.0	-7.0	1.0	1.0	1.0	1.0	1.0	1.0	7.0	7.0	7.0	0.4	0.4	7.0
6	-0.4	-0.0	-0.0	-0.0	-0.0	-0.4	1.0	1.0	1.0	0.0	1.0	0.0	7.0	7.0	7.0	10.0	7.0	10.0
7	-0.0	-0.0	-10.0	-10.0	-0.4	-0.4	0.0	0.0	0.0	1.0	0.0	1.0	10.0	10.0	10.0	7.0	10.0	7.0
8	-0.0	-10.0	-10.4	-10.0	-10.0	-10.0	0.0	0.0	0.4	0.0	0.0	0.0	10.0	10.0	0.0	10.0	10.0	10.0
9	-10.4	-10.0	-11.0	-11.0	-10.0	-10.0	0.0	0.0	0.0	0.4	0.0	0.0	10.0	10.0	10.0	10.0	10.0	10.0
10	-11.0	-11.4	-11.0	-11.0	-11.4	-11.0	0.0	0.0	0.0	0.0	0.0	0.0	10.0	10.0	10.0	10.0	10.0	47.0
11	-11.4	-12.0	-12.0	-12.4	-12.0	-11.0	0.4	0.0	0.4	0.0	0.0	0.0	0.0	10.0	10.0	10.0	10.0	10.0
12	-11.0	-12.4	-12.0	-12.0	-12.0	-12.0	0.4	0.4	0.0	0.0	0.0	0.4	0.0	10.0	10.0	10.0	10.0	10.0
13	-12.0	-12.0	-10.0	-10.0	-10.0	-10.0	0.4	0.4	0.4	0.0	0.4	0.0	0.0	10.0	10.0	10.0	10.0	10.0
14	-12.0	-10.0	-10.0	-14.0	-10.4	-10.0	0.4	0.4	0.0	0.4	0.4	0.4	0.0	10.0	10.0	10.0	10.0	10.0
15	-10.0	-10.0	-14.0	-14.0	-14.0	-10.0	0.4	0.0	0.4	0.0	0.0	0.0	0.0	10.0	10.0	10.0	10.0	10.0
16	-10.4	-14.0	-14.0	-10.0	-14.0	-14.0	0.4	0.4	0.4	0.0	0.0	0.4	0.0	10.0	10.0	10.0	10.0	10.0
17	-10.0	-14.0	-10.0	-10.4	-10.0	-14.4	0.4	0.4	0.4	0.4	0.4	0.4	0.0	10.0	10.0	10.0	10.0	10.0
18	-14.0	-10.0	-10.4	-10.0	-10.0	-14.0	0.4	0.4	0.4	0.4	0.4	0.4	0.0	10.0	10.0	10.0	10.0	10.0
19	-14.0	-10.0	-10.0	-10.0	-10.0	-10.0	0.4	0.0	0.4	0.4	0.4	0.0	0.0	10.0	10.0	10.0	10.0	10.0
20	-14.0	-10.0	-10.0	-10.0	-10.0	-10.0	0.0	0.4	0.4	0.4	0.4	0.0	0.0	10.0	10.0	10.0	10.0	10.0
21	-10.0	-10.0	-10.0	-17.0	-10.0	-10.0	0.0	0.4	0.4	0.4	0.4	0.4	0.0	10.0	10.0	10.0	10.0	10.0
22	-10.0	-10.0	-10.0	-17.0	-17.0	-10.0	0.0	0.0	0.0	0.0	0.0	0.0	0.0	10.0	10.0	10.0	10.0	10.0
23	-10.0	-10.0	-17.0	-17.0	-17.4	-17.0	0.4	0.4	0.4	0.4	0.4	0.4	0.0	10.0	10.0	10.0	10.0	10.0
24	-10.0	-17.0	-17.0	-10.0	-17.0	-17.4	0.4	0.4	0.4	0.4	0.4	0.4	0.0	10.0	10.0	10.0	10.0	10.0
25	-10.4	-17.0	-17.0	-10.4	-10.0	-17.0	0.4	0.0	0.0	0.4	0.4	0.0	0.0	10.0	10.0	10.0	10.0	10.0
26	-10.0	-17.0	-10.0	-10.0	-10.4	-17.0	0.4	0.4	0.4	0.0	0.0	0.0	0.0	10.0	10.0	10.0	10.0	10.0
27	-17.0	-17.0	-10.4	-10.0	-10.0	-10.0	0.4	0.0	0.0	0.4	0.0	0.0	0.0	10.0	10.0	10.0	10.0	10.0
28	-17.4	-10.0	-10.0	-10.0	-10.0	-10.4	0.0	0.4	0.0	0.0	0.4	0.4	0.0	10.0	10.0	10.0	10.0	10.0
29	-17.0	-10.4	-10.0	-10.4	-10.0	-10.0	0.0	0.0	0.4	0.0	0.0	0.0	0.0	10.0	10.0	10.0	10.0	10.0
30	-17.0	-10.0	-10.0	-10.0	-10.0	-10.0	0.0	0.0	0.0	0.4	0.4	0.4	0.0	10.0	10.0	10.0	10.0	10.0
31	-10.0	-10.0	-10.0	-00.0	-00.0	-10.4	0.0	0.4	0.4	0.0	0.4	0.0	0.0	10.0	10.0	10.0	10.0	10.0
32	-10.4	-10.0	-10.0	-00.0	-00.0	-10.0	0.4	0.0	0.0	0.0	0.0	0.0	0.0	10.0	10.0	10.0	10.0	10.0
33	-10.0	-10.0	-00.0	-00.0	-00.4	-10.0	0.0	0.4	0.0	0.4	0.0	0.0	0.0	10.0	10.0	10.0	10.0	10.0
34	-10.0	-10.0	-00.0	-00.0	-00.0	-00.0	0.0	0.0	0.0	0.0	0.4	0.4	0.0	10.0	10.0	10.0	10.0	10.0
35	-10.0	-00.0	-00.0	-01.0	-01.0	-00.4	0.4	0.0	0.4	0.0	0.4	0.0	0.0	10.0	10.0	10.0	10.0	10.0
36	-10.4	-00.0	-01.0	-01.0	-01.4	-00.0	0.0	0.0	0.4	0.0	0.0	0.0	0.0	10.0	10.0	10.0	10.0	10.0
37	-10.0	-00.4	-01.0	-01.0	-01.0	-01.0	0.0	0.0	0.0	0.4	0.0	0.4	0.0	10.0	10.0	10.0	10.0	10.0
38	-10.0	-00.0	-01.4	-00.0	-00.0	-01.0	0.0	0.0	0.0	0.4	0.4	0.0	0.0	10.0	10.0	10.0	10.0	10.0
39	-00.0	-01.0	-01.0	-00.0	-00.0	-01.4	0.4	0.4	0.4	0.0	0.0	0.0	0.0	10.0	10.0	10.0	10.0	10.0
40	-00.4	-01.0	-00.0	-00.4	-00.4	-01.0	0.0	0.0	0.0	0.0	0.0	0.0	0.0	10.0	10.0	10.0	10.0	10.0
41	-00.0	-01.4	-00.0	-00.0	-00.0	-00.0	0.0	0.0	0.0	0.0	0.0	0.0	0.0	10.0	10.0	10.0	10.0	10.0
42	-01.0	-01.0	-00.0	-00.0	-00.0	-00.0	0.4	0.4	0.4	0.4	0.0	0.0	0.0	10.0	10.0	10.0	10.0	10.0
43	-01.4	-00.0	-00.0	-00.0	-00.0	-00.4	0.4	0.0	0.4	0.0	0.0	0.0	0.0	10.0	10.0	10.0	10.0	10.0
44	-01.0	-00.0	-00.0	-00.4	-00.4	-00.0	0.4	0.0	0.0	0.0	0.4	0.0	0.0	10.0	10.0	10.0	10.0	10.0
45	-00.0	-00.4	-00.0	-00.0	-00.0	-00.0	0.0	0.0	0.0	0.0	0.4	0.4	0.0	10.0	10.0	10.0	10.0	10.0

A.1 Archer Landfill Manual DCP Raw Data and CBR Estimations

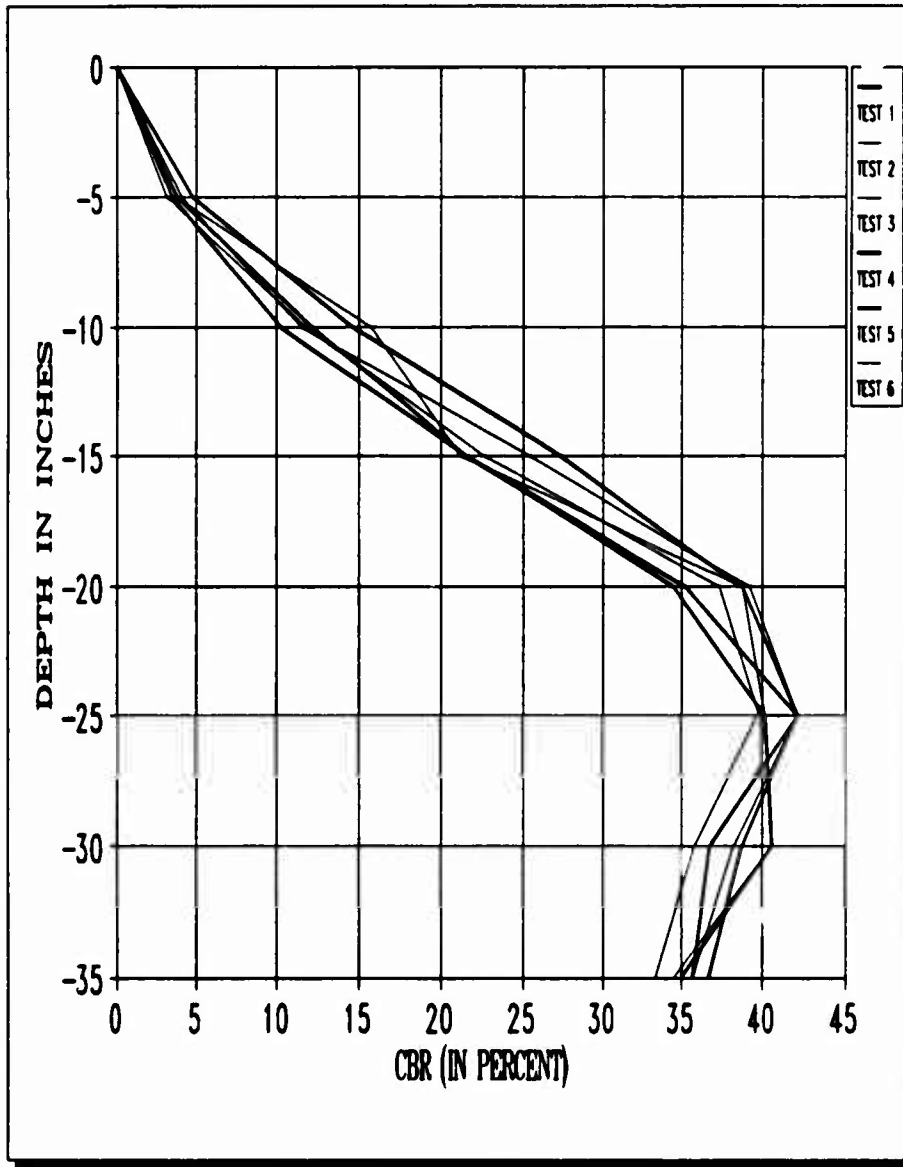
CUMULATIVE DCP PENETRATION (INCHES)							DCP VALUES (IN/BLW)						WES DCP-CBR CORRELATION					
TEST	TEST	TEST	TEST	TEST	TEST	TEST	DCP	DCP	DCP	DCP	DCP	DCP	CBR	CBR	CBR	CBR	CBR	CBR
BLW	1	2	3	4	5	6	1	2	3	4	5	6	1	2	3	4	5	6
46	-32.2	-32.0	-32.4	-34.0	-34.0	-32.2	0.2	0.2	0.2	0.4	0.2	0.2	47.3	47.3	47.3	21.8	47.3	47.3
47	-32.4	-32.8	-32.8	-34.2	-34.2	-32.4	0.2	0.2	0.4	0.2	0.2	0.2	47.3	47.3	21.8	47.3	47.3	47.3
48	-32.0	-32.0	-34.0	-34.0	-34.4	-32.0	0.2	0.2	0.2	0.4	0.2	0.2	47.3	47.3	47.3	21.8	47.3	47.3
49	-32.0	-32.4	-34.2	-34.0	-34.0	-34.0	0.4	0.4	0.2	0.2	0.2	0.4	21.8	21.8	47.3	47.3	47.3	21.8
50	-32.2	-32.0	-34.0	-32.0	-32.0	-34.2	0.2	0.4	0.4	0.2	0.4	0.2	47.3	21.8	21.8	47.3	21.8	47.3
51	-32.4	-34.0	-34.0	-32.2	-32.2	-34.0	0.2	0.2	0.2	0.2	0.2	0.4	47.3	47.3	47.3	47.3	21.8	21.8
52	-32.0	-34.2	-32.0	-32.4	-32.4	-34.0	0.2	0.2	0.2	0.2	0.2	0.2	47.3	47.3	47.3	47.3	47.3	47.3
53	-34.0	-34.4	-32.4	-32.0	-32.0	-32.0	0.4	0.2	0.4	0.2	0.2	0.2	21.8	47.3	21.8	47.3	47.3	47.3
54	-34.2	-34.0	-32.0	-32.0	-32.0	-32.2	0.2	0.2	0.2	0.2	0.4	0.2	47.3	47.3	47.3	47.3	21.8	47.3
55	-34.0	-32.0	-32.0	-32.0	-32.2	-32.4	0.4	0.4	0.2	0.2	0.2	0.2	21.8	21.8	47.3	47.3	47.3	47.3
56	-34.2	-32.2	-32.0	-32.2	-32.4	-32.0	0.2	0.2	0.2	0.2	0.2	0.2	47.3	47.3	47.3	47.3	47.3	47.3
57	-32.0	-32.4	-32.2	-32.4	-32.0	-32.0	0.2	0.2	0.2	0.2	0.4	0.4	47.3	47.3	47.3	47.3	21.8	21.8
58	-32.2	-32.0	-32.4	-32.0	-32.0	-32.2	0.2	0.2	0.2	0.4	0.2	0.2	47.3	47.3	47.3	21.8	47.3	47.3
59	-32.4	-32.0	-32.0	-32.0	-32.2	-32.4	0.4	0.2	0.4	0.2	0.2	0.2	21.8	47.3	21.8	47.3	47.3	47.3
60	-32.2	-32.0	-32.0	-32.2	-32.0	-32.0	0.2	0.2	0.2	0.2	0.4	0.4	47.3	47.3	47.3	47.3	21.8	21.8
61	-32.0	-32.2	-32.0	-32.4	-32.0	-32.0	0.2	0.2	0.0	0.2	0.2	0.2	47.3	47.3	13.0	47.3	47.3	47.3
62	-32.2	-32.4	-32.0	-32.0	-32.0	-32.4	0.2	0.2	0.4	0.4	0.2	0.4	47.3	47.3	21.8	21.8	47.3	21.8
63	-32.4	-32.0	-32.2	-32.0	-32.2	-32.0	0.2	0.4	0.2	0.2	0.2	0.2	47.3	21.8	47.3	47.3	47.3	47.3
64	-32.2	-32.0	-32.0	-32.2	-32.4	-32.0	0.2	0.2	0.0	0.2	0.2	0.2	47.3	47.3	13.0	47.3	47.3	47.3
65	-32.0	-32.2	-32.0	-32.4	-32.0	-32.0	0.2	0.2	0.2	0.2	0.2	0.2	47.3	47.3	47.3	47.3	47.3	47.3
66	-32.0	-32.4	-32.2	-32.4	-32.0	-32.4	0.2	0.2	0.2	0.4	0.2	0.4	47.3	47.3	47.3	21.8	47.3	21.8
67	-32.2	-32.0	-32.4	-32.2	-32.0	-32.0	0.2	0.4	0.2	0.4	0.2	0.2	47.3	21.8	47.3	21.8	47.3	47.3
68	-32.4	-32.0	-32.0	-32.4	-32.2	-32.0	0.2	0.2	0.2	0.2	0.2	0.4	47.3	47.3	47.3	47.3	47.3	21.8
69	-32.0	-32.4	-32.0	-32.0	-32.4	-32.2	0.4	0.4	0.4	0.2	0.2	0.2	21.8	21.8	21.8	47.3	47.3	47.3
70	-32.2	-32.0	-32.2	-32.0	-32.0	-32.4	0.4	0.0	0.2	0.0	0.4	0.0	21.8	47.3	47.3	47.3	21.8	47.3
71	-32.0	-32.0	-32.4	-32.0	-32.2	-32.0	0.4	0.0	0.2	0.2	0.4	0.2	21.8	47.3	47.3	47.3	21.8	47.3
72	-32.0	-32.0	-32.0	-32.2	-32.4	-32.0	0.2	0.2	0.4	0.2	0.2	0.2	47.3	47.3	21.8	47.3	47.3	47.3
73	-32.2	-32.2	-31.0	-32.4	-32.0	-32.0	0.4	0.2	0.2	0.2	0.2	0.2	21.8	47.3	47.3	47.3	47.3	47.3
74	-32.4	-32.4	-31.2	-32.0	-31.0	-32.2	0.2	0.2	0.2	0.4	0.4	0.2	47.3	47.3	47.3	21.8	21.8	47.3
75	-32.0	-32.0	-31.0	-31.2	-31.2	-32.0	0.2	0.4	0.4	0.4	0.2	0.4	47.3	21.8	21.8	21.8	47.3	21.8
76	-32.0	-32.2	-31.0	-31.4	-31.4	-32.0	0.2	0.4	0.2	0.2	0.2	0.2	47.3	21.8	47.3	47.3	47.3	47.3
77	-32.0	-32.4	-32.2	-31.0	-31.0	-31.0	0.2	0.2	0.4	0.2	0.2	0.2	47.3	47.3	21.8	47.3	47.3	47.3
78	-32.2	-32.0	-32.4	-32.0	-32.0	-31.4	0.2	0.4	0.2	0.4	0.4	0.4	47.3	21.8	47.3	21.8	21.8	21.8
79	-32.4	-31.0	-32.0	-32.2	-32.4	-31.0	0.2	0.2	0.2	0.2	0.4	0.4	47.3	47.3	47.3	47.3	21.8	21.8
80	-32.0	-31.4	-32.0	-32.4	-32.0	-32.0	0.2	0.4	0.4	0.2	0.2	0.2	47.3	21.8	21.8	47.3	47.3	47.3
81	-31.0	-31.0	-32.4	-32.0	-32.0	-32.2	0.4	0.2	0.4	0.2	0.2	0.2	21.8	47.3	21.8	47.3	47.3	47.3
82	-31.4	-31.0	-32.0	-32.0	-32.0	-32.4	0.4	0.2	0.2	0.2	0.2	0.2	21.8	47.3	47.3	47.3	47.3	47.3
83	-31.0	-32.0	-34.0	-32.2	-32.2	-32.0	0.2	0.2	0.4	0.4	0.2	0.4	47.3	47.3	21.8	21.8	47.3	21.8
84	-31.0	-32.4	-34.2	-32.4	-32.4	-32.0	0.2	0.4	0.2	0.2	0.2	0.2	47.3	21.8	47.3	47.3	47.3	47.3
85	-32.2	-32.0	-34.4	-32.0	-32.0	-32.4	0.4	0.4	0.2	0.4	0.4	0.4	21.8	21.8	47.3	21.8	21.8	21.8
86	-32.4	-32.2	-34.0	-34.2	-34.2	-32.0	0.2	0.4	0.4	0.4	0.4	0.2	47.3	21.8	21.8	21.8	21.8	47.3
87	-32.0	-32.4	-32.2	-34.0	-34.0	-34.0	0.2	0.2	0.4	0.4	0.0	0.4	47.3	47.3	21.8	21.8	13.0	21.8
88	-32.0	-32.0	-32.4	-34.0	-32.2	-34.2	0.4	0.2	0.2	0.2	0.4	0.2	21.8	47.3	47.3	47.3	21.8	47.3
89	-32.4	-32.0	-32.0	-32.0	-32.4	-34.0	0.4	0.2	0.4	0.2	0.2	0.4	21.8	47.3	21.8	47.3	47.3	21.8
90	-32.0	-34.2	-32.0	-32.2	-32.0	-34.0	0.2	0.4	0.2	0.2	0.4	0.2	47.3	21.8	47.3	47.3	21.8	47.3
91	-34.0	-34.4		-32.0	-32.0	-32.2	0.4	0.2		0.4	0.2	0.4	21.8	47.3		21.8	47.3	21.8
92	-34.2	-34.0		-32.0		-32.4	0.2	0.4		0.2			47.3	21.8		47.3		47.3
93	-34.0	-32.0		-32.2		-32.0	0.4	0.2		0.4		0.0	21.8	47.3		21.8		13.0
94	-34.0						0.2	0.4					47.3	21.8				
95	-32.2	-32.0					0.4	0.2					21.8	47.3				
96	-32.4	-32.0					0.2	0.4					47.3	21.8				
97	-32.0						0.2	0.4					47.3	21.8				
98	-32.0						0.4						21.8					

A.1 Archer Landfill Manual DCP Raw Data and CBR Estimations
(Continued)

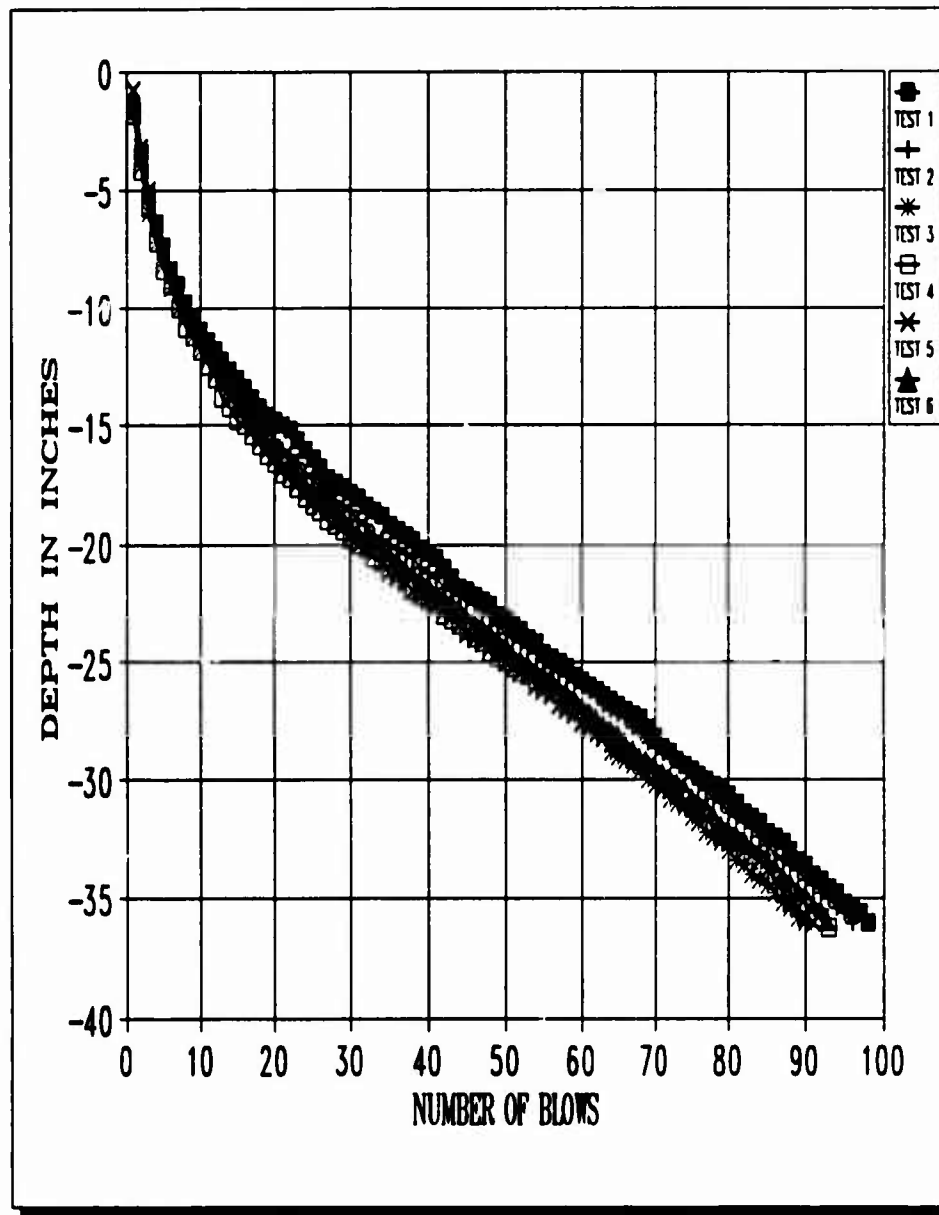
D E P T H*	AVG CBR 1	AVG CBR 2	AVG CBR 3	AVG CBR 4	AVG CBR 5	AVG CBR 6	CBR SITE AVG	ST DEV	CV
-5	4.8	4.1	3.1	3.8	3.5	3.8	3.8	0.5	13.6
-10	14.7	11.5	11.9	12.3	10.3	15.8	12.7	1.9	14.8
-15	27.2	25.3	22.6	21.5	21.6	21.2	23.3	2.3	9.7
-20	38.8	39.2	37.4	35.3	34.5	38.8	37.3	1.8	4.9
-25	42.2	42.2	39.8	42.2	40.2	40.2	41.1	1.1	2.6
-30	36.8	38.3	35.8	38.8	40.6	40.6	38.5	1.8	4.6
-35	35.7	35.7	33.4	36.7	35.0	34.5	35.1	1.0	2.9

* Depths are in inches.

A.2 Archer Landfill Average Estimated CBR Calculations



A.3 Archer Landfill Estimated CBR Profile



A.4 Archer Landfill Manual DCP Blows vs Penetration

MAGUIRE HOUSING AREA

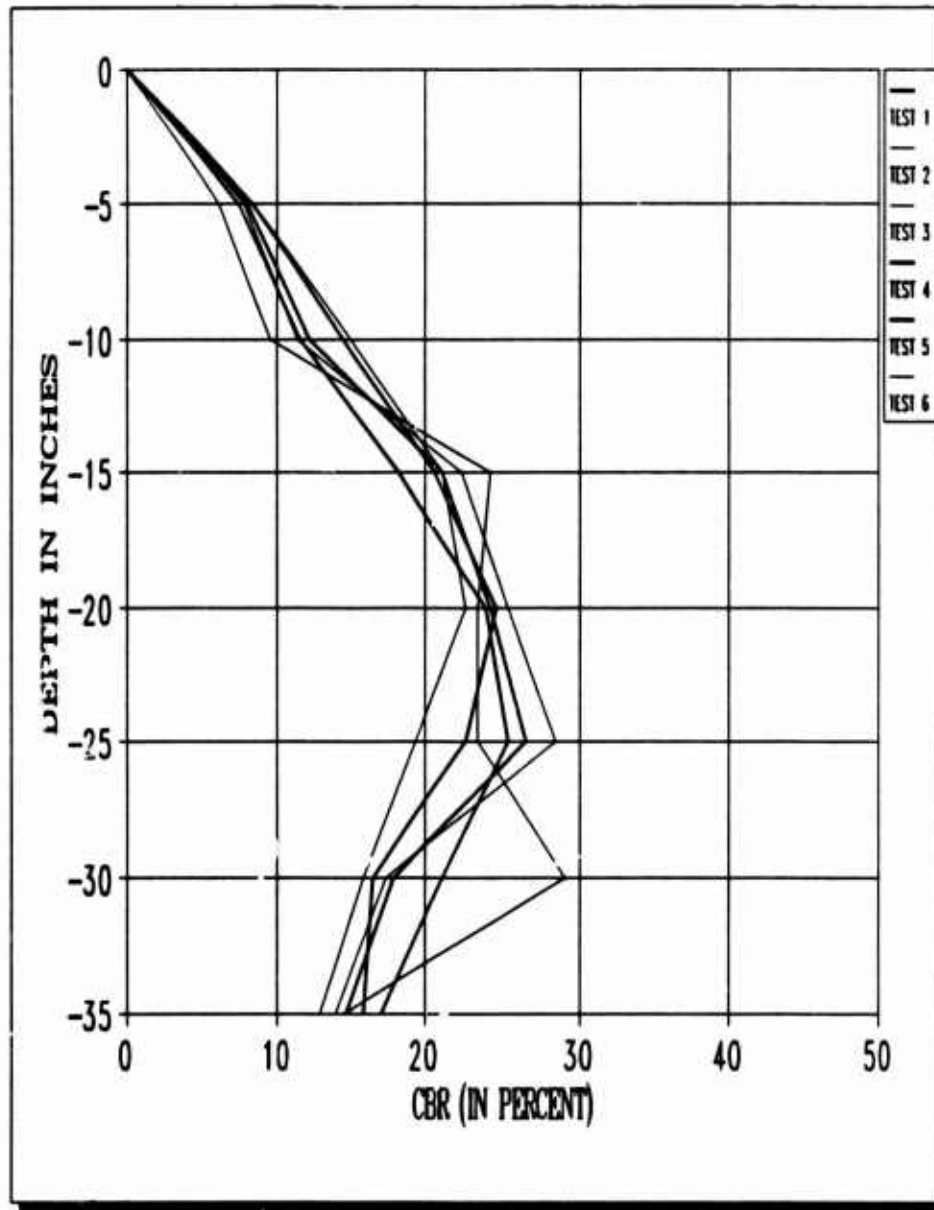
CUMULATIVE DCP PENETRATION (INCHES)							DCP VALUES (INCHES)						WBS DCP CBR CORRELATION					
TEST	TEST	TEST	TEST	TEST	TEST	TEST	DCP	DCP	DCP	DCP	DCP	DCP	CBR	CBR	CBR	CBR	CBR	CBR
NO.	1	2	3	4	5	6	1	2	3	4	5	6	1	2	3	4	5	6
1	1.0	1.0	1.0	0.0	0.4	0.4	1.0	1.0	1.0	0.0	0.4	0.4	7.0	7.0	7.0	13.0	21.0	21.0
2	2.0	2.0	2.4	1.0	1.6	1.2	1.0	1.0	1.4	1.2	1.0	0.0	7.0	7.0	8.5	6.4	6.4	10.0
3	3.0	3.0	2.4	0.0	2.0	0.0	1.0	1.0	1.0	1.4	1.2	1.0	7.0	7.0	7.0	5.3	6.4	7.0
4	4.0	4.2	4.4	4.4	4.0	3.2	1.0	1.2	1.0	1.2	1.2	1.0	7.0	6.4	7.0	6.4	6.4	7.0
5	4.0	3.6	0.4	0.2	0.0	4.2	0.0	1.4	1.0	0.0	1.0	1.0	10.0	3.3	7.0	10.0	7.0	7.0
6	5.0	0.0	0.2	0.2	0.0	0.2	1.0	1.2	0.0	1.0	1.0	1.0	7.0	6.4	10.0	7.0	7.0	7.0
7	6.0	7.0	7.2	7.2	7.0	0.2	1.0	1.0	1.0	1.2	1.0	1.0	7.0	7.0	7.0	7.0	7.0	7.0
8	7.0	0.0	0.0	0.0	7.0	7.2	1.0	1.0	0.0	0.0	0.0	1.0	7.0	7.0	10.0	10.0	10.0	7.0
9	0.0	0.0	0.0	0.0	0.0	0.0	0.0	0.0	0.0	0.0	1.0	1.0	10.0	10.0	13.0	13.0	7.0	7.0
10	0.2	10.4	0.4	0.0	0.0	0.0	0.0	0.0	0.0	1.0	0.0	1.4	13.0	10.0	10.0	7.0	10.0	5.3
11	10.0	11.2	10.2	10.2	10.2	10.2	0.0	0.0	0.0	0.0	0.0	0.0	10.0	10.0	10.0	13.0	13.0	13.0
12	10.0	10.0	10.0	10.0	11.0	11.0	0.0	0.0	0.4	0.0	0.0	0.0	13.0	10.0	21.0	13.0	10.0	10.0
13	11.0	10.0	11.2	11.4	11.0	11.0	0.4	0.0	0.0	0.0	0.0	0.0	21.0	13.0	13.0	13.0	13.0	13.0
14	11.0	13.2	11.0	10.2	10.2	10.2	0.0	0.0	0.0	0.0	0.0	0.0	10.0	13.0	13.0	10.0	13.0	13.0
15	10.2	10.0	10.2	10.0	10.0	10.2	0.4	0.4	0.4	0.0	0.0	1.0	21.0	21.0	21.0	13.0	13.0	7.0
16	10.2	14.2	10.0	13.4	10.4	13.0	0.0	0.0	0.0	0.0	0.0	0.4	13.0	10.0	10.0	10.0	13.0	21.0
17	13.2	14.0	13.4	14.0	14.0	14.0	0.4	0.4	0.0	0.0	0.0	0.4	21.0	21.0	13.0	13.0	13.0	21.0
18	14.0	10.0	14.0	14.4	14.4	14.4	0.0	0.4	0.0	0.4	0.4	0.4	10.0	21.0	13.0	21.0	21.0	21.0
19	14.4	10.4	14.2	14.0	13.0	10.0	0.4	0.4	0.2	0.4	0.0	0.0	21.0	21.0	47.3	21.0	13.0	13.0
20	14.0	10.0	14.0	10.2	10.4	10.0	0.4	0.4	0.4	0.4	0.4	0.0	21.0	21.0	21.0	21.0	21.0	47.3
21	10.2	10.2	10.2	10.0	10.0	10.0	0.4	0.4	0.0	0.4	0.0	0.0	21.0	21.0	13.0	21.0	10.0	10.0
22	10.0	10.4	10.0	10.2	10.4	10.4	0.4	0.2	0.4	0.0	0.4	0.0	21.0	47.3	21.0	13.0	21.0	21.0
23	10.0	17.0	10.0	10.4	10.0	10.0	0.4	0.0	0.4	0.2	0.4	0.4	21.0	10.0	21.0	47.3	21.0	21.0
24	10.4	17.2	10.4	17.0	17.2	17.2	0.4	0.2	0.4	0.0	0.4	0.4	21.0	47.3	21.0	13.0	21.0	21.0
25	10.0	17.0	10.0	17.4	17.0	17.0	0.0	0.0	0.4	0.4	0.0	0.0	21.0	10.0	21.0	21.0	21.0	10.0
26	17.2	10.2	17.4	17.0	10.0	10.2	0.4	0.4	0.0	0.2	0.4	0.4	21.0	21.0	10.0	47.3	21.0	21.0
27	17.0	10.0	17.0	10.2	10.4	10.4	0.4	0.4	0.4	0.0	0.4	0.2	21.0	21.0	21.0	13.0	21.0	47.3
28	10.0	10.0	10.0	10.0	10.0	10.0	0.4	0.4	0.4	0.4	0.4	0.4	21.0	21.0	21.0	21.0	21.0	21.0
29	10.4	10.4	10.0	10.0	10.2	10.2	0.4	0.4	0.4	0.2	0.4	0.4	21.0	21.0	21.0	47.3	21.0	21.0
30	10.0	10.0	10.0	10.2	10.0	10.0	0.4	0.4	0.4	0.4	0.4	0.4	21.0	21.0	21.0	21.0	21.0	21.0
31	10.0	20.2	10.4	10.0	20.0	20.2	0.2	0.4	0.4	0.0	0.4	0.0	47.3	21.0	21.0	13.0	21.0	10.0
32	10.4	20.4	20.0	20.2	20.2	20.0	0.4	0.2	0.0	0.4	0.2	0.4	21.0	47.3	13.0	21.0	47.3	21.0
33	20.0	21.0	20.4	20.0	20.0	20.0	0.0	0.0	0.4	0.0	0.4	0.2	13.0	13.0	21.0	13.0	21.0	47.3
34	20.4	21.4	20.0	21.0	21.0	21.2	0.4	0.4	0.4	0.4	0.4	0.4	21.0	21.0	21.0	21.0	21.0	21.0
35	20.0	21.0	21.0	21.4	21.0	21.0	0.4	0.4	0.2	0.2	0.4	0.4	21.0	21.0	47.3	47.3	21.0	21.0
36	21.0	22.1	21.0	21.0	21.0	20.0	0.2	0.4	0.0	0.4	0.4	0.4	47.3	21.0	10.0	21.0	21.0	21.0
37	21.4	22.0	20.0	20.2	20.2	20.4	0.4	0.4	0.4	0.4	0.4	0.4	21.0	21.0	21.0	21.0	21.0	21.0
38	20.2	20.0	20.4	20.0	20.0	20.0	0.0	0.4	0.4	0.4	0.4	0.4	10.0	21.0	21.0	21.0	21.0	21.0
39	20.2	20.4	20.0	20.2	20.0	20.0	0.4	0.4	0.4	0.0	0.4	0.2	21.0	21.0	21.0	10.0	21.0	47.3
40	20.0	20.0	20.2	20.0	20.4	20.2	0.4	0.4	0.4	0.4	0.4	0.2	21.0	21.0	21.0	21.0	21.0	47.3
41	20.2	24.2	20.0	20.0	20.0	24.0	0.2	0.4	0.4	0.2	0.4	0.0	47.3	21.0	21.0	47.3	21.0	10.0
42	20.0	24.0	24.2	24.2	24.2	24.2	0.4	0.4	0.0	0.4	0.4	0.2	21.0	21.0	13.0	21.0	21.0	47.3
43	24.2	20.0	24.0	24.0	24.0	24.0	0.0	0.4	0.4	0.4	0.4	0.0	13.0	21.0	21.0	21.0	21.0	13.0
44	24.0	20.4	20.0	20.2	24.0	20.2	0.4	0.4	0.4	0.0	0.2	0.4	21.0	21.0	21.0	10.0	47.3	21.0
45	20.0	20.0	20.4	20.0	20.2	20.0	0.4	0.4	0.4	0.4	0.4	0.4	21.0	21.0	21.0	21.0	21.0	21.0
46	20.4	20.4	20.0	20.0	20.0	20.2	0.4	0.4	0.0	0.4	0.4	0.0	21.0	10.0	10.0	21.0	21.0	13.0
47	20.0	20.0	20.4	20.2	20.2	20.0	0.0	0.2	0.4	0.2	0.0	0.4	13.0	47.3	21.0	47.3	13.0	21.0
48	20.4	27.0	27.0	20.0	20.0	27.0	0.4	0.4	0.0	0.0	0.4	0.4	21.0	21.0	13.0	13.0	21.0	21.0
49	20.0	20.0	27.4	27.0	20.0	27.2	0.4	1.0	0.4	0.2	0.2	0.0	21.0	7.0	21.0	47.3	47.3	47.3
50	27.2	20.4	20.0	27.0	27.2	27.0	0.4	0.4	0.0	0.0	0.4	0.0	21.0	21.0	13.0	13.0	21.0	13.0
51	27.0	20.0	20.4	20.0	27.0	20.2	0.4	0.0	0.4	0.4	0.4	0.0	21.0	13.0	21.0	21.0	21.0	21.0
52	10.2	20.0	20.0	20.4	20.2	20.0	0.0	0.0	0.0	0.4	0.0	0.0	13.0	0.0	13.0	21.0	13.0	13.0
53	20.0	20.0	20.0	20.0	20.0	20.0	0.4	0.1	0.0	0.0	0.4	0.4	21.0	10.0	13.0	10.0	21.0	21.0
54	20.0	20.4	20.2	20.0	20.0	20.0	0.0	0.4	0.0	0.4	0.2	0.0	13.0	21.0	13.0	21.0	47.3	13.0
55	20.0	21.2	20.0	20.2	20.2	20.2	0.4	0.0	0.0	0.0	0.4	0.4	21.0	10.0	13.0	13.0	21.0	21.0
56	20.2	21.4	21.2	20.0	20.0	20.0	0.0	0.2	0.4	0.4	0.0	0.0	13.0	47.3	21.0	21.0	13.0	10.0
57	20.0	20.0	21.0	21.2	20.2	21.2	0.0	0.0	0.0	0.0	0.4	0.4	13.0	13.0	13.0	13.0	21.0	21.0
58	21.4	22.4	22.4	21.0	20.0	20.0	0.0	0.4	0.0	0.0	0.0	0.0	13.0	21.0	13.0	13.0	13.0	10.0
59	22.0	20.0	20.0	20.2	21.2	20.0	0.0	0.0	0.0	0.4	0.4	0.0	13.0	13.0	13.0	21.0	21.0	13.0
60	22.4	24.0	24.0	22.0	21.0	20.0	0.4	1.0	0.0	0.0	0.4	0.4	21.0	7.0	10.0	13.0	21.0	21.0
61	20.2	24.4	24.4	20.2	20.2	24.0	0.0	0.4	0.0	0.4	0.0	1.0	10.0	21.0	13.0	21.0	13.0	6.4
62	20.0	20.0	20.0	20.0	20.0	20.0	0.4	0.0	0.0	0.0	0.4	0.0	21.0	10.0	10.0	10.0	21.0	13.0
63	20.2	24.0	20.0	24.4	20.0	20.4	0.0	1.0	0.0	0.0	0.4	0.0	13.0	7.0	13.0	13.0	21.0	13.0
64	24.0		20.2	20.2	20.0	20.0	0.0		0.0	0.0	0.0	0.0	13.0		10.0	13.0	13.0	10.0
65	20.4			20.0	20.2		0.0			0.0	0.0		13.0		10.0	13.0	13.0	10.0
66	20.2			20.2	24.0		0.0			0.4	0.4		10.0		21.0	21.0		
67					20.2						0.0					13.0		
68					20.0						0.0						10.0	
69																		
70																		

A.5 Maguire Field Manual DCP Raw Data and CBR Estimations

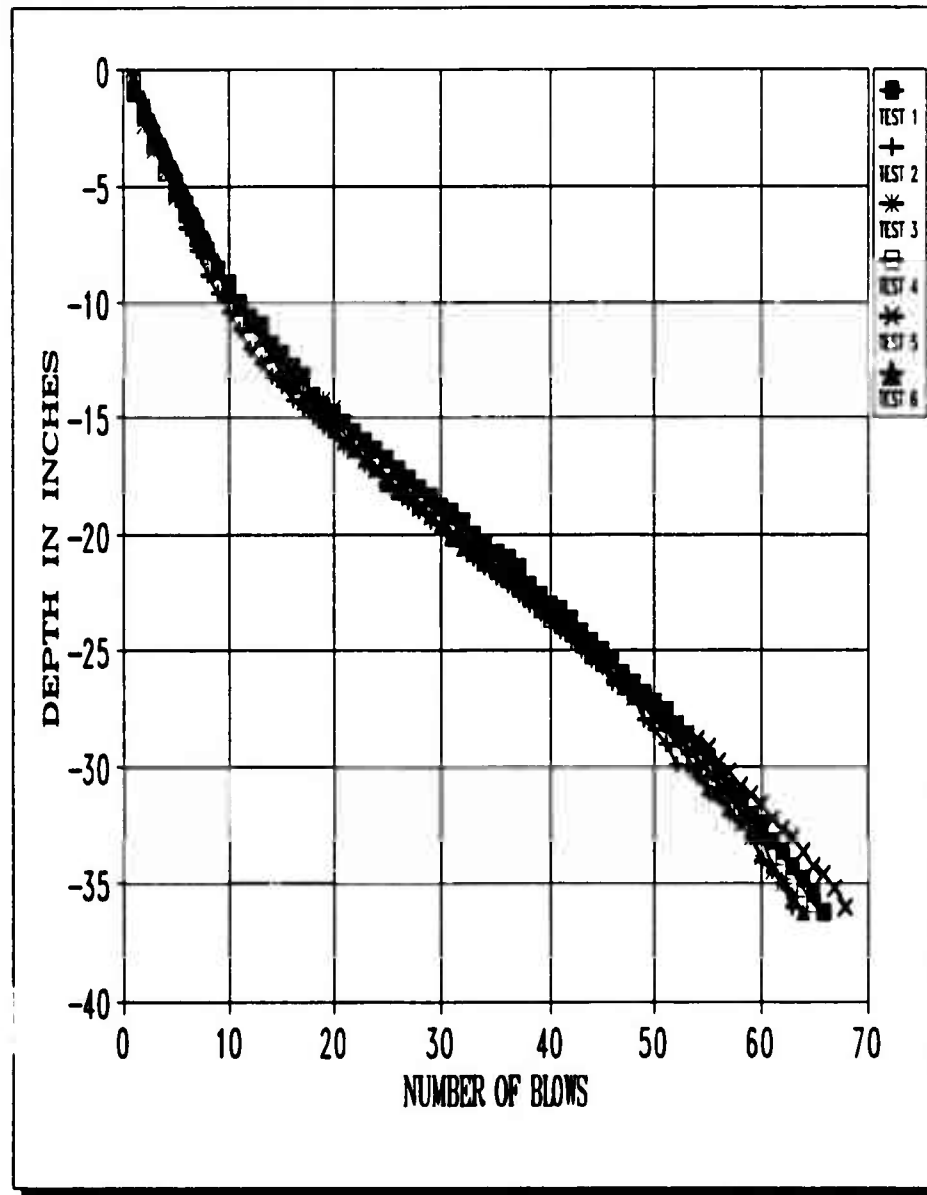
D E P T H*	AVG CBR 1	AVG CBR 2	AVG CBR 3	AVG CBR 4	AVG CBR 5	AVG CBR 6	CBR SITE AVG	ST DEV	CV
-5	8.4	6.0	8.4	8.0	7.4	7.8	7.7	0.8	10.4
-10	14.5	9.6	15.0	12.2	11.5	11.4	12.3	1.9	15.1
-15	20.6	24.2	21.1	21.1	18.2	22.4	21.3	1.8	8.5
-20	24.6	23.4	22.6	24.2	23.9	25.3	24.0	0.8	3.6
-25	22.6	23.4	19.4	26.6	25.3	28.5	24.3	2.9	12.1
-30	16.5	29.1	15.8	17.8	21.1	17.3	19.6	4.6	23.3
-35	15.8	14.5	12.9	14.6	17.0	13.9	14.8	1.3	8.9

* Depths are in inches.

A.6 Maguire Field Average Estimated CBR Calculations



A.7 Maguire Field Estimated CBR Profile



A.8 Maguire Field Manual DCP Blows vs Penetration

LAKE ALICE PARKING LOT

[illegible]

A.9 Lake Alice Pkg Lot Manual DCP Raw Data and CBR Estimations

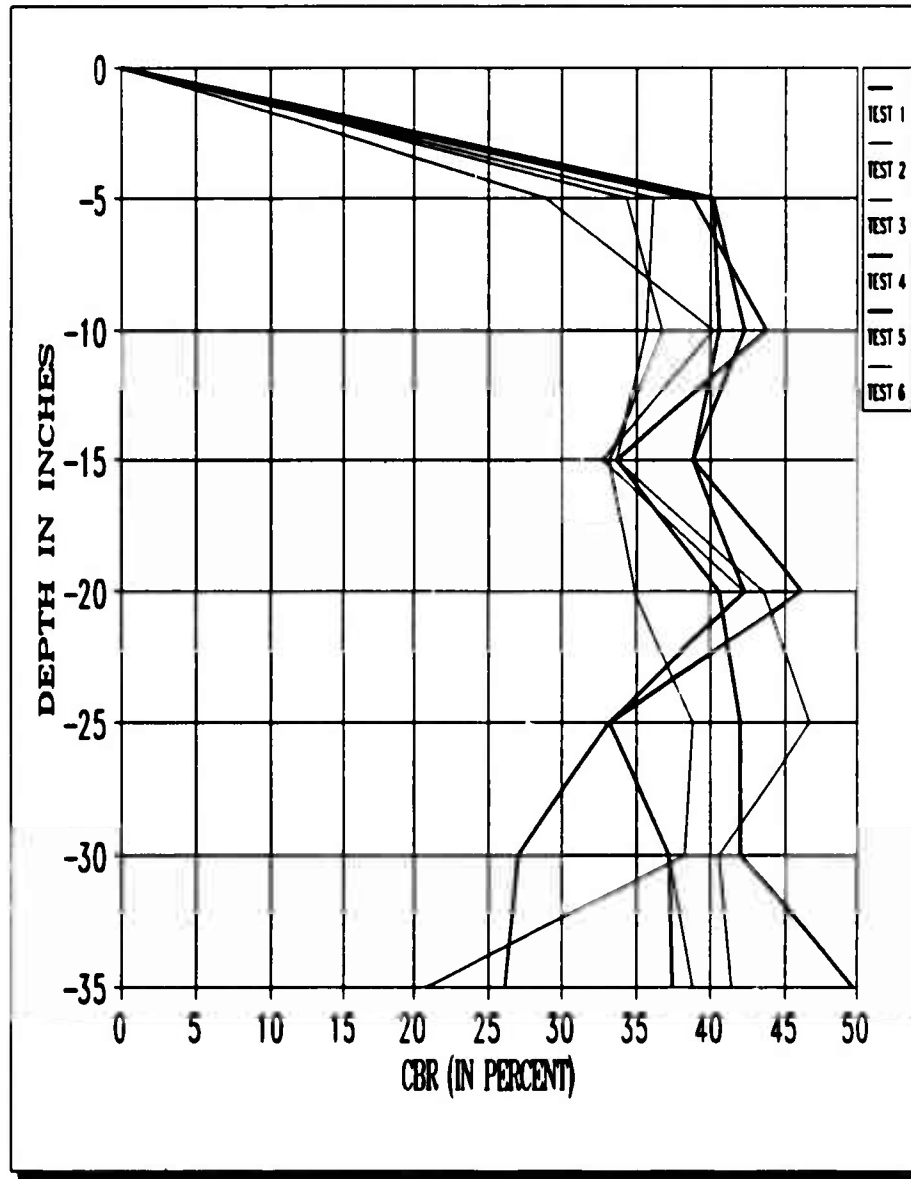
[illegible]

A.9 Lake Alice Pkg Lot Manual DCP Raw Data and CBR Estimations (Continued)

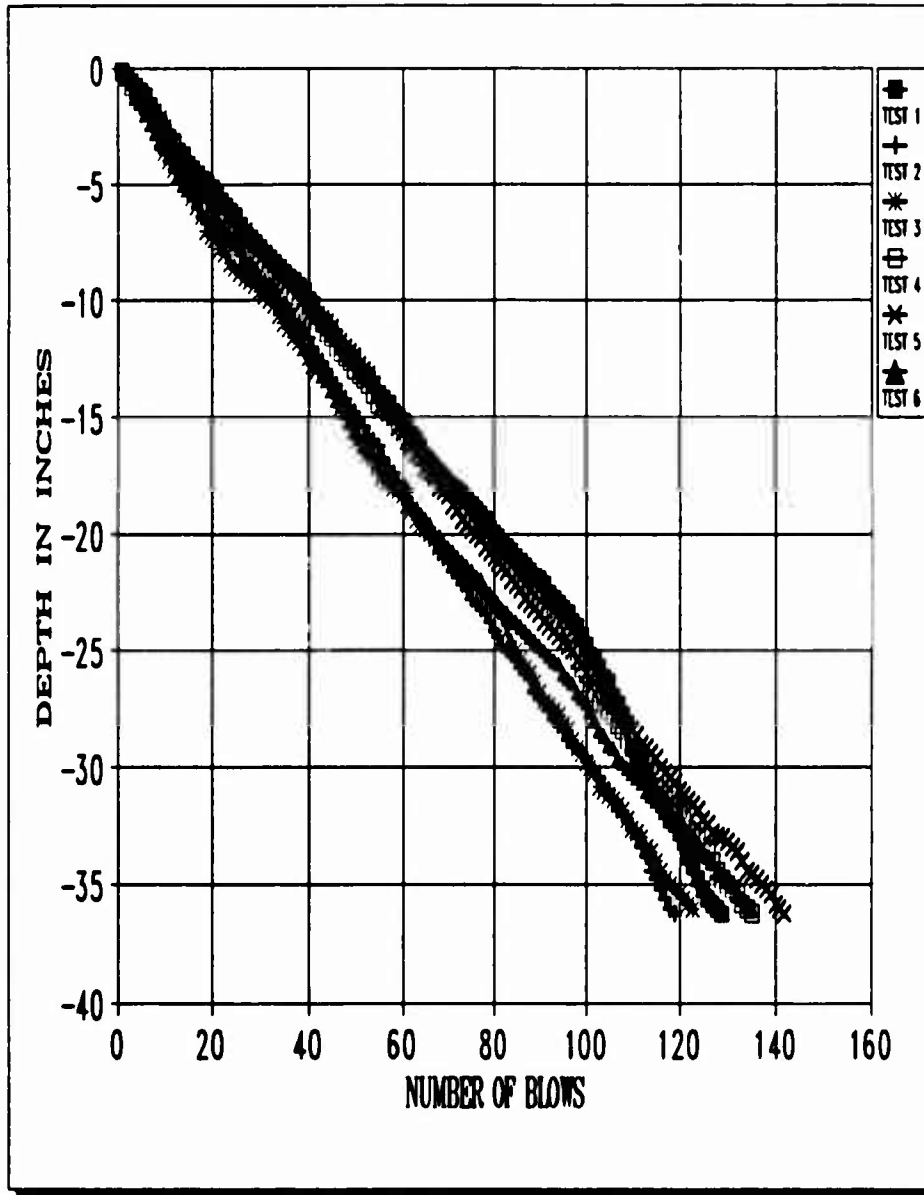
D E P T H*	AVG CBR 1	AVG CBR 2	AVG CBR 3	AVG CBR 4	AVG CBR 5	AVG CBR 6	CBR SITE AVG	ST DEV	CV
-5	40.2	34.3	28.9	40.2	38.7	36.1	36.4	3.9	10.9
-10	42.1	36.7	40.2	40.5	43.6	35.6	39.8	2.8	7.1
-15	38.7	33.1	32.7	38.7	33.6	33.6	35.1	2.6	7.4
-20	46.1	34.8	42.1	42.1	40.5	43.4	41.5	3.4	8.3
-25	33.1	38.8	33.1	33.1	41.9	46.6	37.8	5.1	13.7
-30	27.0	38.2	37.2	37.2	41.9	40.5	37.0	4.7	12.9
-35	26.1	20.8	38.7	37.4	49.7	41.4	35.7	9.6	26.9

* Depths are in inches.

A.10 Lake Alice Pkg Lot Average Estimated CBR Calculations



A.11 Lake Alice Pkg Lot Estimated CBR Profile



A.12 Lake Alice Pkg Lot Manual DCP Blows vs Penetration

LAKE ALICE SHORTLINE

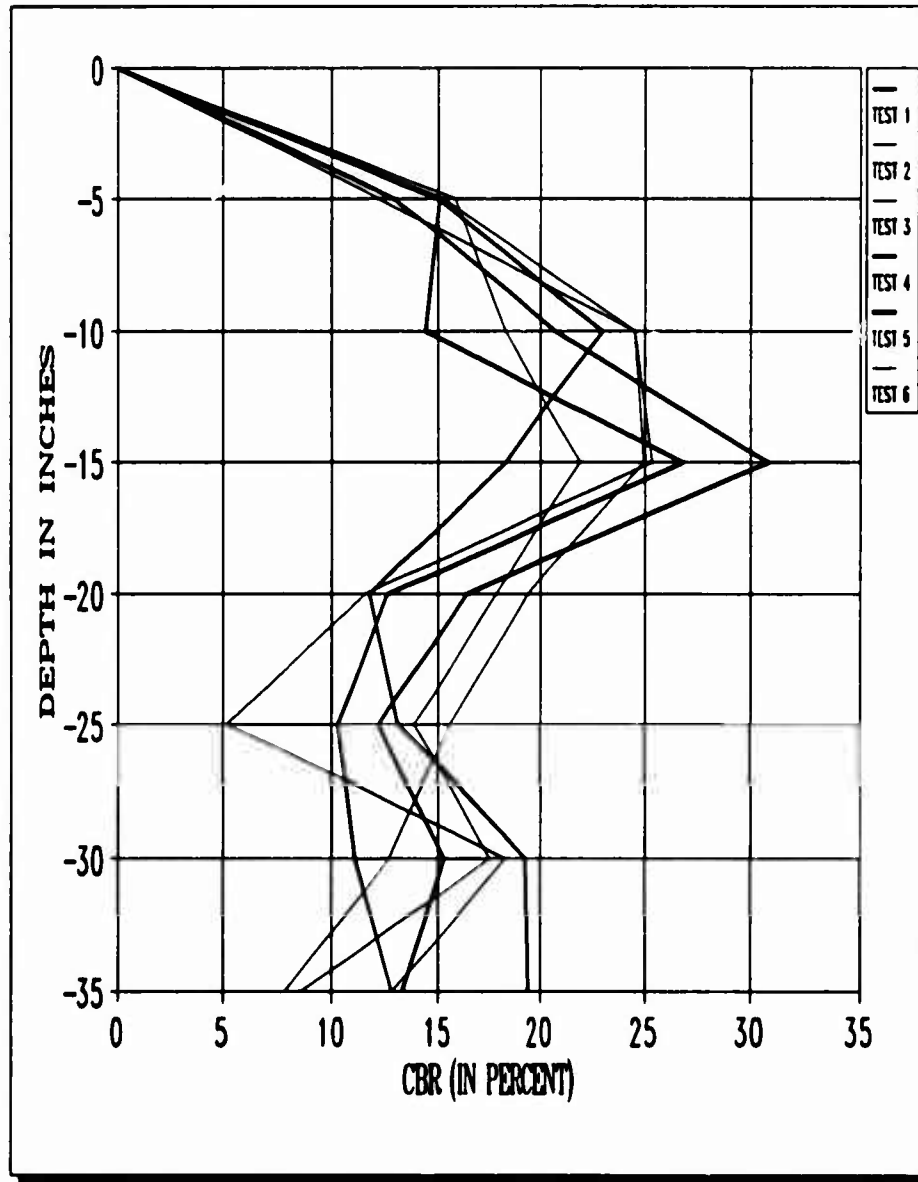
OVERALL DCP PENETRATION (INCHES)							DCP VALUES (KSI/IN)						WED DCP DCP CORRELATION					
TEST	TEST	TEST	TEST	TEST	TEST	TEST	DCP	DCP	DCP	DCP	DCP	DCP	DCP	DCP	DCP	DCP	DCP	DCP
DATE	1	2	3	4	5	6	1	2	3	4	5	6	1	2	3	4	5	6
1	3.0	3.0	3.0	3.0	3.0	3.0	3.0	3.0	3.0	3.0	3.0	3.0	1.7	2.1	2.1	2.1	2.1	2.0
2	4.0	4.2	4.2	4.0	4.0	4.0	1.0	1.0	1.0	0.0	1.0	1.2	7.0	7.0	7.0	10.0	3.0	6.4
3	5.0	5.0	0.0	4.0	0.4	3.0	0.0	0.0	0.0	0.0	0.0	0.0	10.0	10.0	10.0	10.0	10.0	10.0
4	4.0	3.4	0.0	0.0	0.0	0.0	0.0	0.4	1.0	0.4	0.0	0.0	21.0	21.0	7.0	21.0	13.0	10.0
5	4.0	5.0	0.0	3.0	0.0	0.0	0.0	0.0	0.4	0.4	0.0	0.4	10.0	10.0	21.0	21.0	13.0	21.0
6	7.0	0.0	7.0	0.0	7.0	0.0	0.4	0.0	0.0	0.0	0.4	0.0	21.0	10.0	10.0	10.0	21.0	10.0
7	7.0	7.0	0.0	0.0	7.0	7.0	0.0	0.4	1.0	0.0	0.0	0.4	10.0	21.0	7.0	13.0	13.0	21.0
8	0.4	7.0	0.0	7.0	0.0	0.0	0.0	0.4	0.0	0.0	0.4	0.0	10.0	21.0	10.0	10.0	21.0	10.0
9	0.0	0.0	0.0	0.0	0.0	0.4	0.0	0.0	0.0	0.0	0.0	0.4	10.0	10.0	10.0	10.0	10.0	10.0
10	0.0	0.4	0.0	0.0	0.0	0.0	0.0	0.4	0.0	0.0	0.4	0.0	10.0	21.0	10.0	10.0	21.0	10.0
11	10.0	0.0	10.0	0.0	0.0	0.4	0.0	0.0	0.4	0.4	0.0	0.4	10.0	10.0	21.0	21.0	10.0	10.0
12	11.0	0.0	10.0	10.0	10.0	10.0	0.0	0.4	0.4	1.0	0.4	0.0	10.0	21.0	21.0	7.0	21.0	10.0
13	11.4	10.0	11.0	10.4	10.0	10.4	0.4	0.0	0.4	0.4	0.0	0.4	21.0	13.0	21.0	21.0	13.0	21.0
14	10.0	10.4	11.0	11.0	11.0	10.0	0.0	0.4	0.4	0.0	0.4	0.4	10.0	21.0	21.0	13.0	21.0	21.0
15	10.0	11.0	11.0	11.0	11.0	11.4	0.0	0.0	0.0	0.0	0.0	0.0	10.0	10.0	07.0	07.0	10.0	10.0
16	10.0	11.4	10.0	10.0	10.0	11.0	0.0	0.4	0.4	0.0	0.2	0.4	07.0	21.0	21.0	10.0	07.0	21.0
17	10.4	10.0	10.0	10.0	10.4	10.0	0.4	0.0	0.0	0.0	0.4	0.0	21.0	13.0	07.0	07.0	21.0	07.0
18	14.0	10.0	10.0	10.0	10.0	10.0	0.0	0.4	0.4	0.4	0.2	0.0	13.0	21.0	21.0	21.0	07.0	07.0
19	14.0	10.0	13.0	10.0	10.0	10.0	0.0	0.0	0.4	0.4	0.4	0.0	07.0	21.0	21.0	21.0	21.0	13.0
20	14.0	10.0	10.0	10.0	10.0	10.0	0.4	0.4	0.0	0.0	0.0	0.0	21.0	21.0	07.0	10.0	07.0	07.0
21	10.0	10.4	10.0	14.0	10.4	10.4	0.4	0.4	0.4	0.4	0.0	0.4	21.0	21.0	21.0	21.0	21.0	21.0
22	10.4	14.0	14.0	14.0	10.0	10.0	0.4	0.0	0.4	0.0	0.0	0.4	21.0	10.0	21.0	13.0	21.0	21.0
23	10.0	14.0	14.0	10.0	14.0	14.0	0.4	0.0	0.4	0.4	0.2	0.0	21.0	07.0	21.0	21.0	07.0	07.0
24	10.0	14.0	10.0	10.0	14.0	14.0	0.0	0.4	0.0	0.0	0.0	0.2	07.0	21.0	13.0	10.0	07.0	21.0
25	10.4	10.0	10.4	10.0	14.0	14.0	0.4	0.4	0.4	0.4	0.4	0.4	21.0	21.0	21.0	21.0	21.0	21.0
26	17.0	10.0	10.0	10.4	10.0	10.0	0.0	0.0	0.0	0.4	0.4	0.4	10.0	10.0	10.0	21.0	21.0	21.0
27	17.4	10.0	10.0	17.0	10.4	10.0	0.4	0.4	0.0	0.0	0.4	0.4	21.0	21.0	07.0	13.0	21.0	21.0
28	10.0	10.4	10.0	10.0	10.0	10.0	0.0	0.4	0.4	1.0	0.0	0.4	10.0	21.0	21.0	7.0	10.0	21.0
29	10.4	17.0	17.0	10.4	10.0	10.0	0.4	0.0	0.4	0.4	0.0	0.4	21.0	10.0	21.0	21.0	10.0	10.0
30	10.0	17.4	17.4	10.0	17.0	10.0	0.0	0.4	0.0	0.0	0.0	0.4	10.0	21.0	10.0	10.0	07.0	21.0
31	20.0	17.0	10.0	20.0	17.0	17.4	1.0	0.4	0.4	1.0	0.0	0.0	7.0	21.0	21.0	7.0	10.0	10.0
32	20.0	10.0	10.4	21.0	10.0	17.0	0.0	0.4	0.4	1.0	0.4	0.0	10.0	21.0	21.0	7.0	21.0	07.0
33	21.0	10.0	10.0	20.0	10.0	10.0	0.0	0.0	0.0	1.0	0.0	0.0	10.0	10.0	13.0	7.0	10.0	10.0
34	20.0	10.0	10.4	20.0	10.0	10.0	1.0	0.4	0.4	1.0	0.4	0.0	7.0	21.0	21.0	7.0	21.0	10.0
35	20.0	10.0	10.0	24.0	10.0	10.4	1.0	0.4	0.4	1.0	0.0	0.0	7.0	21.0	21.0	7.0	10.0	10.0
36	24.0	20.0	20.0	24.0	20.0	20.0	0.0	0.0	0.4	0.0	0.4	0.0	10.0	10.0	21.0	10.0	21.0	10.0
37	20.0	20.0	20.0	20.0	21.0	21.0	0.0	0.4	0.0	0.4	0.0	1.0	10.0	21.0	13.0	21.0	10.0	7.0
38	20.0	21.0	21.0	20.0	21.0	20.0	0.0	0.4	0.0	0.4	0.0	1.0	10.0	21.0	21.0	7.0	21.0	0.4
39	20.0	21.0	21.0	20.0	20.0	20.0	0.0	0.0	0.0	0.0	0.0	1.4	10.0	13.0	10.0	10.0	10.0	0.0
40	27.4	20.0	20.0	27.0	20.0	21.0	0.0	0.0	0.4	0.0	1.0	1.0	10.0	10.0	21.0	10.0	7.0	7.0
41	20.0	20.0	20.0	20.0	24.0	27.4	0.0	0.0	0.0	0.0	0.0	0.0	10.0	10.0	10.0	10.0	10.0	2.0
42	20.0	24.0	20.4	20.0	24.0	20.0	1.0	0.0	0.4	0.0	0.0	0.0	7.0	10.0	21.0	13.0	10.0	10.0
43	20.0	24.0	24.0	20.0	20.0	20.4	0.0	0.0	0.0	0.4	0.4	0.4	10.0	10.0	10.0	21.0	21.0	21.0
44	20.4	20.0	24.4	20.0	20.0	20.0	0.0	0.4	0.4	0.0	1.0	0.0	10.0	21.0	21.0	10.0	7.0	10.0
45	21.0	20.0	20.0	20.0	27.0	20.4	0.0	0.0	0.0	0.4	1.0	0.4	10.0	10.0	10.0	21.0	7.0	21.0
46	21.0	20.4	20.0	21.0	27.0	20.0	0.0	0.4	0.0	0.0	0.0	0.0	10.0	21.0	10.0	10.0	10.0	10.0
47	22.0	27.0	20.4	21.0	20.0	20.4	0.0	0.0	0.0	0.0	0.4	0.4	10.0	10.0	10.0	07.0	21.0	21.0
48	20.0	20.0	27.0	22.0	20.0	20.0	0.0	0.0	0.0	0.0	0.0	0.4	10.0	10.0	10.0	10.0	10.0	21.0
49	20.0	20.0	27.0	22.0	20.0	21.0	0.0	0.0	0.0	0.0	0.4	0.4	10.0	07.0	10.0	10.0	21.0	21.0
50	20.4	20.0	20.4	20.0	20.0	21.0	0.0	0.0	0.0	0.4	0.0	0.0	10.0	10.0	10.0	21.0	10.0	10.0
51	20.0	20.0	20.0	20.0	20.0	20.4	0.0	0.0	0.0	0.0	0.0	0.0	10.0	10.0	10.0	10.0	10.0	10.0
52	20.0	20.0	20.0	20.0	21.0	20.0	0.0	1.0	0.0	0.2	0.4	0.0	10.0	13.0	10.0	07.0	21.0	10.0
53	21.0	20.0	20.0	20.0	20.0	20.0	0.0	0.0	1.0	1.0	0.0	0.0	10.0	10.0	7.0	7.0	10.0	10.0
54	21.0	20.0	20.0	20.0	20.0	20.4	0.0	0.0	0.0	0.0	0.0	0.0	10.0	10.0	10.0	10.0	10.0	10.0
55	20.0	21.0	20.0	20.4	20.0	20.0	0.0	0.0	0.0	0.4	0.0	0.0	10.0	10.0	10.0	21.0	10.0	10.0
56	20.4	20.0	20.0	20.0	20.0	20.0	0.0	0.0	0.0	1.0	0.0	0.0	10.0	10.0	10.0	7.0	10.0	10.0
57	20.4	20.0	20.0	20.0	20.0	20.0	1.0	1.0	0.0	0.0	0.0	0.0	7.0	7.0	10.0	10.0	10.0	10.0
58	20.4	20.0	20.0	20.0	20.0	20.0	1.0	1.0	0.0	0.0	0.0	0.0	7.0	7.0	10.0	10.0	10.0	10.0
59	27.0	20.0	20.0	20.0	20.0	20.0	1.0	1.0	0.0	0.0	0.0	0.0	4.0	7.0	10.0	10.0	10.0	10.0
60	20.0	20.0	20.0	20.0	20.0	20.0	0.0	0.0	0.0	0.0	0.0	0.0	0.0	0.0	0.0	0.0	0.0	0.0

A.13 Lake Alice Shoreline Manual DCP Raw Data and CBR Estimations

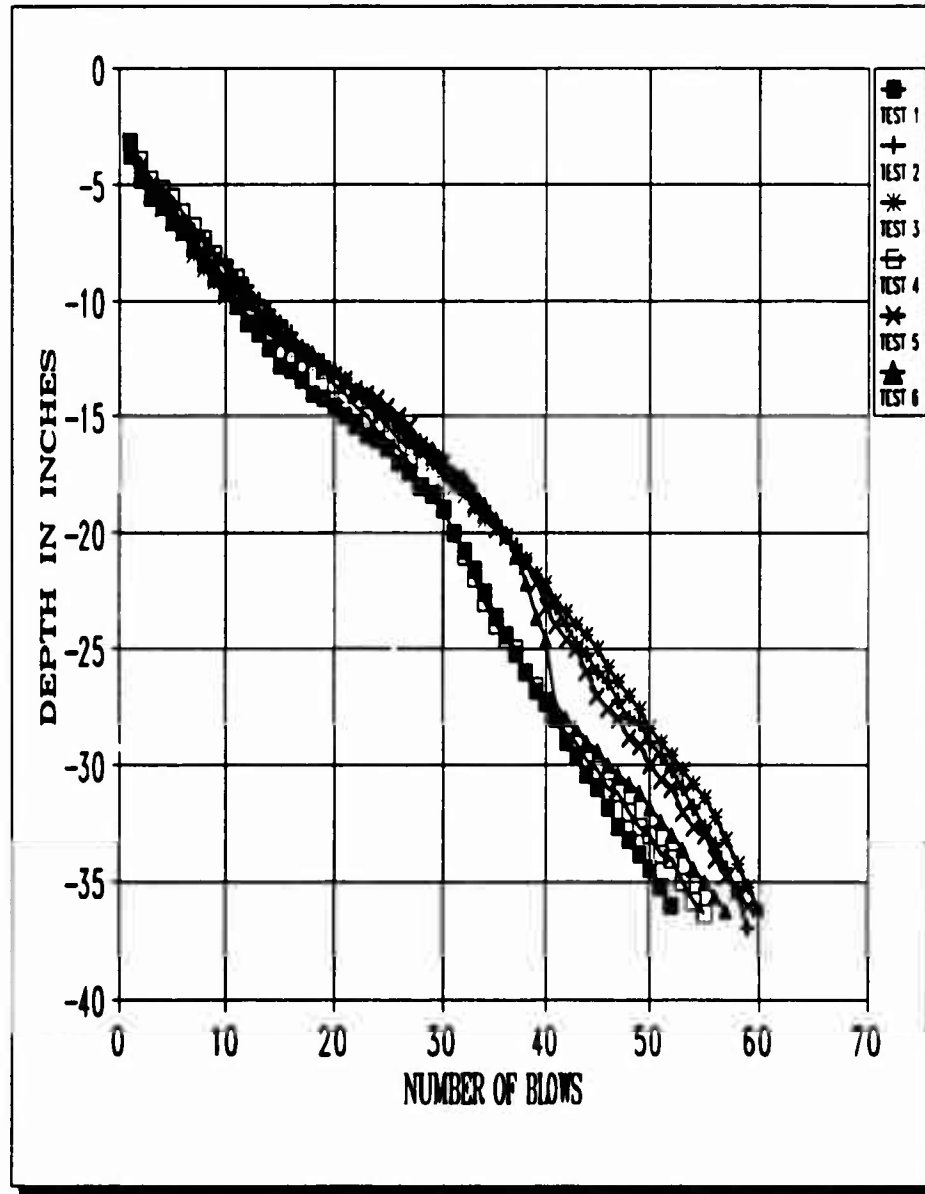
D E P T H*	AVG CBR 1	AVG CBR 2	AVG CBR 3	AVG CBR 4	AVG CBR 5	AVG CBR 6	CBR SITE AVG	ST DEV	CV
-5	15.0	15.8	12.2	15.0	12.9	15.2	14.4	1.3	9.1
-10	14.4	18.2	24.5	22.9	20.8	24.5	20.9	3.6	17.4
-15	26.8	21.9	25.0	18.2	30.8	25.4	24.7	3.9	15.8
-20	12.7	17.8	19.4	11.8	16.4	11.6	14.9	3.1	20.5
-25	10.3	13.9	15.5	13.1	12.2	5.1	11.7	3.4	28.6
-30	11.1	17.5	12.7	19.2	15.3	18.2	15.7	2.9	18.9
-35	12.9	8.5	7.8	19.4	13.4	12.9	12.5	3.8	30.4

* Depths are in inches.

A.14 Lake Alice Shoreline Average Estimated CBR Calculations



A.15 Lake Alice Shoreline Estimated CBR Profile



A.16 Lake Alice Shoreline Manual DCP Blows vs Penetration

QUARRY THE ROCK FILL PAD

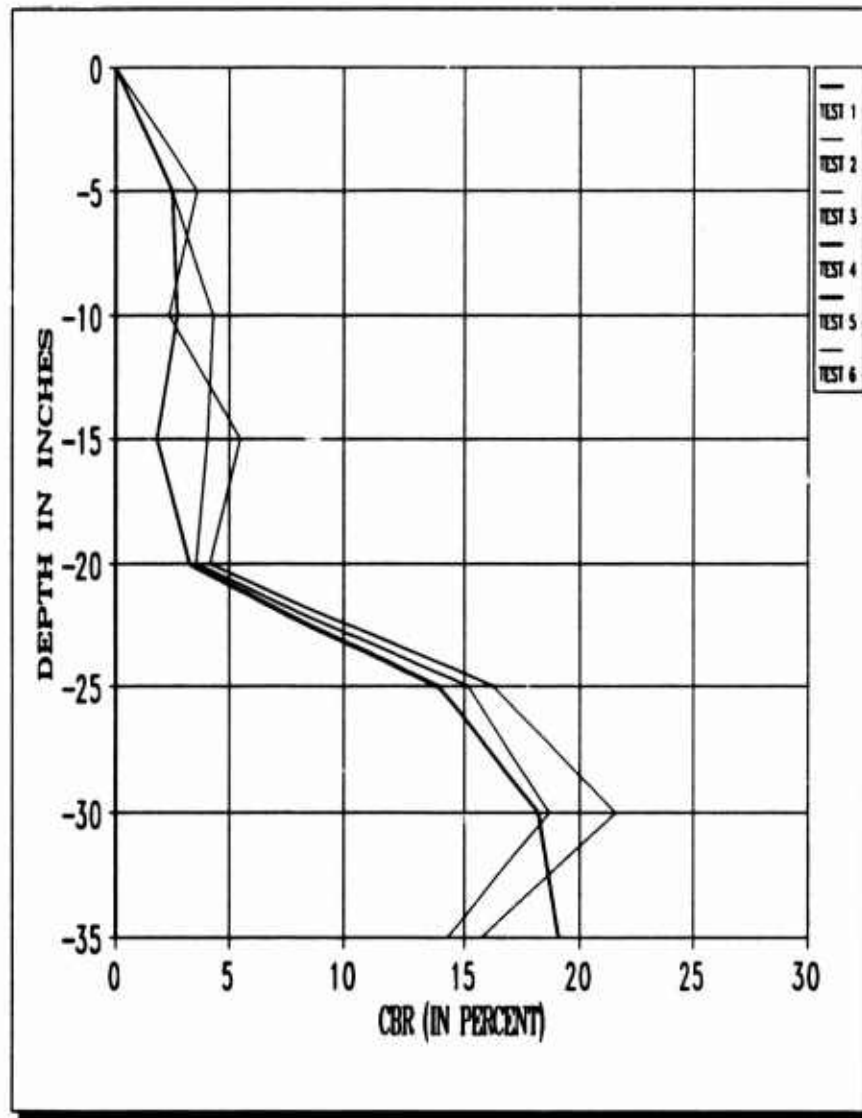
CUMULATIVE DCP PENETRATION (INCHES)							DCP VALUES (IN/BLow)						WES DCP-CBR CORRELATION					
	TEST	TEST	TEST	TEST	TEST	TEST	DCP	DCP	DCP	DCP	DCP	DCP	CBR	CBR	CBR	CBR	CBR	CBR
BLow	1	2	3	4	5	6	1	2	3	4	5	6	1	2	3	4	5	6
1	-2.5	-2.2	-2.2				2.5	2.2	2.2				2.5	2.5	2.5			
2	-4.5	-4.5	-4.5				2.5	2.5	2.5				2.5	2.5	2.7			
3	-6.5	-7.5	-7.5				2.5	2.5	2.5				2.3	3.5	2.5			
4	-11.2	-10.0	-9.5				2.5	3.5	2.2				2.7	2.5	3.2			
5	-15.2	-13.5	-11.2				2.5	3.5	1.4				3.5	2.5	5.3			
6	-17.5	-15.5	-13.5				2.5	2.5	2.5				1.7	3.5	5.5			
7	-23.5	-19.2	-15.5				3.5	1.5	1.5				1.7	7.5	4.5			
8	-25.5	-19.5	-17.5				2.2	1.5	2.5				3.2	4.5	2.7			
9	-34.2	-25.4	-25.4				1.2	2.4	2.5				5.4	2.5	2.5			
10	-35.5	-31.5	-28.5				0.5	1.4	1.5				15.5	5.5	4.5			
11	-35.4	-32.5	-28.5				0.4	1.5	1.2				21.5	7.5	5.4			
12	-35.5	-32.2	-28.5				0.5	0.4	0.5				15.5	21.5	15.5			
13	-35.5	-34.5	-24.5				0.5	0.5	0.4				15.5	15.5	21.5			
14	-37.2	-34.4	-25.5				0.4	0.4	0.5				21.5	21.5	15.5			
15	-35.5	-35.5	-25.5				0.5	0.5	0.5				15.5	15.5	15.5			
16	-35.4	-35.5	-25.2				0.4	0.5	0.4				21.5	15.5	21.5			
17	-35.5	-35.5	-25.5				0.5	0.4	0.5				15.5	21.5	15.5			
18	-35.4	-35.5	-27.7				0.4	0.5	0.5				21.5	15.5	5.5			
19	-35.5	-27.2	-25.5				0.5	0.5	0.5				15.5	15.5	25.5			
20	-35.4	-27.5	-25.5				0.4	0.5	0.5				21.5	15.5	15.5			
21	-34.5	-25.2	-25.5				0.5	0.4	0.4				15.5	21.5	21.5			
22	-34.4	-25.5	-25.5				0.4	0.4	0.5				21.5	21.5	15.5			
23	-35.5	-25.5	-25.5				0.5	0.4	0.4				15.5	21.5	21.5			
24	-35.4	-25.5	-25.4				0.4	0.5	0.4				21.5	15.5	21.5			
25	-35.5	-25.2	-21.2				0.5	0.5	0.5				15.5	15.5	15.5			
26	-35.4	-25.5	-21.5				0.4	0.4	0.4				21.5	21.5	21.5			
27	-34.5	-21.5	-22.2				0.5	0.4	0.5				15.5	21.5	15.5			
28	-34.4	-21.2	-25.5				0.4	0.2	0.5				21.5	47.5	15.5			
29	-35.5	-25.5	-25.5				0.5	0.5	0.5				15.5	15.5	15.5			
30	-35.4	-25.4	-24.5				0.4	0.4	0.4				21.5	21.5	21.5			
31	-35.5	-25.5	-25.5				0.4	0.5	1.5				21.5	15.5	7.5			
32	-35.5	-25.5	-25.5				0.5	0.5	0.5				15.5	15.5	15.5			
33		-24.2	-25.5					0.5	0.4				15.5					
34		-24.5						0.5					15.5					
35		-25.5						0.4					21.5					
36		-25.5						0.5					15.5					
37		-25.4						0.4					21.5					
38		-27.5																
39																		
40																		

A.17 SW 24 Ave Quarry Manual DCP Raw Data and CBR Estimations

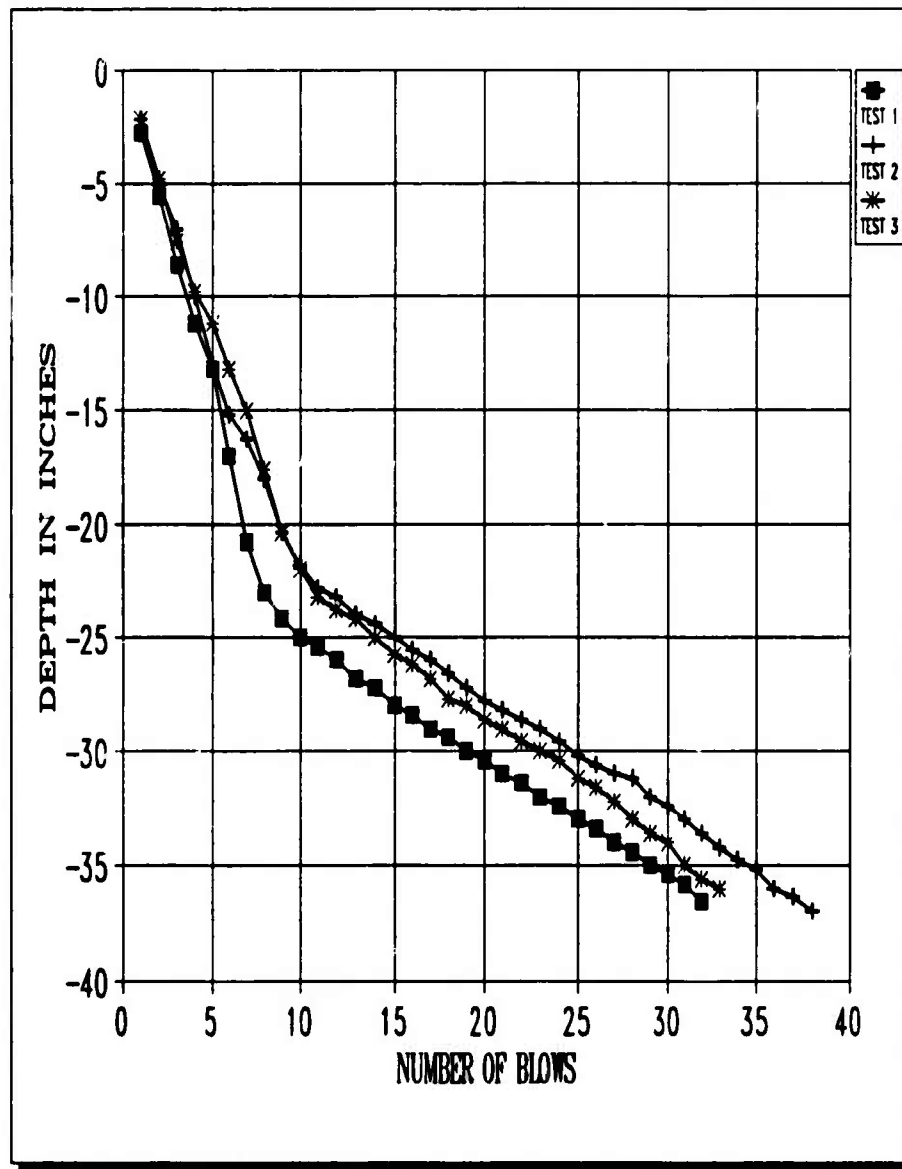
D E P T H*	AVG CBR 1	AVG CBR 2	AVG CBR 3	CBR SITE AVG	ST DEV	CV
-5	2.5	3.6	2.5	2.9	3.9	10.9
-10	2.7	2.3	4.3	3.1	2.8	7.1
-15	1.7	5.5	4.0	3.7	2.6	7.4
-20	3.2	4.1	3.5	41.5	3.4	8.3
-25	13.9	16.3	15.2	37.8	5.1	13.7
-30	18.2	21.5	18.7	37.0	4.7	12.9
-35	19.1	15.8	14.3	35.7	9.6	26.9

* Depths are in inches.

A.18 SW 24 Ave Quarry Average Estimated CBR Calculations



A.19 SW 24 Ave Quarry Estimated CBR Profile



A.20 SW 24 Ave Quarry Manual DCP Blows vs Penetration

NEWBERRY FARM

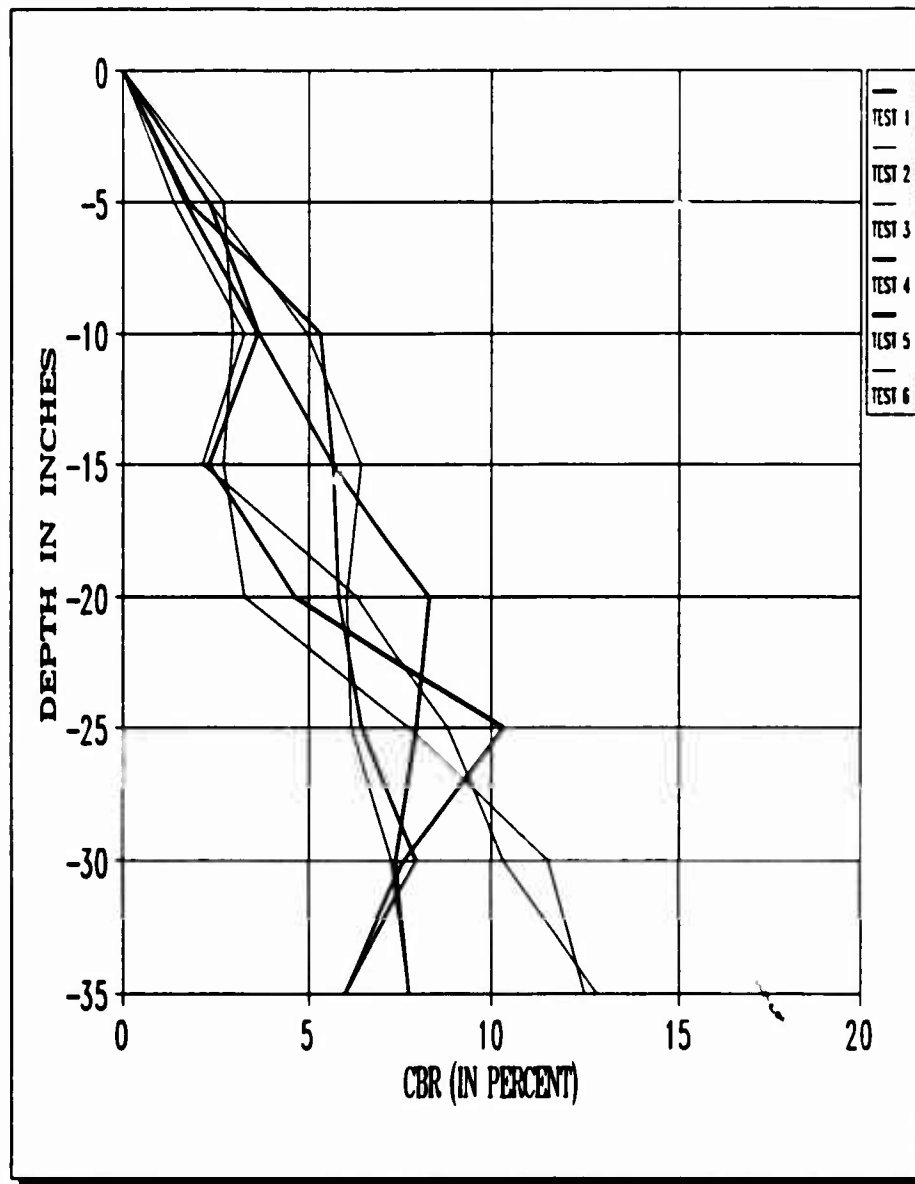
CUMULATIVE DCP PENETRATION (INCHES)							DCP VALUES (IN/BLOW)							WES DCP-CBR CORRELATION						
BLOW	TEST 1	TEST 2	TEST 3	TEST 4	TEST 5	TEST 6	DCP 1	DCP 2	DCP 3	DCP 4	DCP 5	DCP 6	CBR 1	CBR 2	CBR 3	CBR 4	CBR 5	CBR 6		
1	-5.0	-4.0	-1.0	-4.0	-4.0	-5.0	5.0	4.0	1.0	4.0	4.0	5.0	1.3	1.7	7.8	1.7	1.7	1.3		
2	-6.0	-6.8	-7.0	-4.0	-7.8	-6.0	3.0	4.8	6.0	4.0	3.8	3.0	2.3	1.3	1.0	1.7	1.7	2.3		
3	-10.2	-11.0	-8.0	-10.0	-9.8	-10.0	2.2	2.2	2.8	2.0	2.0	2.0	3.2	3.2	2.7	3.0	3.0	3.8		
4	-12.0	-13.0	-12.0	-12.0	-11.4	-11.2	1.8	2.8	2.4	2.0	1.8	1.2	4.0	2.7	2.9	3.0	4.0	6.4		
5	-14.0	-16.8	-14.4	-16.4	-12.4	-12.8	2.0	3.2	2.4	3.4	1.8	1.8	3.8	2.1	2.9	2.0	7.8	4.8		
6	-16.0	-16.2	-17.8	-16.4	-13.4	-14.2	2.0	2.4	2.8	3.0	1.8	1.4	3.8	2.9	2.7	2.3	7.8	5.3		
7	-17.0	-20.4	-19.8	-20.8	-14.8	-15.0	1.8	1.2	2.8	2.4	1.4	0.8	7.8	8.4	2.7	2.9	5.3	10.0		
8	-18.2	-21.8	-21.8	-22.0	-16.0	-16.8	1.2	1.2	2.2	1.2	1.2	1.8	8.4	8.4	3.2	8.4	8.4	4.0		
9	-19.0	-22.8	-23.0	-22.0	-17.4	-19.0	0.8	1.2	1.2	1.0	1.4	1.2	10.0	8.4	8.4	7.8	5.3	8.4		
10	-20.0	-23.8	-24.8	-24.0	-18.8	-19.2	1.0	1.0	1.0	1.0	1.4	1.2	7.8	7.8	7.8	7.8	5.3	8.4		
11	-21.0	-24.8	-25.8	-24.8	-20.0	-21.0	1.0	0.8	1.0	0.8	1.2	1.8	7.8	10.0	7.8	10.0	8.4	4.0		
12	-22.0	-25.8	-26.8	-25.8	-21.4	-22.0	1.0	1.2	1.0	0.8	1.4	1.0	7.8	8.4	7.8	10.0	5.3	7.8		
13	-23.0	-26.8	-27.8	-26.4	-23.0	-23.4	1.0	0.8	1.0	0.8	1.8	1.4	7.8	10.0	7.8	10.0	4.8	5.3		
14	-24.0	-27.4	-28.8	-27.0	-24.8	-25.0	1.0	0.8	1.0	0.8	1.0	1.8	7.8	10.0	7.8	13.8	7.8	4.8		
15	-24.8	-28.2	-29.8	-27.8	-26.2	-26.0	0.8	0.8	1.0	0.8	1.2	1.0	10.0	10.0	7.8	10.0	8.4	7.8		
16	-25.0	-29.0	-30.8	-28.8	-28.0	-27.8	1.2	0.8	0.8	1.0	1.4	1.8	8.4	10.0	13.8	7.8	5.3	4.0		
17	-27.0	-30.0	-30.4	-30.8	-30.0	-30.8	1.0	1.0	0.8	0.8	1.4	2.0	7.8	7.8	10.0	10.0	5.3	3.8		
18	-28.0	-30.8	-31.8	-30.8	-30.8	-30.4	1.0	0.8	0.8	1.2	1.0	0.8	7.8	10.0	13.8	8.4	7.8	13.8		
19	-29.0	-31.4	-31.8	-32.0	-30.8	-32.0	1.0	0.8	0.8	1.2	0.8	1.8	7.8	13.8	10.0	8.4	10.0	4.8		
20	-30.0	-32.2	-32.4	-32.2	-30.8	-32.0	1.0	0.8	0.8	1.2	1.0	1.0	7.8	10.0	13.8	8.4	7.8	7.8		
21	-31.0	-33.0	-33.0	-34.8	-32.0	-34.0	1.0	0.8	0.8	1.4	1.2	1.0	7.8	10.0	13.8	5.3	8.4	7.8		
22	-32.2	-33.8	-33.8	-35.8	-32.2	-35.0	1.2	0.8	0.8	1.2	1.2	1.0	8.4	13.8	13.8	8.4	8.4	7.8		
23	-33.2	-34.2	-34.4	-37.0	-34.4	-36.0	1.0	0.8	0.8	1.2	1.2	1.0	7.8	13.8	10.0	8.4	8.4	7.8		
24	-34.2	-35.0	-35.0	-38.0	-35.8	-37.0	1.0	0.8	0.8	1.0	1.2	1.8	7.8	10.0	13.8	7.8	8.4	7.8		
25	-35.2	-35.8	-35.8	-38.8	-37.8	-38.0	1.0	0.8	0.8	1.8	1.4	1.0	7.8	13.8	13.8	4.8	5.3	7.8		
26	-36.0	-36.8	-36.4	-39.2	-38.8	-39.0	0.8	0.4	0.8	0.8	1.0	1.0	10.0	21.8	10.0	13.8	7.8	7.8		
27			-37.0	-41.0	-39.0	-40.0			0.8	0.8	1.0	1.0			13.8	10.0	7.8	7.8		
28			-38.0	-42.0	-40.0	-40.8			1.0	1.0	1.0	0.8			7.8	7.8	7.8	10.0		
29			-38.8	-42.8	-41.8	-41.8			0.8	0.8	1.0	1.0			10.0	10.0	7.8	7.8		
30			-39.8	-44.0	-42.8	-43.4			0.8	1.2	1.0	1.8			10.0	8.4	7.8	4.8		
31			-40.4	-45.0	-43.4	-45.2			0.8	1.0	1.4	1.8			10.0	7.8	5.3	4.8		
32			-41.2	-46.0	-45.0	-47.0			0.8	1.0	1.8	1.8			10.0	7.8	4.8	4.0		
33			-42.0	-47.2	-47.0	-48.2			0.8	1.2	2.0	1.2			10.0	8.4	3.8	8.4		
34			-43.0	-48.2	-48.4				1.0	1.0	1.4				7.8	7.8	5.3			
35			-44.8						1.0						7.8					
36			-45.8						1.0						7.8					
37			-46.8						1.0						7.8					
38			-48.0																	
39																				
40																				

A.21 Newberry Farm Manual DCP Raw Data and CBR Estimations

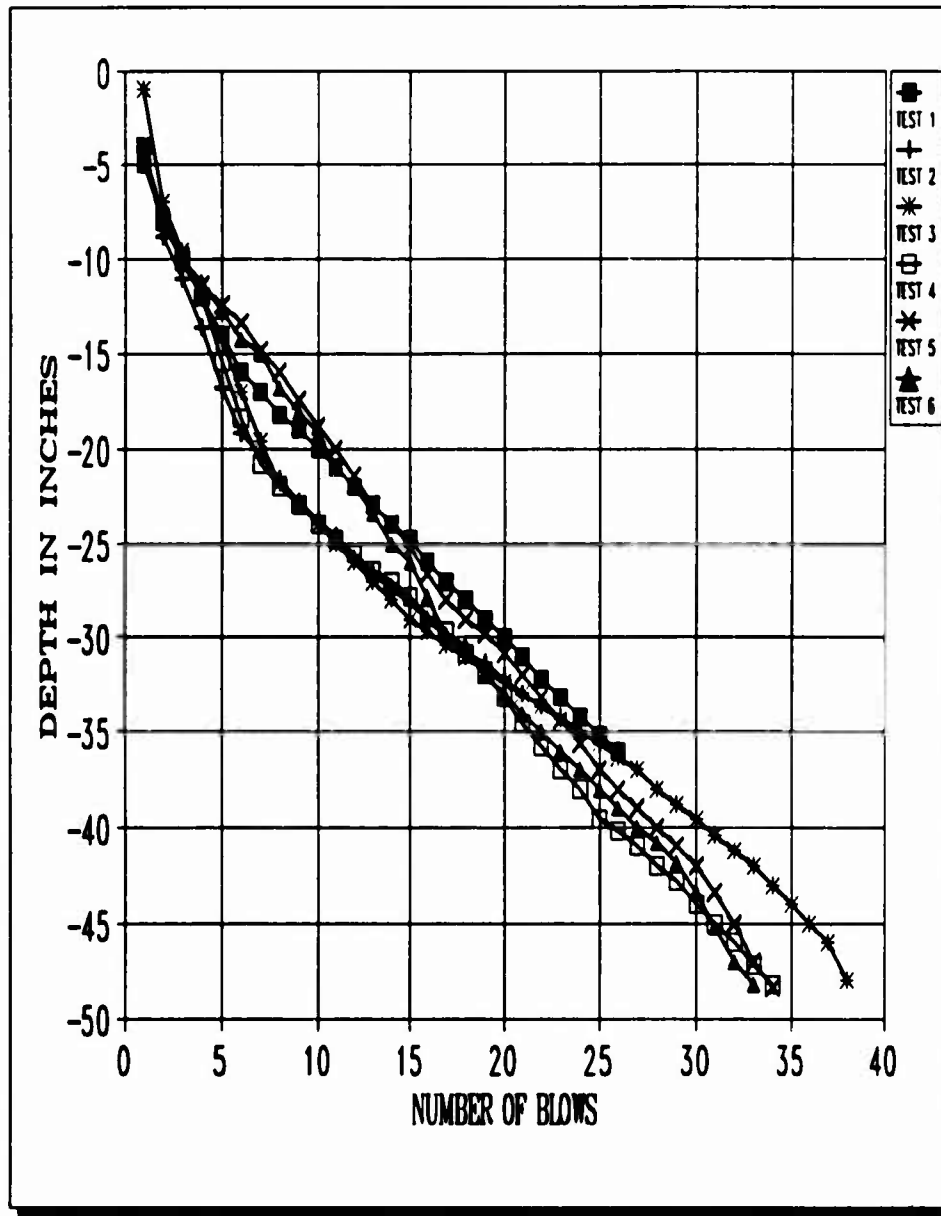
D E P T H*	AVG CBR 1	AVG CBR 2	AVG CBR 3	AVG CBR 4	AVG CBR 5	AVG CBR 6	CBR SITE AVG	ST DEV	CV
-5	2.3	1.4	2.7	1.6	1.7	2.3	2.0	0.4	22.6
-10	3.6	3.2	2.9	3.6	5.3	5.0	3.9	0.9	22.6
-15	5.7	2.1	2.7	2.3	5.7	6.5	4.2	1.8	43.9
-20	8.4	6.4	3.2	4.6	5.9	6.1	5.7	1.6	27.4
-25	8.0	8.8	7.8	10.3	6.5	6.2	8.0	1.4	17.5
-30	7.4	10.3	11.5	7.6	8.0	7.3	8.7	1.6	18.7
-35	7.8	12.9	12.5	6.0	6.0	7.8	8.8	2.8	32.0

* Depths are in inches.

A.22 Newberry Farm Average Estimated CBR Calculations



A.23 Newberry Farm Estimated CBR Profile

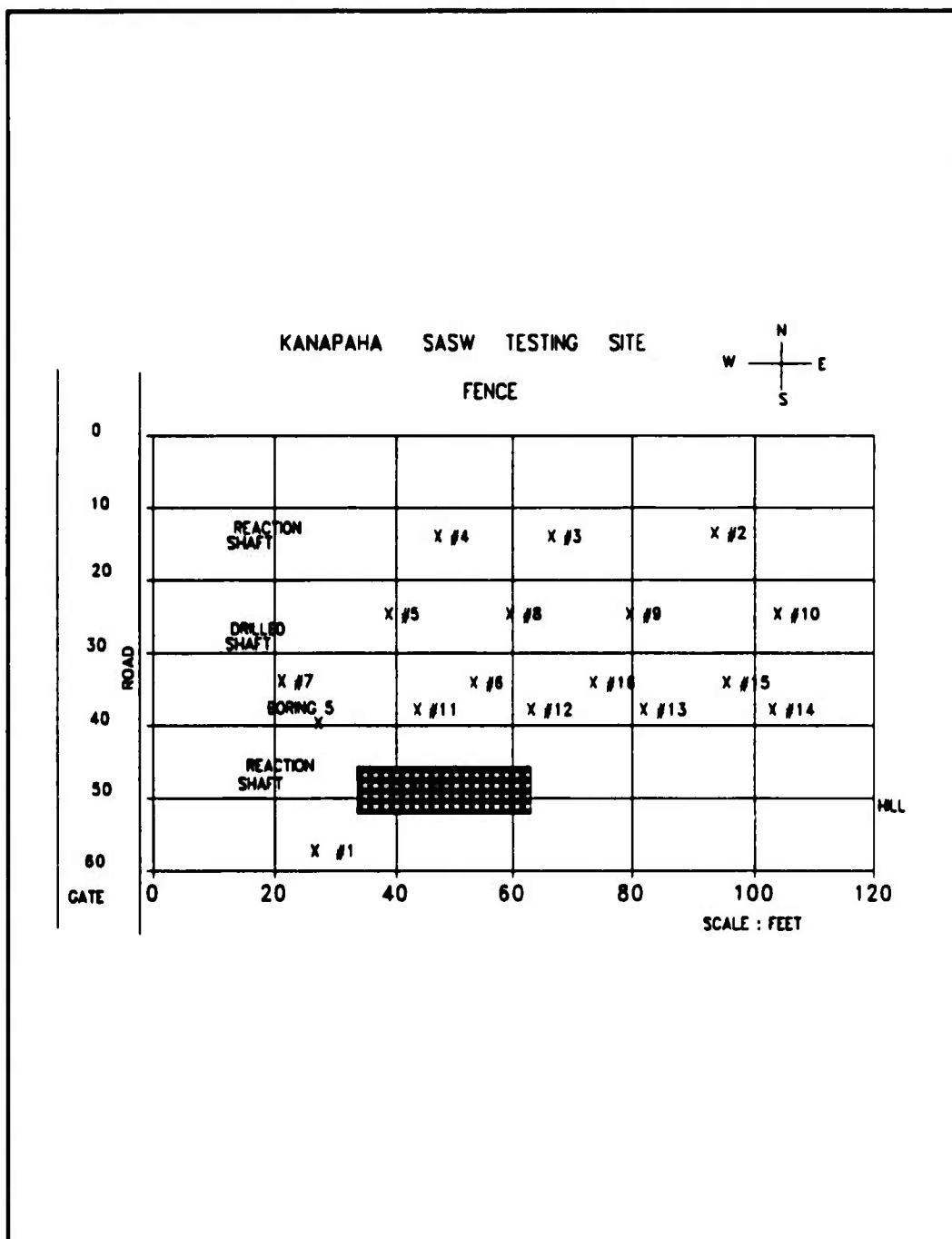


A.24 Newberry Farm Manual DCP Blows vs Penetration

Appendix B

KANAPAHA DCP TESTING DATA

This appendix presents results from DCP testing at the Kanapaha site. Sixteen separate DCP tests were performed at the locations shown in Appendix B.1. The remaining pages present the raw DCP data, calculated DCP penetration indexes, and the estimated CBR values calculated using the WES CBR-DCP correlation. In addition, the sites CBR calculations, CBR profiles, and the blow profiles are presented.



B.1 Kanapaha Site Locations

CUMULATIVE DCP PENETRATION (INCHES)							VES DCP-CBR CORRELATION					
DEPTH	TEST 1	TEST 2	TEST 3	TEST 4	TEST 5	TEST 6	CBR 1	CBR 2	CBR 3	CBR 4	CBR 5	CBR 6
1	-2.0	-2.4	-1.0	-1.2	-2.0	-1.0	2.0	21.0	4.0	2.4	2.0	7.0
2	-4.0	-1.6	-2.4	-2.0	-2.0	-2.1	2.7	2.4	10.0	2.0	2.0	7.0
3	-2.0	-2.4	-2.0	-2.0	-2.1	-2.1	2.0	10.0	12.0	7.0	2.0	7.0
4	-7.0	-2.0	-2.0	-2.2	-2.0	-2.0	7.0	12.0	7.0	12.0	11.0	2.0
5	-2.4	-2.2	-2.0	-2.0	-2.4	-2.0	2.0	20.0	12.0	12.0	12.0	10.0
6	-2.4	-2.0	-2.4	-2.4	-2.0	-2.0	7.0	10.0	12.0	10.0	12.0	10.0
7	-10.0	-2.0	-2.4	-2.0	-2.0	-2.7	2.4	10.0	7.0	21.0	21.0	7.0
8	-11.0	-2.0	-7.0	-2.4	-2.0	-2.4	2.4	21.0	12.0	12.0	11.0	2.0
9	-12.0	-2.2	-7.0	-2.0	-2.4	-10.2	7.0	20.0	12.0	27.0	21.0	2.0
10	-14.2	-2.0	-2.4	-7.0	-2.0	-11.0	2.0	21.0	12.0	21.0	12.0	2.0
11	-12.0	-2.0	-2.4	-7.4	-7.2	-12.0	2.0	20.0	7.0	21.0	20.0	2.0
12	-17.4	-2.2	-10.2	-2.0	-7.0	-10.7	2.0	20.0	12.0	12.0	20.0	2.4
13	-12.0	-2.0	-11.0	-2.4	-2.2	-10.0	2.0	21.0	12.0	21.0	11.0	2.1
14	-21.2	-2.0	-12.0	-2.0	-2.0	-24.1	2.0	20.0	7.0	21.0	20.0	2.0
15	-24.0	-7.2	-12.0	-2.4	-2.0	-20.7	2.0	20.0	2.0	12.0	21.0	2.0
16	-27.2	-7.0	-14.0	-2.0	-2.0	-27.1	2.1	20.0	7.0	21.0	21.0	2.0
17	-22.0	-7.0	-12.1	-10.2	-2.0	-22.0	1.0	20.0	7.0	21.0	20.0	2.0
18	-24.0	-2.1	-10.0	-10.0	-10.0	-20.0	1.7	20.0	12.0	21.0	21.0	2.0
19	-27.0	-2.4	-12.0	-11.0	-10.4	-21.4	2.2	20.0	21.0	11.0	21.0	2.0
20	-20.0	-2.7	-12.0	-11.7	-10.7	-22.2	2.2	20.0	20.0	21.0	20.0	2.0
21	-21.0	-2.0	-17.0	-12.2	-11.0	-22.0	2.0	27.0	2.0	12.0	20.0	2.0
22	-24.0	-2.0	-12.0	-12.0	-11.2	-20.0	2.0	20.0	2.0	12.0	27.0	2.0
23	-27.0	-2.0	-20.7	-12.4	-11.7		2.0	20.0	2.0	12.0	12.0	
24	-20.0	-2.7	-22.2	-12.0	-12.1		2.0	27.0	2.0	21.0	21.0	
25		-10.0	-20.7	-12.0	-12.4			20.0	2.0	12.0	20.0	
26		-10.0	-20.0	-12.0	-12.0			20.0	2.0	21.0	21.0	
27		-10.7	-27.0	-12.0	-12.2			21.0	2.0	12.0	21.0	
28		-11.0	-22.0	-12.0	-12.0			20.0	2.0	12.0	21.0	
29		-11.0	-22.0	-17.4	-10.0			20.0	2.0	12.0	20.0	
30		-11.0	-21.0	-10.2	-12.0			20.0	2.0	12.0	21.0	
31		-11.0	-20.1	-10.0	-12.0			20.0	2.0	12.0	20.0	
32		-12.0	-24.0	-20.0	-12.0			21.0	2.4	7.0	21.0	
33		-12.0	-20.5	-21.2	-12.4			20.0	2.0	2.4	21.0	
34		-12.0	-22.0	-21.0	-12.0			20.0	12.0	21.0	21.0	
35		-12.2	-22.0	-24.0	-12.2			20.0	12.0	2.0	21.0	
36		-12.0	-27.0	-22.2	-12.0			21.0	21.0	2.0	21.0	
37		-12.0	-27.0	-20.0	-17.0			20.0	12.0	2.0	21.0	
38		-12.0	-22.2	-22.4	-17.4			21.0	12.0	2.0	21.0	
39		-12.0	-22.0	-22.0	-17.0			20.0	21.0	2.0	21.0	
40		-12.0	-22.0	-21.0	-12.0			21.0	21.0	2.0	12.0	
41		-12.4	-22.4	-22.4	-12.7			21.0	21.0	2.0	21.0	
42		-12.7	-22.0	-22.0	-12.2			20.0	21.0	2.0	12.0	
43		-12.2	-22.2	-22.2	-12.7			12.0	21.0	2.4	12.0	
44		-12.4	-22.0	-22.0	-22.2			27.0	21.0	2.0	12.0	
45		-12.0	-21.0	-22.2	-22.7			12.0	21.0	2.4	12.0	
46		-17.4	-21.0	-22.0	-21.0			12.0	12.0	2.0	12.0	
47		-17.0	-22.2	-22.0	-21.0			21.0	12.0	2.4	12.0	
48		-12.0	-22.0	-22.2	-22.0			12.0	12.0	2.4	12.0	
49		-12.7	-22.0	-22.0	-22.4			21.0	12.0	2.0	102.0	
50		-12.2	-22.4	-22.4	-22.0			12.0	12.0	12.0	102.0	
51		-12.7	-22.2	-22.4	-22.0			12.0	12.0	7.0	2.0	
52		-22.2	-22.0	-27.0	-24.7			12.0	12.0	12.0	12.0	
53		-22.7	-27.0	-27.0	-22.0			12.0	7.0	12.0	2.0	
54		-21.0	-27.0	-22.0	-22.0			12.0	12.0	12.0	2.0	
55		-21.7	-22.0		-27.2			21.0	12.0		11.0	
56		-22.0			-22.2			12.0			7.0	
57		-22.2			-22.4			2.0			2.4	
58		-22.0			-22.0			20.0			2.4	
59		-22.7			-21.0			27.0			2.0	
60		-22.0			-22.2			27.0			2.0	
61		-24.0			-22.0			102.0			2.0	

B.2 Kanapaha Sites 1-6 Manual DCP Raw Data and CBR Estimations

CUMULATIVE DCP PENETRATION (INCHES)							VES DCP-CBR CORRELATION					
BLOWS	TEST 1	TEST 2	TEST 3	TEST 4	TEST 5	TEST 6	CBR 1	CBR 2	CBR 3	CBR 4	CBR 5	CBR 6
62		-34.1			-36.9			102.0			7.0	
63		-34.2			-37.2			102.0			6.4	
64		-34.3			-38.4			102.0			6.4	
65		-34.4			-40.6			102.0			3.2	
66		-34.5			-42.4			102.0			4.0	
67		-34.6			-44.2			102.0			4.0	
68		-34.7			-46.0			102.0			4.0	
69		-34.8			-47.6			102.0			4.0	
70		-35.0			-48.0			47.3			9.2	
71		-35.1						102.0				
72		-35.2						102.0				
73		-35.3						102.0				
74		-35.9						47.3				
75		-36.6						102.0				
76		-36.8						47.3				
77		-36.9						102.0				
78		-36.9						102.0				
79		-36.9						47.3				
80		-36.4						47.3				
81		-36.6						47.3				
82		-36.9						30.0				
83		-37.1						47.3				
84		-37.4						30.0				
85		-37.6						47.3				
86		-38.8						21.0				
87		-39.8						30.0				
88		-39.6						30.0				
89		-39.1						10.0				
90		-39.3						47.3				
91		-39.9						13.0				
92		-39.2						30.0				
93		-39.6						21.0				
94		-39.9						30.0				
95		-41.3						21.0				
96		-41.4						102.0				
97		-41.8						21.0				
98		-42.1						30.0				
99		-43.4						30.0				
100		-42.0						21.0				
101		-42.2						21.0				
102		-42.6						21.0				
103		-44.0						21.0				
104		-44.4						21.0				
105		-44.6						47.3				
106		-44.8						47.3				
107		-45.0						47.3				
108		-46.4						21.0				
109		-46.7						30.0				
110		-46.0						30.0				
111		-46.2						47.3				
112		-46.0						10.0				
113		-47.1						30.0				
114		-47.6						11.6				
115		-48.3						10.0				
116		-48.9						10.0				
117		-49.2						21.0				
118		-49.0						10.0				
119		-49.6						13.0				
120		-41.2						18.0				

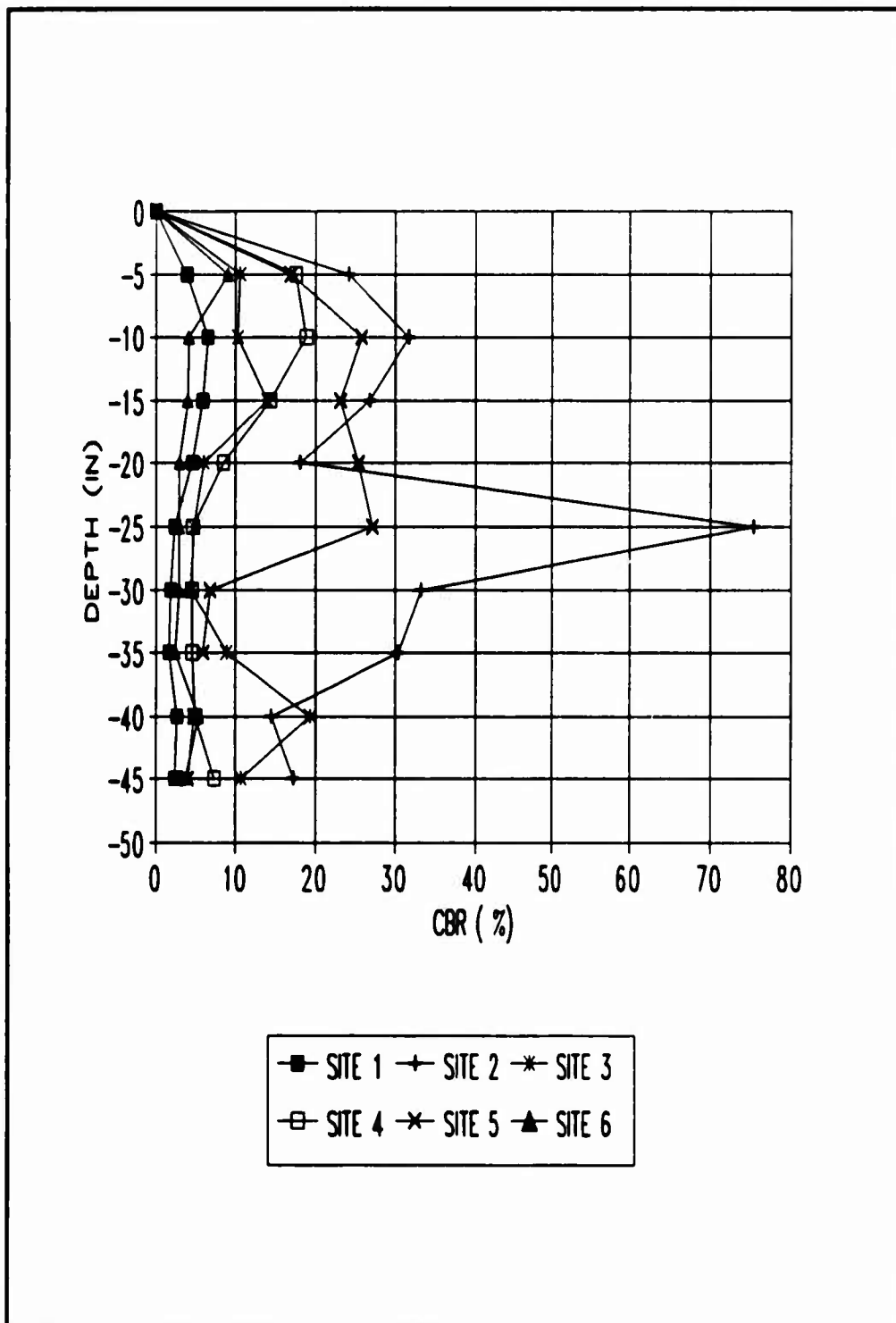
B.2 Kanapaha Sites 1-6 Manual DCP Raw Data and CBR Estimations (Continued)

KANAPAHA

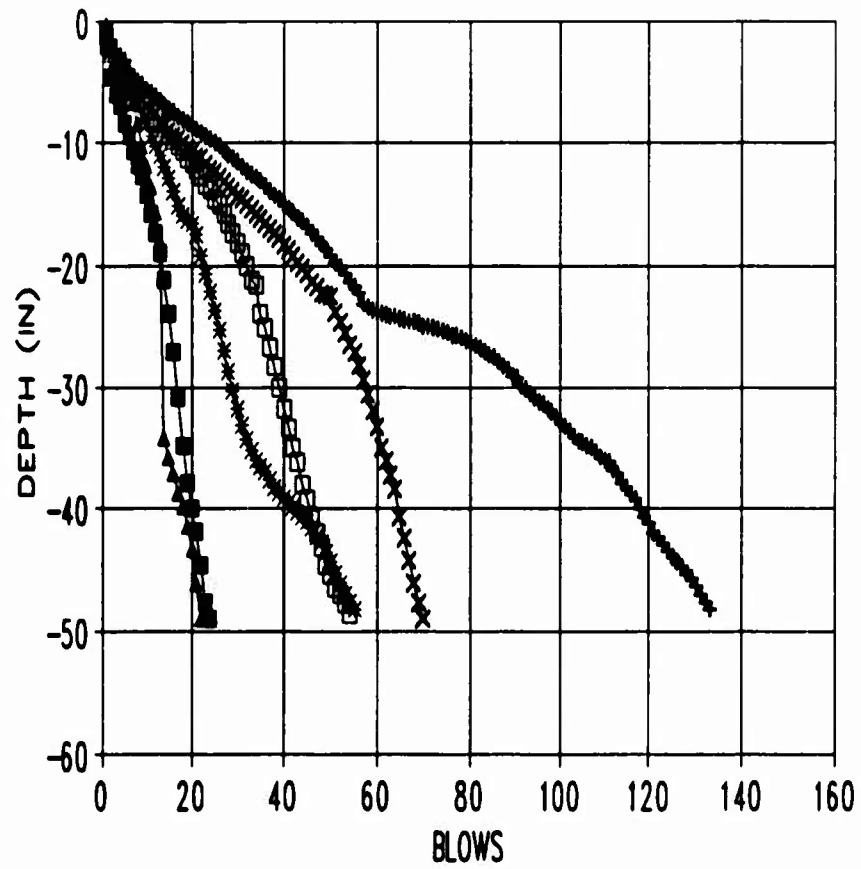
SITES 1 THRU 6

MEAN DEPTH (INCHES)	AVG CBR 1	AVG CBR 2	AVG CBR 3	AVG CBR 4	AVG CBR 5	AVG CBR 6
0	0.00	0.00	0.00	0.00	0.00	0.00
-5	4.01	24.12	10.65	17.69	17.03	9.15
-10	6.50	31.67	10.33	16.87	25.76	4.17
-15	5.92	26.80	14.10	14.46	23.14	4.04
-20	4.61	18.20	6.01	8.54	25.34	3.07
-25	2.46	75.42	4.76	4.64	27.14	3.07
-30	1.86	33.24	4.49	4.61	8.84	3.07
-35	1.65	30.28	8.95	4.61	5.88	2.46
-40	2.75	14.57	19.38	5.00	4.79	5.38
-45	2.46	17.37	10.77	7.38	4.04	3.80

B.3 Kanapaha Sites 1-6 Average Estimated CBR Calculations



B.4 Kanapaha Sites 1-6 Estimated CBR Profile



—■— SITE 1 —+— SITE 2 —*— SITE 3
—□— SITE 4 —x— SITE 5 —▲— SITE 6

B.5 Kanapaha Sites 1-6 Manual DCP Blows vs Penetration

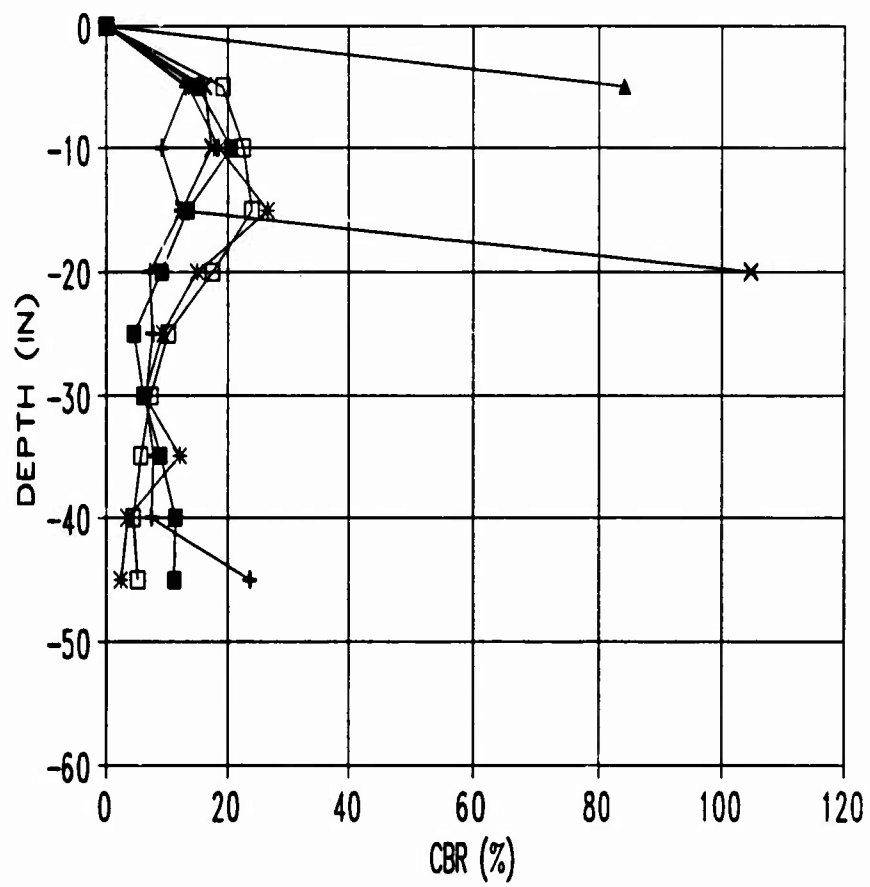
CUMULATIVE DCP PENETRATION (INCHES)							VES DCP-CBR CORRELATION					
BLOWS	TEST 7	TEST 8	TEST 9	TEST 10	TEST 11	TEST 12	CBR 7	CBR 8	CBR 9	CBR 10	CBR 11	CBR 12
1	-8.4	-1.0	-8.0	-1.2	-8.4	-8.2	21.0	4.0	10.0	6.4	21.0	47.3
2	-1.0	-8.4	-1.0	-8.4	-1.0	-8.4	7.0	4.0	10.0	6.4	10.0	47.3
3	-8.7	-8.0	-8.0	-8.4	-8.0	-8.0	8.4	10.0	4.0	7.0	8.4	21.0
4	-5.0	-8.0	-8.0	-8.2	-8.0	-1.0	10.0	10.0	10.0	10.0	10.0	47.3
5	-4.1	-8.2	-8.0	-8.0	-8.4	-1.2	10.0	21.0	10.0	21.0	10.0	47.3
6	-8.0	-8.0	-8.4	-8.0	-8.0	-1.0	11.0	11.0	10.0	21.0	21.0	21.0
7	-8.0	-8.4	-8.0	-8.0	-8.0	-1.0	10.0	10.0	21.0	10.0	10.0	47.3
8	-8.0	-7.0	-8.2	-8.2	-8.0	-8.0	11.0	10.0	21.0	21.0	21.0	47.3
9	-8.0	-7.4	-8.0	-8.0	-8.0	-8.2	20.0	21.0	10.0	10.0	10.0	47.3
10	-8.7	-8.2	-7.4	-7.0	-8.0	-8.4	21.0	10.0	10.0	47.3	21.0	47.3
11	-7.2	-8.0	-7.0	-7.4	-8.0	-8.0	10.0	10.0	21.0	21.0	10.0	47.3
12	-7.0	-10.0	-8.4	-8.0	-7.0	-8.0	10.0	7.0	10.0	10.0	21.0	47.3
13	-8.1	-10.0	-8.0	-8.4	-7.0	-8.2	20.0	8.0	21.0	21.0	10.0	21.0
14	-8.7	-10.0	-8.4	-8.0	-8.0	-8.4	10.0	7.0	10.0	21.0	21.0	47.3
15	-8.1	-10.0	-8.0	-8.0	-8.0	-8.0	21.0	10.0	21.0	47.3	10.0	47.3
16	-8.4	-10.0	-10.0	-8.0	-8.1	-8.0	20.0	11.0	10.0	10.0	20.0	21.0
17	-10.0	-10.0	-10.7	-10.0	-8.7	-8.2	10.0	10.0	21.0	21.0	10.0	47.3
18	-10.0	-10.0	-11.0	-10.4	-10.2	-8.0	20.0	11.0	10.0	21.0	10.0	21.0
19	-11.0	-10.0	-11.7	-10.0	-10.0	-8.0	11.0	11.0	21.0	21.0	10.0	47.3
20	-11.0	-10.0	-10.0	-11.2	-11.2	-8.0	20.0	9.0	10.0	21.0	21.0	47.3
21	-10.0	-17.0	-10.0	-11.0	-11.0	-8.4	11.0	7.0	21.0	21.0	10.0	21.0
22	-10.0	-10.0	-10.7	-10.0	-10.2	-8.0	47.0	7.0	100.0	21.0	21.0	47.0
23	-10.0	-10.0	-10.2	-10.4	-10.0	-8.0	10.0	9.0	10.0	21.0	10.0	47.3
24	-10.0	-11.2	-10.0	-10.0	-10.0	-8.0	10.0	9.0	21.0	21.0	10.0	47.3
25	-14.0	-8.0	-14.0	-10.0	-14.2	-8.2	10.0	9.0	10.0	47.0	10.0	47.0
26	-14.0	-8.4	-14.7	-10.4	-14.0	-8.4	10.0	9.0	10.0	21.0	10.0	47.0
27	-10.2	-8.2	-10.2	-10.0	-10.0	-8.0	10.0	8.4	10.0	21.0	10.0	47.3
28	-10.0	-8.0	-10.0	-14.2	-14.2	-8.7	11.0	10.0	21.0	21.0	10.0	100.0
29	-10.0	-8.0	-10.0	-14.0	-14.0	-8.0	11.0	7.0	21.0	21.0	10.0	100.0
30	-17.0	-8.0	-10.7	-10.0	-17.0	-8.0	10.0	7.0	11.0	21.0	10.0	220.4
31	-10.1	-8.0	-17.4	-10.4	-10.1	-8.0	11.0	7.0	11.0	21.0	10.0	220.4
32	-10.0	-8.4	-17.0	-10.0	-10.0	-7.0	8.0	8.0	21.0	21.0	10.0	200.4
33	-8.1	-8.0	-10.0	-10.2	-10.4	-7.0	7.0	9.0	10.0	21.0	10.0	220.4
34	-11.0	-8.0	-10.0	-10.0	-8.0	-7.1	9.0	7.0	10.0	21.0	10.0	220.4
35	-8.0	-8.0	-10.0	-17.0	-8.0	-7.1	8.0	7.0	11.0	10.0	47.0	200.4
36	-8.0	-8.0	-8.0	-17.0	-8.0		8.0	7.0	21.0	21.0	20.0	
37	-8.0	-8.0	-8.0	-10.2	-8.0		2.7	7.0	10.0	10.0	100.0	
38	-8.0	-8.0	-8.0	-10.0	-8.7		0.2	7.0	10.0	21.0	100.0	
39	-8.0	-8.0	-8.0	-10.0	-8.0		7.0	7.0	11.0	21.0	200.4	
40	-8.0	-8.0	-8.0	-10.0	-8.0		11.0	9.0	10.0	10.0	200.4	
41	-8.4	-8.4	-8.0	-8.0	-8.0		10.0	7.0	7.0	10.0	200.4	
42	-8.0	-11.2	-8.0	-8.0	-8.0		8.0	10.0	7.0	21.0	200.4	
43	-8.0	-11.0	-8.0	-8.0	-8.0		7.0	10.0	7.0	11.0	200.4	
44	-8.0	-8.0	-8.0	-8.0	-8.0		11.0	10.0	7.0	11.0	200.4	
45	-8.0	-8.0	-8.0	-8.0	-8.0		7.0	8.0	7.0	10.0		
46	-8.0	-8.1	-8.0	-8.0	-8.0		7.0	10.0	8.0	10.0		
47	-8.0	-8.0	-8.0	-8.0	-8.0		7.0	11.0	8.0	10.0		
48	-8.0	-8.0	-8.0	-8.0	-8.0		7.0	10.0	2.7	7.0		
49	-8.0	-8.0	-8.0	-8.0	-8.0		8.0	100.0	21.0	10.0		
50	-8.7	-8.0	-8.0	-8.0	-8.0		11.0	10.0	8.0	7.0		
51	-11.1	-8.7	-8.0	-8.0	-8.0		21.0	11.0	8.0	7.0		
52	-11.0	-8.4	-8.0	-8.0	-8.0		11.0	11.0	8.2	7.0		
53	-8.4	-8.0	-8.0	-8.0	-8.0		10.0	10.0	2.0	6.4		
54	-8.0	-8.0	-8.0	-8.0	-8.0		10.0	10.0	2.0	8.4		
55	-8.0	-8.4	-8.4	-8.0	-8.0		10.0	10.0	2.7	9.0		
56	-8.0		-8.0	-8.0	-8.0		11.0		8.0	8.0		
57	-8.0			-8.0	-8.0		10.0			8.4		
58	-8.0			-8.0	-8.0		11.0			8.0		
59	-8.0			-8.0	-8.0		8.0			8.0		
60	-8.0			-8.0	-8.0		11.0			8.0		
61	-8.0			-8.0	-8.0		11.0			8.0		
62	-8.0			-8.0	-8.0		11.0			8.0		
63	-8.0			-8.0	-8.0					8.4		
64				-8.0	-8.0					8.0		
65				-8.0	-8.0					8.0		
66				-8.0	-8.0					8.0		
67				-8.0	-8.0					8.0		
68				-8.0	-8.0					8.0		
69				-8.0	-8.0					8.0		
70				-8.0	-8.0					8.0		
71				-8.0	-8.0					8.0		
72				-8.0	-8.0					8.0		
73				-8.0	-8.0					8.0		
74				-8.0	-8.0					8.0		
75				-8.0	-8.0					8.0		
76				-8.0	-8.0					8.0		
77				-8.0	-8.0					8.0		
78				-8.0	-8.0					8.0		
79				-8.0	-8.0					8.0		
80				-8.0	-8.0					8.0		
81				-8.0	-8.0					8.0		
82				-8.0	-8.0					8.0		
83				-8.0	-8.0					8.0		
84				-8.0	-8.0					8.0		
85				-8.0	-8.0					8.0		
86				-8.0	-8.0					8.0		
87				-8.0	-8.0					8.0		
88				-8.0	-8.0					8.0		
89				-8.0	-8.0					8.0		
90				-8.0	-8.0					8.0		
91				-8.0	-8.0					8.0		
92				-8.0	-8.0					8.0		
93				-8.0	-8.0					8.0		
94				-8.0	-8.0					8.0		
95				-8.0	-8.0					8.0		
96				-8.0	-8.0					8.0		
97				-8.0	-8.0					8.0		
98				-8.0	-8.0					8.0		
99				-8.0	-8.0					8.0		
100				-8.0	-8.0					8.0		

B.6 Kanapaha Sites 7-12 Manual DCP Raw Data and CBR Estimations

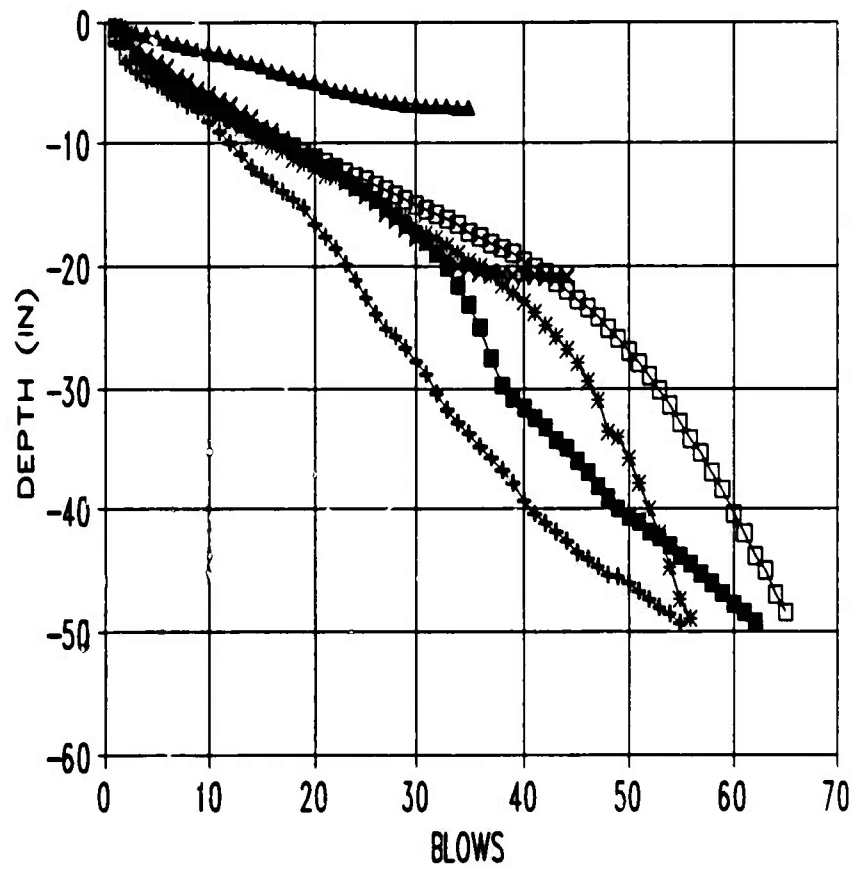
KANAPAHA**SITES 7 THRU 12**

MEAN DEPTH (INCHES)	AVG CBR 7	AVG CBR 8	AVG CBR 9	AVG CBR 10	AVG CBR 11	AVG CBR 12
0	0.00	0.00	0.00	0.00	0.00	0.00
-5	15.27	13.15	13.60	19.28	16.32	84.36
-10	20.66	9.15	18.58	22.64	17.31	-
-15	13.54	12.50	26.61	24.08	12.55	-
-20	9.14	7.14	15.13	17.52	104.84	-
-25	4.61	7.72	9.30	10.33	-	-
-30	6.13	6.59	6.18	7.32	-	-
-35	9.00	7.80	12.22	5.69	-	-
-40	11.43	7.44	3.41	4.47	-	-
-45	11.42	23.68	2.46	5.20	-	-

B.7 Kanapaha Sites 7-12 Average Estimated CBR Calculations



B.8 Kanapaha Sites 7-12 Estimated CBR Profile



—■— SITE 7 +— SITE 8 *— SITE 9
—□— SITE 10 ×— SITE 11 ▲— SITE 12

B.9 Kanapaha Sites 7-12 Manual DCP Blows vs Penetration

CUMULATIVE DCP PENETRATION (INCHES)							WEB DCP-CBR CORRELATION					
BLOWS	TEST 10	TEST 14	TEST 16	TEST 16	TEST 17	TEST 18	CBR 10	CBR 14	CBR 16	CBR 16	CBR 17	CBR 18
1	-0.2	-0.0	-0.6	-1.0			47.0	0.0	13.0	4.0		
2	-0.4	-2.0	-2.0	-2.2			47.0	10.0	9.3	9.3		
3	-0.0	-0.0	-0.2	-4.4			21.0	10.0	0.4	0.4		
4	-1.2	-4.2	-4.4	-5.2			21.0	10.0	0.4	10.0		
5	-1.6	-4.0	-6.0	-6.0			21.0	11.0	13.0	10.0		
6	-2.2	-5.2	-6.7	-6.5			10.0	21.0	11.0	16.0		
7	-2.0	-6.0	-6.0	-7.0			21.0	11.0	10.0	10.0		
8	-0.0	-6.4	-6.0	-7.0			21.0	21.0	10.0	10.0		
9	-0.4	-6.0	-7.0	-8.2			21.0	21.0	10.0	21.0		
10	-3.0	-7.2	-7.0	-8.0			21.0	21.0	16.0	13.0		
11	-4.4	-7.0	-8.2	-8.0			10.0	21.0	21.0	21.0		
12	-5.0	-8.1	-8.0	-8.0			10.0	10.0	21.0	13.0		
13	-5.2	-8.4	-8.1	-10.2			47.0	00.0	10.0	21.0		
14	-8.0	-8.0	-8.0	-10.0			10.0	10.0	47.0	13.0		
15	-8.0	-8.0	-8.0	-11.2			47.0	10.0	10.0	21.0		
16	-8.0	-8.0	-10.2	-11.0			00.0	00.0	21.0	13.0		
17	-8.0	-10.2	-10.0	-12.2			00.0	21.0	21.0	21.0		
18	-7.0	-10.0	-11.0	-12.0			21.0	47.0	21.0	11.0		
19	-7.4	-11.1	-11.4	-10.2			21.0	13.0	21.0	00.0		
20	-7.6	-11.0	-11.0	-10.7			47.0	10.0	21.0	10.0		
21	-8.0	-11.0	-12.1	-14.0			21.0	00.0	00.0	10.0		
22	-8.4	-12.2	-12.4	-14.0			21.0	21.0	00.0	13.0		
23	-8.0	-12.0	-12.0	-10.2			21.0	10.0	10.0	21.0		
24	-9.1	-13.0	-13.2	-10.0			00.0	10.0	00.0	13.0		
25	-9.0	-13.7	-10.0	-10.2			10.0	21.0	21.0	21.0		
26	-10.0	-14.0	-14.0	-10.0			21.0	00.0	21.0	10.0		
27	-10.4	-14.4	-14.0	-17.0			21.0	21.0	13.0	10.0		
28	-10.7	-14.0	-14.0	-10.0			00.0	10.0	00.0	21.0		
29	-11.0	-15.2	-15.0	-10.7			00.0	21.0	21.0	11.0		
30	-11.0	-15.0	-15.7	-10.4			10.0	10.0	21.0	11.0		
31	-11.0	-16.4	-16.2	-00.0			47.0	10.0	10.0	10.0		
32	-12.0	-16.0	-16.0	-00.0			47.0	10.0	21.0	0.0		
33	-12.0	-17.4	-17.0	-21.7			10.0	10.0	21.0	10.0		
34	-13.0	-17.0	-17.7	-22.0			21.0	21.0	11.0	0.0		
35	-13.0	-18.0	-10.0	-23.0			10.0	11.0	00.0	7.0		
36	-10.0	-10.0	-10.0	-04.7			47.0	10.0	10.0	7.0		
37	-14.1	-10.0	-10.0	-20.0			00.0	10.0	21.0	0.0		
38	-14.0	-00.2	-10.7	-27.0			10.0	10.0	11.0	4.0		
39	-10.0	-00.0	-00.0	-20.4			21.0	11.0	00.0	4.0		
40	-10.0	-01.0	-00.0	-31.0			10.0	0.0	10.0	0.0		
41	-10.0	-02.0	-01.0	-30.4			21.0	10.0	11.0	10.0		
42	-10.7	-02.2	-01.0	-30.0			11.0	13.0	13.0	21.0		
43	-17.0	-04.0	-02.0	-00.0			00.0	10.0	11.0	100.0		
44	-17.0	-04.0	-00.2	-00.0			10.0	10.0	10.0	100.0		
45	-10.0	-20.0	-24.0	-00.0			21.0	7.0	10.0	30.0		
46	-10.0	-00.0	-24.0	-00.4			10.0	7.0	10.0	100.0		
47	-10.0	-27.0	-20.0	-00.0			21.0	7.0	7.0	100.0		
48	-10.0	-00.2	-00.0	-00.0			10.0	0.0	7.0	100.0		
49	-00.1	-00.4	-27.0	-33.7			10.0	0.4	7.0	100.0		
50	-00.0	-02.2	-00.0	-32.0			10.0	4.0	7.0	220.4		
51	-01.0	-04.0	-00.0	-30.0			11.0	4.0	7.0	220.4		
52	-00.0	-00.0	-00.0	-00.0			7.0	0.0	0.0	000.4		
53	-20.4	-00.0	-00.7	-00.0			10.0	2.7	4.3	223.4		
54	-24.0	-41.0	-00.0	-04.0			0.4	2.0	3.0	100.0		
55	-25.4	-44.0	-07.0	-04.1			10.0	2.3	3.2	100.0		
56	-00.0	-00.0	-00.0	-04.0			0.4	1.7	0.0	47.0		

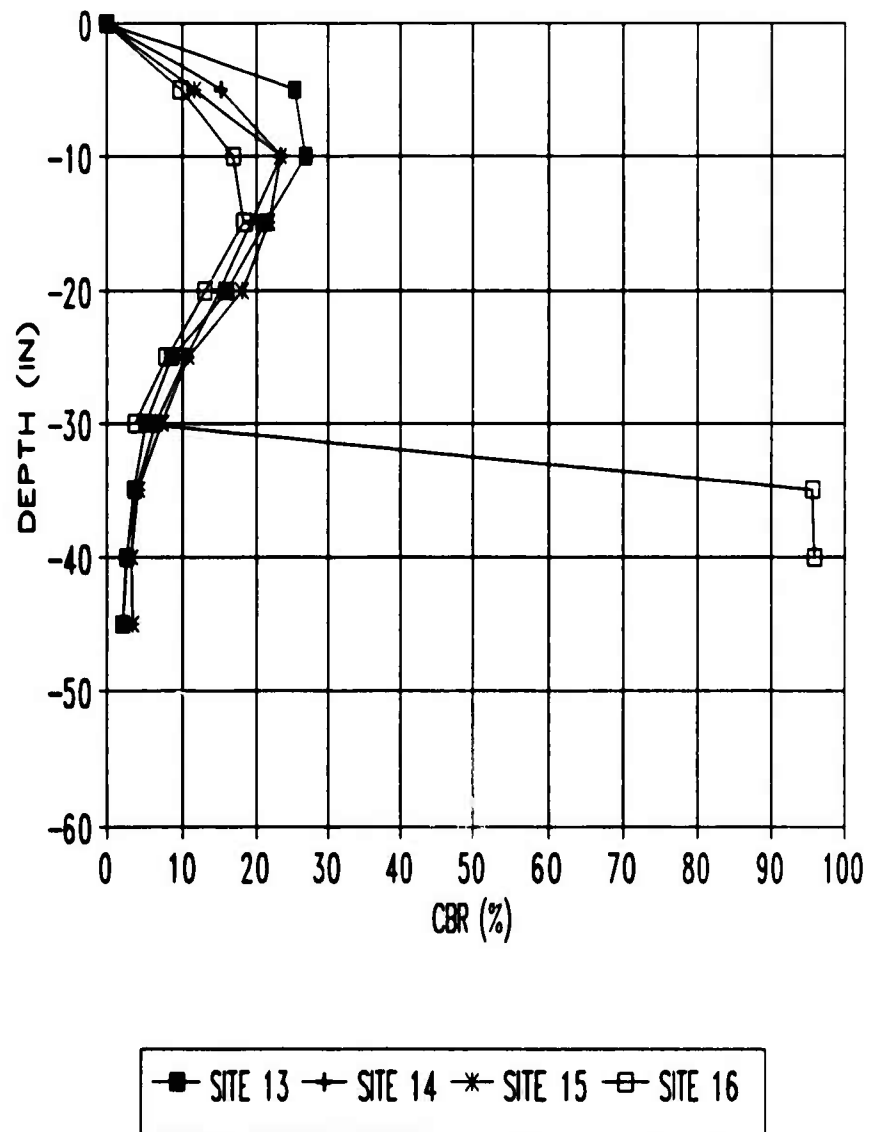
B.10 Kanapaha Sites 13-16 Manual DCP Raw Data and CBR Estimations

KANAPAHA

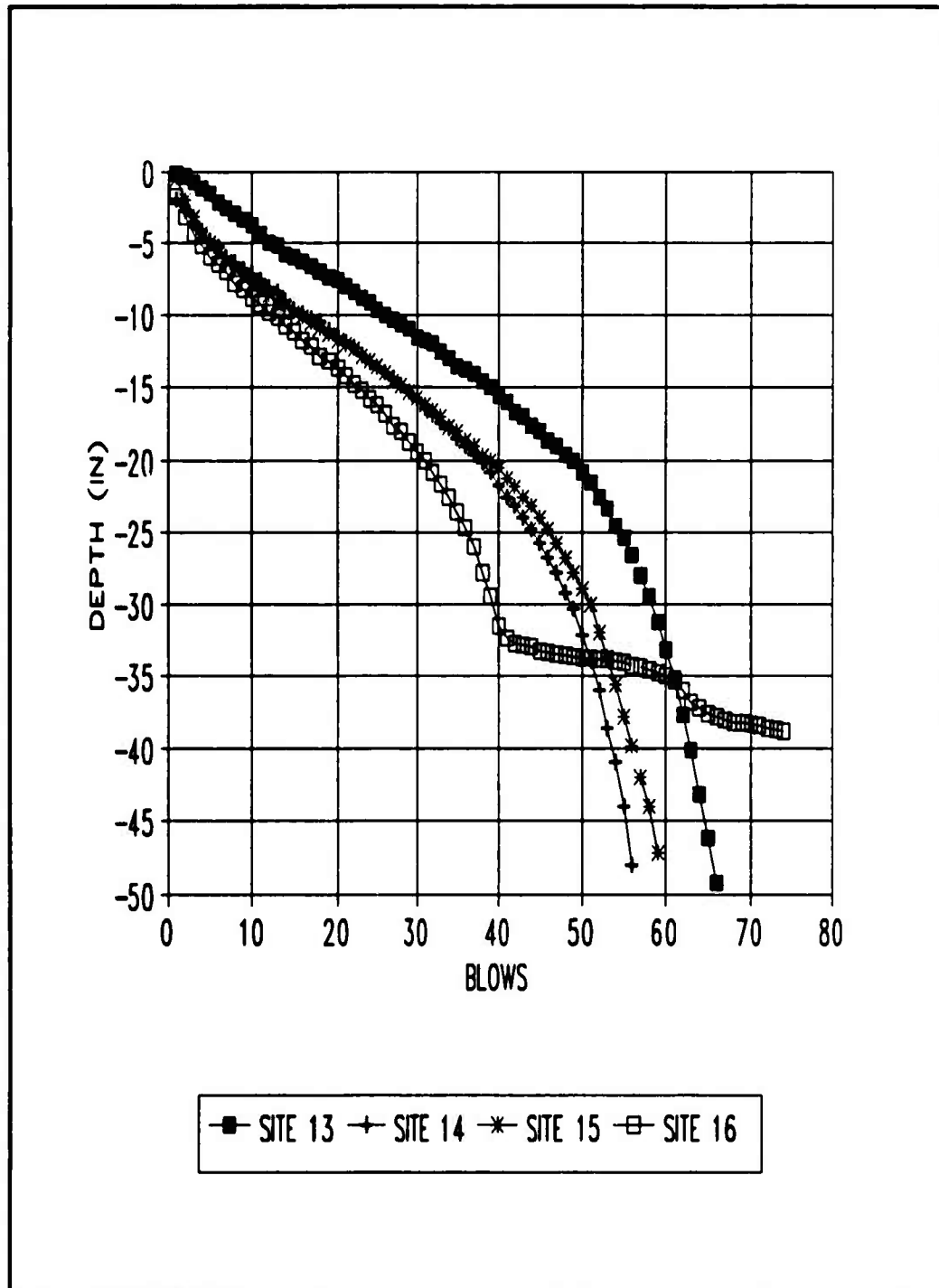
SITE 13 THRU 16

MEAN DEPTH (INCHES)	AVG CBR 13	AVG CBR 14	AVG CBR 15	AVG CBR 16	AVG CBR 17	AVG CBR 18
0	0.00	0.00	0.00	0.00	-	-
-5	25.41	15.30	11.49	9.74	-	-
-10	27.02	23.30	23.37	16.92	-	-
-15	21.26	19.39	21.66	18.34	-	-
-20	15.99	14.93	18.04	12.94	-	-
-25	8.54	10.33	10.65	7.96	-	-
-30	5.35	6.50	7.27	3.96	-	-
-35	3.80	4.04	4.30	95.70	-	-
-40	2.79	2.67	3.41	95.63	-	-
-45	2.28	2.28	3.59	-	-	-

B.11 Kanapaha Sites 13-16 Average Estimated CBR Calculations



B.12 Kanapaha Sites 13-16 Estimated CBR Profile



B.13 Kanapaha Sites 13-16 Manual DCP Blows vs Penetration

APPENDIX C

AADCP AND DCP CORRELATION TESTING

This appendix presents the data associated with the AADCP and DCP correlation testing. The data are grouped by site and are presented in the following order:

(a) Spreadsheet 1 of Cumulative Penetration for both AADCP and DCP instruments

(b) Spreadsheet 2 of Penetration Index values for AADCP and DCP instruments, Standard Deviation, Coefficient of Variability, AADCP-DCP Correlation Penetration Index and Estimated CBR values

(c) Plot of Blows vs Depth of AADCP and DCP Instruments

(d) Plot of Estimated Penetration Index (PI) from AADCP Data and DCP versus depth

(e) Plot of Estimated CBR from AADCP and DCP Instrument

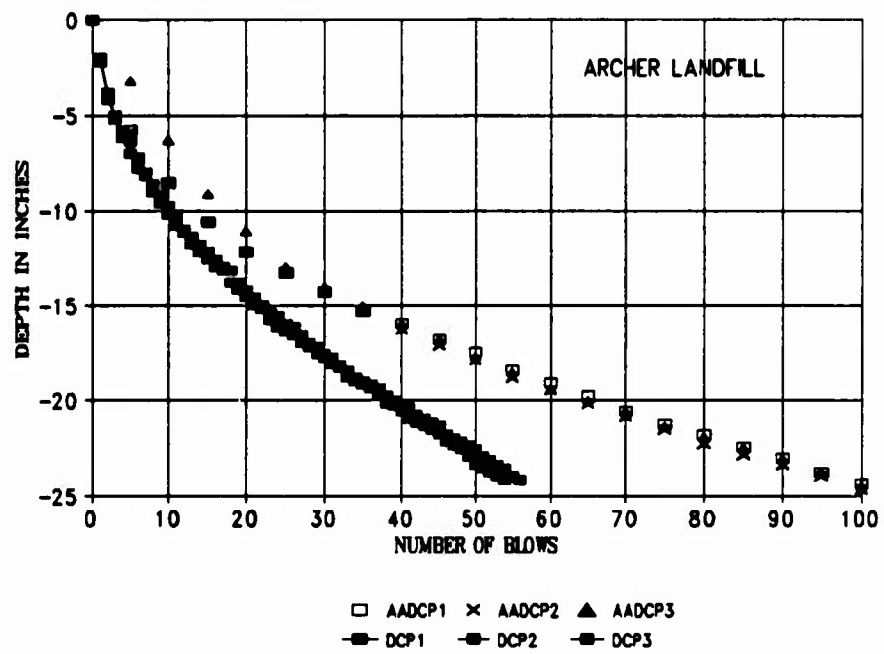
ARCHER LANDFILL

CUMULATIVE PENETRATION (BCHES)							
	AASCP	AASCP	AASCP		DCP	DCP	DCP
	TEST	TEST	TEST		TEST	TEST	TEST
BLOWS	1	2	3	BLOWS	1	2	3
0	-4	-4	-4	0	-4.0	-4.0	-4.0
5	-8.9	-8.9	-10.3	1	-8.2	-8	-8.2
10	-12.6	-12.6	-13.1	2	-7.6	-8	-8.2
15	-14.6	-14.6	-16.1	3	-8	-8	-8.2
20	-16.2	-16.2	-17	4	-8.8	-10	-10.2
25	-17.3	-17.3	-18	5	-10.4	-11	-11
30	-18.3	-18.3	-18	6	-11.2	-11.6	-11.8
35	-19.3	-19.3	-20	7	-12	-12.2	-12.2
40	-20	-20.3	-20.6	8	-12.6	-13	-13
45	-20.9	-21.1	-21.7	9	-13.2	-13.6	-13.6
50	-21.5	-21.9	-22.5	10	-13.6	-14.2	-14.2
55	-22.4	-22.6	-23.4	11	-14.2	-14.6	-14.6
60	-23.1	-23.5	-24	12	-15	-15.2	-15.2
65	-23.9	-24.2	-24.6	13	-15.4	-15.8	-15.8
70	-24.6	-24.9	-25.4	14	-15.8	-16.2	-16.2
75	-25.3	-25.6	-25.9	15	-16.2	-16.6	-16.4
80	-25.8	-26.3	-26.5	16	-16.6	-17	-17
85	-26.5	-26.9	-27.1	17	-17	-17.2	-17.2
90	-27.1	-27.4	-27.8	18	-17.2	-17.6	-17.6
95	-27.9	-28	-28.5	19	-17.8	-18.2	-18.2
100	-28.4	-28.7		20	-18.2	-18.6	-18.6
				21	-18.6	-19	-18.6
				22	-19	-19.2	-19.2
				23	-19.4	-19.8	-19.6
				24	-19.8	-20.2	-19.8
				25	-20	-20.4	-20.2
				26	-20.2	-20.6	-20.4
				27	-20.6	-21	-20.6
				28	-21	-21.2	-21
				29	-21.2	-21.6	-21.2
				30	-21.6	-21.8	-21.6
				31	-21.8	-22.1	-21.8
				32	-22.2	-22.3	-22.2
				33	-22.6	-22.8	-22.4
				34	-22.8	-23	-22.8
				35	-23	-23.2	-23
				36	-23.2	-23.4	-23.2
				37	-23.6	-23.8	-23.4
				38	-23.8	-24.2	-23.6
				39	-24	-24.3	-24
				40	-24.2	-24.6	-24.2
				41	-24.4	-25	-24.4
				42	-24.8	-25.2	-24.8
				43	-25	-25.4	-25
				44	-25.2	-25.6	-25.2
				45	-25.4	-25.8	-25.4
				46	-25.8	-26.2	-25.8
				47	-26	-26.4	-26
				48	-26.2	-26.6	-26.2
				49	-26.4	-27	-26.4
				50	-26.7	-27.4	-26.6
				51	-27	-27.6	-27
				52	-27.2	-27.8	-27.2
				53	-27.4	-28	-27.4
				54	-27.8	-28.2	-27.6
				55	-28		-28
				56	-28.2		-28.2

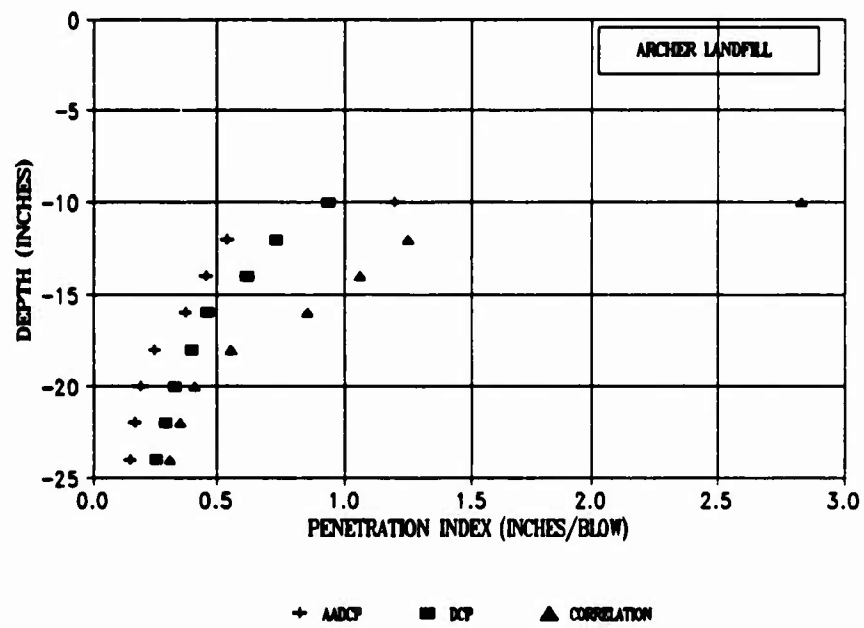
ARCHER LANDFILL

MEAN DEPTH (INCHES)	AVG P.I. AADCP 1	AVG P.I. AADCP 2	AVG P.I. AADCP 3	P.I. SITE AVERAGE	STANDARD DEVIATION	COEFFICIENT OF VARIABILITY	CORRELATION P.I. SITE AVERAGE	CBR ** SITE AVERAGE
0	-	-	-	-	-	-	-	-
-2	-	-	-	-	-	-	-	-
-4	-	-	-	-	-	-	-	-
-6	-	-	-	-	-	-	-	-
-8	-	-	-	-	-	-	-	-
-10	1.16	1.16	1.26	1.20	0.05	4.41	2.72	2.55
-12	0.54	0.54	-	0.54	0.00	0.00	1.20	6.35
-14	0.42	0.40	0.56	0.46	0.09	18.95	1.02	7.65
-16	0.32	0.32	0.46	0.37	0.09	24.74	0.82	9.76
-18	0.21	0.21	0.33	0.25	0.07	27.06	0.53	15.79
-20	0.17	0.20	0.20	0.19	0.02	10.19	0.39	22.09
-22	0.16	0.17	0.17	0.17	0.01	3.08	0.34	26.01
-24	0.15	0.14	0.15	0.15	0.01	4.55	0.30	30.28
AVERAGE						11.62		
* DCP = 2.30 AADCP - 0.04								
** CBR = 292/DCP*1.12								
MEAN DEPTH (INCHES)	AVG P.I. DCP 1	AVG P.I. DCP 2	AVG P.I. DCP 3	P.I. SITE AVERAGE	STANDARD DEVIATION	COEFFICIENT OF VARIABILITY	CBR ** SITE AVERAGE	
0	-	-	-	-	-	-	-	
-2	-	-	-	-	-	-	-	
-4	-	-	-	-	-	-	-	
-6	2.20	2.00	2.20	2.13	0.12	5.41	3.34	
-8	1.40	1.50	2.00	1.63	0.32	19.66	4.50	
-10	0.87	1.00	0.93	0.93	0.07	7.14	6.42	
-12	0.73	0.75	0.70	0.73	0.03	3.50	11.13	
-14	0.60	0.65	0.60	0.62	0.03	4.66	13.40	
-16	0.47	0.44	0.46	0.46	0.02	4.41	18.51	
-18	0.40	0.40	0.40	0.40	0.00	0.00	21.76	
-20	0.34	0.34	0.31	0.33	0.02	4.95	26.69	
-22	0.30	0.30	0.27	0.29	0.01	4.95	31.00	
-24	0.24	0.27	0.24	0.25	0.02	6.93	36.09	
AVERAGE						6.16		

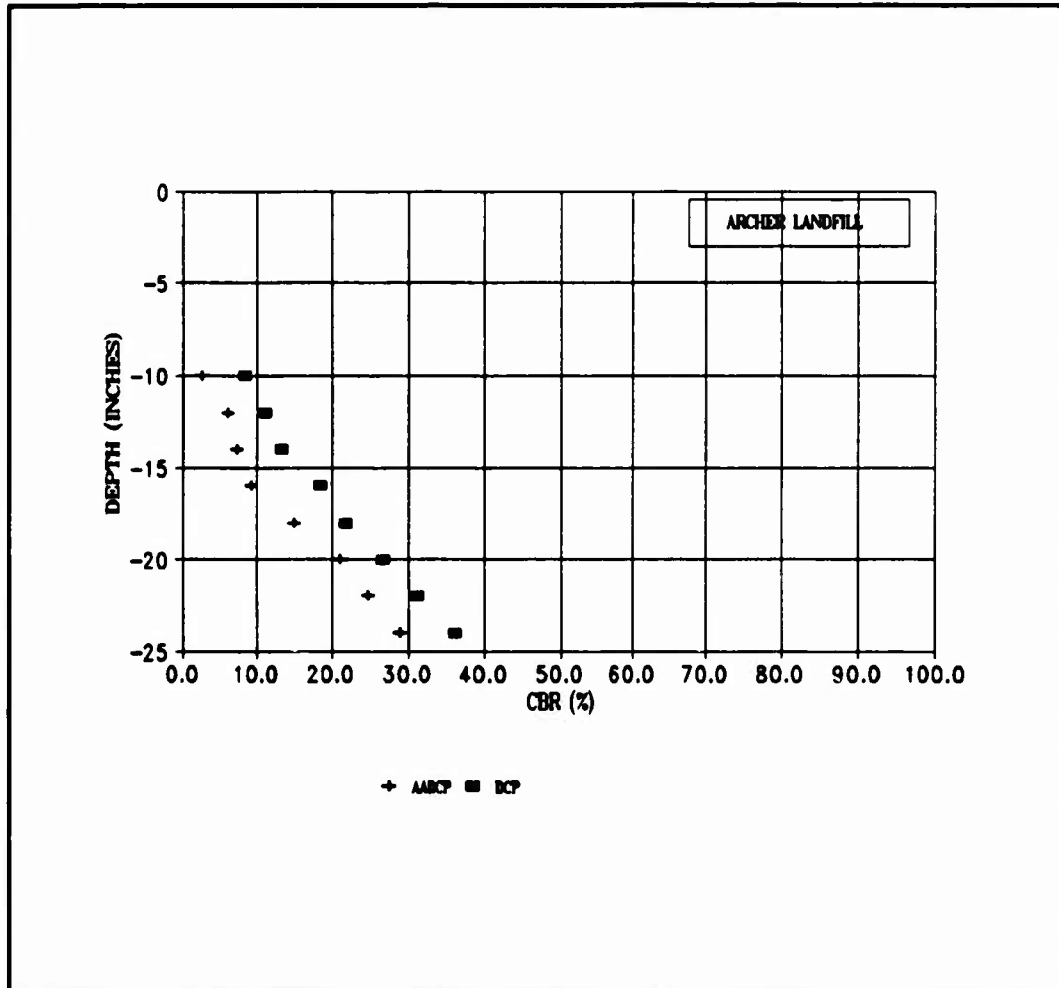
C.2 Archer Landfill Spreadsheet 2



C.3 Archer Landfill AADCP and DCP Blow Profile



C.4 Archer Landfill PI vs Depth



C.5 Archer Landfill Estimated CBR vs Depth

MAQUIRE FIELD

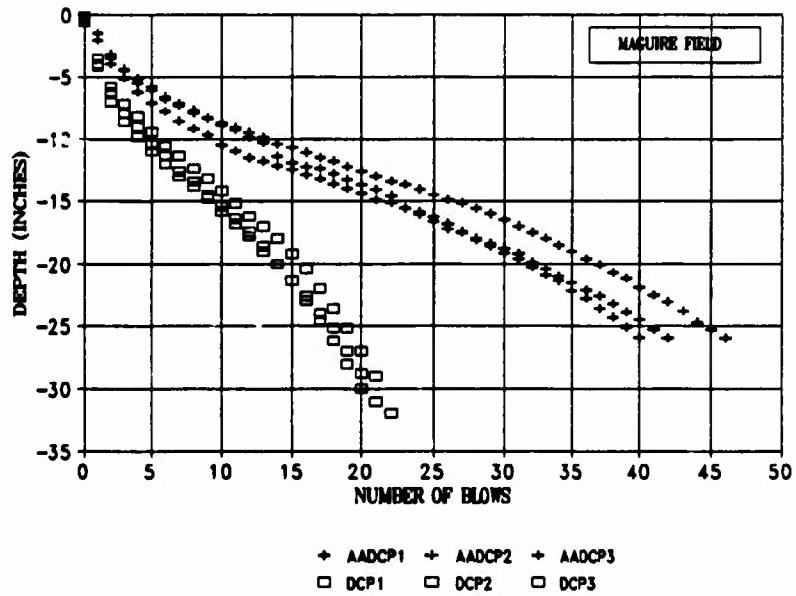
CUMULATIVE PENETRATION (INCHES)							
	AACP	AACP	AACP		DCP	DCP	DCP
	TEST	TEST	TEST		TEST	TEST	TEST
BLOWS	1	2	3	BLOWS	1	2	3
0	-0.4	-0.4	-0.4	0	-0.4	-0.6	-0.2
1	-1.5	-2.1	-2.1	1	-4.2	-4.0	-3.8
2	-4.0	-3.5	-3.2	2	-7.0	-6.2	-5.8
3	-5.1	-4.5	-4.4	3	-8.6	-8.0	-7.2
4	-6.2	-5.5	-5.1	4	-9.8	-9.0	-8.2
5	-7.1	-6.1	-5.8	5	-11.0	-10.4	-9.4
6	-7.8	-6.8	-6.6	6	-12.0	-11.4	-10.6
7	-8.6	-7.3	-7.2	7	-13.0	-12.6	-11.4
8	-9.2	-7.7	-7.9	8	-13.8	-13.4	-12.4
9	-9.7	-8.4	-8.3	9	-14.8	-14.6	-13.2
10	-10.5	-8.7	-8.9	10	-15.8	-15.4	-14.2
11	-11.0	-9.1	-9.3	11	-16.8	-16.4	-15.2
12	-11.5	-9.5	-9.9	12	-17.8	-17.4	-16.2
13	-11.8	-9.9	-10.3	13	-19.0	-18.6	-17.0
14	-12.2	-10.4	-11.4	14	-20.0	-20.0	-18.0
15	-12.5	-10.7	-11.9	15	-21.4	-21.4	-19.2
16	-12.9	-11.1	-12.3	16	-22.6	-23.0	-20.4
17	-13.2	-11.5	-12.4	17	-24.0	-24.6	-22.0
18	-13.6	-11.8	-12.8	18	-25.2	-26.2	-23.6
19	-14.0	-12.3	-13.3	19	-27.0	-28.0	-25.2
20	-14.4	-12.6	-13.7	20	-28.6	-30.0	-27.0
21	-14.9	-13.0	-14.1	21	-31.0		-29.0
22	-15.1	-13.4	-14.6	22			-32.0
23	-15.6	-13.7	-15.6				
24	-15.9	-14.1	-16.1				
25	-16.3	-14.5	-16.6				
26	-16.8	-14.9	-17.2				
27	-17.4	-15.2	-17.5				
28	-18.0	-15.6	-18.1				
29	-18.4	-16.0	-18.6				
30	-18.8	-16.5	-19.1				
31	-19.2	-17.0	-19.6				
32	-19.9	-17.5	-20.3				
33	-20.4	-18.0	-20.9				
34	-21.0	-18.5	-21.4				
35	-21.5	-19.0	-22.2				
36	-22.1	-19.6	-22.6				
37	-22.6	-20.1	-23.6				
38	-23.2	-20.7	-24.3				
39	-23.9	-21.2	-25.1				
40	-24.5	-21.9	-25.9				
41	-25.3	-22.5					
42	-26.0	-23.1					
43		-23.8					
44		-24.7					
45		-25.3					
46		-26.0					

C.6 Maguire Field Spreadsheet 1

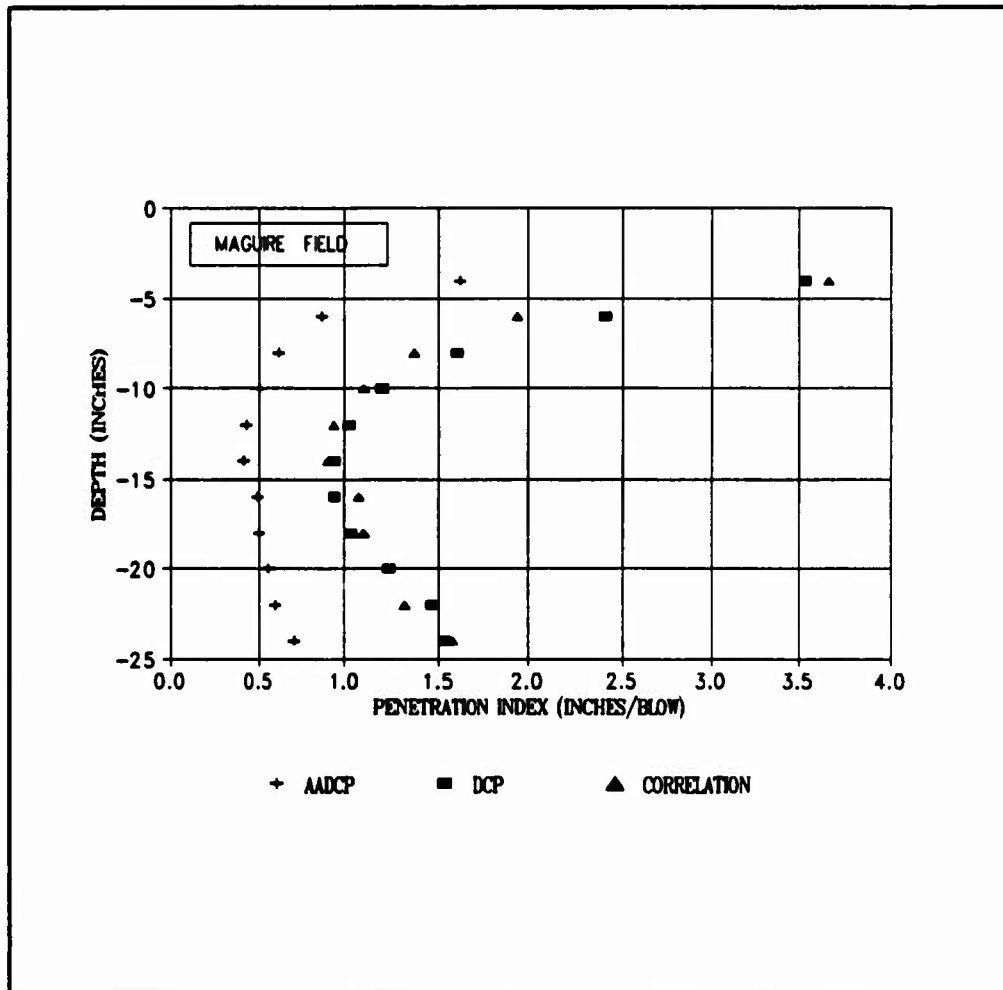
MAGUIRE FIELD

MEAN DEPTH (INCHES)	AVG P.I. AADCP 1	AVG P.I. AADCP 2	AVG P.I. AADCP 3	P.I. SITE AVERAGE	STANDARD DEVIATION	COEFFICIENT OF VARIABILITY	CORRELATION * P.I. SITE AVERAGE	CBR ** SITE AVERAGE
0	-	-	-	-	-	-	-	-
-2	1.10	1.70	1.70	1.80	0.36	23.08	3.41	1.98
-4	2.60	1.20	1.18	1.82	0.77	47.34	3.87	1.82
-6	1.10	0.77	0.73	0.87	0.20	23.40	1.95	3.89
-8	0.80	0.47	0.58	0.82	0.17	26.99	1.38	5.45
-10	0.63	0.40	0.47	0.50	0.12	24.04	1.11	8.94
-12	0.40	0.38	0.50	0.43	0.08	15.07	0.94	8.35
-14	0.40	0.38	0.46	0.41	0.03	8.44	0.91	8.72
-16	0.38	0.42	0.67	0.48	0.18	31.78	1.08	7.13
-18	0.60	0.60	0.50	0.50	0.00	0.00	1.11	8.94
-20	0.66	0.66	0.58	0.68	0.01	2.58	1.24	8.11
-22	0.66	0.60	0.63	0.68	0.04	7.08	1.33	5.88
-24	0.63	0.73	0.75	0.71	0.08	8.84	1.58	4.67
AVERAGE						18.23		
* DCP = 2.30 AADCP - 0.04								
** CBR = 292/DCP ^{1.12}								
MEAN DEPTH (INCHES)	AVG P.I. DCP 1	AVG P.I. DCP 2	AVG P.I. DCP 3	P.I. SITE AVERAGE	STANDARD DEVIATION	COEFFICIENT OF VARIABILITY	CBR ** SITE AVERAGE	
0	-	-	-	-	-	-	-	
-2	-	-	-	-	-	-	-	
-4	3.80	3.40	3.40	3.53	0.23	8.54	1.90	
-6	2.80	2.20	2.20	2.40	0.35	14.43	2.93	
-8	2.20	1.40	1.20	1.80	0.53	33.07	4.81	
-10	1.20	1.20	1.20	1.20	0.00	0.00	6.36	
-12	1.07	1.10	0.90	1.02	0.11	10.48	7.61	
-14	0.93	1.00	0.90	0.94	0.05	5.39	8.31	
-16	1.00	0.90	0.93	0.94	0.05	5.39	8.31	
-18	1.10	1.10	0.90	1.03	0.12	11.17	7.52	
-20	1.10	1.40	1.20	1.23	0.15	12.39	8.17	
-22	1.30	1.60	1.80	1.47	0.15	10.41	5.08	
-24	1.40	1.80	1.80	1.63	0.12	7.53	4.83	
AVERAGE						10.62		

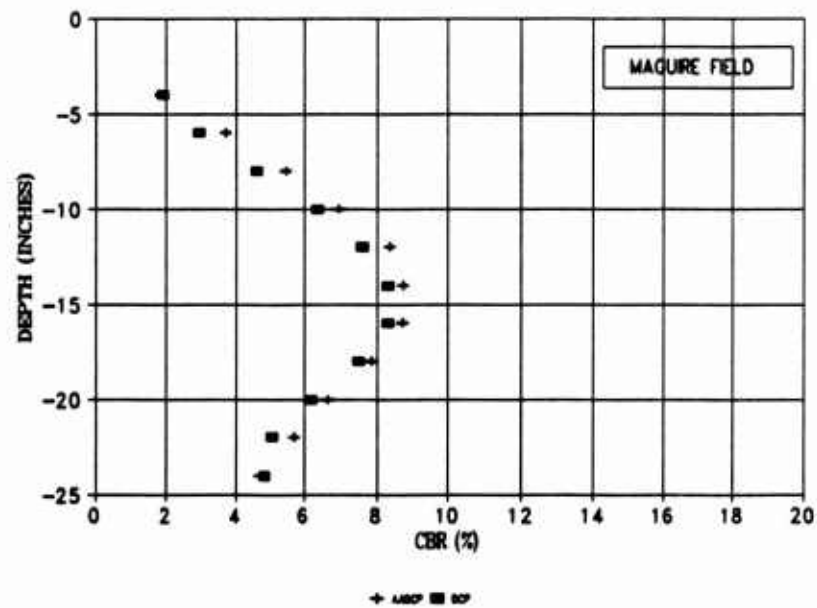
C.7 Maguire Field Spreadsheet 2



C.8 Maguire Field AADCP and DCP Blow Profile



C.9 Maguire Field PI vs Depth



C.10 Maguire Field Estimated CBR vs Depth

LAKE ALICE PARKING LOT

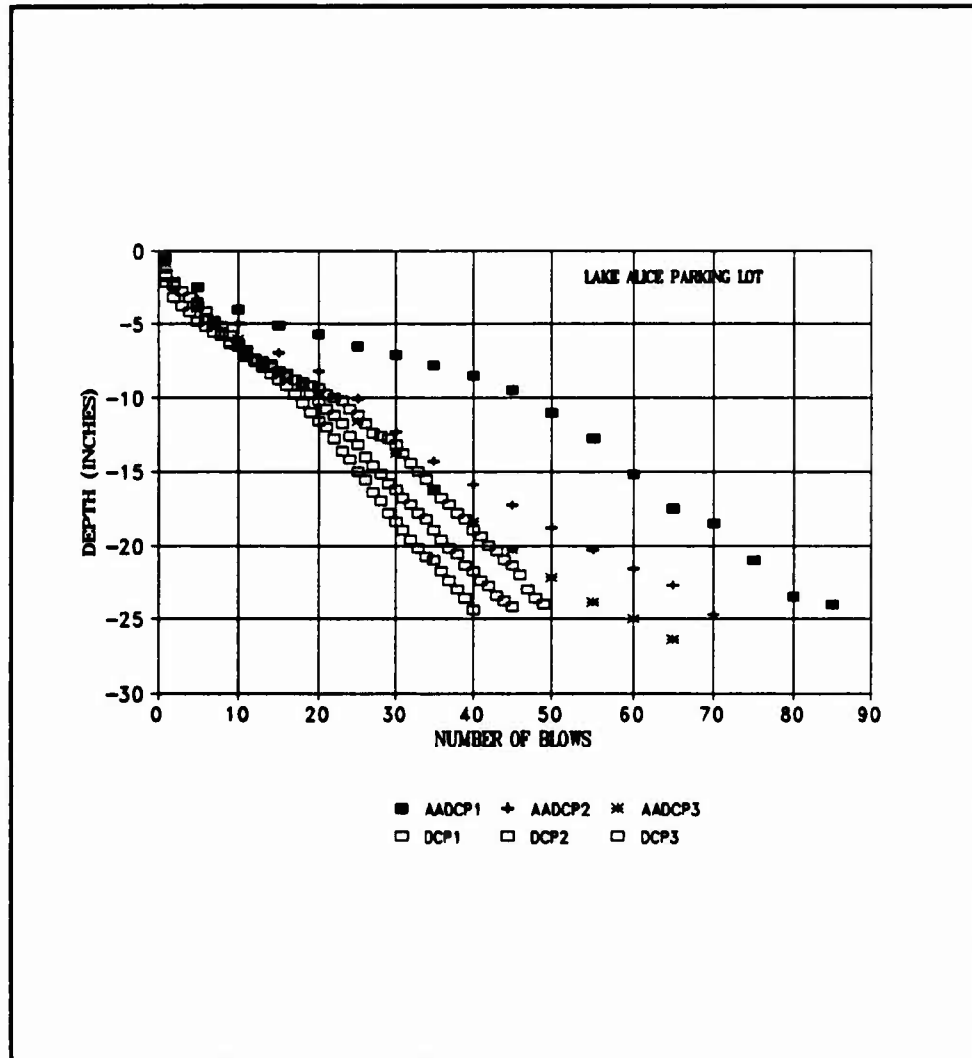
CUMMULATIVE PENETRATION (INCHES)									
BLOWS	AADCP TEST	AADCP TEST	AADCP TEST	BLOWS	DCP TEST	DCP TEST	DCP TEST	BLOWS	DCP TEST
	1	2	3		1	2	3		DCP TEST
0	-0.5	-0.8	-0.9	1	-1.8	-1.8	-2.2	1	-1.8
5	-2.5	-3.3	-3.9	2	-2.4	-2.2	-3.2	2	-2.4
10	-4.0	-5.0	-6.0	3	-2.8	-2.8	-3.8	3	-2.8
15	-5.1	-7.0	-8.3	4	-3.2	-3.2	-4.2	4	-3.2
20	-5.7	-8.2	-9.9	5	-3.8	-3.8	-4.8	5	-3.8
25	-6.5	-10.1	-11.8	6	-4.2	-4.8	-5.2	6	-4.2
30	-7.1	-12.3	-13.8	7	-4.8	-5.0	-5.8	7	-4.8
35	-7.8	-14.3	-16.3	8	-5.2	-5.8	-6.8	8	-5.2
40	-8.5	-15.9	-18.4	9	-5.8	-6.2	-8.4	9	-5.8
45	-9.5	-17.3	-20.3	10	-6.4	-6.8	-8.6	10	-6.4
50	-11.0	-18.8	-22.2	11	-7.2	-6.8	-7.0	11	-7.2
55	-12.8	-20.3	-23.9	12	-7.6	-7.4	-7.4	12	-7.6
60	-15.2	-21.8	-25.0	13	-8.0	-7.8	-7.8	13	-8.0
65	-17.5	-22.7	-26.4	14	-8.4	-7.8	-8.0	14	-8.4
70	-18.6	-24.7		15	-8.8	-8.2	-8.2	15	-8.8
75	-21.0			16	-9.2	-8.8	-8.4	16	-9.2
80	-23.5			17	-9.8	-8.8	-8.8	17	-9.8
85	-24.0			18	-10.4	-9.2	-9.0	18	-10.4
				19	-11.0	-9.8	-9.2	19	-11.0
				20	-11.8	-10.2	-9.4	20	-11.8
				21	-12.0	-10.8	-9.8	21	-12.0
				22	-12.8	-11.2	-10.0	22	-12.8
				23	-13.6	-11.8	-10.2	23	-13.6
				24	-14.2	-12.6	-10.8	24	-14.2
				25	-15.0	-13.2	-11.2	25	-15.0
				26	-15.6	-14.0	-11.8	26	-15.6
				27	-16.4	-14.6	-12.4	27	-16.4
				28	-17.0	-15.2	-12.6	28	-17.0
				29	-17.8	-15.8	-12.8	29	-17.8
				30	-18.4	-16.2	-13.2	30	-18.4
				31	-19.0	-16.8	-13.8	31	-19.0
				32	-19.8	-17.2	-14.4	32	-19.8
				33	-20.2	-17.8	-15.0	33	-20.2
				34	-20.8	-18.2	-15.5	34	-20.8
				35	-21.0	-19.0	-16.2	35	-21.0
				36	-21.8	-19.6	-16.8	36	-21.8
				37	-22.4	-20.2	-17.2	37	-22.4
				38	-23.0	-20.6	-17.8	38	-23.0
				39	-23.6	-21.4	-18.2	39	-23.6
				40	-24.4	-21.8	-19.0	40	-24.4
				41		-22.4	-19.4	41	
				42		-22.8	-20.0	42	
				43		-23.4	-20.4	43	
				44		-23.8	-21.0	44	
				45		-24.2	-21.4	45	
				46			-22.0	46	
				47			-22.4	47	
				48			-23.0	48	
				49			-23.6	49	
				50			-24.0	50	

C.11 Lake Alice Parking Lot Spreadsheet 1

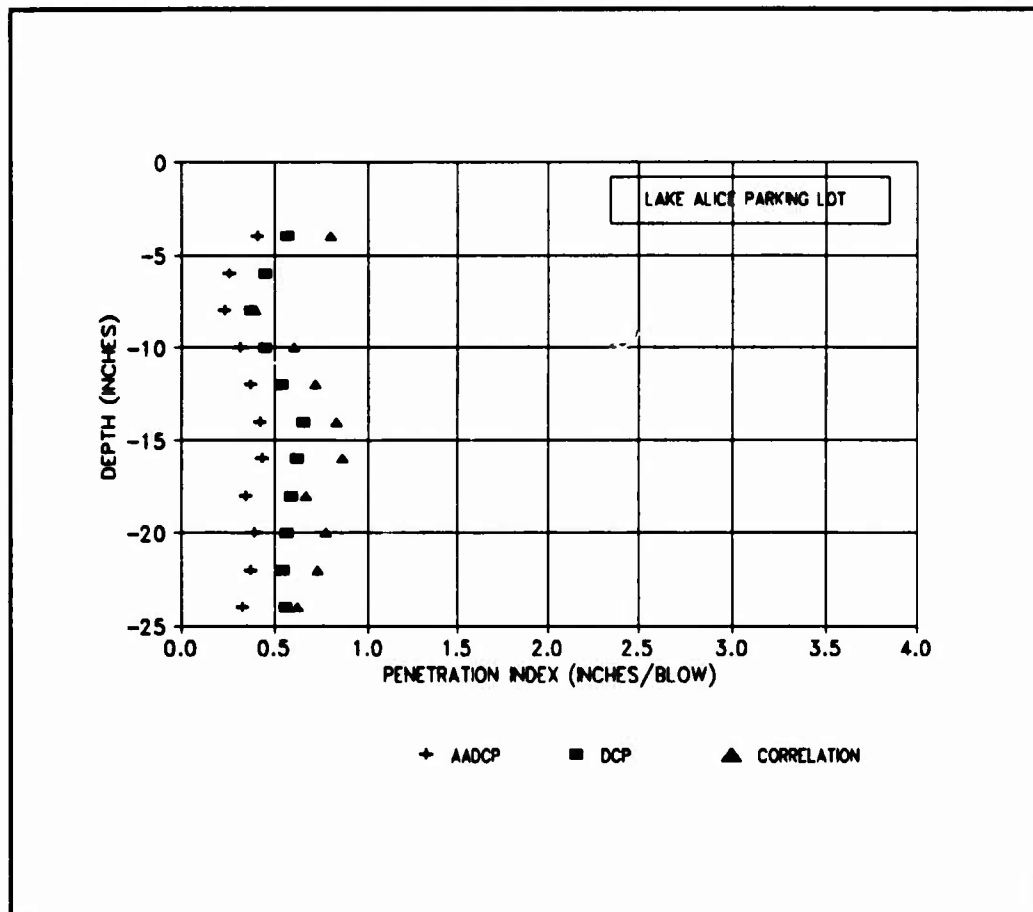
LAKE ALICE PARKING LOT

MEAN DEPTH (INCHES)	AVG P.I. AADCP 1	AVG P.I. AADCP 2	AVG P.I. AADCP 3	P.I. SITE AVERAGE	STANDARD DEVIATION	COEFFICIENT OF VARIABILITY	CORRELATION P.I. SITE AVERAGE	CBR ** SITE AVERAGE
0	-	-	-	-	-	-	-	-
-2	0.40	-	-	-	-	-	-	-
-4	0.30	0.51	0.60	0.41	0.15	36.86	0.80	10.04
-6	0.17	0.34	0.42	0.25	0.12	48.38	0.45	18.88
-8	0.13	0.32	0.46	0.23	0.13	58.23	0.39	22.16
-10	0.25	0.38	0.32	0.32	0.07	20.55	0.80	13.88
-12	0.33	0.44	0.34	0.37	0.06	16.44	0.72	11.29
-14	-	0.40	0.44	0.42	0.03	6.73	0.83	9.59
-16	0.48	0.32	0.50	0.43	0.10	22.77	0.86	9.21
-18	0.33	0.29	0.42	0.36	0.07	19.21	0.67	12.30
-20	0.50	0.30	0.36	0.39	0.10	25.59	0.77	10.43
-22	0.50	0.24	0.36	0.37	0.13	34.86	0.73	11.16
-24	0.30	0.40	0.28	0.33	0.06	19.68	0.62	13.32
AVERAGE						28.10		
* DCP = 2.27 AADCP - 0.12								
** CBR = 292/DCP*1.12								
MEAN DEPTH (INCHES)	AVG P.I. DCP 1	AVG P.I. DCP 2	AVG P.I. DCP 3	P.I. SITE AVERAGE	STANDARD DEVIATION	COEFFICIENT OF VARIABILITY	CBR ** SITE AVERAGE	
0	-	-	-	-	-	-	-	
-2	0.50	0.60	-	0.55	0.07	12.86	15.23	
-4	0.50	0.55	0.65	0.57	0.06	13.48	14.73	
-6	0.53	0.44	0.37	0.45	0.06	18.70	19.23	
-8	0.46	0.33	0.30	0.37	0.10	25.80	23.67	
-10	0.55	0.50	0.29	0.45	0.14	31.53	19.30	
-12	0.60	0.60	0.40	0.53	0.12	21.85	15.77	
-14	0.73	0.67	0.55	0.65	0.09	14.28	12.63	
-16	0.70	0.55	0.60	0.62	0.08	12.39	13.40	
-18	0.65	0.55	0.55	0.58	0.06	9.90	14.26	
-20	0.52	0.60	0.55	0.56	0.04	7.14	14.93	
-22	0.55	0.55	0.52	0.54	0.02	3.21	15.55	
-24	0.67	0.47	0.53	0.56	0.10	18.33	15.06	
AVERAGE						15.77		

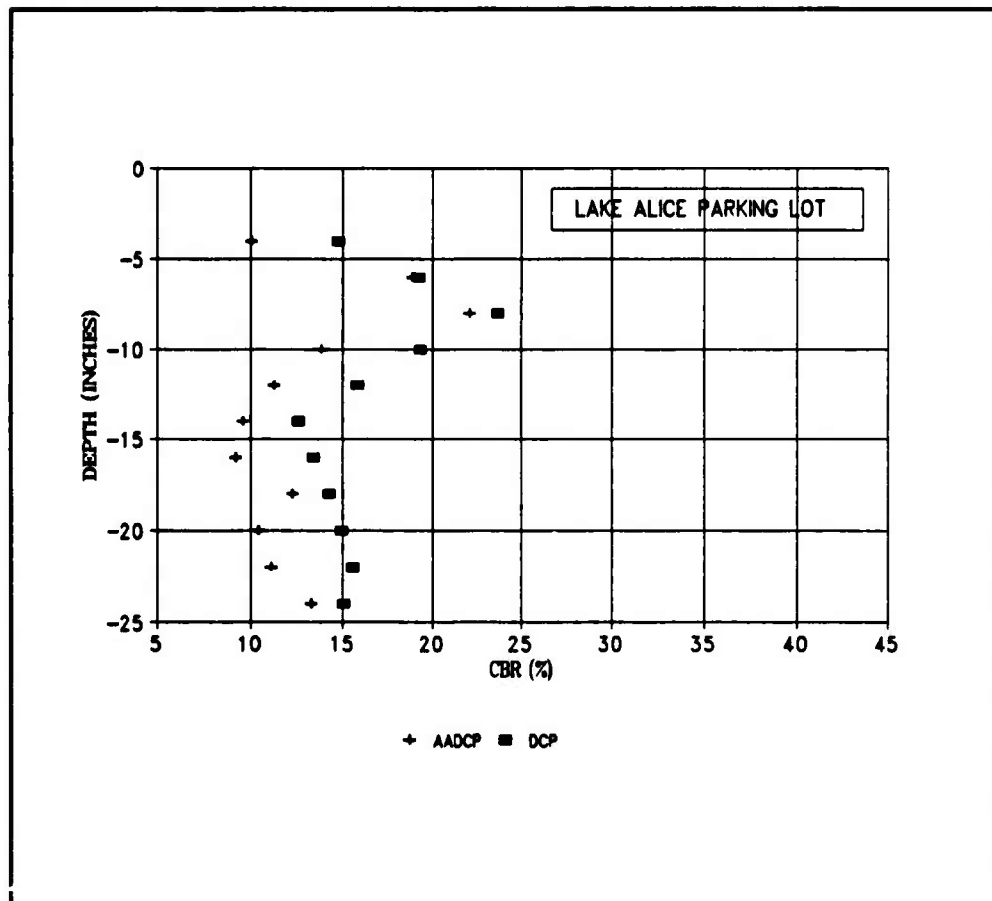
C.12 Lake Alice Parking Lot Spreadsheet 2



C.13 Lake Alice Parking Lot AADCP and DCP Blow Profile



C.14 Lake Alice Parking Lot PI vs Depth



C.15 Lake Alice Parking Lot Estimated CBR vs Depth

LAKE ALICE SHORE LINE

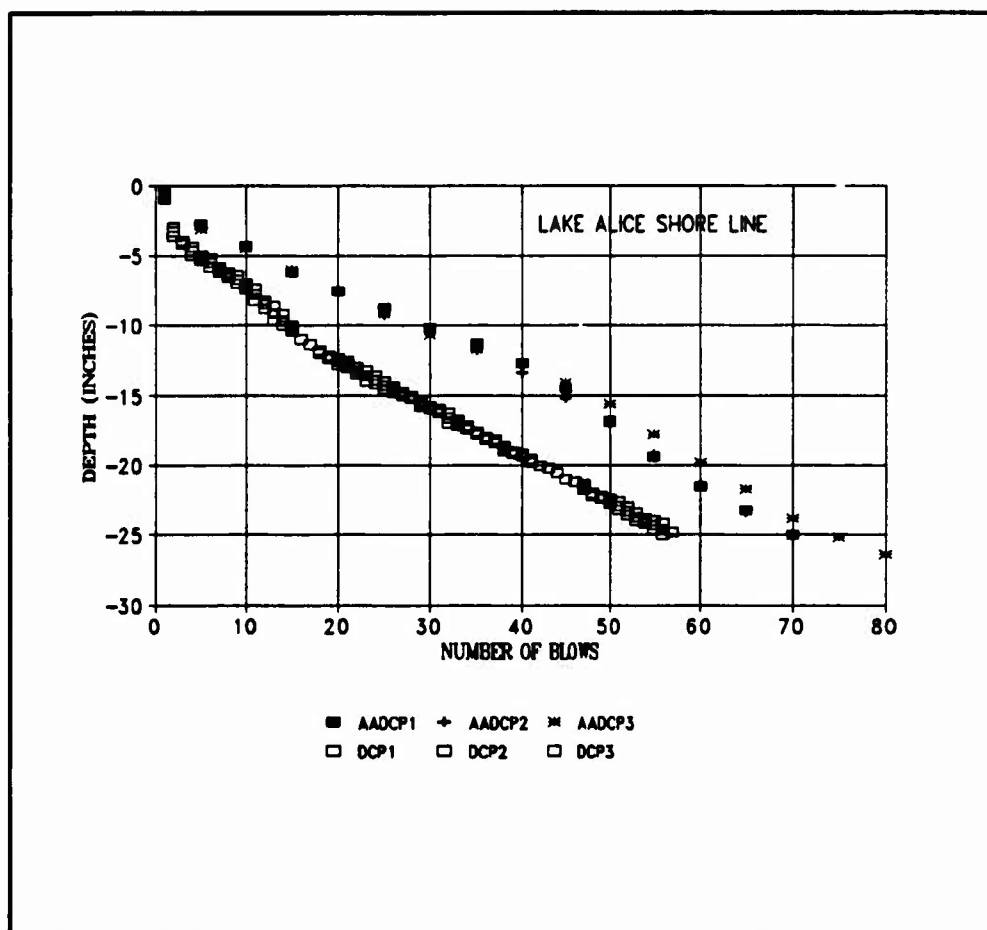
CUMULATIVE PENETRATION (INCHES)								
	ADCP	ADCP	ADCP		DCP	DCP	DCP	
	TEST	TEST	TEST		TEST	TEST	TEST	
BLOWS	1	2	3	BLOWS	1	2	3	
1	-0.8	-0.8	-0.8	1	-1.0	-0.8	-0.8	
5	-2.8	-3.1	-3.1	2	-3.0	-3.0	-3.3	
10	-4.3	-4.5	-4.5	3	-4.2	-4.0	-4.1	
15	-6.2	-6.0	-6.0	4	-5.0	-4.4	-4.7	
20	-7.5	-7.5	-7.5	5	-5.4	-5.0	-5.2	
25	-8.7	-8.3	-8.2	6	-5.8	-5.2	-5.5	
30	-10.2	-10.5	-10.7	7	-6.2	-5.8	-6.0	
35	-11.3	-11.6	-11.7	8	-6.6	-6.2	-6.4	
40	-12.7	-13.4	-12.7	9	-7.0	-6.4	-6.7	
45	-14.5	-15.2	-14.1	10	-7.4	-7.0	-7.2	
50	-16.5	-17.2	-15.8	11	-8.2	-7.4	-7.8	
55	-18.4	-19.2	-17.8	12	-8.8	-8.2	-8.5	
60	-21.5	-21.4	-19.8	13	-9.6	-8.8	-9.1	
65	-23.2	-23.4	-21.7	14	-10.0	-9.2	-9.6	
70	-25.0	-25.0	-23.8	15	-10.4	-10.0	-10.2	
75			-25.2	16	-11.0	-11.0	-11.0	
80			-26.4	17	-11.4	-11.4	-11.4	
				18	-12.0	-11.8	-11.9	
				19	-12.4	-12.2	-12.3	
				20	-12.8	-12.4	-12.6	
				21	-13.0	-12.6	-12.8	
				22	-13.5	-13.0	-13.3	
				23	-14.0	-13.2	-13.6	
				24	-14.2	-13.6	-13.9	
				25	-14.8	-14.0	-14.3	
				26	-14.8	-14.4	-14.6	
				27	-15.0	-14.8	-14.9	
				28	-15.2	-15.0	-15.1	
				29	-15.8	-15.4	-15.6	
				30	-16.0	-15.8	-15.9	
				31	-16.2	-16.0	-16.1	
				32	-17.0	-16.2	-16.6	
				33	-17.2	-16.8	-17.0	
				34	-17.4	-17.2	-17.3	
				35	-17.8	-17.6	-17.7	
				36	-18.2	-18.0	-18.1	
				37	-18.4	-18.2	-18.3	
				38	-19.0	-18.6	-18.8	
				39	-19.2	-19.0	-19.1	
				40	-19.4	-19.2	-19.3	
				41	-19.8	-19.6	-19.7	
				42	-20.0	-20.0	-20.0	
				43	-20.2	-20.2	-20.2	
				44	-20.6	-20.6	-20.6	
				45	-21.0	-21.0	-21.0	
				46	-21.2	-21.2	-21.2	
				47	-21.6	-21.4	-21.6	
				48	-22.2	-22.0	-22.1	
				49	-22.4	-22.2	-22.3	
				50	-22.8	-22.4	-22.6	
				51	-23.2	-22.6	-22.9	
				52	-23.6	-23.0	-23.3	
				53	-24.0	-23.4	-23.7	
				54	-24.2	-23.8	-24.0	
				55	-24.6	-24.0	-24.3	
				56	-25.0	-24.2	-24.6	
				57		-24.6		

C.16 Lake Alice Shore Line Spreadsheet 1

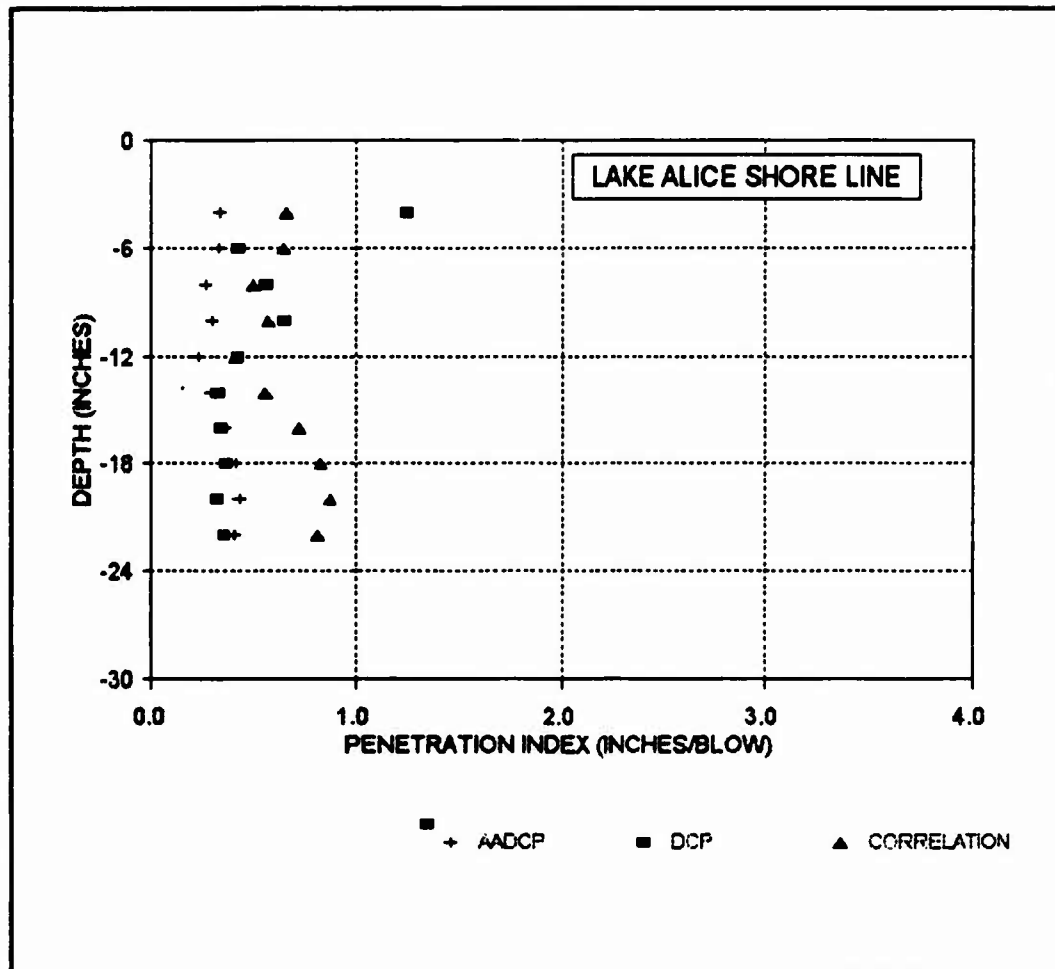
LAKE ALICE SHORE LINE

	AVG	AVG	AVG	P.I.			CORRELATION *	P.I.
MEAN	P.I.	P.I.	P.I.	SITE	STANDARD	COEFFICIENT		
DEPTH	AADCP	AADCP	AADCP	AVERAGE	DEVIATION	OF	P.I.	SITE
(INCHES)	1	2	3			VARIABILITY	AVERAGE	AVERAGE
0	-	-	-	-	-	-	-	-
-2	0.46	-	-	-	-	-	-	-
-4	0.30	0.39	0.41	0.34	0.06	18.45	0.66	12.38
-6	0.36	0.30	0.30	0.34	0.06	16.64	0.65	12.62
-8	0.25	0.30	0.30	0.28	0.04	12.86	0.50	16.83
-10	0.30	0.30	0.32	0.31	0.01	3.77	0.57	14.50
-12	0.25	0.26	0.20	0.24	0.03	13.56	0.42	20.61
-14	0.36	0.32	0.28	0.30	0.03	9.43	0.56	14.94
-16	0.46	0.36	0.30	0.37	0.06	21.65	0.73	11.16
-18	-	0.40	0.44	0.42	0.03	6.73	0.63	9.59
-20	0.62	0.40	0.40	0.44	0.07	15.75	0.66	9.03
-22	0.42	0.44	0.36	0.41	0.03	7.39	0.62	9.78
-24	0.34	0.36	0.42	0.37	0.04	11.15	0.73	11.16
AVERAGE						12.48		
								* DCP = 2.27 AADCP - 0.12
								** CBR = 292/DCP^1.12

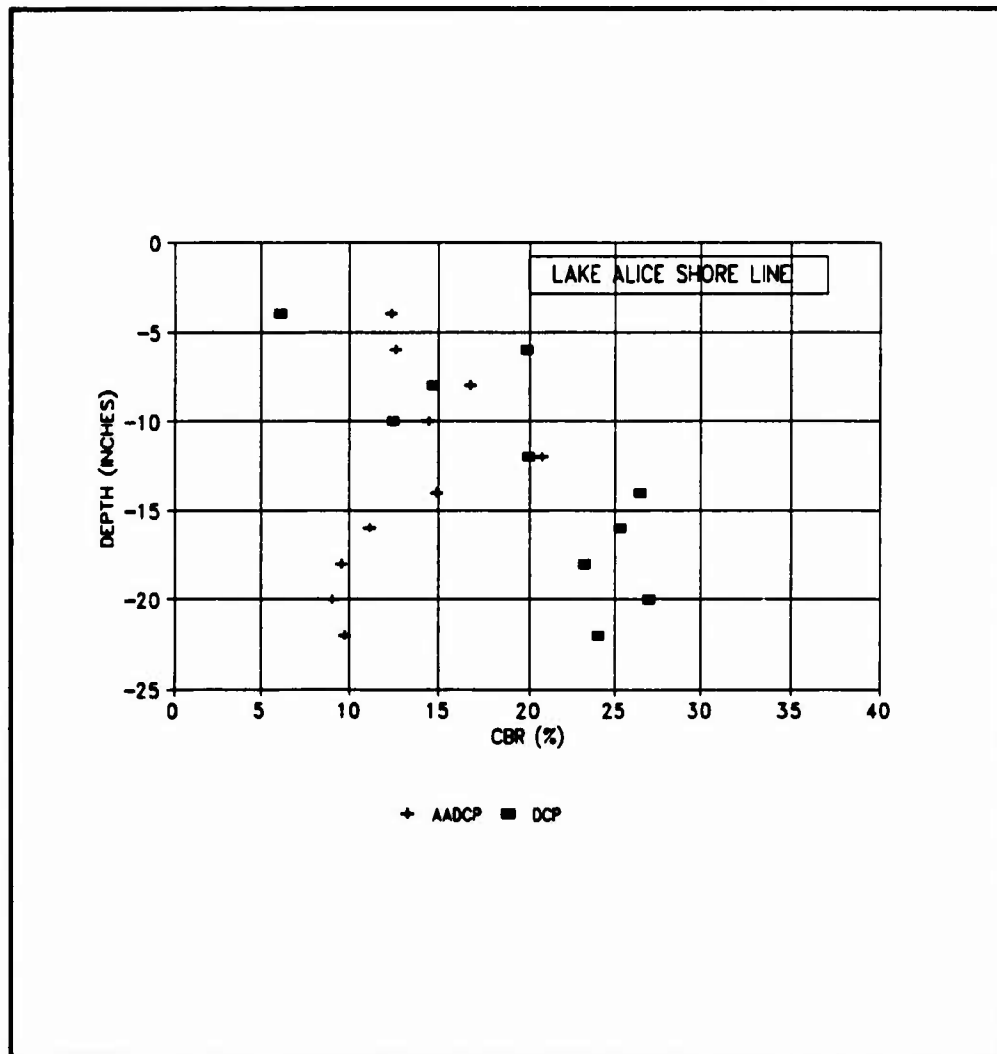
	AVG	AVG	AVG	P.I.			CBR **
MEAN	P.I.	P.I.	P.I.	SITE	STANDARD	COEFFICIENT	
DEPTH	DCP	DCP	DCP	AVERAGE	DEVIATION	OF	SITE
(INCHES)	1	2	3			VARIABILITY	AVERAGE
0	-	-	-	-	-	-	-
-2	-	2.40	-	-	-	-	-
-4	1.33	1.10	1.30	1.24	0.13	10.14	6.10
-6	0.47	0.43	0.40	0.43	0.03	7.89	19.89
-8	0.66	0.66	0.60	0.67	0.03	5.09	14.73
-10	0.66	0.60	0.63	0.66	0.13	19.49	12.45
-12	0.43	0.43	0.43	0.43	0.00	0.64	19.96
-14	0.31	0.34	0.35	0.34	0.02	5.63	26.48
-16	0.37	0.33	0.36	0.36	0.02	4.76	26.27
-18	0.40	0.37	0.37	0.38	0.02	5.09	23.20
-20	0.33	0.34	0.31	0.33	0.01	4.41	26.96
-22	-	0.40	0.33	0.37	0.05	12.86	23.99
-24	-	-	-	-	-	-	-
AVERAGE						7.56	



C.18 Lake Alice Shore Line AADCP and DCP Blow Profile



C.19 Lake Alice Shore Line PI vs Depth



C.20 Lake Alice Shore Line Estimated CBR vs Depth

FDOT TEST PIT #1

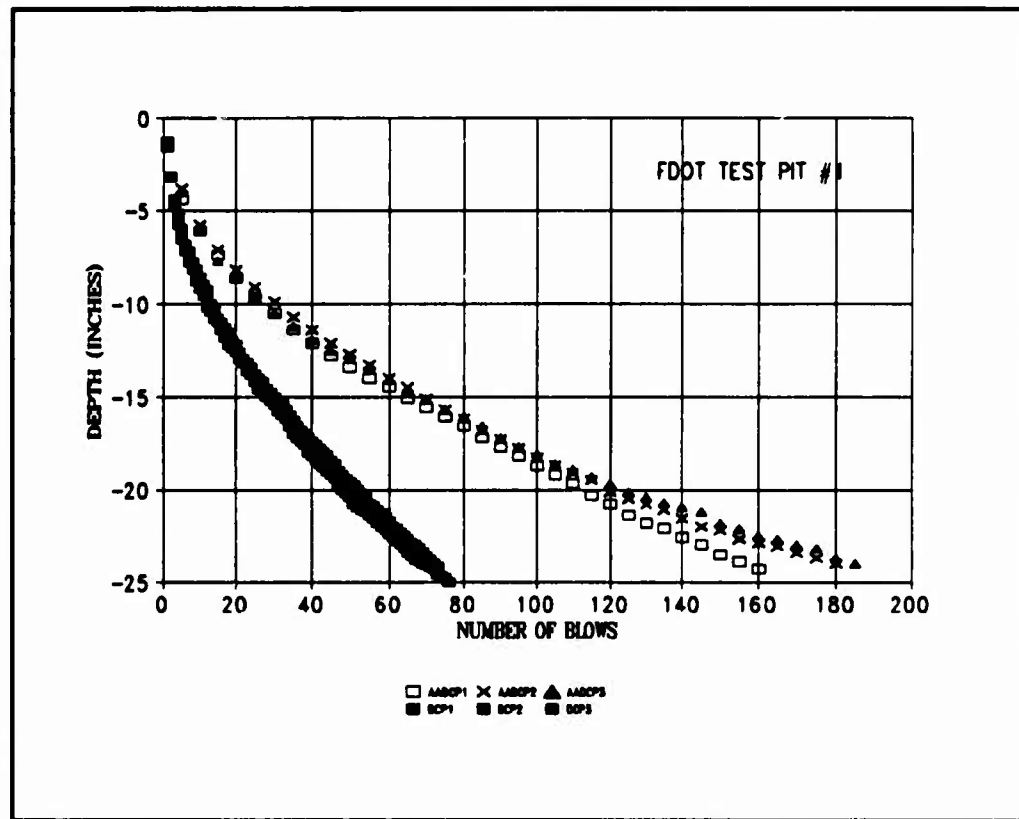
CUMULATIVE PENETRATION (INCHES)											
AACDP			AACDP			AACDP			DCP		
TEST			TEST			TEST			TEST		
BLOWS	1	2	3	BLOWS	1	2	3	BLOWS	1	2	3
0	-1.0	-1.3	-1.5	0	-1.3	-1.6	-1.5	0	-1.3	-1.6	-1.5
5	-4.4	-3.0	-4.0	1	-3.2	-3.2	-3.2	1	-3.2	-3.2	-3.2
10	-8.1	-6.0	-8.1	2	-6.0	-4.4	-4.0	2	-6.0	-4.4	-4.0
15	-7.4	-7.1	-7.7	3	-5.0	-5.2	-5.5	3	-5.0	-5.2	-5.5
20	-8.8	-8.2	-8.5	4	-6.0	-6.0	-6.3	4	-6.0	-6.0	-6.3
25	-9.7	-9.1	-9.0	5	-7.2	-6.0	-7.0	5	-7.2	-6.0	-7.0
30	-10.5	-9.0	-10.5	6	-7.0	-7.2	-7.5	6	-7.0	-7.2	-7.5
35	-11.4	-10.7	-11.2	7	-8.2	-7.0	-8.0	7	-8.2	-7.0	-8.0
40	-12.1	-11.4	-11.0	8	-8.0	-8.2	-8.5	8	-8.0	-8.2	-8.5
45	-12.0	-12.1	-12.5	9	-9.2	-8.0	-8.9	9	-9.2	-8.0	-8.9
50	-13.4	-12.7	-13.0	10	-9.0	-9.0	-9.3	10	-9.0	-9.0	-9.3
55	-14.0	-13.3	-13.5	11	-10.2	-9.1	-9.0	11	-10.2	-9.1	-9.0
60	-14.5	-14.0	-14.1	12	-10.4	-10.0	-10.2	12	-10.4	-10.0	-10.2
65	-16.1	-14.5	-14.7	13	-10.0	-10.2	-10.5	13	-10.0	-10.2	-10.5
70	-16.0	-15.1	-16.1	14	-11.0	-10.0	-10.0	14	-11.0	-10.0	-10.0
75	-16.1	-16.7	-16.7	15	-11.4	-11.0	-11.2	15	-11.4	-11.0	-11.2
80	-16.6	-16.2	-16.1	16	-11.0	-11.3	-11.0	16	-11.0	-11.3	-11.0
85	-17.2	-16.0	-16.0	17	-12.2	-11.0	-11.0	17	-12.2	-11.0	-11.0
90	-17.7	-17.3	-17.2	18	-12.4	-12.0	-12.2	18	-12.4	-12.0	-12.2
95	-18.2	-17.0	-17.7	19	-12.6	-12.2	-12.4	19	-12.6	-12.2	-12.4
100	-18.7	-18.3	-18.1	20	-13.0	-12.6	-12.0	20	-13.0	-12.6	-12.0
105	-19.2	-18.7	-18.0	21	-13.2	-13.0	-13.1	21	-13.2	-13.0	-13.1
110	-19.7	-19.1	-18.0	22	-13.6	-13.2	-13.4	22	-13.6	-13.2	-13.4
115	-20.3	-19.5	-19.3	23	-13.0	-13.4	-13.0	23	-13.0	-13.4	-13.0
120	-20.0	-20.1	-19.7	24	-14.2	-13.0	-14.0	24	-14.2	-13.0	-14.0
125	-21.4	-20.5	-20.1	25	-14.0	-14.0	-14.3	25	-14.0	-14.0	-14.3
130	-21.0	-20.0	-20.4	26	-14.0	-14.2	-14.5	26	-14.0	-14.2	-14.5
135	-22.1	-21.1	-20.7	27	-15.0	-14.0	-14.0	27	-15.0	-14.0	-14.0
140	-22.0	-21.0	-20.0	28	-15.2	-14.0	-15.0	28	-15.2	-14.0	-15.0
145	-23.0	-22.0	-21.2	29	-15.4	-15.0	-15.2	29	-15.4	-15.0	-15.2
150	-23.5	-22.2	-21.0	30	-16.0	-15.2	-15.5	30	-16.0	-15.2	-15.5
155	-23.0	-22.7	-22.1	31	-16.0	-15.4	-15.7	31	-16.0	-15.4	-15.7
160	-24.3	-22.0	-22.5	32	-16.2	-15.7	-16.0	32	-16.2	-15.7	-16.0
165		-23.1	-22.7	33	-16.0	-16.0	-16.3	33	-16.0	-16.0	-16.3
170		-23.4	-23.0	34	-17.0	-16.3	-16.7	34	-17.0	-16.3	-16.7
175		-23.7	-23.2	35	-17.2	-16.0	-16.0	35	-17.2	-16.0	-16.0
180		-24.0	-23.7	36	-17.4	-16.0	-17.1	36	-17.4	-16.0	-17.1
185			-24.0	37	-17.0	-17.0	-17.3	37	-17.0	-17.0	-17.3
				38	-18.0	-17.2	-17.6	38	-18.0	-17.2	-17.6
				39	-18.2	-17.4	-17.0	39	-18.2	-17.4	-17.0
				40	-18.4	-17.0	-18.0	40	-18.4	-17.0	-18.0
				41	-18.0	-17.0	-18.2	41	-18.0	-17.0	-18.2
				42	-18.0	-18.0	-18.4	42	-18.0	-18.0	-18.4
				43	-18.0	-17.2	-18.0	43	-18.0	-17.2	-18.0
				44	-18.2	-18.4	-18.0	44	-18.2	-18.4	-18.0
				45	-18.4	-18.0	-18.0	45	-18.4	-18.0	-18.0
				46	-18.0	-18.0	-18.4	46	-18.0	-18.0	-18.4
				47	-20.0	-18.2	-18.0	47	-20.0	-18.2	-18.0
				48	-20.2	-18.4	-18.0	48	-20.2	-18.4	-18.0
				49	-20.4	-18.0	-20.0	49	-20.4	-18.0	-20.0
				50	-20.0	-18.0	-20.3	50	-20.0	-18.0	-20.3
				51	-21.0	-20.0	-20.5	51	-21.0	-20.0	-20.5
				52	-21.1	-20.2	-20.7	52	-21.1	-20.2	-20.7
				53	-21.2	-20.4	-20.0	53	-21.2	-20.4	-20.0
				54	-21.4	-20.0	-21.1	54	-21.4	-20.0	-21.1
				55	-21.0	-20.0	-21.3	55	-21.0	-20.0	-21.3
				56	-21.0	-21.1	-21.5	56	-21.0	-21.1	-21.5
				57	-22.0	-21.3	-21.7	57	-22.0	-21.3	-21.7
				58	-22.2	-21.5	-21.0	58	-22.2	-21.5	-21.0
				59	-22.4	-21.7	-22.1	59	-22.4	-21.7	-22.1
				60	-22.0	-22.0	-22.3	60	-22.0	-22.0	-22.3
				61	-22.0	-22.1	-22.5	61	-22.0	-22.1	-22.5
				62	-23.0	-22.3	-22.7	62	-23.0	-22.3	-22.7
				63	-23.2	-22.5	-22.0	63	-23.2	-22.5	-22.0
				64	-23.4	-22.7	-23.1	64	-23.4	-22.7	-23.1
				65	-23.0	-22.0	-23.3	65	-23.0	-22.0	-23.3
				66	-23.0	-23.0	-23.4	66	-23.0	-23.0	-23.4
				67	-23.0	-23.2	-23.0	67	-23.0	-23.2	-23.0
				68	-24.0	-23.4	-23.7	68	-24.0	-23.4	-23.7
				69	-24.1	-23.0	-23.0	69	-24.1	-23.0	-23.0
				70	-24.2	-23.0	-24.0	70	-24.2	-23.0	-24.0
				71	-24.3	-24.0	-24.2	71	-24.3	-24.0	-24.2
				72	-24.0	-24.2	-24.4	72	-24.0	-24.2	-24.4
				73	-24.7			73	-24.7		
				74	-24.0			74	-24.0		
				75	-25.0			75	-25.0		

C.21 FDOT Test Pit #1 Spreadsheet 1

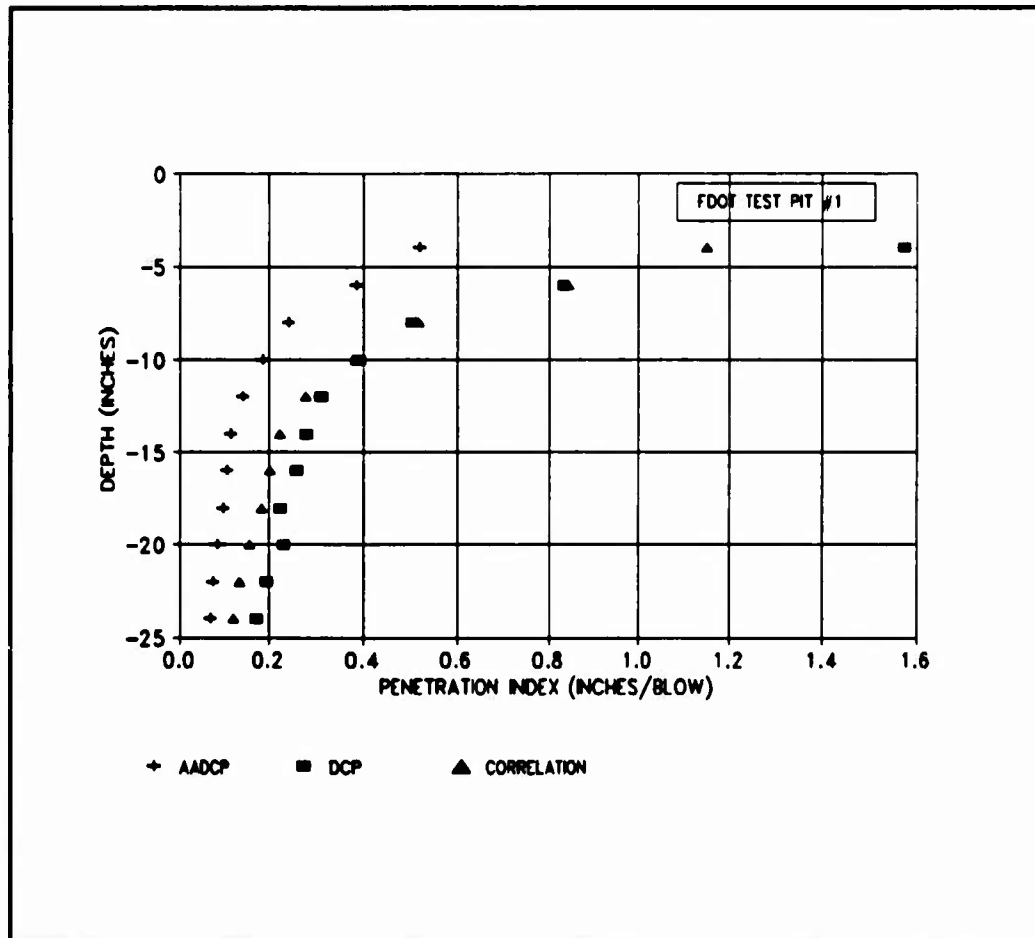
FDOT TEST PIT #1

MEAN DEPTH (INCHES)	AVG P.I. AADCP 1	AVG P.I. AADCP 2	AVG P.I. AADCP 3	P.I. SITE AVERAGE	STANDARD DEVIATION	COEFFICIENT OF VARIABILITY	CORRELATIO P.I. SITE AVERAGE	CBR ** SITE AVERAGE
0	-	-	-	-	-	-	-	-
-2	-	-	-	-	-	-	-	-
-4	0.56	0.50	0.50	0.52	0.03	6.66	1.16	6.64
-6	0.34	0.40	0.42	0.39	0.04	10.77	0.85	9.37
-8	0.25	0.24	0.24	0.24	0.01	2.37	0.52	16.23
-10	0.19	0.17	0.20	0.19	0.02	9.22	0.39	22.58
-12	0.15	0.13	0.13	0.14	0.01	8.25	0.28	32.13
-14	0.11	0.12	0.11	0.11	0.01	4.45	0.22	41.70
-16	0.10	0.12	0.09	0.10	0.01	9.52	0.20	46.74
-18	0.11	0.09	0.09	0.10	0.01	6.99	0.18	51.77
-20	0.11	0.08	0.07	0.09	0.02	21.45	0.16	61.60
-22	0.09	0.07	0.07	0.08	0.01	14.45	0.13	73.92
-24	0.09	0.06	0.07	0.07	0.02	23.06	0.12	83.45
AVERAGE						10.65		
* DCP = 2.30 AADCP - 0.04								
** CBR = 292/DCP^1.12								
MEAN DEPTH (INCHES)	AVG P.I. DCP 1	AVG P.I. DCP 2	AVG P.I. DCP 3	P.I. SITE AVERAGE	STANDARD DEVIATION	COEFFICIENT OF VARIABILITY	CBR ** SITE AVERAGE	
0	-	-	-	-	-	-	-	
-2	-	-	-	-	-	-	-	
-4	1.75	1.40	1.57	1.58	0.17	11.11	4.69	
-6	0.90	0.80	0.80	0.83	0.06	6.93	9.56	
-8	0.56	0.44	0.52	0.50	0.06	11.30	16.82	
-10	0.37	0.40	0.40	0.39	0.02	4.95	22.46	
-12	0.31	0.31	0.32	0.32	0.00	0.44	28.43	
-14	0.30	0.27	0.27	0.28	0.02	6.18	32.37	
-16	0.27	0.24	0.26	0.26	0.02	5.89	35.16	
-18	0.24	0.22	0.21	0.22	0.02	6.84	41.80	
-20	0.24	0.23	0.22	0.23	0.01	4.86	40.01	
-22	0.18	0.19	0.21	0.19	0.01	5.69	49.20	
-24	0.16	0.19	0.17	0.17	0.01	8.32	56.11	
AVERAGE						6.59		

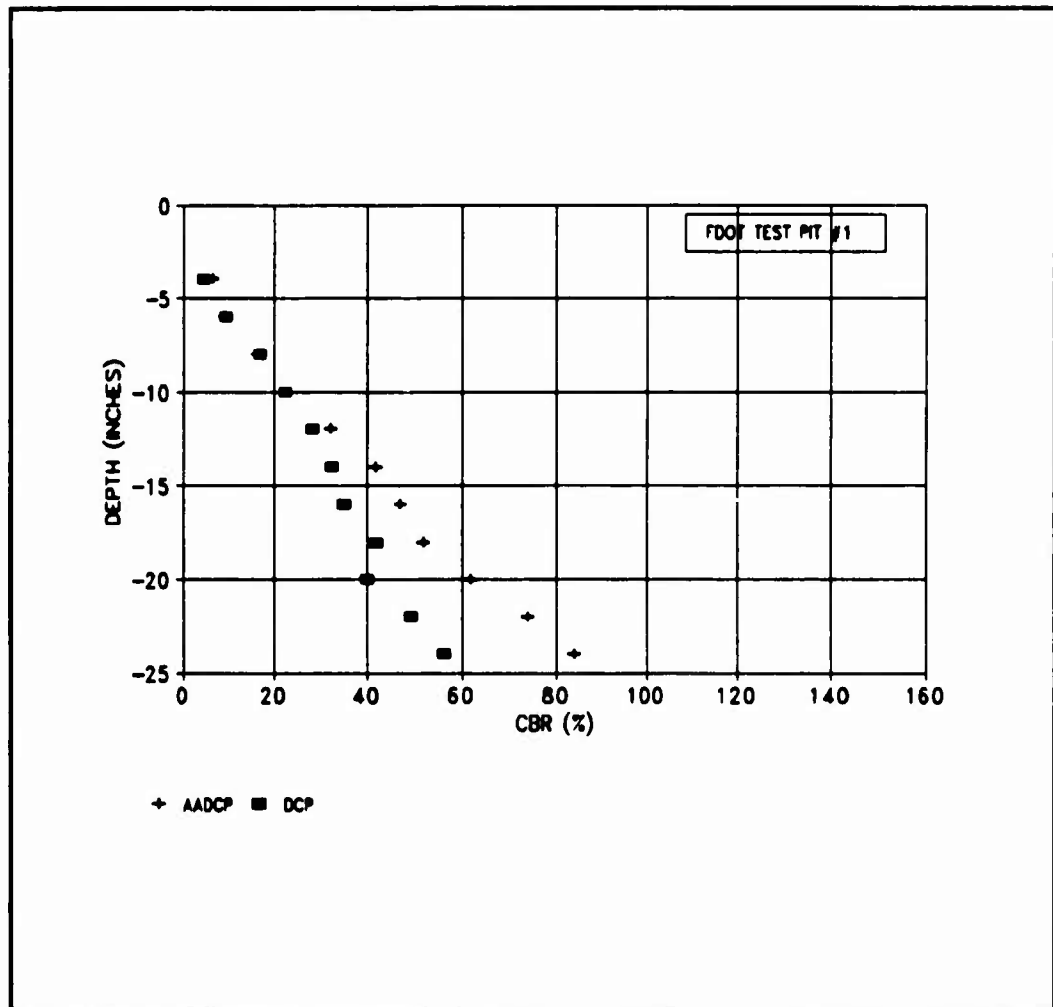
C.22 FDOT Test Pit #1 Spreadsheet 2



C.23 FDOT Test Pit #1 AADCP and DCP Blow Profile



C.24 FDOT Test Pit #1 PI vs Depth



C.25 FDOT Test Pit #1 Estimated CBR vs Depth

APPENDIX D
FORCE AND ENERGY MEASUREMENT OF THE AADCP AND DCP
INSTRUMENTS

This appendix describes and presents the equipment, procedures and results of force and energy measurement of the AADCP and DCP instruments. It is placed in an appendix and not in the main text due to the lack of conclusive results.

D.1 Force and Energy Measurement Test Equipment and Procedures

A force measurement method developed after Chua and Lytton (1989) was used to determine the force in the penetration rod of both the DCP and the AADCP. The force is actually computed from measuring accelerations. The acceleration time plot is first integrated to yield a velocity time plot. The velocity over time is then multiplied by the impedance of the penetration rod yielding the force-time plot (see Chapter 2 for theory). A schematic of the test equipment is shown in Figure D.1. The equipment consisted of a Lecroy Oscilloscope, a PCB Constant Current Power Supply, an Endevco High g Accelerometer, a HP plotter, coaxial cables, and BNC connectors. The accelerometer, mounted to the penetration rod just under the anvil, was connected to the constant current power supply which was in turn connected to the Lecroy oscilloscope. Each test consisted of one blow which was analyzed by the oscilloscope and plotted out to the HP plotter.

Energy calculations of the first compression wave were made by applying the following equation from ASTM 1586

$$E_i = \frac{CK_1K_2K_c}{AE} \int [F(t)]^2 dt \quad (D.1)$$

where

E_i = compression energy

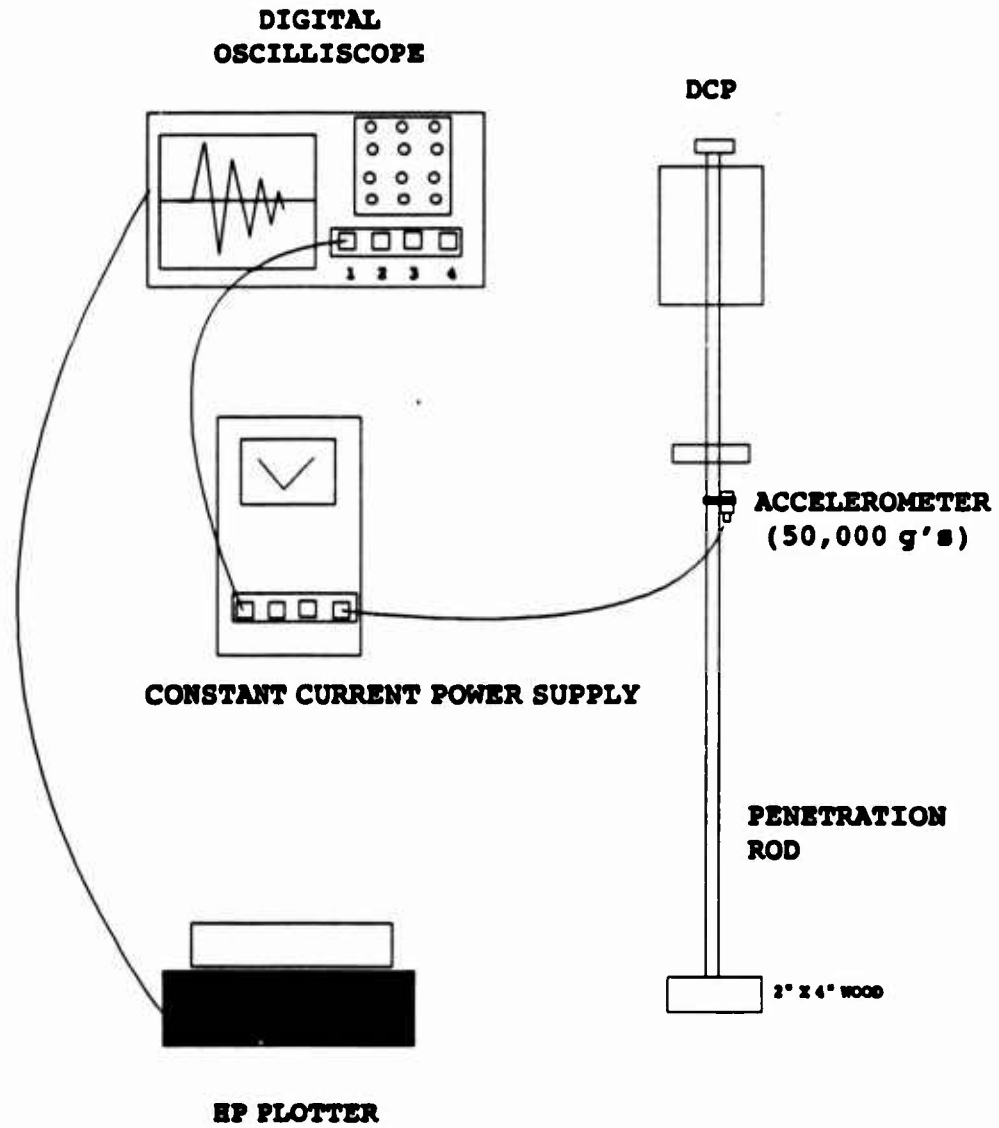


Figure D.1 Force Measurement Equipment

c = wave speed

K_1, K_2, K_c = constants

A = area

E = Young's Modulus

F = force

t = time

The three K values were set to 1.0 and not used since they did not apply in a practical manner to the DCP and AADCP instruments.

D.2 Force and Energy Measurement Results

Figures D.2, D.3, and D.4 show results of the force and energy measurement testing at Weil Hall on an asphalt site. Figure D.2 shows a velocity-time plot of the AADCP and DCP instruments. Figure D.3 shows the force-time plot of both instruments while Figure D.4 shows the cumulative energy of both instruments.

The following equations were used to calculate the force in the penetration rod

$$F = I v \quad (D.2)$$

$$I = E(A)/C \quad (D.3)$$

$$A = \pi d^2/4 \quad (D.4)$$

where

F = force in penetration rod (lbs)

I = Impedance (lb-sec/ft)

v = particle velocity (ft/sec)

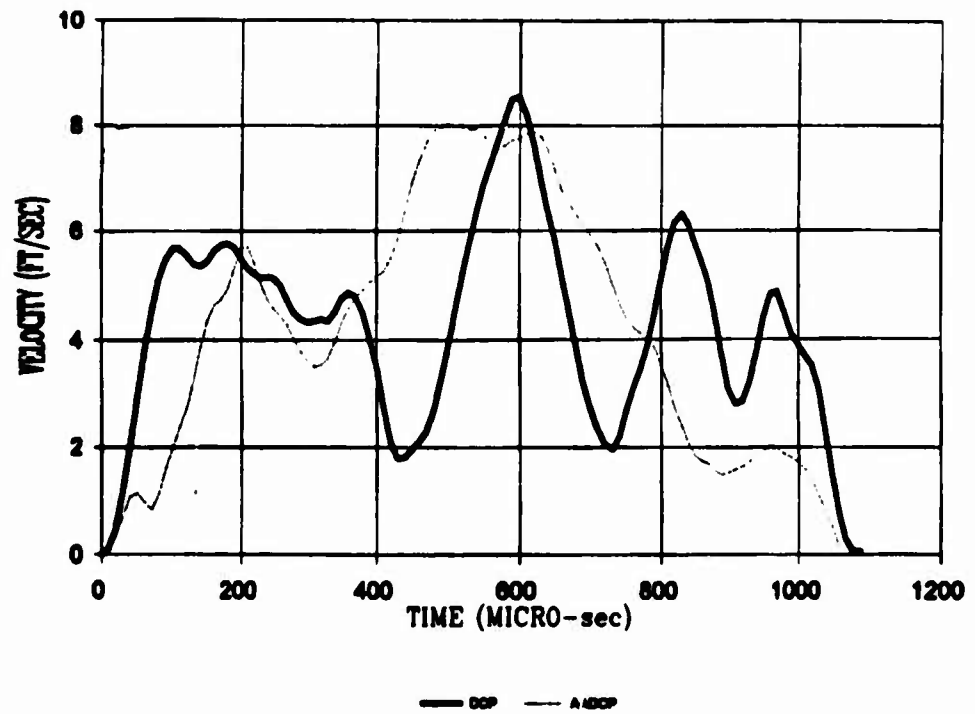


Figure D.2 Velocity-Time Plot

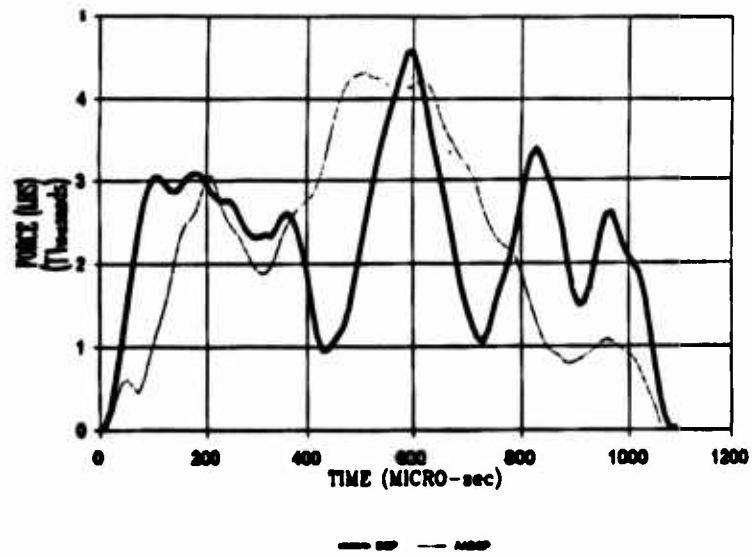


Figure D.3 Force-Time Plot

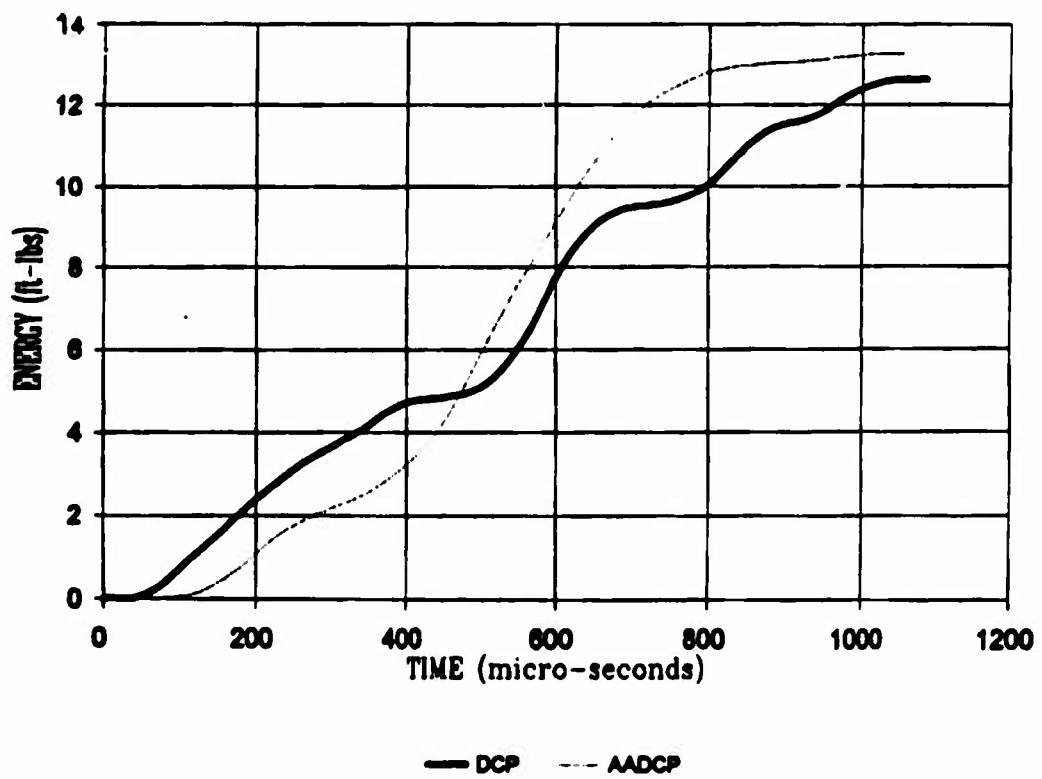


Figure D.4 Cumulative Energy-Time Plot

E = Young's Modulus (29,000,000 psi)

A = cross sectional area of penetration rod (in²)

C = wave speed in steel (17,000 ft/sec)

From Equation D.3

$$\begin{aligned} I &= [(29,000,000)(144)][\pi(0.629)^2/(4)(144)]/[(17,000)] \\ &= 530 \text{ lb-sec/ft} \end{aligned}$$

and therefore the force in the rod becomes

$$F = (530)v \quad (D.5)$$

D.3 Discussion of Force and Energy Measurement Results

The results of the force measurement testing indicate that the AADCP is striking its penetration rod with about the same force that the DCP is striking. This result is somewhat surprising since the correlation testing concluded that the AADCP requires approximately 2.5 times the number of blows that the manual DCP requires.

The potential energy of the AADCP is

$$\begin{aligned} PE &= [(1/2)(K)(X^2)] + [(W)(X)] \quad (D.5) \\ &= [(1/2)(285)(2^2)] + [(11)(2)] \\ &= 592 \text{ in-lbs} \end{aligned}$$

and the potential energy of the manual DCP is

$$\begin{aligned} PE &= [(W)(X)] \quad (D.6) \\ &= [(17.6)(22.6)] \\ &= 398 \text{ in-lbs} \end{aligned}$$

where

PE = potential energy (in-lbs)

K = spring constant (lb/in)

X = deflection (in)

W = weight of hammer

Therefore, the potential energy available to the AADCP is almost 50% higher than the manual DCP.

In Figure D.4 the energy of both instruments is essentially the same despite the field testing results. The most likely reason for the lack of energy in the AADCP penetration rod lies with the reaction of the compression spring. When the piston raises the hammer and compresses the spring, two forces act in opposite directions. Those forces acting down are the weight of the hammer and the compression resistance in the spring. The force acting up is the pressure in the cylinder. Once the cylinder has reached the top position, the air is "immediately" released. The compression spring is then free to strike in both directions, up and down. The spring will move more in the direction of least resistance whether it be down towards the penetration rod or up towards the top of the cylinder. If the spring is not securely prevented from moving in the up direction, valuable energy is lost. Practical solutions to secure the instrument from rebounding up were attempted using the one-way gripper as described in Section 3.3.6.3. However, this solution was not successful in that it scarred the rod.

APPENDIX E
INSTRUCTION MANUAL FOR AADCP TESTING

This appendix is an instructional manual for the AADCP. It includes the procedures to be used to run the instrument and determine the estimated CBR value for the site. Also included are sample data sheets that can be used in the field.

**INSTRUCTION MANUAL FOR THE AUTOMATED AIRFIELD DYNAMIC CONE
PENETROMETER (AADCP)**



**BY
CAPTAIN DAVID WEINTRAUB**

E.1 AADCP General Description

The purpose of this section is to provide a complete description of the Automated Airfield Dynamic Cone Penetrometer (AADCP). The AADCP is composed of three basic components, the penetration system, the control system and the power system. The penetration system consists of the penetration rod, cone tip, anvil, pneumatic air cylinder and piston, hammer, compression spring, counter weight and quick exhaust valve. The control system includes the piston position switch, the double solenoid air valve, the trigger switch, the vertical tape measuring rod, and the digital counter. The power system consists of the gas powered motor, air compressor, air tank, and 12 volt DC battery. In general, the AADCP works somewhat like a single acting pile driver. The AADCP requires two operators with one person reading the measuring rod and the other operating the trigger switch. Testing begins by an operator turning the toggle switch to the "on" position which allows air to flow into the cylinder, Figure E.1. Notice in Figure E.1 that the toggle switch has a lead to the positive side of the battery and one to the fill side of the solenoid. The air, supplied by an adjacent air compressor to port 1, travels through the fill side of the directional control valve from port 1 to port 2. Port 2 is directly connected to the air cylinder and acts as a pivot point for air to fill and exhaust the cylinder. Notice that when it is time to

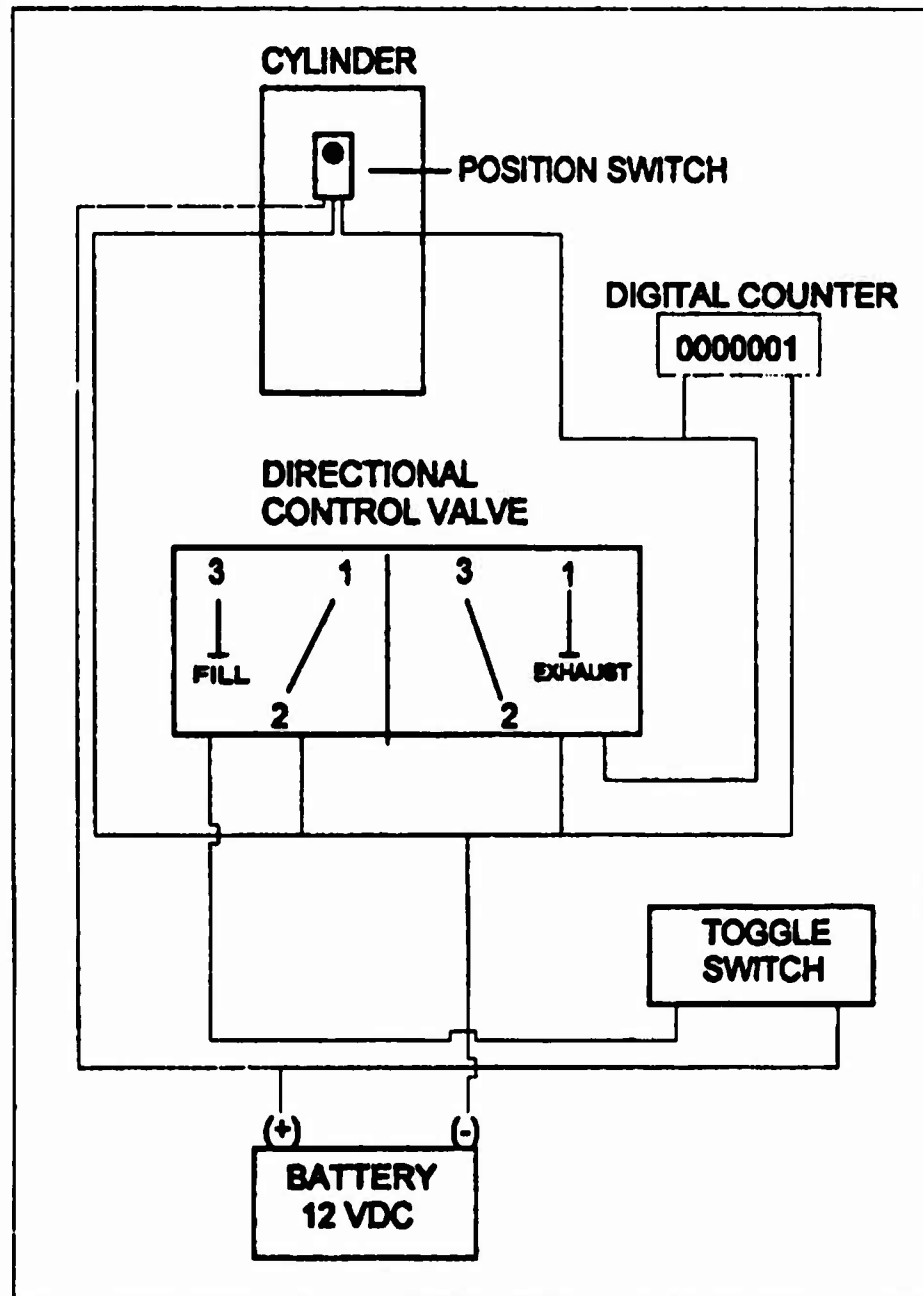


Figure E.1 General Flow of AADCP Operation

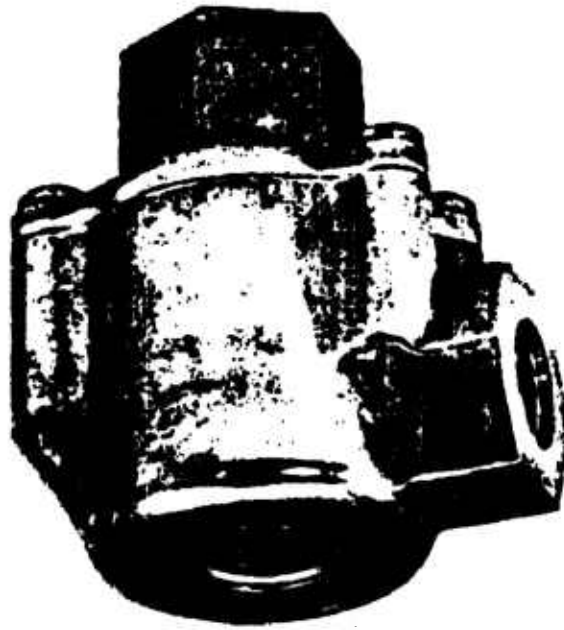
exhaust the air that port 2 pivots and is now connected with port 3 on the exhaust side of the directional control valve. As the 100 psi pressurized air fills the cylinder, the piston is raised approximately two inches. The air overcomes the resistance of both the hammer mass and the 285 lb/in spring. Generally, 100-120 psi of air pressure is required to quickly raise the piston two inches. Once the piston reaches the top of the stroke, a magnet attached to the piston, triggers the position switch mounted on the outside of the cylinder. The position switch then sends a signal to the exhaust side of the directional control valve to stop the air flow into the cylinder and to exhaust this air. Notice in Figure E.1, the position switch has three leads with two of them connected to the battery terminals. The third lead is connected to the exhaust side of the directional control valve. Immediately, the piston is driven down by the spring and mass of the hammer and strikes the anvil which is rigidly connected to the penetration rod. The trigger operator starts the process again by moving the toggle switch back to the "on" position. This is the basic operation of the AADCP. The following sections describe the various functions of the AADCP in more detail.

E.2 Penetration System

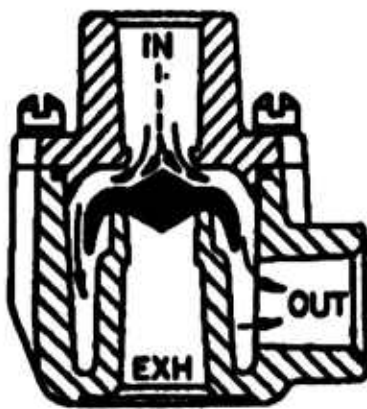
The penetration system consists of the penetration rod, the cone tip, the anvil, the hammer, the pneumatic air

cylinder, the compression spring, the counter weight and the quick exhaust valve. The penetration steel rod has a diameter of 16 mm and can penetrate to a depth of 36 inches. The hardened steel cone tip, which is threaded to the penetration rod, has a diameter of 20 mm and a 60 degree cone apex. The air cylinder has a 2.5 inch diameter piston that has a 10 inch stroke capability with no attached mass. Note that an 11 lb mass is mounted to the piston rod. This leaves a maximum of two inches in stroke. The compression spring is mounted inside the piston with teflon guide rings used to stabilize the spring. The spring rests on top of the piston and pushes against the top of the cylinder when compressed. The operating air pressure is approximately 100 psi. A 20 lb weight is used to counter the large rebound force from the compression spring.

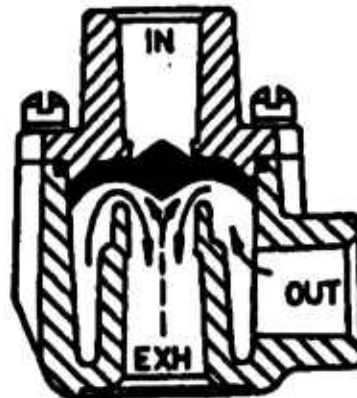
One of the key elements of the penetration system is the quick exhaust valve, Figure E.2(a). This valve is used to expel the air inside the cylinder as quickly as possible. As previously mentioned, once the position switch triggers the exhaust side of the directional control valve, the air into the cylinder is cutoff, port 1 closed, and the air begins to exhaust from port 2 to port 3 through the directional control valve. Since the openings inside the directional control valve are relatively small, the air does not escape fast enough through the valve. However, the drop in pressure from the directional control valve creates a



A



B



C

Figure E.2 Quick Exhaust Valve

backpressure on the quick exhaust valve diaphragm which "instantly" dumps the air out of its large 3/4" exhaust port, Figure E.2(c). Figure E.2(b) shows the filling of the air cylinder through the exhaust valve while Figure E.2(c) shows the air exhausting out the valve. Notice the pressure of the in-coming air forces the diaphragm to block the exhaust port during filling and the backpressure causes the diaphragm to seal the "in" port during the exhaustion phase.

E.3 Control System

The control system consists of the piston position switch, the directional control valve, the toggle switch, the digital blow counter, and the vertical tape measure. The purpose of the control system is to direct the air flow into and out of the cylinder. When the piston is at the bottom (striking) position, high pressure air flows through the normally open solenoid valve into the quick exhaust valve and then into the cylinder. The piston rises and eventually aligns with the top position switch. The top position switch is a magnetic operated switch that is activated when the piston travels near its position. The magnet, mounted in the piston, closes the top position switch which sends a 12 VDC impulse to the solenoid valve. The solenoid valve then ceases the flow of air into the piston and forces the air to escape through its exhaust port.

The other control components are the trigger switch and the digital blow counter. The trigger switch is used to pulse the fill side of the directional control valve as discussed in the previous section. The digital blow counter is activated by the impulse from the position switch. Each time the piston rises to the top position, the counter is pulsed. A measuring rod, divided into tenths of an inch, is used to measure the penetration.

E.4 Power System

The power system includes the gas powered motor, air compressor, air tank, and 12 volt DC battery. A light-weight gas powered motor ideally should run the air compressor. However, the focus of this research was to design and develop a penetration system. It was decided that an electric air compressor run by a gas powered generator would suffice to supply the 100 psi air pressure. A 12 volt DC battery was used to power the solenoids, digital blow counter and the position switches.

E.5 AADCP Test Procedures

The AADCP test consists of attaching the air supply to the pneumatic cylinder, connecting the 12 VDC battery to the three-way solenoid valve and attaching a measuring rod to the instrument. Air pressure is released into the air lines at about 100-120 psi pressure which is required to compress

the 285 lb/inch spring. The hand switch is used to trip the solenoid valve to allow air into the air cylinder while the counter is triggered to measure the number of blows. The hand-switch allows air into the cylinder while the position switch is used to redirect the air out of the cylinder and release the hammer. Generally, a measurement is made every five blows. The stiffer the soil, the greater the number of blows before a measurement is made, generally five to ten blows.

Data is recorded on the sample form in Table E.1. This form records the number of blows with penetration. The average penetration is calculated in the last column. Table E.2 calculates the estimated CBR profile using the AADCP raw data. The penetration index is calculated by subtracting the previous penetration from the present penetration and dividing by the number of blows. If the type of soil penetrated is sand, the sand correlation at the bottom of Table E.2 is used. However, if soil penetrated is not known then the overall correlation should be used. The overall correlation of the AADCP and DCP is

$$\text{DCP} = 2.7 \text{ AADCP} - 0.12$$

A profile of the CBR can be plotted by using the average penetration column versus the CBR column.

Table E.1 AADCP FIELD TESTING FORM

	PENETRATION (INCHES)			
BLOWS	TEST 1	TEST 2	TEST 3	AVERAGE
0	0	0	0	0
5	- 7.1	- 6.1	-5.8	-6.3
10	-10.5	-8.7	-8.9	-9.4
15	-12.5	-10.7	-11.9	-11.7
20	-14.4	-12.6	-13.7	-13.6
25	-16.3	-14.5	-16.6	-15.8
30	-18.8	-16.5	-19.1	-18.1
35	-21.5	-19.0	-22.2	-20.9

Table E.2 AADCP Sample Data Correlation Worksheet

BLOWS	AVERAGE PENETRATION (INCHES)	PENETRATION INDEX (P.I.) (IN/BLOW) ¹	AADCP-DCP CORRELATION P.I. (IN/BLOW) ²	DCP-CBR CORRELATION CBR (%) ³
0	0	0	0	0
5	-6.3	1.26	3.28	2.04
10	-9.4	0.62	1.55	4.71
15	-11.7	0.46	1.12	6.78
20	-13.6	0.38	0.91	8.56
25	-15.8	0.44	1.07	7.1
30	-18.1	0.46	1.12	6.78
35	-20.9	0.56	1.39	5.33

Notes:

- (1) This column subtracts previous penetration and divides by 5 blows, $(9.4 - 6.3)/5 = 0.62$
- (2) This column uses one of two correlations of AADCP-DCP sands: $DCP = 2.3 \text{ AADCP} - 0.04$
silty-sands: $DCP = 2.7 \text{ AADCP} - 0.12$
- (3) This column uses the Webster (1992) DCP-CBR Correlation
 $\text{Log CBR} = 2.46 - 1.12 [(\text{Log DCP} \times 25.4 \text{ mm/in})]$

REFERENCE LIST

- Bowles, J.E., (1988) Foundation Analysis and Design, 4th Edition, McGraw-Hill, Inc., New York, pp. 788.
- Brabston, W.N., and Hammitt, G.M., (1974) "Soil Stabilization for Roads and Airfields in the Theater of Operations," U.S. Army Engineer Waterways Experiment Station, AD-787-257.
- Brown, R.W. Letter to 61 MAG/CC. 7 August 1986.
- Caudle, W.N., Pope, A.Y., McNeill, R.L., and Magason, B.E. (1977) "Feasibility of Rapid Soil Investigations Using High Speed Earth Penetrating Projectiles," International Symposium on Wave Propagation and Dynamic Properties of Earth Materials, Albuquerque, NM, (August).
- Chua, K. M., and Lytton, R. L., (1989) "Dynamic Analysis Using the Portable Pavement Dynamic Cone Penetrometer," Transportation Research Record 1192, TRB, National Research Council, Washington, D.C., pp. 27-38.
- Durgunoglu, H. T., and Mitchell, J. K., (1974) "Influence of Penetrometer Characteristics on Static Penetration Resistance," Proceedings of the European Symposium on Penetration Testing, Stockholm, pp. 133-139.
- Fenwick, W.B., (1965) "Description and Application of Airfield Cone Penetrometer," U.S. Army Engineer Waterways Experiment Station, Instruction Report No. 7.
- Hammitt, G.M., (1970) "Thickness Requirements For Unsurfaced Roads and Airfields," U.S. Army Engineer Waterways Experiment Station, Technical Report S-70-5, (July).
- Harison, J. A., (1986) "Correlation of CBR and Dynamic Cone Penetrometer Strength Measurement of Soils," Technical Note No. 2, Australian Road Research, 16(2), (June), pp. 130-136.

- Harison, J. A., (1989) "In Situ CBR Determination by DCP Testing Using a Laboratory-Based Correlation," Technical Note No. 2, Australian Road Research 19(4), December, pp. 313-317.
- Kleyn, E. G., (1975) "The Use of the Dynamic Cone Penetrometer," Transvaal Roads Department, Report 12/74, July, Pretoria, South Africa.
- Ladd, D.C., (1965) "Ground Flotation Requirements for Aircraft Landing Gear," U.S. Army Engineer Waterways Experiment Station, Misc Paper No. 4-459.
- Ladd, D.M. and Ulery, H.H. Jr., (1967) "Aircraft Ground Flotation Investigations; Part I, Basic Report," Technical Documentary Report AAFDL-TDR-66-43 Air Force Flight Dynamics Laboratory, WPAFB, Ohio.
- Livneh, M., (1987) "The Correlation Between Dynamic Cone Penetrometer Values (DCP) and CBR Values," Transportation Research Institute, Technion-Israel Institute of Technology, Pub. No. 87-065.
- Livneh, M., and Greenstein, J., (1978) "A Modified California Bearing Ratio Test for Granular Materials," Geotechnical Testing Journal, ASTM, Vol 1, No. 3, Sep, pp. 141-147.
- Livneh, M., and Ishai, I., (1989) "Carrying Capacity of Unsurfaced Runways for Low Volume Aircraft Traffic - Phase I: Review of Current Technology," August, Technion-Israel Institute of Technology, Transportation Research Institute, Haifa, Israel, Prepared for AFESC, Tyndall AFB, FL 32403.
- Livneh, M., Ishai, I., and Livneh, N., (1990) "Carrying Capacity of Unsurfaced Runways for Low Volume Aircraft Traffic - Phase III: Application of the Dynamic Cone Penetrometer," April, (Draft Copy), Technion-Israel Institute of Technology, Transportation Research Institute, Haifa, Israel, Prepared for AFESC, Tyndall AFB, FL 32403.
- Livneh, M., Ishai, I., and Livneh, N., (1992) "Carrying Capacity of Unsurfaced Runways for Low Volume Aircraft Traffic -Supplement to Phase III: Automated DCP Device Vs. Manual DCP Device," February, (Draft Copy), Technion-Israel Institute of Technology, Transportation Research Institute, Haifa, Israel, Prepared for AFESC, Tyndall AFB, FL 32403.

- MACP 50-8, (1989) "Combat Control - The Quick Action Force," Department of the Air Force - Military Airlift Command Regulation, Scott Air Force Base, Illinois, (June).
- Melzer, K. J., and Smoltczyk, U., (1982) "Dynamic Penetration Testing - State of the Art Report," Proceedings of the Second European Symposium on Penetration Testing, Amsterdam, 24-27 May, pp. 191-202.
- Metcalf, J.B., (1976) "Pavement Materials - The Use of California Bearing Ratio Test in Controlling Quality," Report 48, Australia Road Research Board, Vermont Victoria, Australia.
- Meyerhof, G. G., (1961) "The Ultimate Bearing Capacity of Wedge-Shaped Foundations," Proceedings, Fifth International Conference on Soil Mechanics and Foundation Engineering, Vol. 2, pp. 105-109.
- Molineux, C.E., (1955) "Remote Determination of Soil Trafficability By the Aerial Penetrometer," Report No. 77, Air Force Cambridge Research Center, Bedford, Mass.
- Roesset, J.M., Chang, D., Stokoe, K., and Aouad, M., (1990) "Modulus and Thickness of the Pavement Surface Layer from SASW Tests," Transportation Research Record 1260, TRB, National Research Council, Washington, D.C., pp. 53-63.
- Rohani, B. and Baladi, G.Y., (1981) "Correlation of Mobility Cone Index with Fundamental Engineering Properties of Soil," Miscellaneous Paper SL-81-4, U.S. Army Engineer Waterways Experiment Station, Vicksburg, MS.
- Scala, A. J., (1956) "Simple Methods of Flexible Pavement Design Using Cone Penetrometers," New Zealand Engineering, Vol 11, No. 2, pp. 34-44.
- Schmertmann, J.H., (1979) "Statics of SPT," Journal of the Geotechnical Division, ASCE, Vol. 105, No. GT5, Proc. Paper 14573.
- Seed, B., Wong, R.T., Idriss, I.M., and Tokimatsu, K., (1986) "Moduli and Damping Factors for Dynamic Analysis of Cohesionless Soils," Journal of Geotechnical Engineering, November, Vol 112, No. 11.
- Smith, R.B., and Pratt, D.N., (1983) "A Field Study of In-Situ California Bearing Ratio and Dynamic Cone Penetrometer Testing for Road Subgrade Investigations," Australian Road Research 13(4), December, pp. 283-294.

- Stokoe, K.H., Nazarian, S., Rix, G.J., Sanchez-Salinero, Ignacio, Sheu, J., and Mok, Y., (1988) "In Situ Seismic Testing of Hard-to-Sample Soils by Surface Wave Method," Proceedings, Earthquake Engineering and Soil Dynamics II, ASCE Specialty Conference - Recent Advances in Ground Motion Evaluation, June, Park City, Utah, pp. 264-278.
- Townsend, F.C., Theos, J.F., Shields, M.D., Hussein, M., Coastal Caisson Drill Co., and Florida DOT, (1991) "Dynamic Load Testing of Drilled Shaft," March, Final Report to the Association of Drilled Shaft Contractors
- Turnbull, W. J., Maxwell, A.A., and Burns, C. D., (1961) "Strength Requirements in Unsurfaced Soils for Aircraft Operations," Proceedings of the 5th International Conference of Soil Mechanics and Foundation Engineering, Paris, pp. 347-357.
- Van Vuuren, D. J., (1969) "Rapid Determination of CBR with the Portable Dynamic Cone Penetrometer," The Rhodesian Engineer, September, Paper No. 105, pp. 852-854.
- Vesic, A. S., (1972) "Expansion of Cavities in Infinite Soil Mass," Journal of the Soil Mechanics and Foundations Division, March, pp. 265-290.
- Webster, S.L., Grau, R.H., and Williams, Thomas P., (1992) "Description and Application of Dual Mass Dynamic Cone Penetrometer," Instruction Report GL-92-3, Waterways Experiment Station, Mississippi.
- Womack, L.M., (1965) "Tests with a C-130E Aircraft on Unsurfaced Soils," U.S. Army Engineer Waterways Experiment Station, Vicksburg, MS.

SUPPLEMENTARY REFERENCES

- Air Force Engineering and Services Center, "Aircraft Characteristics for Airfield Pavement Design and Evaluation," Tyndall Air Force Base, 1990.
- Aun, O. T., and Hui, T. W., "The Use of a Light Dynamic Cone Penetrometer in Malaysia," 4th Southeast Asian Conference on Soil Engineering, Kuala Lumpur, Malaysia, 7-10 April 1975, pp. 3-62 - 3-79.
- Ayers, M. E., Thompson, M. R., and Uzarski, D. R., "Rapid Shear Strength Evaluation of In Situ Granular Materials," Transportation Research Record 1227, pp. 134-146.
- Cearns, P. J., and McKenzie, A., "Application of Dynamic Cone Penetrometer Testing in East Anglia," Penetration Testing in the UK, Thomas Telford, London, 1988, pp. 123-127.
- Chua, K. M., "Determination of CBR and Elastic Modulus of Soils using a Portable Pavement Dynamic Cone Penetrometer," ISOPT-1 Orlando, Fl, 20-24 March 1988.
- Harison, J. A., 1987 (December). "Correlation Between California Bearing Ratio and Dynamic Cone Penetrometer Strength Measurements of Soils," Proceedings of Instn. Civil Engineers, Part 2, pp. 833-844.
- Headquarters, Department of the Army. 1990 (September). "Design of Aggregate Surfaced Roads and Airfields," Technical Manual TM 5-822-12, Washington, DC.
- Khedr, S. A., Kraft, D.C., and Jenkins, J. L., "Automated Cone Penetrometer: A Nondestructive Field Test for Subgrade Evaluation," Transportation Research Record 1022, pp. 108-115.
- Kleyn, E.G., Maree, J. H., Savage, P. F., "The Application of a Portable Pavement Dynamic Cone Penetrometer to Determine In-Situ Bearing Properties of Road Pavement Layers and Subgrades in South Africa," Proceedings of the Second European Symposium on Penetration Testing, Amsterdam, 24-27 May 1982, pp. 277-282.

- Livneh, M., "Validation of Correlations Between a Number of Penetration Tests and In Situ California Bearing Ratio Tests," Transportation Research Record 1219, pp. 56-67.
- Livneh, M., and Ishai, I., "The Relationship Between In-situ CBR Test and Various Penetration Tests," ISOPT-1 Orlando, Fl, 20-24 March 1988, pp. 445-452.
- Livneh, M., and Ishai, I., 1987 (July). "Pavement and Material Evaluation by a Dynamic Cone Penetrometer," Proceedings of the Sixth International Conference on Structural Design of Asphalt Pavements, Vol. I, pp. 665-676, University of Michigan, Ann Arbor, MI.
- McElvaney, J., and Bunadidjatnika, I., "Strength Evaluation of Lime-Stabilized Pavement Foundations Using the Dynamic Cone Penetrometer," Australian Road Research 21(1), March 1991, pp. 40-52.
- Nazarian, S., Stokoe, K.H., Briggs, R.C., and Rogers, R., "Determination of Pavement Layer Thicknesses and Moduli by SASW Method," Transportation Research Record 1190, pages 133-150, 1988.
- Overby, C., "A Comparison between Benkelman Beam, DCP, and Clegg-Hammer measurements for Pavement Strength Evaluation," International Symposium on Bearing Capacity of Roads and Airfields, Norway, June 23-25, 1982, pages 138-147.
- Schmertmann, J. H., and Palacios, A., "Energy Dynamics of SPT," Journal of the Geotechnical Engineering Division, GT8, August 1978, pp. 909-926.
- Smith, R. B., "Cone Penetrometer and In Situ CBR Testing of an active Clay," ISOPT-1 Orlando, Fl, 20-24 March 1988, pp. 459-465.
- Sowers, G. F., and Hedges, C. S., "Dynamic Cone for Shallow In-Situ Penetration Testing," Vane Shear and Cone Penetration Resistance Testing of In-Situ Soils, ASTM STP 399, Am. Soc. Testing Mats., 1966, pp. 29-37.
- U.S. Army Engineer Waterways Experiment Station, "Dynamic Cone Penetrometer - Instruction Manual, August 1989.
- Van Heerden, M. J., and Rossouw, A. J., "An Investigation to Determine the Structural Capacity of an Airfield Pavement Using the Pavement Dynamic Cone Penetrometer," International Symposium on Bearing Capacity of Roads and Airfields, June 23-25, 1982 Trondheim, Norway, pp. 1092-1094.

BIOGRAPHICAL SKETCH

David Weintraub earned a Bachelor of Science in Civil Engineering degree from the United States Air Force Academy in 1986. His first assignment was at Shaw AFB, SC. The basic skills as a civil engineer were acquired while he worked as a construction manager, runway project officer and a pavements engineer. As Deputy Chief of Contract Management at Shaw AFB, he coordinated inspection of \$20 million of Air Force construction and was part of a 1988 Unit Effectiveness Inspection "Excellent Rating" for the construction management section. As runway project officer, he was responsible for the construction and inspection of a \$10 million runway reconstruction project. His responsibilities included negotiating with contractors, writing and approving modifications, and review and approval of project material submittals for technical sufficiency. In addition, he authored the first TAC Runway Construction Management and Inspection Plan which later became the standard for all construction of runways in the Tactical Air Command. Based on this and other projects, he was presented the 1989 Tactical Air Command Design Excellence Award in Construction Management by the TAC commander. As a

pavements engineer he contributed to the design of a \$3 million fighter parking ramp. His design duties included calculations of ramp grades, ramp and base thickness, and the design of joint patterns. In addition, quarterly runway construction briefings to the wing, base, and squadron commanders honed his communication skills as did two years in the Shaw AFB Toastmasters Club.

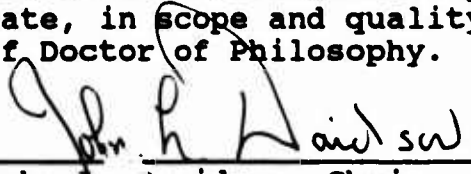
His experience also includes leading a tiger team to Saudi Arabia to maintain and repair the USCENTAF ELF-ONE E-3A Command Center. With an assignment to Squadron Officer School in-residence, and then the selection to AFIT at the University of Florida, his professional and engineering qualifications were greatly enhanced. The University of Florida accepted him in their civil engineering graduate construction management program in August of 1989 where he graduated in December of 1990. He later accepted a position in their Ph.D. geotechnical engineering program in January of 1991. His next assignment is a base level job in Guam in January of 1994 and a follow on assignment as a Civil Engineering instructor at the United States Air Force Academy in January of 1996.

His off-base leadership experience has been enhanced tremendously with extra curricular activities such as a Gainesville youth soccer coach (11-14 year olds) for six seasons, leading a bi-monthly bible study for the last three

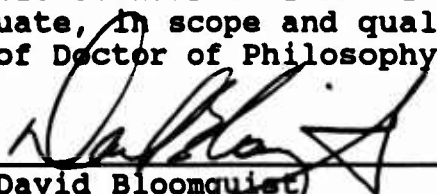
years, and assisting with University of Florida Engineering fairs.

He is married to [REDACTED] They have one daughter, [REDACTED] and are awaiting their son's birth in [REDACTED]

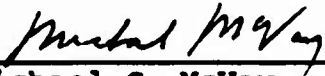
I certify that I have read this study and that in my opinion it conforms to acceptable standards of scholarly presentation and is fully adequate, in scope and quality, as a dissertation for the degree of Doctor of Philosophy.


John L. Davidson, Chair
Professor of Civil Engineering

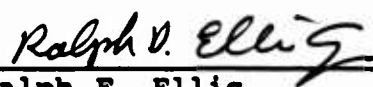
I certify that I have read this study and that in my opinion it conforms to acceptable standards of scholarly presentation and is fully adequate, in scope and quality, as a dissertation for the degree of Doctor of Philosophy.


David Bloomquist
Assistant Professor of
Civil Engineering

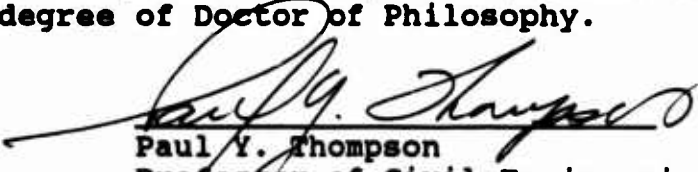
I certify that I have read this study and that in my opinion it conforms to acceptable standards of scholarly presentation and is fully adequate, in scope and quality, as a dissertation for the degree of Doctor of Philosophy.


Michael C. McVay
Associate Professor of
Civil Engineering


I certify that I have read this study and that in my opinion it conforms to acceptable standards of scholarly presentation and is fully adequate, in scope and quality, as a dissertation for the degree of Doctor of Philosophy.


Ralph E. Ellis
Assistant Professor of
Civil Engineering

I certify that I have read this study and that in my opinion it conforms to acceptable standards of scholarly presentation and is fully adequate, in scope and quality, as a dissertation for the degree of Doctor of Philosophy.


Paul Y. Thompson
Professor of Civil Engineering

I certify that I have read this study and that in my opinion it conforms to acceptable standards of scholarly presentation and is fully adequate, in scope and quality, as a dissertation for the degree of Doctor of Philosophy,


Brisbane Brown
Professor of Building
Construction

This dissertation was submitted to the Graduate Faculty of the College of Engineering and to the Graduate School and was accepted as partial fulfillment of the requirements for the degree of Doctor of Philosophy.

December 1993

Winfred M. Phillips
Dean, College of Engineering

Karen A. Holbrook
Dean, Graduate School

2 ms. Man. Inq.
of the copyright of the volume on the subject of
leading into them for similar treatment. - (JAMES W. L. 18-2)
Sept 1876, pp. 241-242, many authorities would refer to the
following material as part of his observations on the
subject of the University of Illinois in December of 1876.

THE NEW YORK PUBLIC LIBRARY
ASTOR LENOX TILDEN FOUNDATION
125 WEST 4TH STREET
NEW YORK, N. Y.

SECRET

100 - 1000 (100)

1977 School - (top page for) 8 students (10)

I (the donor) intend this contribution to University Libraries International, Inc. solely, and solely for the purpose of reproducing and distributing electronic copies of the manuscript.

Maria Theresia 1755-1807

Blackney

100

**Copyright © 1991
Copyright © 1991
Copyright © 1991**

THE UNIVERSITY OF CHICAGO PRESS
530 N. Dearborn Ave., Chicago, IL 60610-3139
Tel: 773/936-7329 Fax: 773/936-7329

**Special Agent
in Charge**

Identifying a group of people

